

CARDIFF
UNIVERSITY

PRIFYSGOL
CAERDYDD

Acetylene Hydrochlorination using Gold Catalysts



Simon Rhys Dawson

Thesis submitted in accordance with the requirement of Cardiff
University for the degree of Doctor of Philosophy

2015 - 2019

Statements and Declaration

STATEMENT 1

This thesis is being submitted in partial fulfilment of the requirements for the degree of PhD

Signed _____

Date _____

STATEMENT 2

This work has not been submitted in substance for any other degree or award at this or any other university or place of learning, nor is it being submitted concurrently for any other degree or award (outside of any formal collaboration agreement between the University and a partner organisation)

Signed _____

Date _____

STATEMENT 3

I hereby give consent for my thesis, if accepted, to be available in the University's Open Access repository (or, where approved, to be available in the University's library and for inter-library loan), and for the title and summary to be made available to outside organisations, subject to the expiry of a University-approved bar on access if applicable.

Signed _____

Date _____

DECLARATION

This thesis is the result of my own independent work, except where otherwise stated, and the views expressed are my own. Other sources are acknowledged by explicit references. The thesis has not been edited by a third party beyond what is permitted by Cardiff University's Use of Third Party Editors by Research Degree Students Procedure.

Signed _____

Date _____

WORD COUNT _____

(Excluding summary, acknowledgements, declarations, contents pages, appendices, tables, diagrams and figures, references, bibliography, footnotes and endnotes)

Abstract

The use of different solvents and modified carbon supports was investigated to determine their effect on the catalytic activity of gold on carbon catalysts for the hydrochlorination of acetylene.

By changing the solvent from that of highly oxidising and harmful aqua regia to simple organic solvents such as acetone, the conversion of acetylene was maintained and the initial activation period of the catalyst reduced. This was attributed to the high dispersion of Au(I) species, stabilised on the carbon support. Furthermore, the drying temperature used in the preparation of the catalyst was greatly reduced, from 140 to 45 °C, owing to the high volatility of the solvent. Catalytic activity was correlated with the polarity of the solvent; decreasing the polarity resulted in higher acetylene conversions whilst higher polarities suffered from deactivation due to water present in the solvent and higher drying temperatures.

Doping the Au/C catalyst with low concentrations of sulfur increased the conversion of acetylene significantly, simultaneously reducing the induction period. The most effective method for increasing the catalytic activity was found to be pre-washing the carbon in dilute H₂SO₄, before the addition of gold. By this method, variation of the concentration of H₂SO₄ had little effect on the catalytic activity, in all cases producing a high initial conversion.

Carbons were prepared with a modified Hummers' oxidation method, resulting in a greater oxygen concentration and greater catalytic activity. The optimum oxygen concentration was found to be 21 %; introduction of ether groups increased acetylene conversion whilst carbonyls were deemed responsible for reduced conversion. Notably, these oxidised carbon catalysts were active at temperatures as low as 130 °C, which would be beneficial for industrial applications. Other oxidation methods resulted in variation in the oxygen concentration, indicating that specific functional groups were responsible for changes in activity, not solely the abundance of oxygen.

Acknowledgements

I would first like to thank Graham Hutchings for allowing me to carry out the PhD in the CCI group. Thanks also for being a referee, helping me get my foot on the ladder that is industrial chemistry. I would like to thank Johnson Matthey for funding my PhD and particularly Peter Johnston. I will always remember your genuine interest in first my wellbeing and second my work (always in that order). I hope I can be half the mentor you are if ever I reach such a position of responsibility. Thanks go to Martin Hayes and all the Johnson Matthey team who made me feel welcome and valued during meetings and conferences.

Thank you to Tom Davies and Qian He for their technical assistance in acquiring the SEM data at Lehigh University, to Stewart Parker and Emma Campbell for their assistance with XAFS at the Diamond Light Source and to Dave Morgan for his help with XPS analysis at Cardiff University.

Thanks to Sam Pattison. Your supervision and genuine support were at times the only reasons I carried on with this thesis. More researchers should have your can-do, positive attitude.

Colleague-come-supervisor Grazia, thank you for being honest with your feedback. We may not have agreed on everything but the science was sound and I'm sure you'll go far.

The Simons (Kondrat and Freakley), thanks for starting me out on the PhD. Kondrat, your passion was at times infectious, I'm glad you're making a name for yourself in Loughborough and inspiring more new minds.

I am grateful for all of the members of CCI who I had the pleasure to work with during the past 4 years and more. A special mention goes to Stefano "Steve" Cattaneo, who inspired/forced me to play volleyball, which has led to many more friends and fun times. Even in the lab, you kept me going through the frustrating days of broken equipment and troublesome reactions. We will always have ABBA to keep us going! Tanja P helped me through the long days writing endless papers and reports, thank you for taking on that burden when I left. And thanks for all the lunches, with Jonathan too, enjoying the weather come rain or shine. Laura, Meg, you were always good for a gossip.

To the old timers, Parag, Nia, Luke and Eoin, thanks for sharing the journey, through the good times and the bad. The next chapters of our lives can only be better.

Steve, Lee and Julian, thank you for all the help you've provided fixing machines and equipment. It was always a delight to head down to the workshop and inspired me to get my first job. You always made it look effortless and I'll miss the random conversations whilst we worked. And to Greg, cheers for your calm manner and all your help. I hope you manage to get into teaching sooner rather than later, you'll be great at it!

Adam, Liz and Alex, thanks for never talking about catalysts. You were always a welcome break from work and inspirational for trying new restaurants. Long may we continue to explore.

Finally, I'd like to thank my parents. A weekly query of "how's the writing" may have been a tad annoying at times but by the end I was writing this just as much for you as me. Thanks for always being there.

Publication List

List of publications produced during the course of this PhD:

G. Malta, S. A. Kondrat, S. J. Freakley, C. J. Davies, L. Lu, S. R. Dawson, A. Thetford, E. K. Gibson, D. J. Morgan, W. Jones, P. P. Wells, P. Johnston, C. R. A. Catlow, C. J. Kiely and G. J. Hutchings. **Identification of single-site gold catalysis in acetylene hydrochlorination.** 2017. *Science* 355(6332), pp. 1399-1403. (10.1126/science.aal3439)

G. Malta, S. A. Kondrat, S. J. Freakley, C. J. Davies, S. R. Dawson, X. Liu, L. Lu, K. Dymkowski, F. Fernandez-Alonso, S. Mukhopadhyay, E. K. Gibson, P. P. Wells, S. F. Parker, C. J. Kiely and G. J. Hutchings. **Deactivation of a single-site gold-on-carbon acetylene hydrochlorination catalyst: An X-ray absorption and inelastic neutron scattering study.** 2018. *ACS Catalysis* 8(9), pp. 8493-8505. (10.1021/acscatal.8b02232)

T. E. Parmentier, S. R. Dawson, G. Malta, L. Lu, T. E. Davies, S. A. Kondrat, S. J. Freakley, C. J. Keily and G. J. Hutchings. **Homocoupling of phenylboronic acid using atomically dispersed gold on carbon catalysts: catalyst evolution before reaction.** 2018. *ChemCatChem*, 10(8), pp. 1853-1859. (10.1002/cctc.201701840)

X. Sun†, S. R. Dawson†, T. E. Parmentier, G. Malta, T. E. Davies, Q. He, L. Luc, D. J. Morgan, N. Carthey, P. Johnston, S. A. Kondrat, S. J. Freakley, C. J. Kiely and G. J. Hutchings. **A Facile Synthesis of Precious Metal Single Site Catalysts using Organic Solvents.** *Nature Chemistry*. 2020. Accepted for publication.

† These authors contributed equally to this work.

Contents

Statements and Declaration	i
Abstract.....	iii
Acknowledgements.....	v
Publication List.....	vii
1. Introduction	1
1.1. Catalysis	1
1.2. Heterogeneous catalysts.....	3
1.3. Catalysis by gold.....	5
1.4. Activated carbon – catalyst and support	6
1.5. VCM production methods.....	11
1.5.1. The balanced process.....	12
1.5.2. The acetylene hydrochlorination reaction.....	13
1.5.2.1. Mercury-based catalysts	13
1.5.2.2. Gold-based catalysts	15
1.5.2.3. Reaction kinetics of Au/C catalyst.....	17
1.6. Project aims.....	20
1.7. Project Overview.....	20
1.8. References	20
2. Experimental	23
2.1. Introduction	23
2.2. Chemicals	23
2.3. Catalyst preparation methods	23
2.3.1. Preparation of supported gold catalysts via wet impregnation	23
2.3.2. Preparation of modified Au/C catalysts.....	24
2.4. Catalyst characterisation techniques.....	24
2.4.1. Brunauer-Emmett-Teller (BET) surface area analysis.....	24
2.4.2. X-ray Absorption Fine Structure (XAFS) Spectroscopy.....	25
2.4.3. Gas chromatography.....	27
2.4.4. Mass spectrometry	30
2.4.5. ICP-MS.....	30

2.4.6.	Fourier Transform Infrared Spectroscopy (FTIR)	31
2.4.7.	Powder x-ray diffraction	32
2.4.8.	In-situ powder x-ray diffraction	34
2.4.9.	Scanning/transmission electron microscopy	34
2.4.10.	Thermogravimetric analysis.....	37
2.4.11.	X-ray photoelectron spectroscopy.....	37
2.5.	Acetylene hydrochlorination reaction	38
2.6.	References	41
3.	Carbon supported single-site gold catalysts prepared using low polarity solvents, for the acetylene hydrochlorination reaction.....	47
3.1.	Introduction	47
3.2.	Single site gold catalysts prepared with aqua regia.....	48
3.3.	Experimental conditions	49
3.4.	Catalysts prepared with different polarity solvents	49
3.5.	Effect of drying temperature on catalytic activity	52
3.6.	Effect of water introduced in preparation on catalytic activity.....	55
3.7.	Investigation of the catalyst stability	60
3.8.	XAFS study of catalyst gold species.....	65
3.9.	Conclusions	69
3.10.	References	70
4.	Acetylene hydrochlorination using sulfur treated, carbon supported gold catalysts	72
4.1.	Introduction	72
4.2.	Experimental Conditions.....	73
4.2.1.	Preparation of pre-treated carbons.....	73
4.2.2.	Preparation of post-treated carbons	73
4.2.3.	Reaction conditions.....	74
4.3.	Catalyst Nomenclature	74
4.4.	Bimetallic catalysts.....	74
4.5.	Catalysts prepared with salt sulfates	81
4.5.1.	(NH ₄) ₂ SO ₄ treatment	82
4.5.2.	Na ₂ SO ₄ treatment.....	84
4.6.	Sulfuric acid catalysts.....	86

4.6.1.	Pre-treatment of carbon supports with sulfuric acid	86
4.6.2.	The effect of temperature on sulfuric acid pre-treated catalysts	91
4.6.3.	The effect of water washing on pre-treated carbon supports	99
4.6.4.	Post-treatment of catalyst with sulfuric acid.....	102
4.6.5.	Other sulfuric acid treatments.....	105
4.7.	Acid treated catalysts.....	107
4.8.	Conclusions	109
4.9.	References	110
5.	Acetylene Hydrochlorination using oxidised carbon supported gold catalysts.....	112
5.1.	Introduction	112
5.2.	Experimental conditions	113
5.2.1.	Treatment of carbon via modified Hummers' method.....	113
5.2.2.	Reaction conditions.....	113
5.3.	Oxidising carbons via modified Hummers' method.....	114
5.3.1.	Effect of amount of oxidant on catalytic activity	114
5.3.2.	Characterisation via XPS	118
5.3.3.	Other characterisation techniques	123
5.3.4.	Effect of temperature on catalytic activity of 1 % Au/Ox C – 2.5	129
5.3.4.1.	Effect of temperature on gold oxidation state	134
5.3.5.	Effect of varying temperature on catalytic activity of 1 % Au/Ox C – 5.....	144
5.4.	The effect of washing the carbon	146
5.5.	Combining oxidised carbon supports with acetone	148
5.6.	Oxidising the support via different methods	149
5.7.	Conclusions and future work	156
5.8.	References	158
6.	Conclusions and future work	160
6.1.	Carbon supported single-site gold catalysts prepared using low polarity solvents .	160
6.2.	Sulfur treated, carbon supported gold catalysts	161
6.3.	Oxidised carbon supported gold catalysts	161

1. Introduction

1.1. Catalysis

The understanding of the principles of catalysis were founded in the early 1800s. Of the first catalytic reactions performed, the most notable was that discovered by Louis Jacques Thenard in 1813; the decomposition of ammonia to nitrogen and hydrogen, performed by passing ammonia over very hot metals.¹ This was further investigated in collaboration with Pierre Dulong, where it was discovered that the catalytic activity was dependent on the metal employed, in the order of iron > copper > silver > gold > platinum, a trend hitherto unobserved.² Although platinum displayed lower activity than the other metals for the decomposition of ammonia, significant research was carried out on its use by Humphry Davy. Davy placed a platinum wire above a coal-gas lamp flame. When an excess of coal-gas was introduced, the flame was extinguished but the wire continued to be very hot and bright. The wire was also incandescent and hot in the presence of coal-gas and air. This was the first indication of heterogeneous catalytic oxidation.³ This research went on to be applied in the preparation of the miner's safety-lamp. Edmund Davy continued this research, by using a fine platinum mesh in place of the wire, showing that smaller divisions of metal resulted in higher catalytic activity.⁴ This catalyst was even found to be active at room temperature, becoming very hot when mixed with alcohol on a porous substance due to rapid oxidation, forming acetic acid. This same theory, using finely divided or nanoscale metal was applied to gold catalysts which were previously thought to be inactive.

Although these were clear examples of catalytic processes, the understanding of how catalysis occurred was not agreed on for several decades. It wasn't until 1836 that the term catalysis was coined by Berzelius, from the Greek words kata (translated as down) and luein (loosen), which were combined to form kataluein (dissolve) and then katalusis.⁵ The early understanding of catalytic processes progressed from theories of catalytic forces or "sleeping energy" released upon catalyst initiation,⁶ to the determination that catalytic processes could involve multiple steps, including multiple intermediate products, due to rearrangement of atoms to more stable systems. This led to the definition by Ostwald in 1901, where he stated that a catalyst is "a substance that alters the chemical reaction rate without itself being part of the final products".⁷ This definition can be illustrated by the energy diagram shown in Figure 1.1. A catalyst can provide an alternative pathway for a reaction mechanism which lowers the activation energy of the reaction. The rate of reaction will increase in the catalysed process, without the catalyst itself being consumed, thereby only affecting the kinetics of the reaction. However, the catalyst

will have no effect on the thermodynamics of the chemical reaction, shown by an equal Gibbs free energy (ΔG) in both the catalysed and uncatalysed pathways.

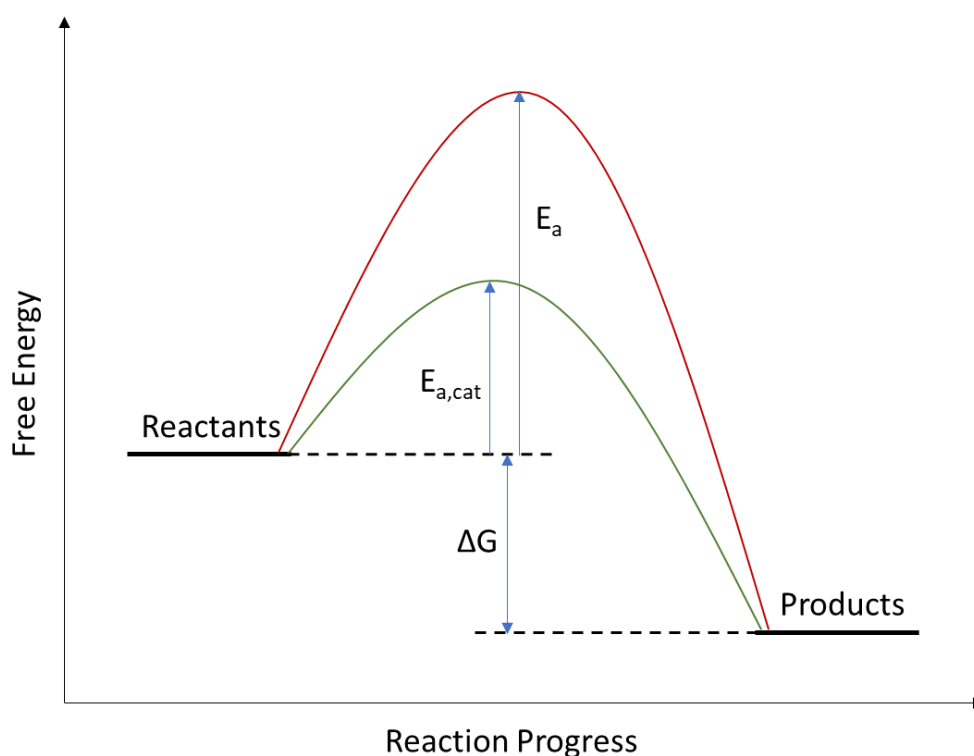
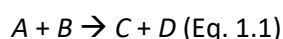


Figure 1.1. An energy level diagram showing the lower activation energy barrier for a catalysed ($E_{a,cat}$) versus uncatalysed (E_a) reaction, where ΔG is the Gibbs free energy.

The kinetics of a reaction can be better appreciated using equation 1.1.



In this instance, the reactants A and B form products C and D . The rate of this reaction (r) can be expressed as shown in equation 1.2.

$$r = k [A]^m [B]^n \text{ (Eq. 1.2)}$$

Where $[A]$ and $[B]$ represent the concentrations of reactants A and B , respectively. m and n are exponential factors representing the orders of reaction of $[A]$ and $[B]$. k is the kinetic constant, given by equation 1.3.

$$k = A e^{-\frac{E_a}{RT}} \text{ (Eq. 1.3)}$$

Where A is the pre-exponential factor, E_a is the activation energy (J mol^{-1}), R is the gas constant ($\text{J mol}^{-1} \text{K}^{-1}$) and T is the temperature (K). Therefore, by decreasing the activation energy of the reaction (via the use of a catalyst), the kinetic constant will be increased, thereby increasing the rate of reaction. Another factor that can increase the rate of reaction is temperature; as temperature is increased the kinetic constant increases and therefore the rate too. Without a

catalyst present, temperature is one of the few factors which may be used to increase the rate of a reaction. Clearly the use of a catalyst therefore decreases the external energy input necessary for a reaction, resulting in a more efficient process. This is one of the key facets of green chemistry; the environmental impact of chemical reactions and how formation of pollution and use of non-renewable resources should be minimised. The 12 principles of green chemistry are summarised in the list below.^{8,9}

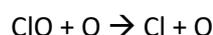
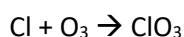
1. Waste prevention is preferable to treating or cleaning waste.
2. Methods should aim to ensure that as much starting material as possible is incorporated into the final product in order to minimise waste production.
3. The use of or generation of materials toxic to the environment and/or humans should be avoided.
4. The product chemicals formed should be minimally toxic whilst still functional.
5. The use of auxiliary substances should be avoided, or non-toxic if essential.
6. Energy requirements of the reaction should be minimised. Those performed using ambient temperature and pressure are desirable.
7. The use of renewable or raw materials is always preferable to non-renewable sources.
8. The use of derivatives should be avoided to minimise the use of extra reagents or the generation of more waste materials.
9. Catalysts (which are reusable) should be used where possible in place of stoichiometric reagents (which are consumed during the reaction).
10. The products formed from the reaction should be environmentally friendly and, where possible, biodegradable.
11. Analytical methods should be developed in order to perform real-time analysis of the reaction. This will help to monitor and thus prevent formation of hazardous substances.
12. General safety should be considered when choosing the substances needed for a process; these should minimise the risk of hazards such as explosions, fires or releases into the environment.

As the impact of chemical processes results in ever more visible effects to our planet, it is more important than ever to focus on green chemistry and, as is discussed in this work, the use of catalysts to improve reaction efficiencies and minimise the production of waste materials.

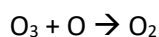
1.2. Heterogeneous catalysts

Catalysis was first indirectly noted in biological catalysts aka enzymes, the name coined by Kühne

in 1877 to describe cellular fermentation¹⁰ to form alcohol from sugar. This term was later adapted to only include rate enhancement by non-living substances. Enzymes are considered to be the example by which all metallic catalysts should be compared to in terms of activity. However, the cost for such high activity is typically low reaction condition tolerances, as slight changes in temperature or pressure can often result in a rapid reduction in performance or deactivation. Non-biological catalysts can be split into two forms, homogeneous and heterogeneous. Homogeneous catalysts are in the same phase as the reactants. An example of this is the decomposition of ozone to form oxygen, using chlorine as the homogeneous catalyst.



Overall reaction:



The use of homogeneous catalysts can result in difficulties separating the catalyst from the reactants and products post-reaction, as well as often suffering from short catalyst lifetimes, thermal instability and general fragility.¹¹ Heterogeneous catalysts are in a different phase to the reactants. Industrial processes typically favour the use of heterogeneous catalysts; indeed 85 – 90 % of industrial reactions rely on the use of heterogeneous catalysts.¹² However, these catalysts are not without problems as high reaction temperatures can lead to over consumption of reactants and low selectivities, which again may cause concern for their environmental impact.¹¹ Generally speaking, these issues are offset by the benefits of heterogeneous catalysts, such as their durability, ease of practical handling and separation of the catalyst post-reaction. Typically, reactions involving heterogeneous catalysts occur on the surface of the catalyst, where nanoparticles have been deposited on bulk materials. The use of nanoparticles or, smaller still, atoms of metals finely dispersed on supports, helps to mitigate the cost of catalysts in industry. Using bulk metals would not only be prohibitively expensive but would also often result in a poorer catalytic activity.

The size of the supported metal has a significant impact on the catalytic activity.¹³ Although different metals and metal sizes are chosen dependent on the reaction, there are several factors which hold true in all cases. Visually, the catalysts will change in colour as the size of supported metal is decreased from nanoparticle to cluster to single atoms. This will affect the photocatalysis as the plasmon of the catalyst is altered.¹⁴ Single atom catalysts are more likely to be geometrically stable than metal clusters, for example, as clusters have a greater number of configurations available to them. They are therefore more likely to be affected by factors such

as the support, reactants, reaction conditions and cluster charge.¹⁵ Increasing the size of clusters to metal nanoparticles results in greater stability for the overall particle, however the exposed surface atoms at the corners, edges and metal-support interfaces may change under reaction conditions.^{16,17} The electronic structures of the systems are also affected by their size (Figure 1.2). In single atoms the electronic structure is highly dependent on the surrounding ligands and solvent.¹⁷ Metal clusters have more complex electronic interactions as multiple metal atoms result in more orbital overlaps. The electronic interactions become cluster size dependent,¹⁸ especially significant as the cluster changes from planar to 3D geometry as a result of a greater number of atoms, resulting in less efficient orbital overlaps.¹⁹ Increasing the size to nanoparticles results in a much smaller band gap between HOMO and LUMO, which forms a continuous energy level in particles larger than 2 nm.²⁰

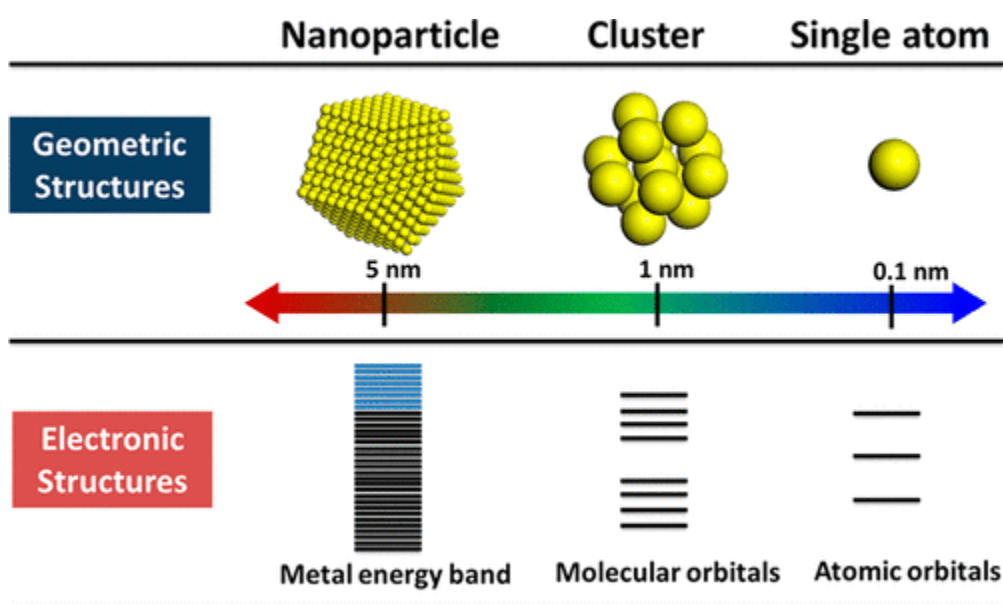


Figure 1.2. Nanoparticle, cluster and single atom geometric and electronic structures.

1.3. Catalysis by gold

Bulk gold has been known as an inert material for centuries, hence its most common application in jewellery and coinage.^{21–23} This is due to the full 5d-orbital prohibiting interaction with elements such as hydrogen and oxygen,^{24,25} and the contracted, stabilised 6s shell.^{26,27} Only within the past 40 years was it discovered that, upon reducing the size of gold materials to nanoparticles, the metal becomes highly active, with huge implications for catalytic applications.²⁸ The breakthrough discovery for catalytically active gold was discovered due to work performed by Haruta *et al.* on the CO oxidation reaction.²⁹ This was closely followed by

Hutchings and his work on the acetylene hydrochlorination reaction,³⁰ discussed in greater depth in section **1.5.2.2**.

Decreasing the size of gold from bulk to nanometer scale results in a greater coverage of metal on the surface of the catalyst support, which causes a greater mobility of gold atoms. As the number of individual surface gold atoms increases, the number of individual reaction sites increases and the surface area of gold in contact with the support increases, introducing more reaction possibilities. These all explain the high reactivity of gold nanoparticles for the CO oxidation reaction.²⁹ The optimum size of gold nanoparticles for the CO oxidation is still under debate, although generally it has been shown that a range of 0.5 – 5.0 nm results in active catalysts,^{31–33} whilst decreasing the size to atomically supported gold has had mixed results,^{34,35} complicated by such factors as the nature of the support, the gold-support interaction, and gold valence state.³⁵

Supported gold atoms can, however, be very active for other reactions such as methanol steam reforming,³⁶ ethanol dehydrogenation reactions³⁷ and the water-gas-shift reaction,^{38,39} with more being discovered due to advances in spectroscopy techniques such as scanning transmission electron microscopy.^{40,41}

1.4. Activated carbon – catalyst and support

In catalysis, the nature of the support can directly influence the catalytic activity, for example as observed in gold catalysts for the CO oxidation reaction; the support may influence the activation of reactant species, as observed with the activation of O₂,⁴² participate in redox processes, by supplying oxygen from the surface lattice,⁴³ or work in synergy with the supported metal to form the product, such as the Au-Ti interface of Au/TiO₂ forming CO-O₂ complexes,⁴⁴ or the electron transfer between Au and ZnO to facilitate the oxidation of CO.⁴⁵

The support used in this work was activated carbon. Carbon has been used for several applications in catalysis; as a catalyst itself,⁴⁶ for the production of phosgene⁴⁷ and sulfur halides,⁴⁸ or the catalytic removal of SO₂/NO_x from flue gases;^{49,50} or as a catalyst support, well documented in several industrial and fine chemical roles.⁵¹

Activated carbon can be easily recovered from precious metal catalysts via combustion, making it a very useful support for catalytic reactions performed on an industrial scale.⁵² The stability of the support in acidic and basic media^{52,53} is an advantage over the use of supports such as alumina and silica, which are dissolved at high pHs and the former also in low pHs.^{54,55} This makes carbon especially suitable for use in the acetylene hydrochlorination reaction (section **1.5.2**), where the reactant, pure HCl, is present in excess. Carbon will naturally reduce metals such as

gold during the catalyst preparation, as noted when using deposition-precipitation for Au/C catalysts.⁵⁶

As there are such a large variety of carbon sources available, variation between batches of carbon materials is common resulting in differences in surface structure and chemical group distribution. Impurities such as calcium, potassium and iron are also a common feature of carbons, caused by various washing treatments.⁵³ This may affect the distribution of the supported metal, directly influencing the catalytic performance. It is this variation that can make it difficult to determine the useful components of the support.

Activated carbon is derived from a graphitic structure, typically comprised of a much higher surface area than graphite and a large variation in pore structures. The addition of heteroatoms to the carbon results in different functionalities, dependant on the concentration and species added. Nitrogen groups may be added by the reaction of a nitrogen containing compound, such as ammonia,⁵⁷ or via the use of nitrogen-containing precursors.⁵⁸ Oxygen functionality can be readily introduced via exposure of carbon to the atmosphere.⁵⁹ Further oxidation is made possible by other methods such as the Hummers' oxidation, covered in greater detail in **5.1**.

The amount of oxygen present also relates to the pH of the carbon in aqueous dispersion; generally more oxygen results in a more acidic dispersion,⁶⁰ resulting in more cationic exchange properties, whilst carbons with a lower oxygen content have a more basic dispersion and anionic exchange behaviour.⁶¹ Species such as carboxylic acids, anhydrides, lactones/lactols and phenols are acidic, whilst carbonyl and ether oxygen may form quinone, chromene and pyrone basic groups. The majority of oxygen groups present are removed from the surface upon heating the carbon to 1000 °C under an inert atmosphere or vacuum. Examples of nitrogen and oxygen groups introduced to the carbon are shown in Figure 1.3.

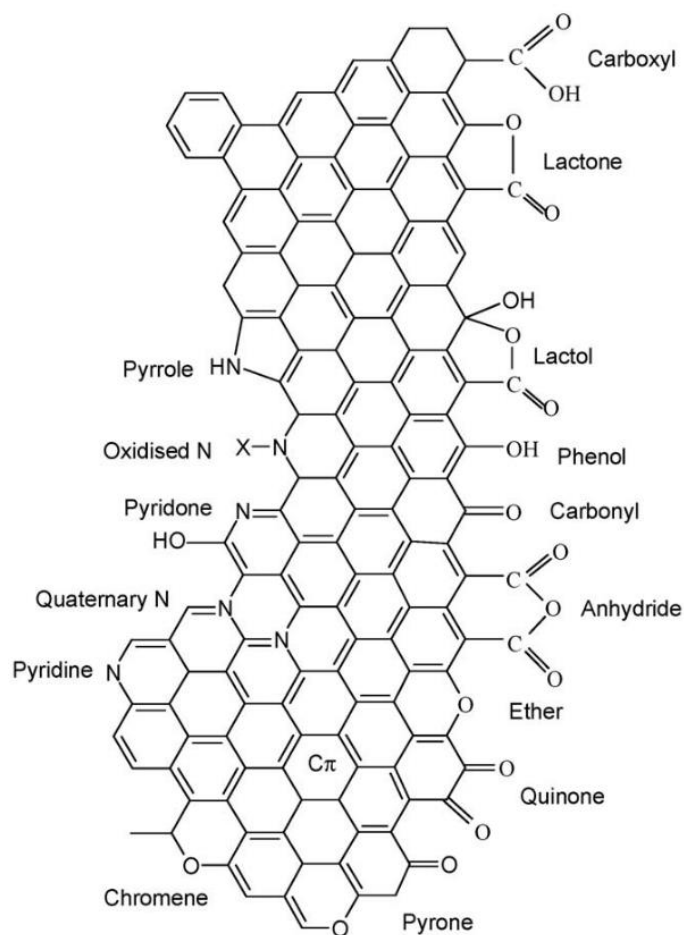


Figure 1.3. Nitrogen and oxygen containing surface groups on carbon. Reproduced from figure 1.⁵⁹

The methods for determining the amount of oxygen on the surface of the carbon began with Boehm's⁶² acid and base titrations for basic and acidic sites respectively. Limitations of this method⁶³ resulted in further development of the following techniques.

- Fourier-transform infra-red (FTIR) in conjunction with diffuse reflectance (DRIFTS),⁶⁴ measuring vibrational absorption bands of C=O groups or C=C and C-O bonds for example.
- X-ray photoelectron spectroscopy (XPS), measuring the binding energy of electrons excited from surface groups, determined by analysing the C 1s or O 1s energies.⁶⁵ The main oxygen-containing groups observable in the C 1s spectrum of an oxidised carbon fibre are shown in Figure 1.4 and in the O 1s spectrum in Figure 1.5.
- Temperature Programmed Desorption (TPD), deconvoluting the thermal desorption peaks of CO and CO₂ evolved from oxygen containing groups.⁶⁶ The temperatures at which the main oxygen functionalities desorb are shown in Figure 1.6.

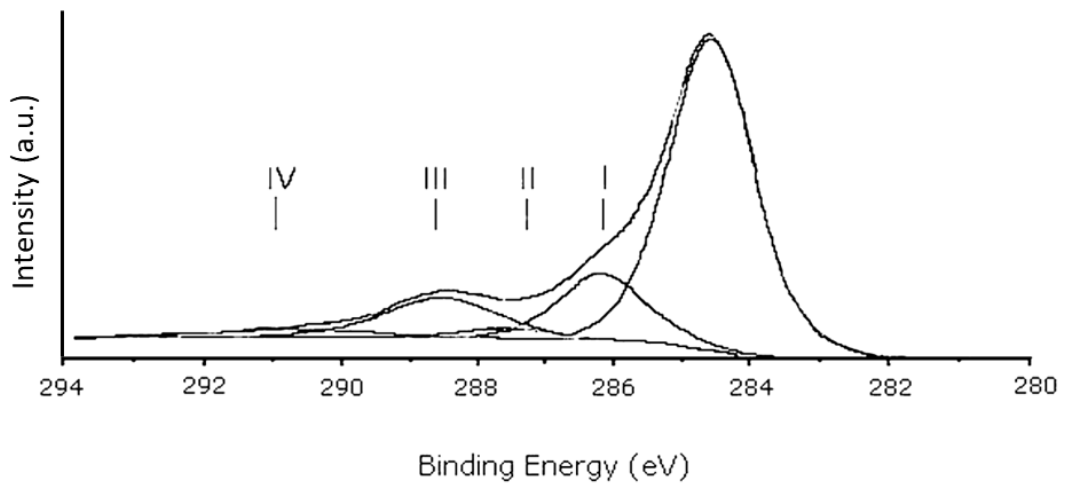


Figure 1.4. Typical C 1s XPS spectrum of oxidised carbon fibres: (I) phenols, (II) carbonyl groups, (III) carboxyl groups, (IV) plasmon peak. Peak at 284.8 due to sp^3 carbon. Black solid line indicates raw data, grey dotted line indicates raw data fit, inner grey lines indicate fitting of functional groups. Reproduced from figure 4.⁶³

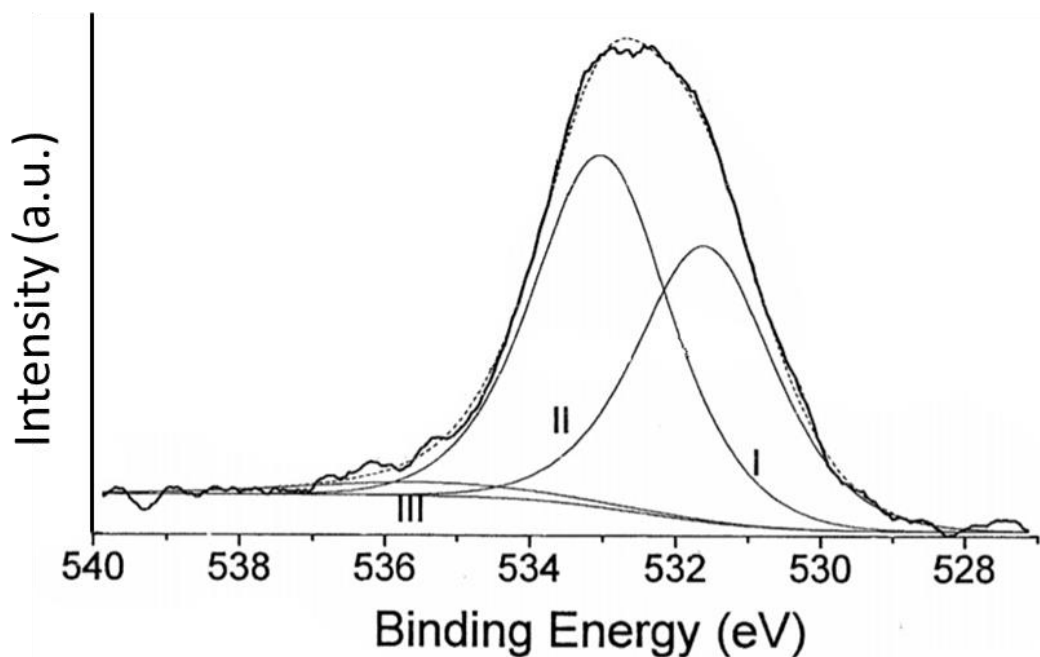


Figure 1.5. Typical O 1s XPS spectrum of oxidised carbon fibres: (I) carbonyl groups, (II) alcohol/ether groups, (III) chemisorbed oxygen/adsorbed water groups. Black solid line indicates raw data, grey dotted line indicates raw data fit, inner grey lines indicate fitting of functional groups. Reproduced from figure 4.⁶⁷

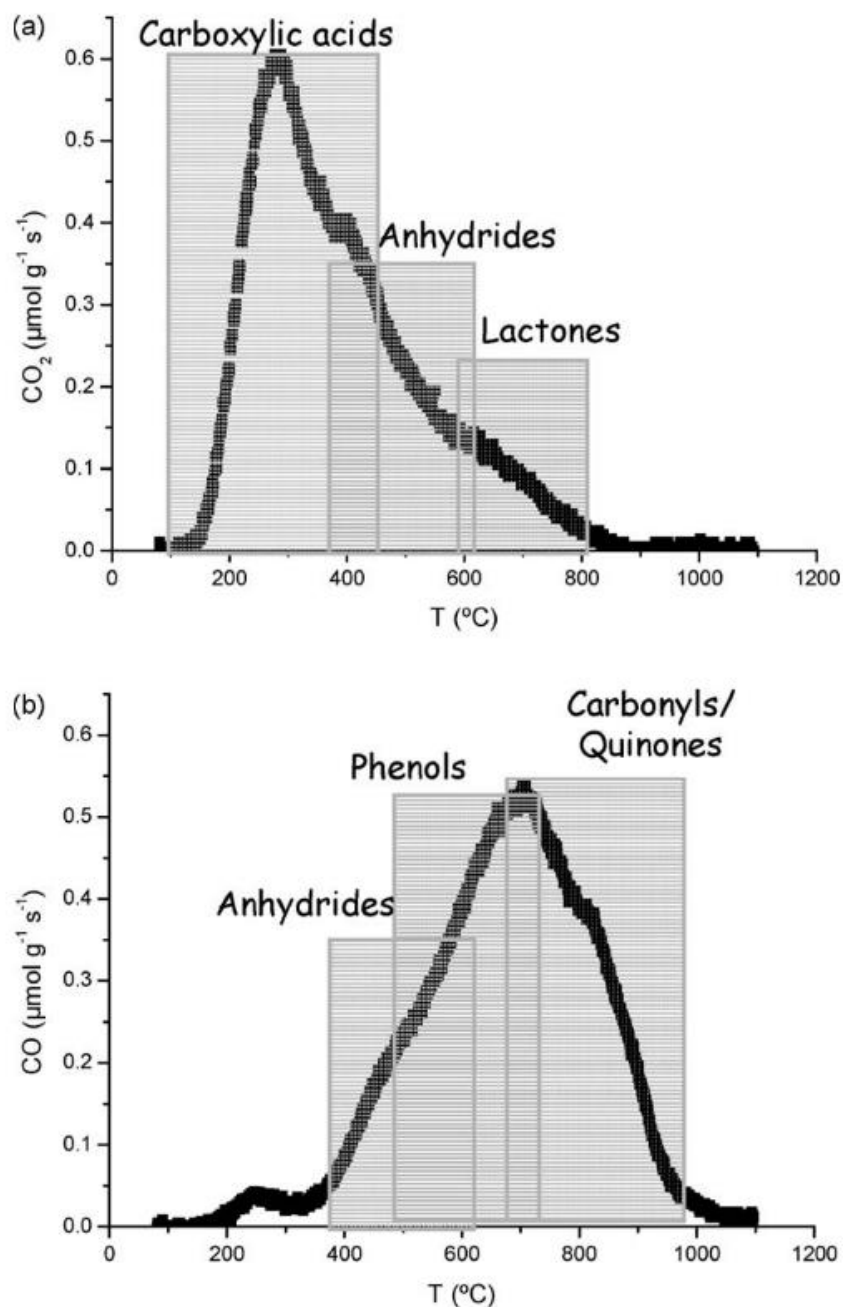


Figure 1.6. Temperature ranges of functional groups desorbed from carbon, from the evolution of (a) CO_2 and (b) CO . Reproduced from figure 2.⁵⁹

It is important to use an appropriate characterisation technique depending on the carbon in question as each has their limitations. Using DRIFTS, functional groups may produce multiple bands that may overlap, making deconvolution of the different groups difficult.⁶⁴ XPS fittings must be performed using fittings dependent on the nature of the carbon, be it more graphitic or aliphatic.⁶⁶ XPS can also lead to an over-estimation of the total oxygen content in microporous carbons, whereas both TPD and XPS perform similarly with mesoporous materials.^{66,68} A combination of the above techniques is most useful to form an accurate qualitative and

quantitative description of the oxygen functionality.⁶⁹

Activated carbon was chosen as the support in this work due to:

- A high stability under harsh acidic conditions and reaction temperature
- A large surface area, to facilitate dispersion of atomic gold species
- A low impact on catalytic selectivity
- Adaptable surface chemistry, to introduce different functionality which may affect catalytic activity
- Suitability for scale-up and industrial application.

1.5. VCM production methods

Over 30 million tonnes of the vinyl chloride monomer (chloroethene, VCM) is produced annually,⁷⁰ the majority of which goes onto be used in the formation of polyvinyl chloride ((C₂H₃Cl)_n, PVC) typically via suspension polymerisation,⁷¹ although emulsion and bulk polymerisation are also viable methods.⁷² PVC is the third most commonly used polymer in the world⁷³ owing to its versatility; it can form soft, flexible materials such as electrical cable insulation and clothing or strong rigid materials, useful for engineering applications such as piping and furniture trimmings.⁷⁴

There are several methods for the production of VCM; however, there are two predominant methods favoured by USA and China; the balanced process and acetylene hydrochlorination, respectively, shown in Figure 1.7.

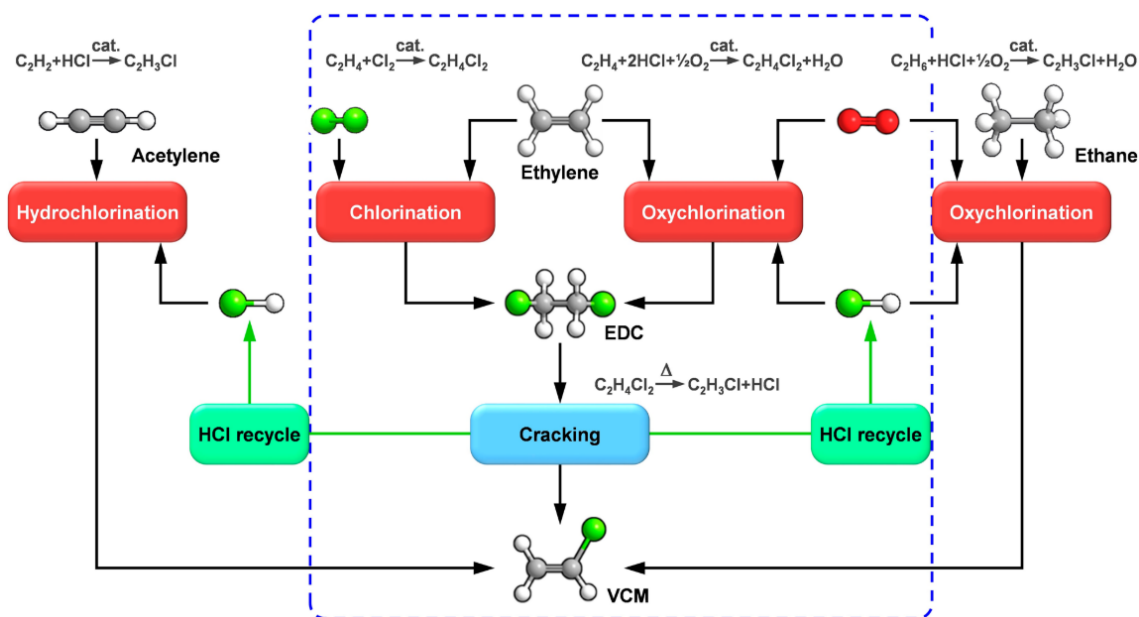


Figure 1.7. Schematic of the various routes available for the production of VCM. Balanced process represented in dashed box. Reproduced from figure 6.⁷⁵

1.5.1. The balanced process

The balanced process involves multiple reaction steps. First ethylene is chlorinated to form ethylene dichloride (EDC) catalysed by $FeCl_3$. Second, EDC is thermally cracked to form VCM. A third step occurs in parallel with these two reactions, the oxychlorination of ethylene, in which ethylene reacts with HCl and O_2 catalysed by $CuCl_2$, consuming the HCl produced during the cracking of EDC.

As shown in Figure 1.8, multiple extra reactions can occur during the oxychlorination of ethylene. EDC can undergo substitution, elimination and addition, forming unwanted chlorinated carbon materials, or undergo over-oxidation to form CO and CO_2 .⁷⁶ This shows the necessity for highly selective catalysts when the balanced process is utilised. Current research is looking into the use of ethane to replace ethylene, thereby forming VCM directly from the oxychlorination of ethane, removing the need for the cracking of EDC step.⁷⁷

This process is particularly favoured in the US due to the availability of oil,⁷⁸ used to produce ethylene, and the reduced safety implications when not handling concentrated acetylene on an industrial scale.^{79,80}

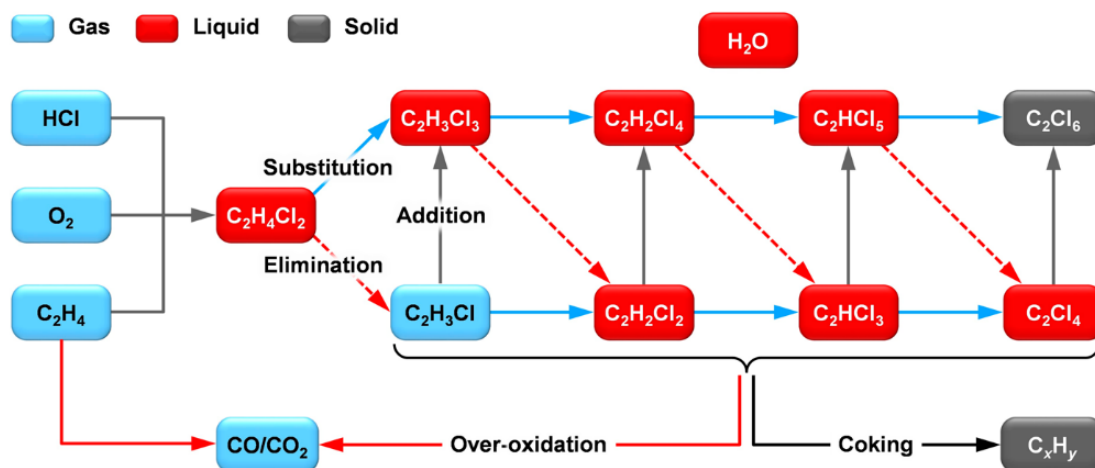


Figure 1.8. The multiple reaction pathways available during ethylene oxychlorination to produce ethylene dichloride. Reproduced from figure 10.⁷⁵

1.5.2. The acetylene hydrochlorination reaction

China uses coal for acetylene production;^{76,81} the coal is cracked with lime to form calcium carbide, which in turn is used to produce acetylene for the hydrochlorination reaction. This accounts for over 95 % of Chinese produced PVC.⁸² This method helps to reduce the cost of PVC production, due to large coal reserves available in China. In contrast to the balanced process, the acetylene hydrochlorination reaction involves just one step, the reaction of acetylene and hydrogen chloride (Figure 1.9). This method utilises 100 % of the reactants and typically results in high product selectivity. The acetylene hydrochlorination reaction is typically performed with a mercuric or gold chloride-based catalyst.

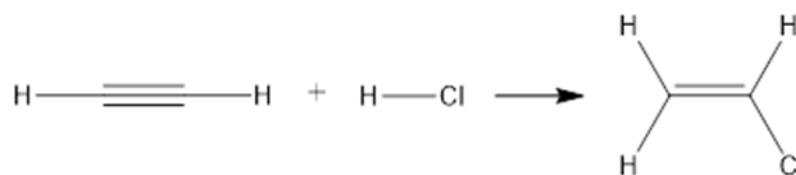


Figure 1.9. Reaction of acetylene with hydrogen chloride to produce the vinyl chloride monomer.

1.5.2.1. Mercury-based catalysts

In 1985, Hutchings determined that there was a correlation between the standard electrode potential of metals and their catalytic activity for the acetylene hydrochlorination reaction, when supported on carbon (Figure 1.10).⁸³ Hg was second only to Pd for VCM production, the latter of which suffers from rapid deactivation due to coke formation,⁸⁴ hence mercury's

abundant use in industry.

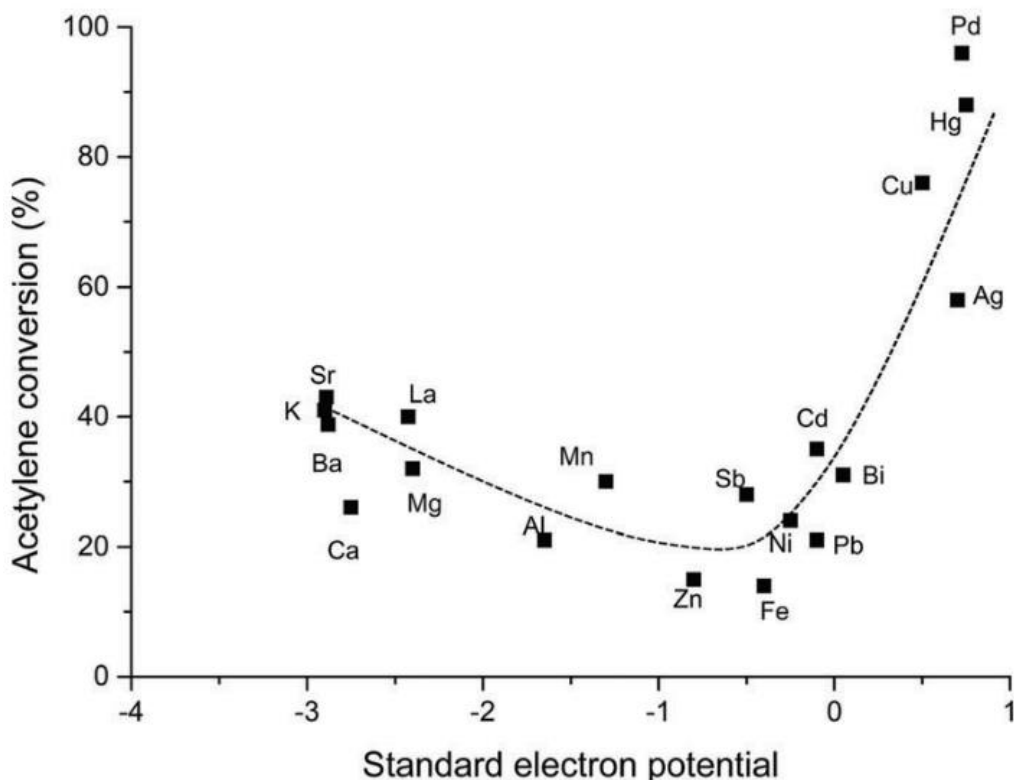


Figure 1.10. Standard electron potential versus acetylene conversion for metal chloride catalysts supported on carbon. Reproduced from figure 2.⁸⁵

Even before this trend was observed, Hg had been used for this reaction since its discovery in 1912 by Fritz Klatté,⁸⁶ typically with a 10 wt. % loading.⁸¹ However, there were two main issues surrounding the use of this metal for this reaction. Firstly, the high metal loading was undesirable due to cost, especially as the HgCl_2 would sublime at the typical reaction temperature of 180 °C, thereby leaving an inactive carbon support.⁸⁷ This resulted in limited catalyst lifetimes, little over a hundred days,⁸⁸ which directly correlated with metal loading.⁸⁹ The volatile HgCl_2 and reduced Hg would typically be found downstream of the reactor or worse, find their way into the environment. This leads to the second main issue, health. The implications of increased levels of mercury being released into the environment were discussed in detail at the Minamata Convention on Mercury in the three years leading to 2013.⁹⁰ Mercury is toxic to humans and other species, therefore release of significant quantities into the environment, especially during the VCM reaction, should be avoided at all costs. The convention took its name from the Japanese city Minamata which suffered heavily from mercury poisoning due to mercury-containing industrial wastewater. The agreement, signed by nearly 140 countries, stipulated that the use of mercury in numerous products will be prohibited by 2020.

For mercury-based catalysts, specifically for the VCM reaction, the production of new plants utilising this catalyst was banned from 2017 and all plants currently using the catalyst must be mercury-free by 2022. This has led to a flurry of new research on the use of alternative metals for the VCM reaction.⁹¹⁻⁹³

1.5.2.2. Gold-based catalysts

The most significant contribution to this field was the discovery by Hutchings that gold could catalyse the production of VCM. This breakthrough came from replotting the previous work on acetylene hydrochlorination catalysts,⁸³ using two-electron, metal chloride reduction potentials instead of metal potentials (Figure 1.11).

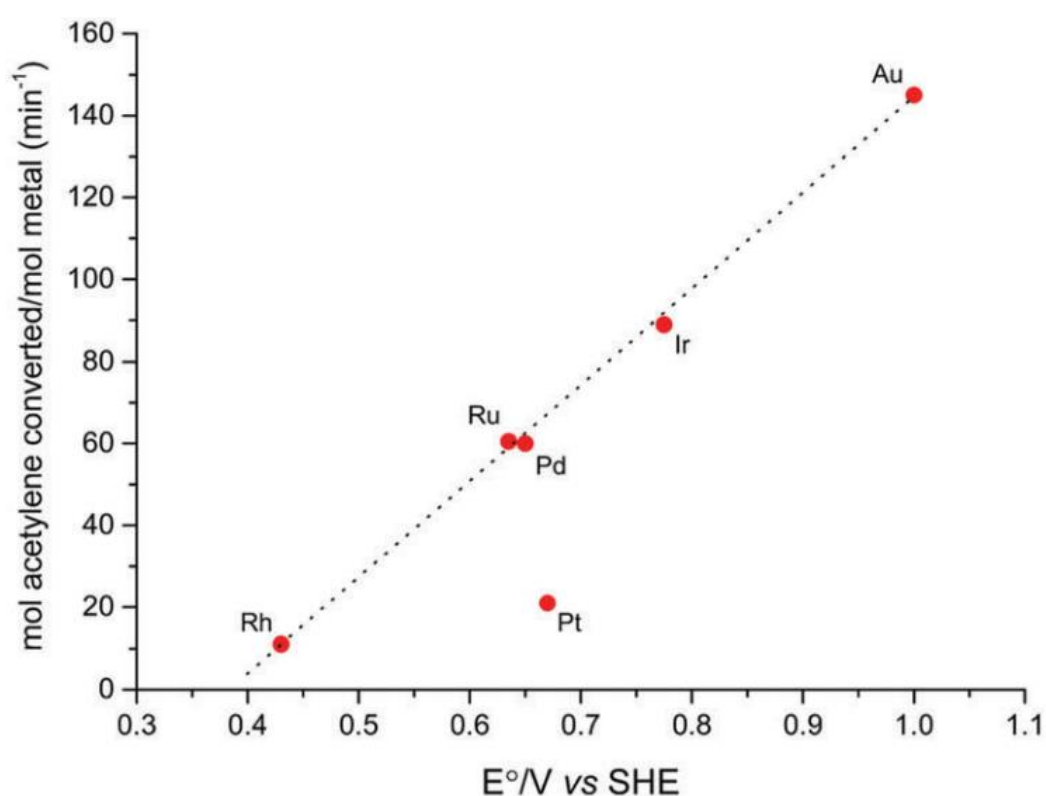


Figure 1.11. Plot of standard electrode potential versus acetylene conversion per mol of metal. Reproduced from figure 2.⁹⁴

Not only was the catalyst more active compared to Hg by an order of magnitude,⁹⁵ but gold did not suffer from metal sublimation as was observed in the mercury catalyst. Particle growth and sintering of Au were considered negligible during the reaction.^{96,97} Unlike the mercury catalyst, the gold catalyst could be reactivated. This could be achieved during or post-reaction by flowing Cl_2 , NO or N_2O , or by boiling in aqua regia^{98,99} to oxidise any reduced gold, rendering it active

again.¹⁰⁰

The active species of the gold catalyst during the acetylene hydrochlorination reaction has been narrowed down from suggestions of a mixture of gold cations and nanoparticles^{97,100} to solely single site atomic Au(I) and Au(III), found using in-situ x-ray absorption fine structure (XAFS) spectroscopy.⁴⁰ This is due to the development of methods such as traditional transmission electron microscopy (TEM), which would not be able to resolve sub-nanometer structures to recently more sophisticated techniques such as aberration-corrected annular dark field scanning transmission electron microscopy (ac-ADF/STEM)^{101–103}, used to view angstrom level resolution for sub-nanometer clusters and atoms. XAFS was also used to detect individual cationic species (such as Au³⁺)^{104,105} and monitor in-situ changes to the catalyst. Using this technique, it was determined that oxidised gold readily switches from Au(I) to Au(III) and back during the reaction, and that Au(I) is the more active of the two species. This was proven by correlating the proportion of Au(I/III) during the reaction with VCM production, shown in Figure 1.12. Here the white line height (normalised absorption energy) is proportional to the Au oxidation state, where a white line height equal to 1.1 is obtained with an entirely Au(III) reference and 0.6 with a Au(I) reference; hence values between 1.1 and 0.6 indicate a mixture of Au(III/I) states, respectively.

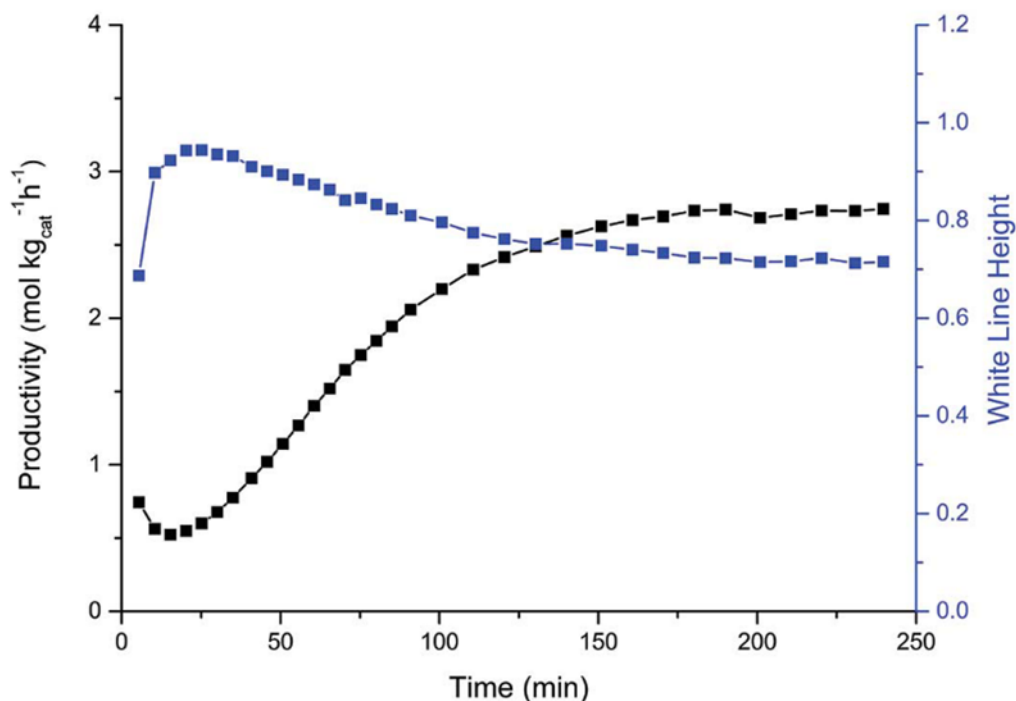


Figure 1.12. White line height and VCM productivity of 1 wt. % Au/C catalyst over time, during the acetylene hydrochlorination reaction. Reproduced from figure 2.⁴⁰

The use of different solvents¹⁰⁶ and ligands^{107,108} has a direct effect on the activity of the gold

catalysts due to their ability to stabilise the Au(I) species. This has led to highly active gold catalyst with metal loadings as low as 0.1 %.^{109,110} From this, the main cause of gold catalyst deactivation is clearly reduction of Au(I) and Au(III) to form Au(0).¹¹¹ In fact, the formation of gold nanoparticles under reaction conditions facilitates further sintering, resulting in a lower dispersion of oxidised gold and hence poor catalytic activity; however, it is also possible to observe formation of oligomers of acetylene if the concentration of acetylene is high with respect to HCl, which can preclude carbon fibre formation.^{109,112} This is one of the reasons why an excess of HCl is always used during the reaction.

1.5.2.3. Reaction kinetics of Au/C catalyst

Literature has speculated numerous mechanisms for the acetylene hydrochlorination reaction with a Au/C catalyst; some suggesting it follows a homogeneous-like pathway as observed in K_2PtCl_6 salts¹¹³, whilst other work suggests this is unlikely owing to the need for an intermediate pathway which involves the co-adsorption of HCl and C_2H_2 , resulting in a weak six-membered-ring interaction.¹¹⁴ Literature also has not conclusively determined whether the reactants are co-adsorbed⁹⁶, or if HCl is added first followed by the addition of C_2H_2 . It is clear that C_2H_2 cannot be added first or separately as this results in the formation of a stable metal complex which facilitates the polymerisation of C_2H_2 , resulting in the deactivation of the catalyst.^{109,114,115} This can be avoided using an excess of HCl and choosing a suitable reaction temperature.¹¹⁵ It has been suggested that the reaction is first order with respect to both reactants⁹⁶ and significantly in all of these articles it is noted that an oxidised gold redox is necessary for the reaction to occur. Upon partial reduction to Au^0 the catalyst will not be as active as the oxidised Au(I)/Au(III) species.

To explore the kinetics of the reaction, a 1 % Au/C catalyst prepared with aqua regia was tested at low gas concentrations to measure the effect of acetylene and hydrogen chloride, separately, on acetylene conversion.

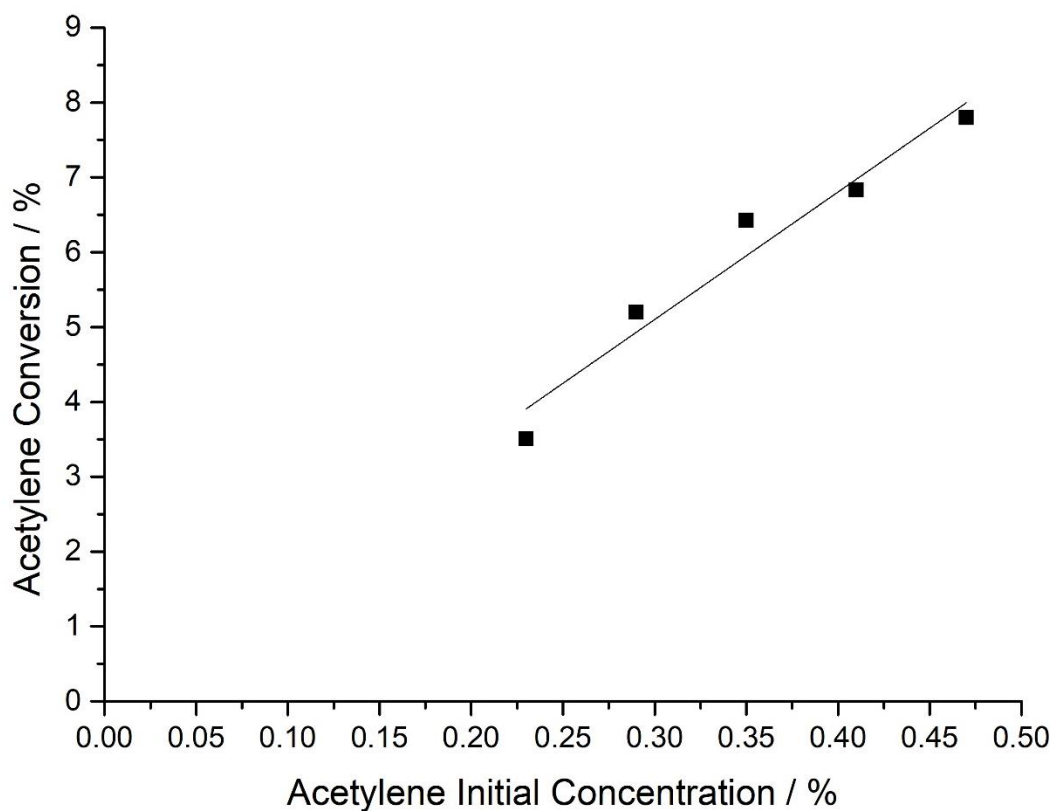
In order to observe the reaction profile at rates suitable for reaction kinetics to be observed, a number of conditions were used, as follows;

1. Low reactant gas concentrations were used to maintain low conversion of acetylene at 200 °C, thus ensuring the reaction was at a viable rate of reaction for kinetic studies. This also ensured that if adsorption of the reactant gases to the catalyst surface occurred during the reaction, the catalyst surface would not become saturated with reactants, which would lead to a zero order of reaction with respect to either of the reactants.
2. To remove the variable of changing gold oxidation state from the experiments, the

reaction was first allowed to proceed until steady state conversion was maintained. It was assumed from this point on in the reaction that the gold oxidation state was optimised and stable. The concentrations of gases were then altered to determine the order of reaction.

3. A high total gas flow and half the mass (0.045 g) of catalyst used in reactions ensured a low acetylene conversion. Therefore, it could be assumed that the reaction remained unaffected by concentration gradients through the catalyst bed.

In both experiments, the concentration of HCl was kept in excess to inhibit the reduction of Au(I/III) by acetylene. The results of this investigation are shown in



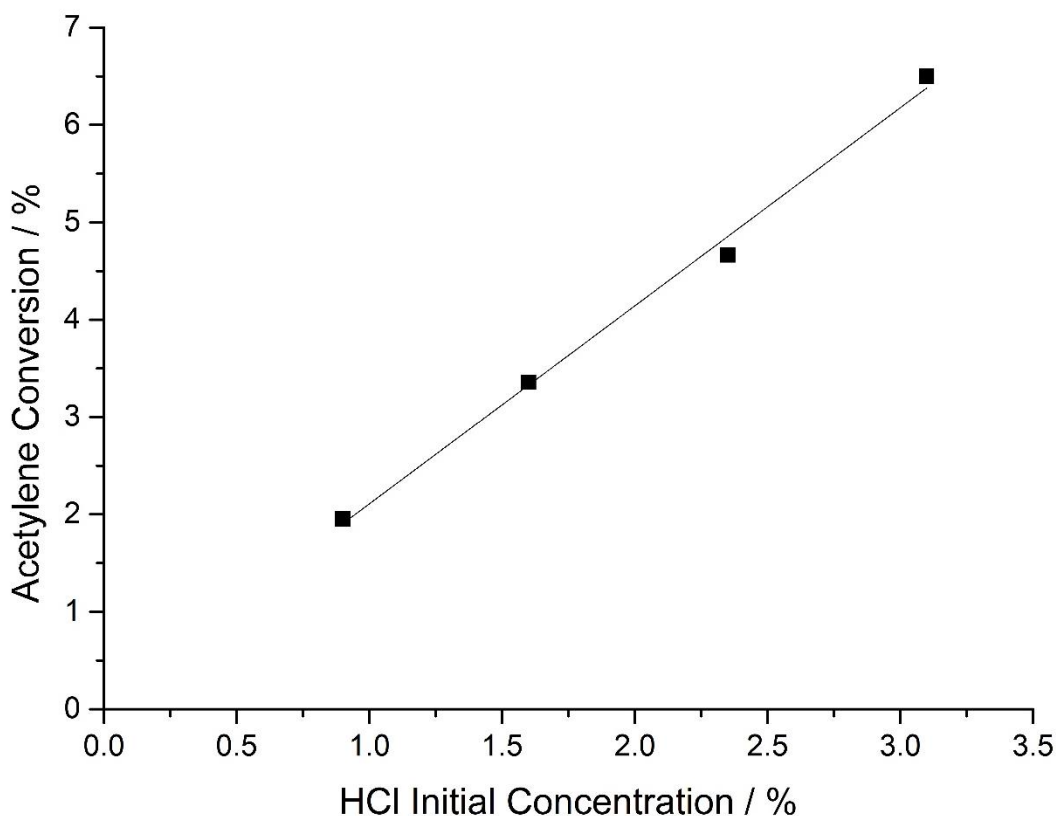


Figure 1.13. Determination of orders of reaction with respect to (top) C_2H_2 and (bottom) HCl concentration. A linear dependence was found in both. Reaction conditions: Catalyst (0.045 g), 200 °C, ambient pressure, various concentrations of gases (HCl in excess) balanced with Ar at fixed flow of 50 mL min^{-1} .

These show that the reaction is first order with respect to acetylene and first order with respect to hydrogen chloride. Therefore, the overall reaction kinetics is second order. These results concur with XAFS studies performed in this group, in which a concerted addition of acetylene and hydrogen chloride to Au(I)-Cl is observed to be the first step of the reaction mechanism.¹¹¹ This also explains the lack of observed 1,1-dichloroethene, which would result from the addition of more than one dissociated HCl molecule per C_2H_2 molecule; even in an excess of HCl this product was not observed, nor in any of the experiments carried out in this work.⁹⁶ It can be assumed that from this point in the reaction the Au(I)/Au(III) redox cycle continues with the reductive elimination of the vinyl chloride monomer, regenerating the more Au(I)-like state to re-start the catalytic cycle.^{40,111}

In summary, of the two main processes for the production of PVC precursor VCM, the hydrochlorination of acetylene is still in high demand, especially in areas such as China. However, the use of high metal loading, low stability mercury-based catalysts must be phased out due to their high toxicity and resultant environmental impact. The most suitable alternative catalyst is that of the low metal loading, more active and stable gold-based catalyst, supported

on robust activated carbon.

1.6. Project aims

The aims of this work were to:

- Remove the need for the harsh, highly acidic solvent aqua regia in order to make the catalyst preparation more environmentally benign whilst maintaining a high dispersion for atomically dispersed Au(I) and Au(III) species.
- Introduce surface functionality to the carbon support, with an aim towards increasing the conversion of acetylene for the production of VCM.

1.7. Project Overview

Chapter 3 focuses on the use of alternative solvents for the preparation of gold on carbon catalysts. The primary aim of this work was to negate the necessity for high boiling point, high polarity, acidic solvents, which are detrimental to catalyst stability and impractical for industrial scale-up. Evidence for the activity and increased stability of these catalysts was explored.

Chapter 4 investigates the effect of acid treatment on the gold on carbon catalyst, both before and after preparation. The role of different acids and their concentration is discussed with respect to the initial acetylene conversion and overall stability of the catalysts under reaction conditions.

Chapter 5 provides an insight into different oxidation methods that can be performed on the carbon support. The effects of different oxidants and the amount of oxidant used were explored. A brief discussion on the effect of combining alternate solvents and oxidation is also included.

1.8. References

- 1 S. Califano, in *Pathways to modern chemical physics*, Springer, New York, 2012, pp. 40–51.
- 2 A. J. B. Robertson, *Platin. Met. Rev.*, 1975, **19**, 42–77.
- 3 H. Davy, *Philos. Trans. R. Soc.*, 1817, **107**, 77–85.
- 4 E. Davy, *Philos. Trans. R. Soc.*, 1820, **110**, 108–125.
- 5 B. Lindström and L. J. Pettersson, *CATTECH*, 2003, **7**, 130–138.
- 6 R. L. Burwell, in *Heterogeneous Catalysis - Selected American Histories*, American Chemical Society, Washington D.C., 1983, pp. 3–12.
- 7 W. Ostwald, *Zeitschrift für Elektrotechnik und Elektrochemie*, 2008, **7**, 995–1003.
- 8 G. Rothenberg, in *Catalysis*, Wiley-VCH Verlag GmbH & Co. KGaA, Weinheim, Germany, 2008, pp. 1–38.
- 9 R. A. Sheldon, I. W. C. E. Arends and U. Hanefeld, in *Green Chemistry and Catalysis*, Wiley-VCH, Weinheim, 2007, pp. 1–2.
- 10 W. Kühne, in *Erhandlungen des naturhistorisch-medizinischen vereins zu heidelberg*,

- Neue Folge, Heidelberg, 1877, pp. 194–198.
- 11 J. D. A. Pelletier and J.-M. M. Basset, *Acc. Chem. Res.*, 2016, **49**, 664–677.
- 12 I. Chorkendorff and J. W. Niemantsverdriet, *Concepts of Modern Catalysis and Kinetics*, Wiley-VCH, Weinheim, 3rd edn., 2003.
- 13 L. Liu and A. Corma, *Chem. Rev.*, 2018, **118**, 4981–5079.
- 14 K. L. Kelly, E. Coronado, L. L. Zhao and G. C. Schatz, *J. Phys. Chem. B*, 2003, **107**, 668–677.
- 15 E. M. Fernández, J. M. Soler, I. L. Garzón and L. C. Balbás, *Int. J. Quantum Chem.*, 2005, **101**, 740–745.
- 16 S. Schauer mann, J. Hoffmann, V. Johánek, J. Hartmann, J. Libuda and H.-J. Freund, *Angew. Chemie Int. Ed.*, 2002, **41**, 2532–2535.
- 17 T. V. W. Janssens, B. S. Clausen, B. Hvolbæk, H. Falsig, C. H. Christensen, T. Bligaard and J. K. Nørskov, *Top. Catal.*, 2007, **44**, 15–26.
- 18 M. Boronat, A. Leyva-Pérez and A. Corma, *Acc. Chem. Res.*, 2014, **47**, 834–844.
- 19 J. Wang, G. Wang and J. Zhao, *Phys. Rev. B Condens. Matter*, 2002, **66**, 035418.
- 20 D. Buceta, Y. Piñeiro, C. Vázquez-Vázquez, J. Rivas and M. A. López-Quintela, *Catalysts*, 2014, **4**, 356–374.
- 21 B. Hammer and J. K. Nørskov, *Nature*, 1995, **376**, 238–240.
- 22 B. Hammer and J. K. Nørskov, *Surf. Sci.*, 1995, **343**, 211–220.
- 23 T. Inasaki and S. Kobayashi, *Electrochim. Acta*, 2009, **54**, 4893–4897.
- 24 G. C. Bond, *Catal. Today*, 2002, **72**, 5–9.
- 25 R. J. Davis, *Science*, 2003, **301**, 926–927.
- 26 G. C. Bond, *Platin. Met. Rev.*, 2000, **44**, 146–155.
- 27 P. Pyykkö, *Chem. Rev.*, 1988, **88**, 563–594.
- 28 G. J. Hutchings, *Catal. Today*, 2002, **72**, 11–17.
- 29 M. Haruta, N. Yamada, T. Kobayashi and S. Iijima, *J. Catal.*, 1989, **115**, 301–309.
- 30 G. J. Hutchings, *Gold Bull.*, 1996, **29**, 123–130.
- 31 M. Haruta, *Chem. Rec.*, 2003, **3**, 75–87.
- 32 B. Hvolbaek, T. V. W. Janssens, B. S. Clausen, H. Falsig, C. H. Christensen and J. K. Nørskov, *Nano Today*, 2007, **2**, 14–18.
- 33 A. A. Herzing, C. J. Kiely, A. F. Carley, P. Landon and G. J. Hutchings, *Science*, 2008, **321**, 1331–1335.
- 34 A. Sanchez, S. Abbet, U. Heiz, W. D. Schneider, H. Häkkinen, R. N. Barnett and U. Landman, *J. Phys. Chem. A*, 1999, **103**, 9573–9578.
- 35 B. Qiao, J. X. Liang, A. Wang, J. Liu and T. Zhang, *Chinese J. Catal.*, 2016, **37**, 1580–1586.
- 36 X.-K. Gu, B. Qiao, C.-Q. Huang, W.-C. Ding, K. Sun, E. Zhan, T. Zhang, J. Liu and W.-X. Li, *ACS Catal.*, 2014, **4**, 3886–3890.
- 37 C. Wang, G. Garbarino, L. F. Allard, F. Wilson, G. Busca and M. Flytzani-Stephanopoulos, *ACS Catal.*, 2016, **6**, 210–218.
- 38 M. Flytzani-Stephanopoulos, *Acc. Chem. Res.*, 2014, **47**, 783–792.
- 39 J. C. J. Bart, S. Cavallaro, G. Lefebvre, M. Lazarus, A. Kollmuss, J. H. Teles, C. S. Slaten, M. Seapan, M. W. Lower, P. E. Tomlinson, M. Aoki, R. Noyori, O. A. Kholdeeva, S. H. Jhung, J. S. Chang, K. Holmberg, K. Wang and J. Chen, *Science*, 2014, **346**, 1498–1502.
- 40 G. Malta, S. A. Kondrat, S. J. Freakley, C. J. Davies, L. Lu, S. R. Dawson, A. Thetford, E. K. Gibson, D. J. Morgan, W. Jones, P. P. Wells, P. Johnston, C. R. A. Catlow, C. J. Kiely and G. J. Hutchings, *Science*, 2017, **355**, 1399–1403.
- 41 J. (Jimmy) Liu, *ChemCatChem*, 2011, **3**, 934–948.
- 42 M. M. Schubert, S. Hackenberg, A. C. van Veen, M. Muhler, V. Plzak and R. J. Behm, *J. Catal.*, 2001, **197**, 113–122.
- 43 L. Li, A. Wang, B. Qiao, J. Lin, Y. Huang, X. Wang and T. Zhang, *J. Catal.*, 2013, **299**, 90–100.
- 44 I. X. Green, W. Tang, M. Neurock and J. T. Yates Jr., *Science*, 2011, **333**, 736–739.

- 45 X. Liu, M.-H. H. Liu, Y.-C. C. Luo, C.-Y. Y. Mou, S. D. Lin, H. Cheng, J.-M. M. Chen, J.-F. F. Lee and T.-S. S. Lin, *J. Am. Chem. Soc.*, 2012, **134**, 10251–10258.
- 46 R. W. Coughlin, *Ind. Eng. Chem. Prod. Res. Dev.*, 1969, **8**, 12–23.
- 47 W. Schneider and W. Diller, in *Ullmann's Encyclopedia of Industrial Chemistry*, Wiley-VCH Verlag GmbH & Co. KGaA, Weinheim, Germany, 2000.
- 48 H.-D. Lauss and W. Steffens, in *Ullmann's Encyclopedia of Industrial Chemistry*, Wiley-VCH Verlag GmbH & Co. KGaA, Weinheim, Germany, 2000.
- 49 K. Tsuji and I. Shiraishi, *Fuel*, 1997, **76**, 555–560.
- 50 H. Jüntgen, E. Richter, K. Knoblauch and T. Hoang-Phu, *Chem. Eng. Sci.*, 1988, **43**, 419–428.
- 51 F. Rodriguez-Reinoso, *Carbon N. Y.*, 1998, **36**, 159–175.
- 52 E. Auer, A. Freund, J. Pietsch and T. Tacke, *Appl. Catal. A Gen.*, 1998, **173**, 259–271.
- 53 C. L. Bianchi, S. Biella, A. Gervasini, L. Prati and M. Rossi, *Catal. Letters*, 2003, **85**, 91–96.
- 54 P. Roisson, J.-P. Brunelle and P. Nortier, *Catalyst supports and supported catalysts: theoretical and applied concepts*, Butterworths, Boston, 1987.
- 55 P. Roisson, J.-P. Brunelle and P. Nortier, *Catalyst supports and supported catalysts: theoretical and applied concepts*, Butterworths, Boston, 1987.
- 56 L. Prati and M. Rossi, *J. Catal.*, 1998, **176**, 552–560.
- 57 R. J. J. Jansen and H. van Bekkum, *Carbon N. Y.*, 1994, **32**, 1507–1516.
- 58 K. Stańczyk, R. Dziembaj, Z. Piwowarska and S. Witkowski, *Carbon N. Y.*, 1995, **33**, 1383–1392.
- 59 J. L. Figueiredo and M. F. R. Pereira, *Catal. Today*, 2010, **150**, 2–7.
- 60 A. Bagreev, F. Adib and T. J. Bandoz, *Carbon N. Y.*, 2001, **39**, 1897–1905.
- 61 J. Lahayeaqb, *Fuel*, 1998, **77**, 543–547.
- 62 H. P. Boehm, *Carbon N. Y.*, 1994, **32**, 759–769.
- 63 H. P. Boehm, *Carbon N. Y.*, 2002, **40**, 145–149.
- 64 P. E. Fanning and M. A. Vannice, *Carbon N. Y.*, 1993, **31**, 721–730.
- 65 P. Albers, K. Deller, B. M. Despeyroux, A. Schäfer and K. Seibold, *J. Catal.*, 1992, **133**, 467–478.
- 66 J. L. Figueiredo, M. F. R. Pereira, M. M. A. Freitas and J. J. M. Órfão, *Carbon N. Y.*, 1999, **37**, 1379–1389.
- 67 Z. R. Yue, W. Jiang, L. Wang, S. D. Gardner and C. U. Pittman Jr., *Carbon N. Y.*, 1999, **37**, 1785–1796.
- 68 P. V. Samant, F. Gonçalves, M. M. A. Freitas, M. F. R. Pereira and J. L. Figueiredo, *Carbon N. Y.*, 2004, **42**, 1321–1325.
- 69 I. I. Salame and T. J. Bandoz, *J. Colloid Interface Sci.*, 2001, **240**, 252–258.
- 70 H. Schobert, *Chem. Rev.*, 2014, **114**, 1743–1760.
- 71 W. R. Sorenson, in *Encyclopedia of Materials: Science and Technology*, Pergamon, Washington, DC, 2001, pp. 7752–7755.
- 72 L. I. Nass, *Encyclopedia of PVC*, M. Dekker, New York, 1976.
- 73 J. Zhong, Y. Xu and Z. Liu, *Green Chem.*, 2018, **20**, 2412–2427.
- 74 I.-T. Trotsu, T. Zimmermann and F. Schüth, *Am. Chem. Soc.*, 2014, **114**, 1761–1782.
- 75 R. Lin, A. P. Amrute and J. Pérez-Ramírez, *Chem. Rev.*, 2017, **117**, 4182–4247.
- 76 B. Yan, W. Lu and Y. Cheng, *Green Process. Synth.*, 2012, **1**, 33–47.
- 77 *US Pat.*, US 3173962, 1962.
- 78 Y. Y. Turov and G. A. Parshina, *Chem. Technol. Fuels Oils*, 1967, **3**, 890–893.
- 79 R. E. Gannon, R. M. Manyik, C. M. Dietz, H. B. Sargent, R. O. Thribolet and R. P. Schaffer, *Kirk-Othmer encyclopedia of chemical technology.*, Wiley, New York, 2004.
- 80 R. J. Tedeschi, *Acetylene-Based Chemicals from Coal and Other Natural Resources*, New York, 1982.
- 81 J. Zhang, N. Liu, W. Li and B. Dai, *Front. Chem. Sci. Eng.*, 2011, **5**, 514–520.

- 82 X. Liu, B. Zhu, W. Zhou, S. Hu, D. Chen and C. Griffy-Brown, *Int. J. Greenh. Gas Control*, 2011, **5**, 1240–1249.
- 83 G. J. Hutchings, *J. Catal.*, 1985, **96**, 292–295.
- 84 Q. L. Song, S. J. Wang, B. X. Shen and J. G. Zhao, *Pet. Sci. Technol.*, 2010, **28**, 1825–1833.
- 85 G. Malta, S. J. Freakley, S. A. Kondrat and G. J. Hutchings, *Chem. Commun.*, 2017, **53**, 11733–11746.
- 86 A. Iles, A. Martin and C. M. Rosen, *Undoing Chemical Industry Lock-ins: Polyvinyl Chloride and Green Chemistry*, 2017, vol. 23.
- 87 X. Xu, H. He, J. Zhao, B. Wang, S. Gu and X. Li, *Chinese J. Chem. Eng.*, 2017, **25**, 1217–1221.
- 88 G. J. Hutchings and D. T. Grady, *Appl. Catal.*, 1985, **17**, 155–160.
- 89 G. J. Hutchings and D. T. Grady, *Appl. Catal.*, 1985, **16**, 411–415.
- 90 Minamata Convention on Mercury, <http://www.mercuryconvention.org/>, (accessed October 2017).
- 91 H. Xu and G. Luo, *J. Ind. Eng. Chem.*, 2018, **65**, 13–25.
- 92 K. C. O’Connell, J. R. Monnier, J. R. R. Regalbuto, K. C. O’Connell, J. R. Monnier and J. R. R. Regalbuto, *Appl. Catal. B Environ.*, 2018, **225**, 268–272.
- 93 M. Zhu, Q. Wang, K. Chen, Y. Wang, C. Huang, H. Dai, F. Yu, L. Kang and B. Dai, *ACS Catal.*, 2015, **5**, 5306–5316.
- 94 M. Conte, A. F. Carley, G. Attard, A. A. Herzing, C. J. Kiely and G. J. Hutchings, *J. Catal.*, 2008, **257**, 190–198.
- 95 B. Nkosi, N. J. Coville and G. J. Hutchings, *Appl. Catal.*, 1988, **43**, 33–39.
- 96 B. Nkosi, M. D. Adams, N. J. Coville and G. J. Hutchings, *J. Catal.*, 1991, **128**, 378–386.
- 97 B. Nkosi, N. J. Coville, G. J. Hutchings, M. D. Adams, K. Friedl and F. E. Wagner, *J. Catal.*, 1991, **128**, 366–377.
- 98 M. Conte, A. F. Carley and G. J. Hutchings, *Catal Lett*, 2008, **124**, 165–167.
- 99 M. Conte, C. J. Davies, D. J. Morgan, T. E. Davies, D. J. Elias, A. F. Carley, P. Johnston and G. J. Hutchings, *J. Catal.*, 2013, **297**, 128–136.
- 100 B. Nkosi, N. J. Coville, G. J. Hutchings, M. D. Adams, J. Friedl and F. E. Wagner, *J. Catal.*, 1991, **128**, 378–386.
- 101 M. Yang, L. F. Allard and M. Flytzani-Stephanopoulos, *J. Am. Chem. Soc.*, 2013, **135**, 3768–3771.
- 102 L. F. Allard, A. Borisevich, W. Deng, R. Si, M. Flytzani-Stephanopoulos and S. H. Overbury, *J. Electron Microsc. (Tokyo)*, 2009, **58**, 199–212.
- 103 J. Lu, C. Aydin, N. D. Browning and B. C. Gates, *Angew. Chemie Int. Ed.*, 2012, **51**, 5842–5846.
- 104 J. Guzman and B. C. Gates, *J. Phys. Chem. B*, 2002, **106**, 7659–7665.
- 105 J. Guzman and B. C. Gates, *J. Catal.*, 2004, **226**, 111–119.
- 106 X. Liu, M. Conte, D. Elias, L. Lu, D. J. Morgan, S. J. Freakley, P. Johnston, C. J. Kiely and G. J. Hutchings, *Catal. Sci. Technol.*, 2016, **6**, 5144–5153.
- 107 C. Huang, M. Zhu, L. Kang and B. Dai, *Catal. Commun.*, 2014, **54**, 61–65.
- 108 K. Zhou, J. Jia, C. Li, H. Xu, J. Zhou, G. Luo and F. Wei, *Green Chem.*, 2015, **17**, 356–364.
- 109 P. Johnston, N. Carthey and G. J. Hutchings, *J. Am. Chem. Soc.*, 2015, **137**, 14548–14557.
- 110 US Pat., US 2013008004, 2013.
- 111 G. Malta, S. A. Kondrat, S. J. Freakley, C. J. Davies, S. R. Dawson, X. Liu, L. Lu, K. Dymkowski, F. Fernandez-Alonso, S. Mukhopadhyay, E. K. Gibson, P. P. Wells, S. F. Parker, C. J. Kiely and G. J. Hutchings, *ACS Catal.*, 2018, **8**, 8493–8505.
- 112 S. Hirata, H. Torii, Y. Furukawa, M. Tasumi and J. Tomkinson, *Chem. Phys. Lett.*, 1996, **261**, 241–245.
- 113 S. A. Mitchenko, E. V. Khomutov, A. A. Shubin and Y. M. Shul’ga, *J. Mol. Catal. A Chem.*, 2004, **212**, 345–352.

- 114 M. Conte, A. F. Carley, C. Heirene, D. J. Willock, P. Johnston, A. A. Herzing, C. J. Kiely and G. J. Hutchings, *J. Catal.*, 2007, **250**, 231–239.
- 115 J. Zhang, Z. He, W. Li and Y. Han, *RSC Adv.*, 2012, **2**, 4814.

2. Experimental

2.1. Introduction

The aim of this section is to list the preparation methods of catalysts and to explain how the various analytical techniques operate and were used in this work. A list of the main chemicals used is also provided.

2.2. Chemicals

The chemicals used in this work, including their suppliers and purities are listed below.

Table 2.1. List of chemicals.

Chemical	Supplier	Purity / %
5 % Acetylene/argon (C ₂ H ₂ /Ar) - gas mix	BOC	> 95
5 % Hydrogen chloride/argon (HCl/Ar) - gas mix	BOC	> 95
Argon, Ar	BIP	99.9999
Hydrochloric acid, HCl	Fisher	37
Nitric acid, HNO ₃	Fisher	70
Sulfuric acid, H ₂ SO ₄	Fisher	95
Chloroauric acid, HAuCl ₄ .3H ₂ O, 49.0 % Au	Alfa Aesar	99.99
Chloroauric acid solution, HAuCl ₄ , 41.76 % Au	JM	-
Activated carbon, Norit ROX 0.8	JM	-
Potassium permanganate, KMnO ₄	Sigma Aldrich	97
Hydrogen Peroxide, H ₂ O ₂	Fluka	30
Extra Dry Acetone, CH ₂ O	Acros Organics	99.8
HPLC-Grade Acetone	Fisher	99.8
Methanol, CH ₃ OH	Fisher	> 99.5
Ethanol, C ₂ H ₅ OH	VWR	≥ 99.8
1-Propanol, C ₃ H ₇ OH	Alfa Aesar	99.5
1-Butanol, C ₄ H ₉ OH	Sigma Aldrich	99.8
2-Propanol, C ₂ H ₅ OH	Fisher	≥ 99.5
2-Butanol, C ₄ H ₉ OH	Sigma Aldrich	99.5
2-Butanone, C ₄ H ₈ O	Acros Organics	99
Ethyl acetate, C ₄ H ₈ O ₂	Fisher	> 99

Diethyl ether, (C ₂ H ₅) ₂ O	Acros Organics	99.5
THF, C ₄ H ₈ O	Sigma Aldrich	≥ 99.9
DMSO, C ₂ H ₆ OS	Alfa Aesar	> 99
DMF, C ₃ H ₇ NO	Alfa Aesar	99
Cyclohexanone, C ₆ H ₁₀ O	Sigma Aldrich	≥ 99.0
Ammonium sulfate, (NH ₄) ₂ SO ₄	Sigma Aldrich	99
Sodium sulfate, Na ₂ SO ₄	Sigma Aldrich	99
Sodium thiosulfate, Na ₂ S ₂ O ₃	Alfa Aesar	99

2.3. Catalyst preparation methods

2.3.1. Preparation of supported gold catalysts via wet impregnation

Chloroauric acid (20 mg) was dissolved in aqua regia (3 HCl : 1 HNO₃), or other solvents (eg. acetone, H₂SO₄, water) as stated, (2.7 mL) and allowed to stir for 10 min. The metal precursor solution was added drop wise, with stirring to ground, activated, dry carbon (0.99 g). This solution was left to stir for 1 h then dried under nitrogen at 140 °C for 16 h. Unless specified otherwise, all catalysts were prepared with a 1 wt. % gold loading, denoted 1% Au/C – solvent and the carbon support was used without any additional treatment.

2.3.2. Preparation of modified Au/C catalysts

In chapters 4 and 5, carbon and Au/C catalysts are modified using sulfur containing solutions and the Hummers' oxidation method, respectively. The details of these methods are detailed in the experimental section at the start of each respective chapter.

2.4. Catalyst characterisation techniques

2.4.1. Brunauer-Emmett-Teller (BET) surface area analysis

Background

Branauer-Emmett-Teller theory uses multiple molecular layers to determine the surface area of a given sample, removing the inaccuracy of Langmuir theory which only considers monolayer coverage.¹ This theory can be applied to obtain information such as total surface area, pore-size distribution and morphology. In practice, nitrogen gas (at 77 K) condenses on the surface of the sample particles as a monolayer. Since the size of the nitrogen gas molecules are known, the amount of adsorbed gas can be correlated to the total surface area, including the pores.

The BET equation can be given as:

$$v = \frac{v_m c p}{(p_0 - p) \left[1 + (c - 1) \left(\frac{p}{p_0} \right) \right]}$$

Where v = absorbed volume of gas, v_m = adsorbed monolayer volume, p = equilibrium gas pressure, p_0 = saturation pressure and c = BET constant:

$$c = \exp\left(\frac{E_1 - E_2}{RT}\right)$$

Where E_1 = heat of adsorption for monolayer formation, E_2 = heat of adsorption for multilayer formation, R = gas constant and T = temperature (K).

The BET constant provides a value to determine the affinity between adsorbent and adsorbate. Values between 100 and 200 are ideal, whilst below this the adsorbent/adsorbate interaction is too substantial, rendering the method invalid. A value higher than 200 indicates the sample is significantly porous.²

The BET equation can be rearranged to form the linear equation:

$$\frac{p}{v(p_0 - p)} = \frac{c - 1}{v_m c} \left(\frac{p}{p_0} \right) + \frac{1}{v_m c}$$

This equation can be plotted using the form $y = mx + c$ where $y = \frac{p}{v(p_0 - p)}$ and $x = \left(\frac{p}{p_0} \right)$ to find gradient, $m = \frac{c-1}{v_m c}$ and y-intercept = $\frac{1}{v_m c}$. Once v_m is known, S can be found using the equation:

$$S = \frac{v_m N_A A m}{V}$$

Where S = specific surface area, N_A = Avagadro's constant, V = molar volume of nitrogen and m = mass of the solid sample.

Experimental

Samples were degassed at 120 °C overnight with a Quantachrome Flovac degasser and then weighed accurately before analysis using a Quantachrome Quadrasorb BET. Nitrogen porosimetry was performed at -196 °C, over the range $P/P_0 = 0.05 - 0.2$.

2.4.2. X-ray Absorption Fine Structure (XAFS) Spectroscopy

Background

X-ray absorption fine structure (XAFS) spectroscopy studies the transmission or fluorescence of x-rays as a result of the interactions of the beam with a solid, liquid or gas sample. XAFS can be explained in two areas; x-ray absorption near edge structure (XANES) and extended x-ray absorption fine structure (EXAFS) (Figure 2.1). XANES is the study of the absorption edge; when the x-ray beam is of the specific energy for a core electron to be excited and removed, it gives rise to a sharp increase in the absorption at that particular energy. This transition energy is atomically specific. For the catalysts studied in this work, the focus is solely on the Au L_3 -edge ($2p_{3/2} \rightarrow 5d$ transition), which has an absorption edge at ~ 11920 eV. The absorption edge has a strong feature known as the white line intensity due to this transition, which gives an indication of the oxidation state of the gold, with a greater intensity signifying an increase in oxidation state.³ Using XANES, information on the electronic and geometric structure can be determined, as well as the formal oxidation state and coordination chemistry. A Linear Combination Fitting (LCF) of the XANES data can be performed, which fits standard data to the sample in order to quantify the proportion of different species present. The use of Au standards from different oxidation states enables calculation of the proportion of different states in the heterogeneous Au catalyst. These calculations were performed using the Athena software package.^{4,5} EXAFS studies the interaction of the ejected electrons with the surrounding atoms in the compound. The electron can be seen to be emitted as a wave, which is back scattered by the nearest neighbours of the emitting atom. This backscattering will interfere with the emitted electron wave constructively and destructively, depending if the waves are in phase or out of phase, respectively. This interference gives rise to fine structure; the change in absorption which occurs after the absorption edge. The frequency of these observed fine-structure oscillations is dependent on the distance between absorber atoms and atoms causing back-scattering, whilst the amplitude is proportional to the number of back-scattering atoms. Therefore, studying this post-edge absorption gives information on the local geometric structure, the coordination number and species of nearest neighbours.

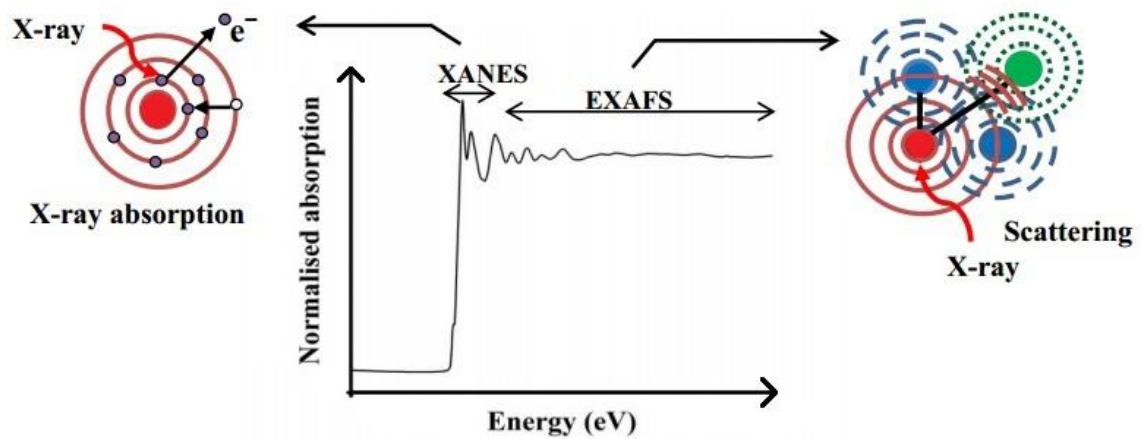


Figure 2.1. XAFS spectrum showing XANES and EXAFS regions and the respective diagrams showing absorption and scattering of the x-ray beam.

XAFS is typically performed in transmission mode, where the analysis can be performed at high temperatures and pressures. The sample is placed in the path of a monochromatic x-ray beam and the intensity before and after analysis is measured. From this, the absorbance, proportional to the excitation energy, can be calculated using the equation:

$$\mu_t x = -\ln\left(\frac{I_t}{I_0}\right)$$

Where μ_t = absorption coefficient, x = thickness of the sample, I_t = intensity of beam after transmission through sample and I_0 = initial intensity of beam. A reference material should also be analysed as a standard, for calibration purposes. XAFS analysis can also be performed in fluorescence mode, which is typically used for dilute samples due to the technique's higher sensitivity. Fluorescence occurs when high energy electrons from upper shells relax into the hole created when a photoelectron is ejected from a core shell (Figure 2.2). The absorbance is monitored by measuring the intensity of these fluorescence x-rays. This is calculated using the equation:

$$\mu_t = \left(\frac{F}{I_0}\right)$$

Where F = intensity of fluorescence x-rays.

The Auger Effect is another method whereby the generated hole is de-excited as an electron from an upper core shell relaxes, also releasing a second electron out of the sample (Figure 2.2).

Gold requires hard x-rays (>5 keV)⁶ to ionise the core electrons, therefore fluorescence is the dominant emission, whereas Auger emission typically occurs after lower energy (soft) x-ray absorption.⁷

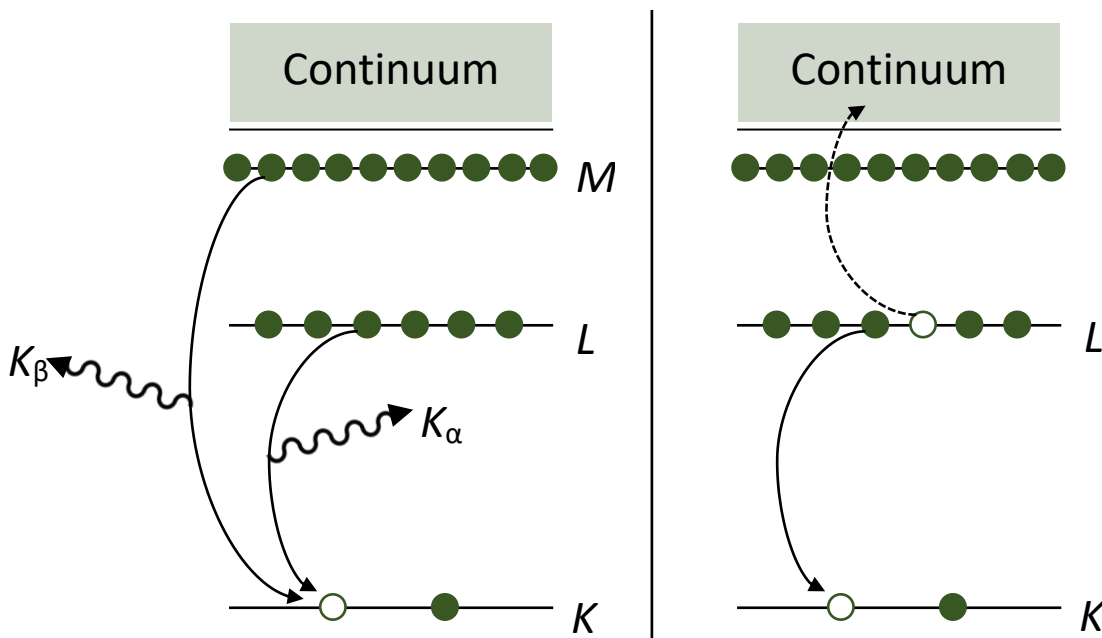


Figure 2.2. De-excitation caused by (left) x-ray fluorescence and (right) Auger emission.

Experimental

X-ray Absorption Fine Structure (XAFS) spectra were recorded at the B18 beamline of Diamond Light Source in Harwell, UK. Measurements were performed using a QEXAFS setup with a fast-scanning Si (111) double crystal monochromator or a 36 element Ge fluorescence detector. Data were analysed using Athena, from the Demeter software package.^{4,5} Samples were analysed at the Au L_3 absorption edge in transmission mode either *in-situ* or *ex-situ*. All analysis was performed with reference to a Au foil standard and KAuCl_4 and AuCl_2^- standard compounds. A minimum of 5 scans were performed on each sample for XANES analysis and the data averaged, resulting in an error value of $\pm 5\%$. The assistance of Stewart Parker and Emma Campbell in performing the XAFS experiments at the Diamond Light Source, Harwell and to both and Simon Kondrat for their assistance in elaborating the data is gratefully acknowledged.

2.4.3. Gas chromatography

Background

Gas chromatography (GC) is commonly used to accurately determine the concentration of

compounds in a liquid or gas phase samples. The GC consists of three main components, the injector, the column with oven and the detector (Figure 2.3). Firstly, the compound mixture is injected into the GC; in this work gas samples are analysed on-line – continuously throughout the reaction. These are injected via a six-port injection loop, which allows an empty section of the loop to be filled with the gas sample without interrupting the flow of the carrier gas during an analysis. The sample then flows through the column using nitrogen as a carrier gas. The use of nitrogen ensures there is no interaction of the carrier gas with the mobile phase. The flow rate is adjusted to ensure good separation of analytes, due to differences in the analytes' affinity for the stationary phase, whilst maintaining a reasonable analysis speed. The column itself consists of a packed stationary phase made of N-Vinyl-2-pyrrolidone (surface area 225-350 m²/g) contained in a stainless steel tube. These columns can be between 1.5-10 m in length and have an internal diameter of 2-4 mm. This allows a large volume of gas to be analysed, which can produce a higher sensitivity than capillary columns; however, capillary columns are used for almost all other analysis due to their high resolution and short analysis times. The column is heated according to the retention of the sample; the higher the temperature, the quicker the sample elutes through the column, but less separation will occur. Therefore, as with column flow rate, a compromise must be made between speed of analysis and separation of analytes.

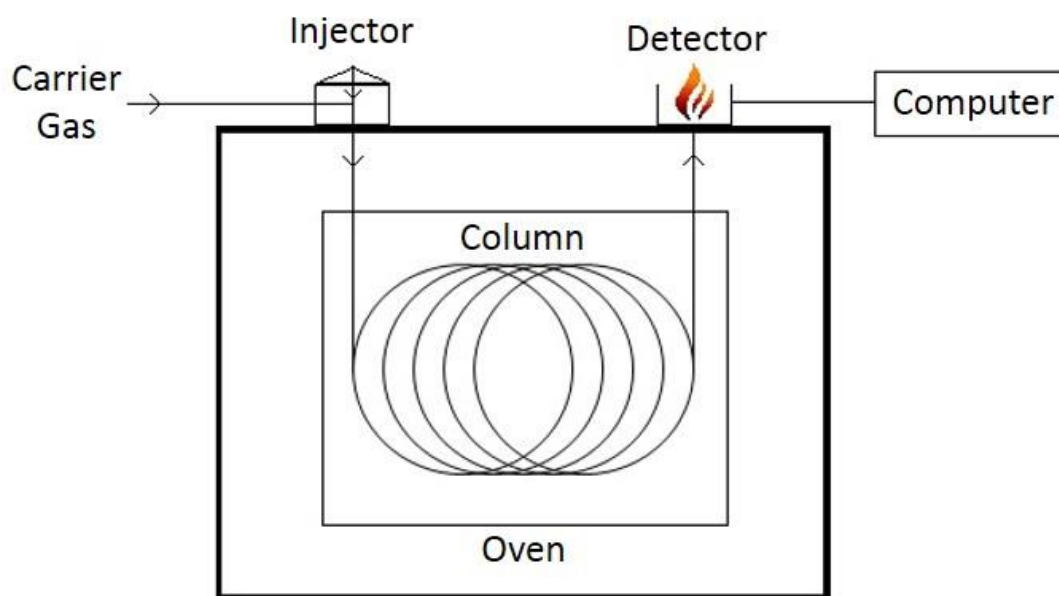


Figure 2.3. Schematic diagram of a gas chromatograph.

Once separated, the analytes are then detected by a flame ionisation detector (FID, Figure 2.4). After leaving the column the sample is pyrolysed by a hydrogen flame. The use of hydrogen results in no detectable trace in the chromatograph. The pyrolysis splits the sample into

hydrocarbon cations and electrons. These ions generate a current between the electrodes situated next to the pyrolysis source. This current is then translated into a signal, resulting in a peak on the chromatograph. Using known concentrations of a standard, a calibration curve can be formed that can then be used to find the unknown concentration of a sample. Various other detectors can also be used on a GC; the thermal conductivity detector (TCD) measures a change in the thermal conductivity of the sample stream compared to a reference stream which, unlike the FID, does not result in the sample's destruction, and the mass spectrometer (MS) ionises the sample to determine the individual masses present. However, FIDs are the preferred detector when analysing hydrocarbons owing to their higher resolution. Mass spectrometry is discussed in further detail in 2.4.4.⁸

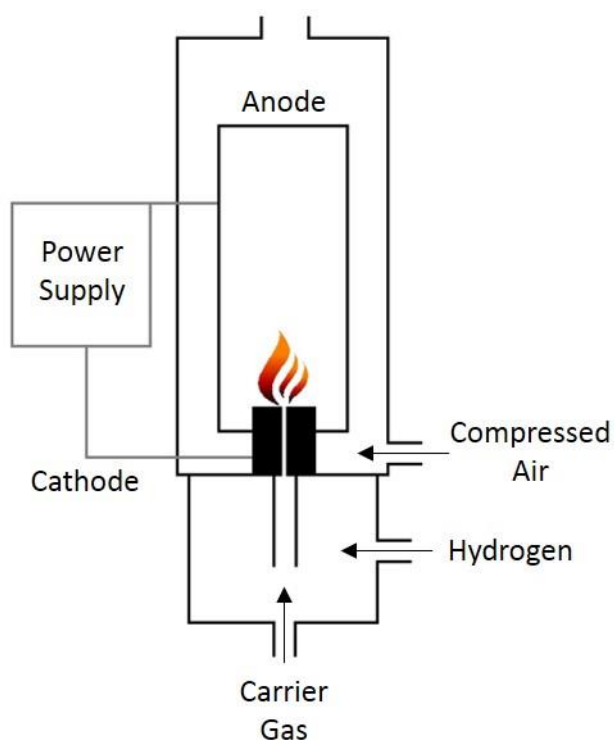


Figure 2.4. Schematic diagram of a flame ionisation detector.

Experimental

Analysis of the acetylene hydrochlorination reaction was carried out using a Varian CP-3800 GC fitted with a Poropak-N packed column and an FID detector. The standard reaction conditions were as follows: injection temperature 100 °C, initial column temperature 130 °C held for 2.5 min, heated at a ramp rate of 10 °C min⁻¹ to 150 °C and held for a further 2 min, detector temperature 180 °C. This sequence was repeated continuously throughout the reaction to provide time-on-line data.

Conversion of acetylene was calculated using the formula:

$$\begin{aligned} & \textit{Acetylene conversion (\%)} \\ &= \frac{\textit{Initial acetylene peak area} - \textit{Final acetylene peak area}}{\textit{Initial acetylene peak area}} \times 100 \end{aligned}$$

Calibration of the main product, VCM could not be performed due to the hazardous nature of the chemical. For this reason, a mass balance could also not be determined. In all reactions a selectivity greater than 99 % was achieved, and the only by-product formed was 1,2-dichloroethane.⁹⁻¹¹ VCM selectivity was determined by correlating the conversion of acetylene with VCM peak area counts when no other products were observed during the reaction. This produced an r^2 value equal to 0.99. The theoretical VCM counts from all reactions, calculated from acetylene conversion, were compared to those of the experimental values with a greater than 99 % correlation.

2.4.4. Mass spectrometry

Background

Mass spectrometry (MS) can be used in-line with gas chromatography or, as in this work, in tandem. This technique is especially useful for identifying unknown compounds produced during a reaction, owing to its high accuracy. To analyse the gas stream, an aliquot is injected through a capillary column, before being introduced to a vacuum. The sample is then bombarded by an electron stream, resulting in a positively charged, ionic sample, although in rare cases a negative sample can also be formed and detected. The peak resulting from the highest mass/charge ratio is the molecular ion, which is the weight of the original sample. Multiple smaller ion fragments are also formed and detected, which are indicative of the sample composition. Various methods of mass selection are available such as ion traps, time-of-flight or, as used in this work, quadrupoles. A quadrupole consists of four equidistant, parallel rods which each exert an electric field when a radio frequency alternating voltage is applied. The sample is attracted and repelled to each charged pair of rods, whilst also being accelerated down the rods, before settling into a steady path to the detector. Ions which are not of the selected mass/charge ratio are discharged on the rods or removed by the vacuum. This radio frequency quadrupole field is highly selective for certain mass/charge ratios and can be continuously tuned during the

reaction to scan for different mass/charge ratios. The positively charged sample contacts the detector, forming a current which is translated into a peak signal, whose intensity is proportional to the concentration of the ion.¹²

Experimental

Analysis was carried out using a Hiden Analytical, QGA gas analysis mass spectrometer, equipped with a quadrupole detector. The gas flow from the reaction stream was analysed continuously to confirm the production of vinyl chloride monomer and to determine if there was any by-product formation. This was used for qualitative analysis purposes only.

2.4.5. ICP-MS

Background

Elemental analysis of solutions can be performed using Inductively Coupled Plasma - Mass Spectrometry (ICP-MS). This technique uses a plasma torch to ionise the sample, which is then directed to a mass spectrometer. No separation between the elements of interest and the bulk sample occurs during the ionisation process, so full elemental detection and quantification is assured.

The sample is first introduced to a nebuliser via a peristaltic pump. Here, small droplets of the sample solution are hit with a perpendicular stream of argon, creating an aerosol. The majority of this aerosol is condensed on the spray chamber walls and removed as waste, whilst a small fraction is directed to the torch. In the ICP torch, argon is flowed through the outermost two of three concentric quartz tubes. The argon forms a plasma when a spark is introduced to the gas stream; ionised argon cations and electrons (from the spark and those released from argon atoms, accelerated by the surrounding induction coil) continuously collide and recombine, resulting in high temperatures in the order of 6,000 - 10,000 K at different regions of the cone shaped plasma. A second flow of argon through the first and second tubes determines the height and hence temperature of the plasma cone.

The aerosol containing the sample of interest is introduced to the plasma via the central quartz tube. The sample undergoes atomisation – firstly the sample is dried at the high temperature, then heated to a gas. These atoms absorb energy from the plasma, resulting in ionisation upon emission of an electron. The temperature is adjusted dependent on the element being analysed in order to maximise first ionisation efficiency and minimise second ionisation (removal of two electrons). These ions then travel to the interface. The interface is an intermediary zone between the ICP and the MS. Here the sample ions are cooled, resulting in expansion of the gas.

A fraction of this is then directed to a vacuum chamber before introduction to the quadrupole mass spectrometer at the correct temperature and pressure.¹³

Experimental

200 mg of oxidised carbon prepared with 2.5 g of KMnO_4 was stirred in 50.0 mL of deionized water for 16 h. The powder was allowed to settle, then an aliquot of the solution was filtered using a PTFE micropore filter (Fisherbrand®, 0.45 μm). Analysis was performed by the Analytical Department in Cardiff University using an Agilent 7900 ICP-MS with I-AS autosampler. A five point calibration curve was run using certified potassium and manganese SRMs and Internal Standard infused inline during analysis. Analysis was carried out using Helium mode in the ORS3 (Collision/Reaction Cell). The sample solution was injected three times and the average value was taken.

2.4.6. Fourier Transform Infrared Spectroscopy (FTIR)

Background

Infrared detectors measure the absorption of different wavelengths of light by solid, liquid or gaseous samples. This is achieved by directing a set of discrete wavelengths at a sample, measuring the absorption of light, then directing a second set of wavelengths, measuring this absorption, and repeating this with continually differing wavelengths over a short time period. The Fourier Transform is an algorithm used to calculate the absorptions by the sample at the different wavelengths.

Infrared spectrometers can analyse a wide spectral range; for the study of catalysts, analysis is commonly performed in the mid infrared region (5000 – 400 cm^{-1}). This is the range in which functional groups and probe molecules (for example CO) vibrate due to a change in dipole, resulting in different absorptions of infrared radiation.¹⁴ Conversely, homonuclear diatomic molecules such as H_2 , O_2 & N_2 are not infrared active as no change in dipole occurs. Analysis can also be performed in the near infrared (12800 – 4000 cm^{-1}) and far infrared (50 – 1000 cm^{-1}) regions.

Experimental

All samples were analysed using a Shimadzu IRAffinity-1S fourier transform infrared spectrophotometer. Scans were performed in the range 400 – 4000 cm^{-1} .

2.4.7. Powder x-ray diffraction

Background

Powder x-ray diffraction (XRD) is used to determine the crystallinity of a sample and is especially useful in catalysis to determine the size of metal nanoparticles on the catalyst. Fingerprints of known crystalline phases have been compiled in databases so can readily be compared for identification. A sample is prepared by placing the powder in a flat, disc-shaped holder. X-rays are generated by bombarding a metal, for example Cu, Fe, Mo with an electron beam. These x-rays are directed through a monochromator to form a parallel, uniform beam, collimated, and directed at the sample. The wavelength of x-rays emitted is related to the distance between atoms in a sample, so when the x-rays are scattered by the sample atoms, a diffraction pattern is formed. Scattering occurs according to Bragg's law:¹⁵

$$n\lambda = 2d \sin \theta$$

Where n = an integer, λ = wavelength of x-rays, d = inter-planar distance and θ = angle between the beam and the normal of the reflecting plane (Figure 2.5).

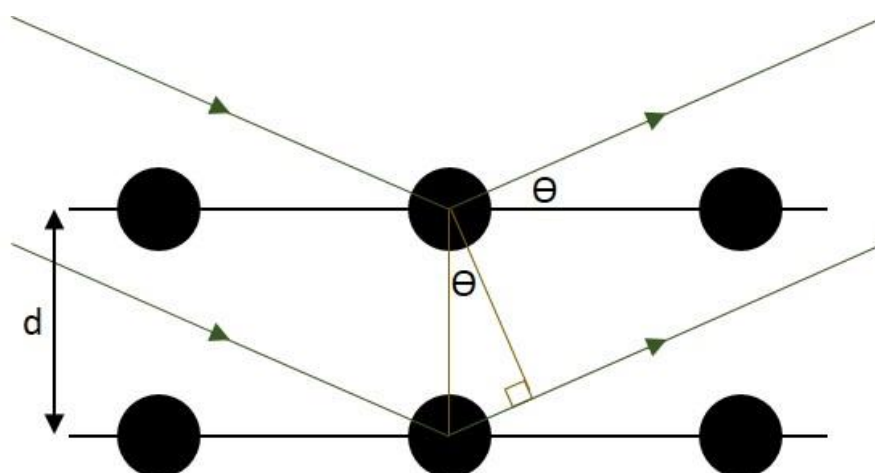


Figure 2.5. Diagram showing Bragg diffraction of x-rays.

Constructive interference occurs when the difference in wavelengths of the scattered x-rays is equal to an integer number. This results in an increase in detection of x-rays at a certain angle, causing a more intense signal. The more amorphous the sample, the less coherent the scattering, resulting in low intensity scattering over a wide angle and therefore a broader peak. As the x-ray wavelength is fixed, peaks will only result from certain angles of reflection, 2θ , specific to certain crystalline structures (Figure 2.6). Thus, a plot of angle, versus intensity is formed, showing the distinct crystal planes of the sample.

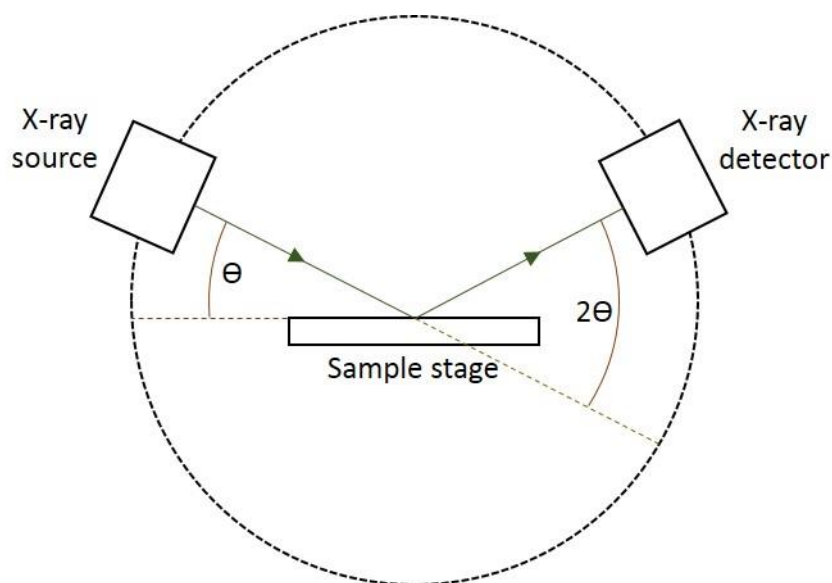


Figure 2.6. Schematic diagram of x-ray diffractometer.

When used in conjunction with the Scherrer equation, an estimate of nanoparticle size can be calculated:¹⁶

$$\tau = \frac{K\lambda}{\beta \cos \theta}$$

Where τ = mean size of the crystalline, K = dimensionless shape factor and β = peak width at full width half maximum. The Scherrer equation relates line width to crystallite size and can be performed for crystals up to 1 μm in size, depending on the diffraction angle.¹⁷ This is especially useful when performing in-situ XRD measurements, to obtain a quantitative measure of particle size growth whilst the catalyst is subject to heat or reaction gases (2.4.8).

Experimental

Powder X-ray Diffraction (XRD) analysis was performed between 10° and 80° 2 θ using an X'Pert Pro PAN Analytical powder diffractometer employing a Cu K α radiation source operating at 40 keV and 40 mA. Analysis of the spectra obtained was carried out using X'Pert High Score Plus software. Figure 2.7 shows the XRD pattern of carbon, the catalyst support used in this work. Two broad reflections are seen due to turbostratic arrangement of carbon - a random stacking of parallel layers. These comprise of (002), at 24°, due to stacked layers and (10), at 43°, where changes in the height of the stacked layers results in no l index of the $00l$ indices. Reflections observed in some samples at 79° can be attributed to carbon (11) structure.^{18,19}

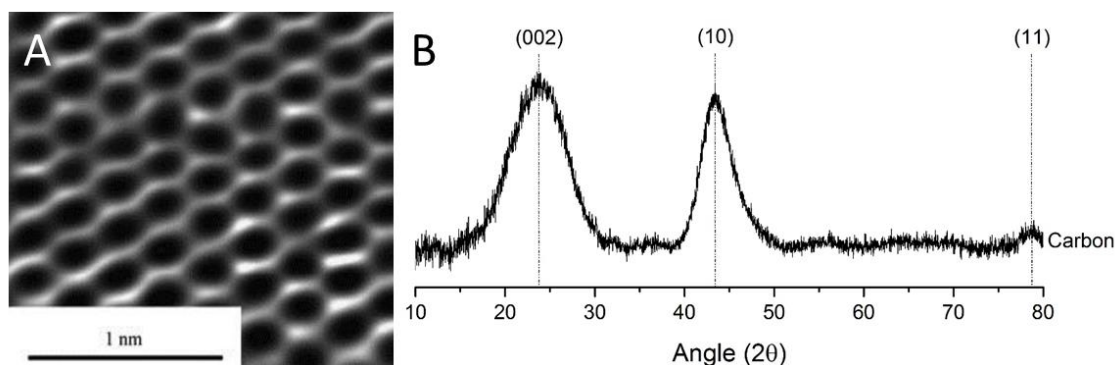


Figure 2.7. STEM showing turbostratic stacking arrangement of carbon (A) and XRD pattern of carbon (B).

2.4.8. In-situ powder x-ray diffraction

Background

Analysis via powder XRD can also be performed whilst subjecting the sample to heat in air or under the flow of a gas mixture. This in-situ analysis can provide information on the evolution of the size of nanoparticles and the bulk material, whilst mimicking reaction conditions.

Experimental

In-situ powder XRD analysis was performed using an X'pert Pro XRD fitted with an Anton-Parr XRK900 in-situ cell between 20° and 80° 2θ at different temperatures, whilst heating under a nitrogen flow, 50 mL min⁻¹. Analysis of the spectra obtained was carried out using X'Pert High Score Plus software.

2.4.9. Scanning/transmission electron microscopy

Background

Scanning or transmission electron microscopy (SEM/TEM) can be used to find structural, morphological and chemical information of the sample, all non-destructively. In scanning electron microscopy, an electron beam is generated from an electron gun which is focused onto a small spot on the sample. The beam is scanned in a rectangular raster pattern over the sample and signal intensities are recorded. The signal intensity is formed from secondary electrons, which are a consequence of the electron beam interacting with electrons from the k-shell, releasing inelastically scattered secondary electrons. The signal is amplified and can be translated into an image in which variation in brightness is used to depict the sample's topography. By altering the size of the rectangular raster, the image can be "magnified"; the

smaller the size, the higher the magnification. The electron beam also results in elastically scattered electrons. These are electrons that reflect off the core electrons, known as back scattered electrons, which are used to determine the distribution of elements in a sample. The elements with a higher atomic mass scatter the electrons more, thereby appearing brighter on the image, hence a distribution pattern of elements can be formed.

Energy dispersive x-rays (EDX) can also be used to determine which elements are present. If the electron beam results in the ejection of an inner shell core electron, a higher energy electron drops down to fill the generated electron hole and concurrently releases an energy packet in the form of an x-ray. This x-ray has a highly element specific wavelength.

Transmission electron microscopy (TEM) is similar in principle to SEM but uses a static beam instead of the mobile raster beam of SEM. Significantly the sample for TEM must be ultra-thin as the beam is required to penetrate the sample, forming an image from the transmission of electrons through the sample. For this same reason, the beam is a much higher voltage than that used in the SEM. Focusing of the image onto a fluorescent screen occurs via electromagnetic lenses, altered by changing the current through the lens coil. This operation is performed under vacuum so no air can interfere with the passage of electrons. Provided the sample is thin enough, both SEM and TEM can be used in conjunction, known as STEM (Figure 2.8). Samples were analysed using high-angle annular dark-field (HAADF)-STEM. This imaging method ignores the unscattered electron beam, typically forming an image with a dark background, collecting electrons from an annulus around the beam which have been inelastically Rutherford scattered at high angles. High angle ADF detectors are also able to determine the atomic number of the atoms which scatter the beam, forming Z-contrast images which are especially useful for determining dispersion of elements in catalyst samples.

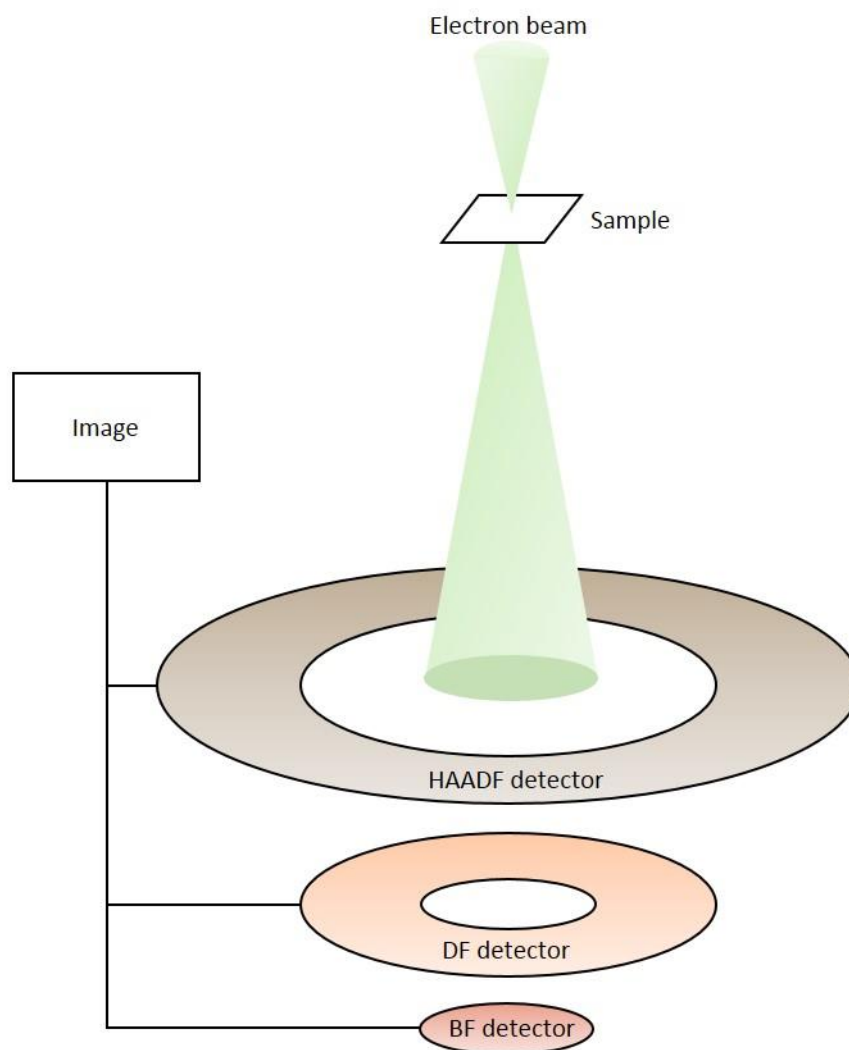


Figure 2.8. Schematic diagram of a STEM.

In contrast to dark field-STEM, bright-field (BF) -STEM utilises the unscattered electrons to form an image, whilst the scattered electrons are not detected. This is typically used as a complementary technique to DF-STEM.

Experimental

Catalysts analysed by STEM were dispersed on a holey carbon TEM grid and analysed using BF-HAADF-STEM imaging mode in an aberration corrected JEOL ARM-200CF scanning transmission electron microscope operating at 200kV. This microscope was also equipped with a Centurio silicon drift detector (SDD) system for x-ray energy dispersive spectroscopy (XEDS) analysis. SEM imaging on the used catalysts was performed on a Tescan MAIA3 field emission gun scanning electron microscope (FEG-SEM). Samples were dry dispersed onto 300 mesh Cu grid supported holey carbon film and imaged using the backscattered electron detector at 15 kV. Samples were uncoated. EDS analysis was performed using an Oxford Instruments X-Max^N 80

SDD. Thank you to Tom Davies and Qian He for their technical assistance in acquiring the SEM and TEM data at Cardiff University and Lehigh University.

2.4.10. Thermogravimetric analysis

Background

Thermogravimetric analysis (TGA) monitors the change in mass of a sample during heating. Typically, a few milligrams of sample are loaded onto a balance which hangs inside a furnace. The temperature is then increased at a controlled rate whilst the sample is subject to a purge gas to control the environment. Gases not limited to hydrogen, oxygen or nitrogen could be used to interact with the sample, depending on the analysis type. The mass or percentage mass is measured and then plotted as a function of time which can be correlated to water loss, decomposition, oxidation, reduction and other chemical processes depending on the analysis. This technique can also be coupled with GC-MS for the separation and identification of gases produced during heating.

Experimental

TGA was carried out in a Perkin Elmer TGA-4000. 20 milligrams of sample were deposited in the auto sampler and heated from 30 - 900 °C at 5 °C/min, under N₂ flow of 20 mL/min.

2.4.11. X-ray photoelectron spectroscopy

Background

X-ray photoelectron spectroscopy (XPS) is primarily a surface analysis technique, used to determine the composition and electronic state of many different materials. XPS works on the same principles as the photo-electric effect; a sample is irradiated with a light source, in this case x-rays, which are absorbed by the surface atoms, resulting in the emission of electrons. These electrons have a kinetic energy that is determined by the binding energy of the atom and the energy of the x-ray source. This is summarised by the following equation:

$$E_k = h\nu - E_b$$

Where E_k = kinetic energy of the emitted photoelectron, h = Planck's constant, ν = frequency of x-ray radiation and E_b = binding energy of the absorbing atom. If the kinetic energy of the emitted electrons is recorded and plotted against photoelectron intensity, it is possible to quantitatively ascertain the abundance of different atoms in the sample. The basic set up for

XPS analysis requires an x-ray source, a sample chamber under high-vacuum, an electron energy analyser and a detector, shown in Figure 2.9.

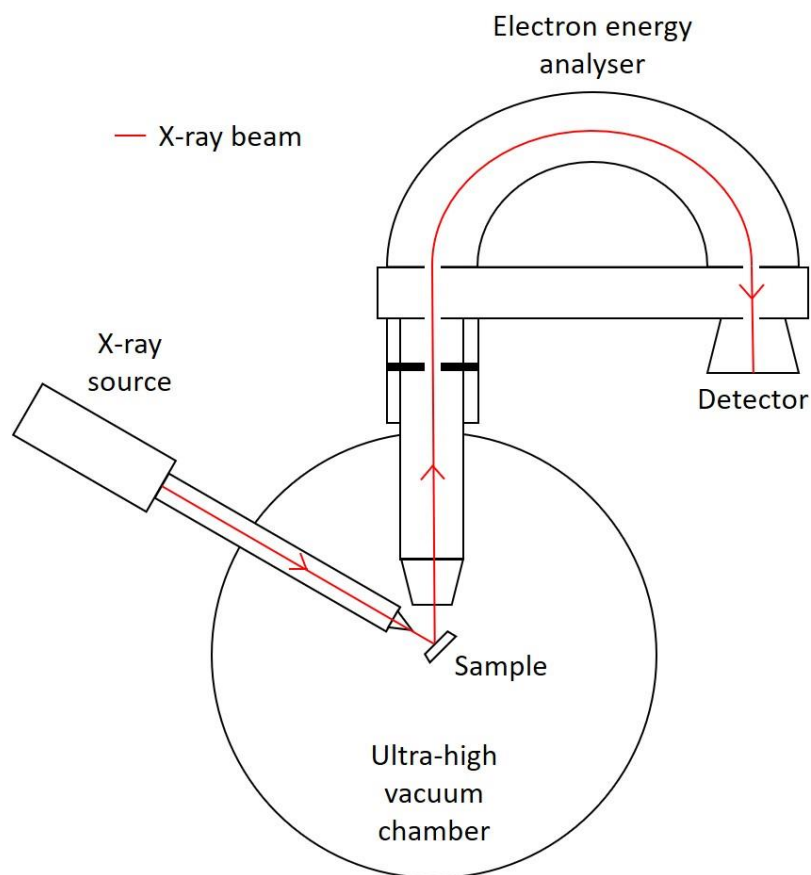


Figure 2.9. Schematic diagram of an x-ray photoelectron spectrometer.

Experimental

X-ray photoelectron spectroscopy (XPS) was performed on a Thermo Fisher Scientific K-alpha⁺ spectrometer. Samples were analysed using a micro-focused monochromatic Al X-ray source (72 W) over an area of approximately 400 microns. Data was recorded at pass energies of 150 eV for survey scans and 40 eV for high resolution scan with 1 eV and 0.1 eV step sizes respectively. Charge neutralisation of the sample was achieved using a combination of both low energy electrons and argon ions. Data analysis was performed in CasaXPS using a Shirley type background and Scofield cross sections. The assistance of Dave Morgan at Cardiff University, performing analysis and helping with data elaboration, is gratefully acknowledged.

2.5. Acetylene hydrochlorination reaction

Reactions were performed in a dedicated reactor, commissioned and assembled by myself, as

shown in Figure 2.10. The gases used were 5 % acetylene/argon, 5% hydrogen chloride/argon and argon as balance. Gases would first flow through moisture traps (Agilent, CP17971) to reduce the amount of moisture entering the rig, to prevent corrosion of the stainless-steel components when exposed to HCl. Where possible, inert PFA (perfluoroalkoxy) tube fittings were used in place of stainless steel. All flows were regulated using electronic mass flow controllers (Brookes, GF40, Ar 0 – 100 mL/min, acetylene and HCl 0 – 50 mL/min). Reactant gases could flow to the reactor when at temperature, or by-pass the reactor during ramping, in which case argon alone would flow through the reactor. The gases would then flow to the detector – primarily a gas chromatograph but for certain analyses also a mass spectrometer. Exit gases were bubbled through a basic solution to neutralise excess HCl and trap any VCM before being vented.

The reactor was made up of a quartz tube (230 x 6 mm), clamped in place inside a vertical tube furnace (Carbolite, MTF 10/15/130). The reactor was made of quartz to remove the possibility of the reaction gases interacting with stainless steel at high temperature. The catalyst would sit in the centre of the quartz tube, fixed by 1 cm of glass wool placed above and below. The temperature of the reactor was monitored during heating and throughout the reaction using a K-type thermocouple.

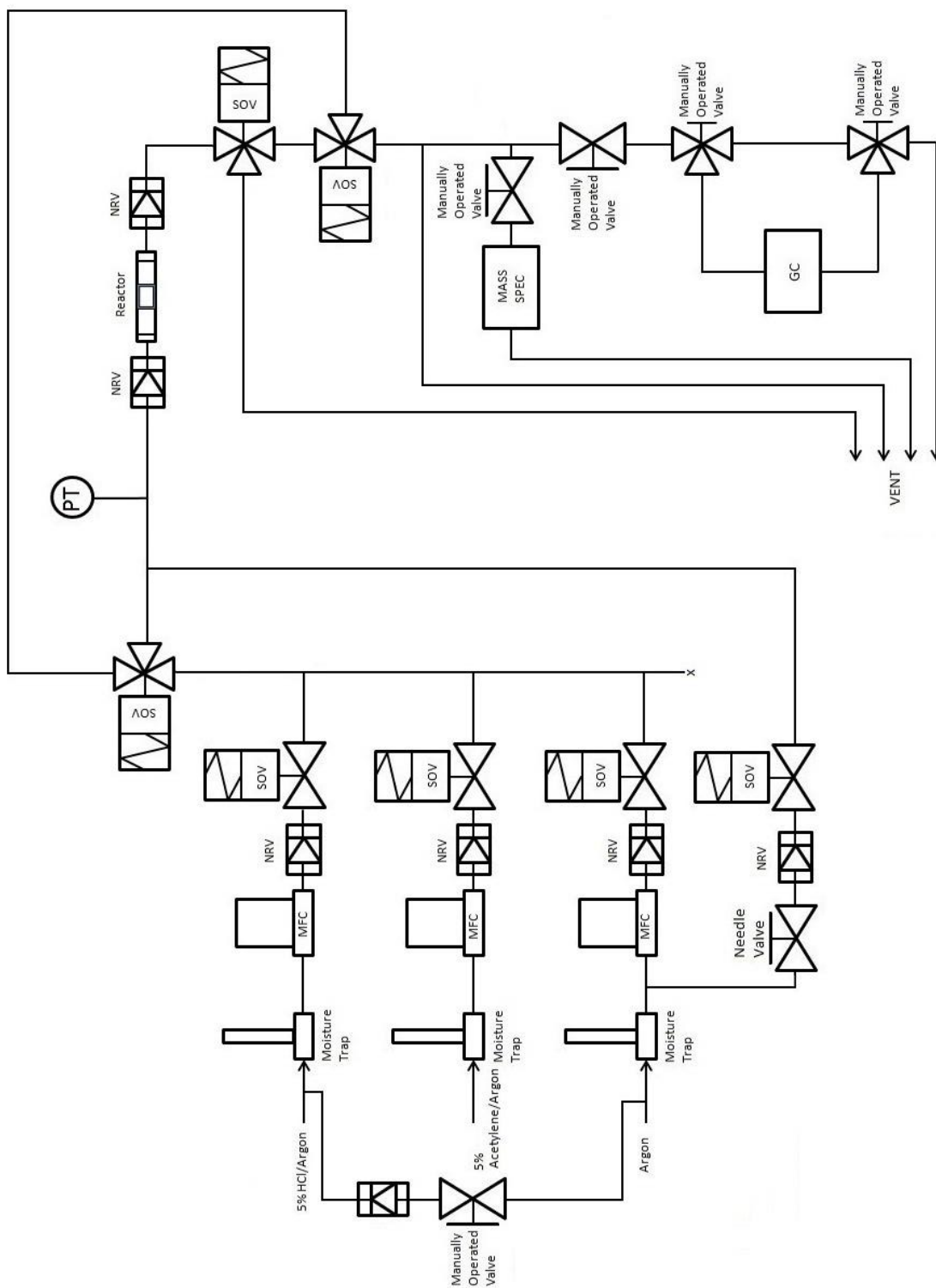


Figure 2.10. Schematic diagram of the acetylene hydrochlorination reactor. NRV = no-return valve, PT = pressure transducer and SOV = solenoid operated valve.

Experimental

Blank analysis was first carried out using a mixture of 5 % acetylene/argon, 5 % HCl/argon and

argon to achieve a 1:1.02 acetylene:HCl ratio and total flow of 50 mL/min. In a standard reaction, 0.089 g of catalyst was heated at 5 °C/min from room temperature to 200 °C under a 50 mL/min flow of argon. 200 °C was chosen to produce acetylene conversions of ~20 % with the Au/C catalyst based on previous temperature studies performed within the group.²⁰ When performed at temperatures other than 200 °C, the reaction temperature is noted in the text. Once at temperature, the flow of reaction gases was directed through the heated catalyst bed and analysed on-line with GC. Post reaction, catalysts were allowed to cool under a 50 mL/min flow of argon. All time-on-line data was reported with a ±1 % acetylene conversion, determined by repeat analysis with the same catalyst (1 % Au/C-Acetone and 1 % Au/C-AR) under the same reaction conditions.

2.6. References

- 1 S. Brunauer, P. H. Emmett and E. Teller, *J. Am. Chem. Soc.*, 1938, **60**, 309–319.
- 2 D. Dollimore, P. Spooner and A. Turner, *Surf. Technol.*, 1976, **4**, 121–160.
- 3 A. Pantelouris, G. Küper, J. Hormes, C. Feldmann and M. Jansen, *J. Am. Chem. Soc.*, 1995, **117**, 11749–11753.
- 4 B. Ravel and M. Newville, *J. Synchrotron Radiat.*, 2005, **12**, 537–541.
- 5 M. Newville, *J. Synchrotron Radiat.*, 2001, **8**, 322–324.
- 6 D. Attwood, *Soft X-rays and Extreme Ultraviolet Radiation*, Cambridge University Press, Cambridge, 1st edn., 2017.
- 7 L. C. Feldman and J. W. Mayer, *Fundamentals of surface and thin film analysis*, P T R Prentice Hall, 1986.
- 8 F. G. Kitson, B. S. Larsen and C. N. McEwen, *Gas chromatography and mass spectrometry*, Academic Press, 1996.
- 9 J. Zhao, J. Xu, J. Xu, J. Ni, T. Zhang, X. Xu and X. Li, *Chempluschem*, 2015, **80**, 196–201.
- 10 M. Conte, A. F. Carley, G. Attard, A. A. Herzing, C. J. Kiely and G. J. Hutchings, *J. Catal.*, 2008, **257**, 190–198.
- 11 P. Johnston, N. Carthey and G. J. Hutchings, *J. Am. Chem. Soc.*, 2015, **137**, 14548–14557.
- 12 W. Clarke, *Mass Spectrom. Clin. Lab.*, 2017, 1–15.
- 13 A. K. Singh, *Experimental Methodologies for the Characterization of Nanoparticles*, Academic Press, 2016.
- 14 A. Villa, N. Dimitratos, C. E. Chan-Thaw, C. Hammond, G. M. Veith, D. Wang, M. Manzoli, L. Prati and G. J. Hutchings, *Chem. Soc. Rev.*, 2016, **45**, 4953–4994.
- 15 W. H. Bragg and W. L. Bragg, *Proc. R. Soc. A*, 1913, **17**, 428–438.
- 16 A. L. Patterson, *Phys. Rev.*, 1939, **56**, 978–982.
- 17 F. T. L. Muniz, M. A. R. Miranda, C. Morilla dos Santos and J. M. Sasaki, *Acta Crystallogr. Sect. A Found. Adv.*, 2016, **72**, 385–390.
- 18 M. Inagaki, in *Handbook of Advanced Ceramics*, ed. S. Somiya, Academic Press, 2nd edn., 2013, pp. 25–60.
- 19 M. Pawlyta, J.-N. Rouzaud and S. Duber, *Carbon N. Y.*, 2015, **84**, 479–490.
- 20 C. J. Davies, *PhD Thesis*, 2012, Cardiff University.

3. Carbon supported single-site gold catalysts prepared using low polarity solvents, for the acetylene hydrochlorination reaction

3.1. Introduction

In this chapter, the use of different solvents for the preparation of heterogeneous single site catalysts for the acetylene hydrochlorination reaction will be explored. A single-site heterogeneous catalyst is defined as: “A catalyst constituted by a metal atom, ion, or small cluster of atoms, held by surface ligands to a rigid framework”.¹

Single site catalysts are typically prepared with a low metal loading; too high and the support will become saturated with metal, leading to nanoparticle formation. Recent advances in the preparation of these catalysts means that loadings of 2.0 wt. % or more can be achieved whilst maintaining a homogeneous single site dispersion.² The use of sub-nanometer precious metal catalysts has already been proven to be more active than its nanometer or larger sized counterparts for several reactions, such as alkynol hydrogenation and CO oxidation³⁻⁵, indicating that the specific activity of metals increases with decreasing metal particle size. Ensuring that the coverage is purely single site is crucial as an inhomogeneous mixture of sizes will reduce the metal atom efficiency and can lead to sometimes unwanted side reactions.^{6,7} From an industrial point of view, it is financially beneficial to maximise the efficiency of a catalyst prior to commercial application. Single site catalysts offer, by definition, the highest atom efficiency achievable and therefore the maximum output from expensive precious metal catalysts.

Single site gold catalysts have been used for several reactions such as water-gas shift⁸⁻¹⁰, methanol steam reforming¹¹, ethanol dehydrogenation¹², and CO oxidation.¹³⁻¹⁵ These catalysts, as well as those using other precious metals, have been prepared using a variety of different methods; some which are pH dependent (deposition precipitation¹⁶) some specific to certain supports such as carbon (pyrolysis synthesis¹⁷) others adapted for low surface area supports (mass-selected soft-landing¹⁸), with many more widely reported in literature.¹⁹ In each case it is important to choose an appropriate support for the catalyst.²⁰ Differences in the surface area, structure and defects will result in different interactions with the metal atoms which will impact the catalytic activity.¹⁹ At such small particle/atom sizes, the surface free energy of the metals will be large,²¹ thereby promoting the aggregation of small atoms and clusters. Many single atom catalysts sinter via Ostwald ripening and particle migration and coalescence.²² Therefore, it is important to choose an appropriate support to minimise this effect, typically one that has a high

surface area and is suitably robust to anchor the metal.^{13,19} Herein, the support used was activated carbon, chosen due to its low cost, high surface area, and high stability under acidic, high temperature conditions.²³

The focus of this chapter was to find an alternative solvent to aqua regia for the preparation of gold on carbon catalysts. Previous work performed by this group focused on aqua regia, as detailed in **3.2**, as this solvent facilitates a high dispersion of oxidised atomic gold on the carbon support, resulting in a high catalytic activity.^{24–27} In the pursuit of alternatives, literature describes the use of solvents such as organic aqua regia – a mixture of thionyl chloride (SOCl₂) and organic solvents/reagents (pyridine, N,N - dimethylformamide, and imidazole).²⁸ Organic aqua regia was an improvement over traditional aqua regia as it was shown to be able to selectively dissolve different metals by changing the organic reagent and conditions, useful for selective recovery of metals from bimetallic catalysts or for microelectronic applications.²⁹ This solvent has been applied to the preparation of gold on carbon catalysts, resulting in improved performance for the acetylene hydrochlorination reaction compared with those prepared using aqua regia;³⁰ however, both traditional and organic aqua regia are still highly oxidising, toxic solvents, not considered to be environmentally friendly nor suitable for commercial application. Therefore, the use of alternative simple, non-oxidising nor acidic solvents were investigated as alternatives.

3.2. Single site gold catalysts prepared with aqua regia

Aqua regia (3:1 HCl : HNO₃) has been used to dissolve gold since the 8th century. Using this solvent, bulk gold is first oxidised by nitric acid to Au(III), followed by reaction with HCl to form tetrachloroaurate anions (AuCl₄⁻). In such an acidic environment, the anions are readily protonated to form chloroauric acid (HAuCl₄). Chloroauric acid was the starting compound used in the preparation of the gold catalysts discussed in this thesis.

Aqua regia has been used as the solvent for the preparation of gold on carbon catalysts owing to its oxidising nature. This inhibits the reduction of gold on the highly reducing carbon support surface. Comparing the use of aqua regia as a solvent to its constituent acids, HNO₃ and HCl, aqua regia produces catalysts with a higher acetylene conversion.^{24,25} This is as a result of both the oxidising HNO₃, maintaining the gold as a mixture of Au(III) and Au(I), and the nucleation ability of Cl⁻ anions of HCl for gold clusters, providing bonding sites for the gold to carbon.^{25,31} Both of these factors result in a high dispersion of homogeneous oxidised gold atoms on the carbon support.²⁶ This ideal catalyst for the acetylene hydrochlorination reaction has been used for the *in-situ* and *ex-situ* study of the gold species on the catalyst^{26,27,32–35} and serves as a good

comparison catalyst for those discussed in the following results chapters.

3.3. Experimental conditions

All catalysts were prepared to a theoretical 1 wt. % Au loading on carbon. All reactions were performed using the following conditions unless stated otherwise: C₂H₂ : HCl = 1:1.02, total gas flow of 50 mL min⁻¹, 0.09 g catalyst, temperature 200 °C, ambient pressure.

3.4. Catalysts prepared with different polarity solvents

Solvents with a wide range of polarities and able to dissolve chloroauric acid were chosen for the preparation of 1% Au/C catalysts, as listed in Table 1. The name of each catalyst is denoted Au/C-*solvent* for clarity. Catalysts were prepared by wet impregnation, as described in Chapter 2 (2.3.1).

Table 3.1. List of solvents and respective polarities, boiling points and the type of solvent used.

Solvent	Polarity ($E_T(30)$) (kcal mol ⁻¹)	Boiling Point (°C)	Dried solvent
H ₂ O	63.1	100	
Methanol	55.5	64	✓
Ethanol	51.8	78	✓
1-Propanol	50.7	97	
1-Butanol	50.2	118	
2-Propanol	48.6	82	✓
2-Butanol	47.1	108	✓
Acetone	42.2	57	✓
2-Butanone	41.3	80	✓
Ethyl Acetate	38.1	77	✓
Tetrahydrofuran	37.4	66	✓
Diethyl Ether	34.6	35	✓
Aqua regia	-	140	

Each catalyst was tested under the reaction conditions stated in section 3.3; a representative time-on-line profile of the 1 % Au/C-AR catalyst is shown in Figure 3.1. The maximum initial conversion (within first 30 min of reaction) of the different solvent polarity catalysts was

recorded, as shown in Figure 3.2. The polarity of each solvent was assigned according to the $E_T(30)$ scale, defined as the molar electronic transition energy of N-phenoxide betaine dye dissolved in solvent, measured in kcal mol^{-1} .^{36,37} According to this scale, which encompasses more than 300 organic solvents,³⁶ a high value of $E_T(30)$ signifies a high solvent polarity. Aqua regia has no recorded $E_T(30)$ value because it is a mixture of two solvents.

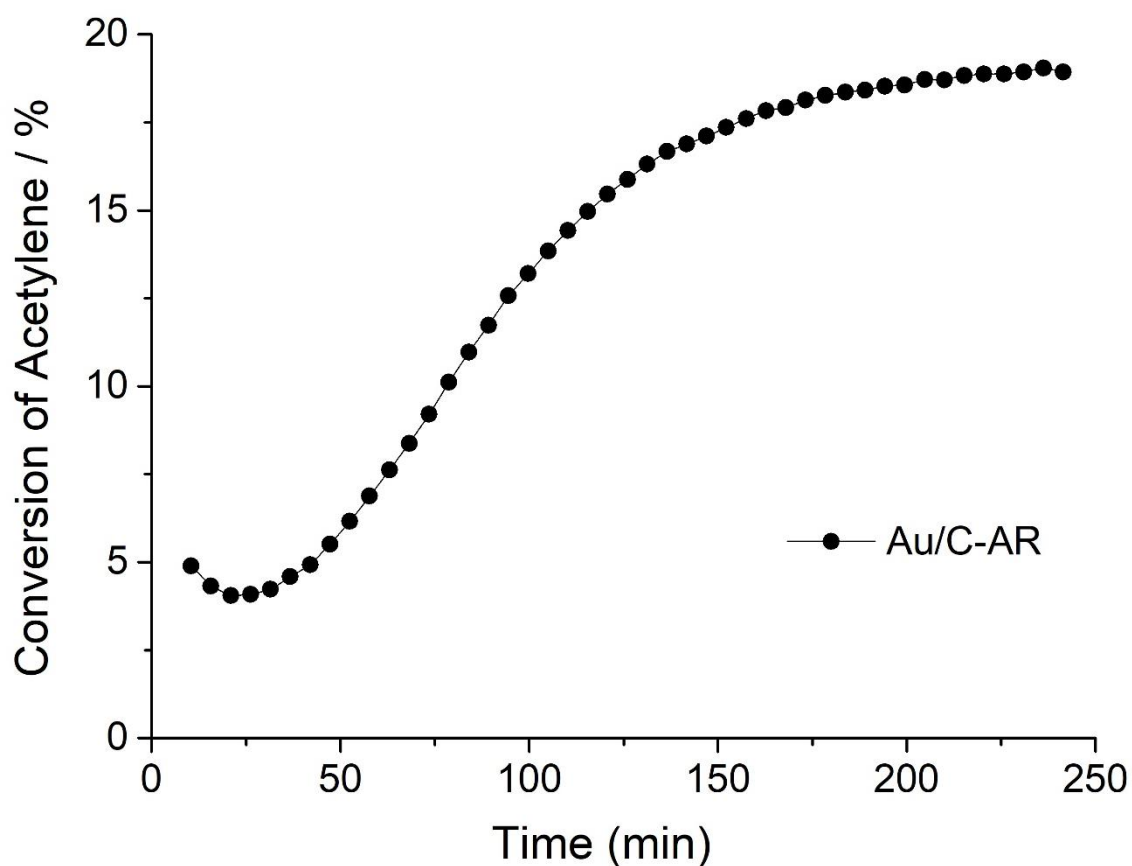


Figure 3.1. Time-on-line profile of 1 % Au/C-AR. Reaction conditions as stated in section 3.3.

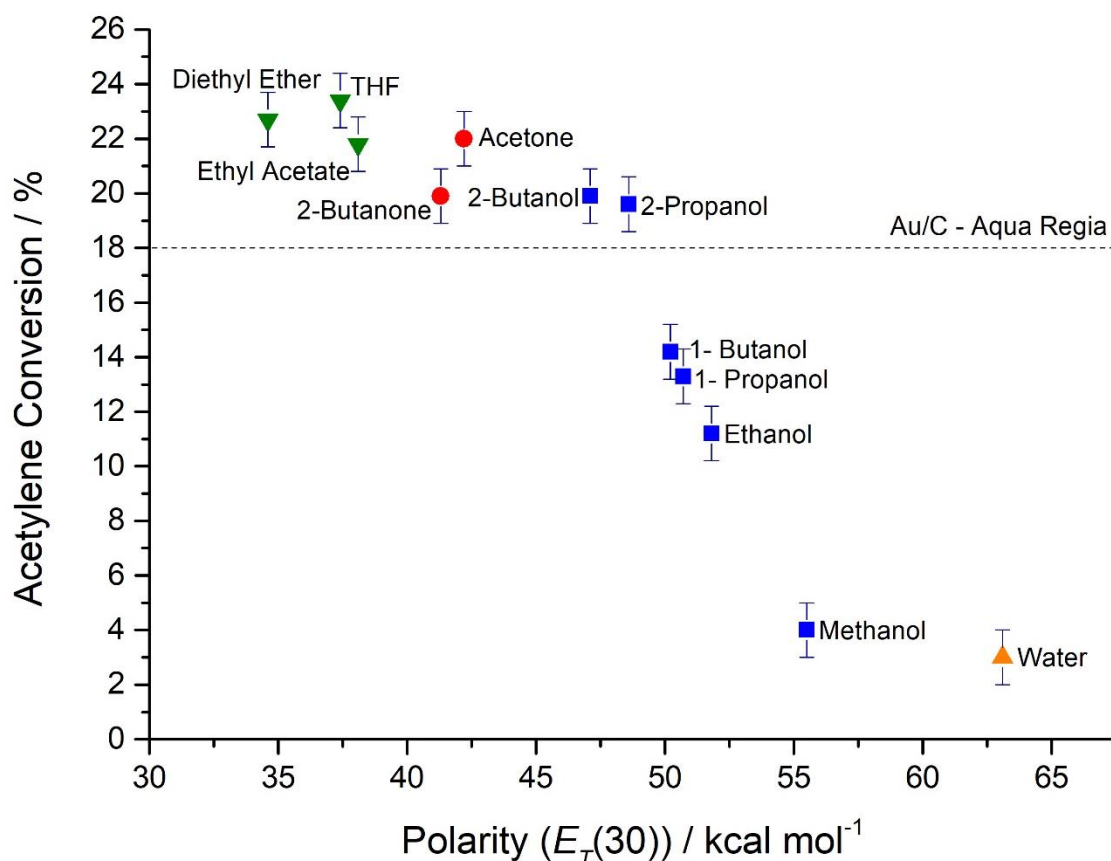


Figure 3.2. Steady state acetylene conversion of 1% Au/C catalysts prepared by wet impregnation of HAuCl_4 from various alcohol (■), ketone (●), ether (▼) and aqueous solvents (▲); the dashed line indicates the activity of the previously prepared Au/C-Aqua regia catalyst, under conditions stated in 3.3.

Initially, the conversion increases as the polarity of the solvents decreases until reaching a plateau (around 20-24% of conversion) when using solvent with polarity below 49 kcal mol⁻¹ (observed at 2-propanol). Notably, these conversions are slightly higher than observed for the catalyst prepared with aqua regia (denoted by a dashed line on the figure). This shows that, by using simple, neither highly oxidising nor acidic solvents, an active catalyst can be prepared which out-performs that prepared using aqua regia.

The similar conversion of the catalysts prepared with polarities below 49 kcal mol⁻¹ was attributed to the limit of dispersion of the gold-chloride species on the surface of the carbon at a 1 wt. % metal loading. X-ray diffraction was used to observe the nucleation of gold observed in some of the catalysts. Figure 3.3 shows that, as the polarity of the solvent decreases, the intensity of the reflections corresponding to gold nanoparticles also decreases, indicating and overall reduction in size and quantity of gold nanoparticles. There are no observable reflections in the catalysts prepared at the lowest polarities, consistent with a high dispersion of gold and hence no gold agglomerations of gold larger than clusters present. There are two possible explanations as to why the low polarity solvent catalysts have such high activity. These are; the

drying temperature required when preparing the catalyst and the amount of water present in the solvent. Both factors are explored in the next section.

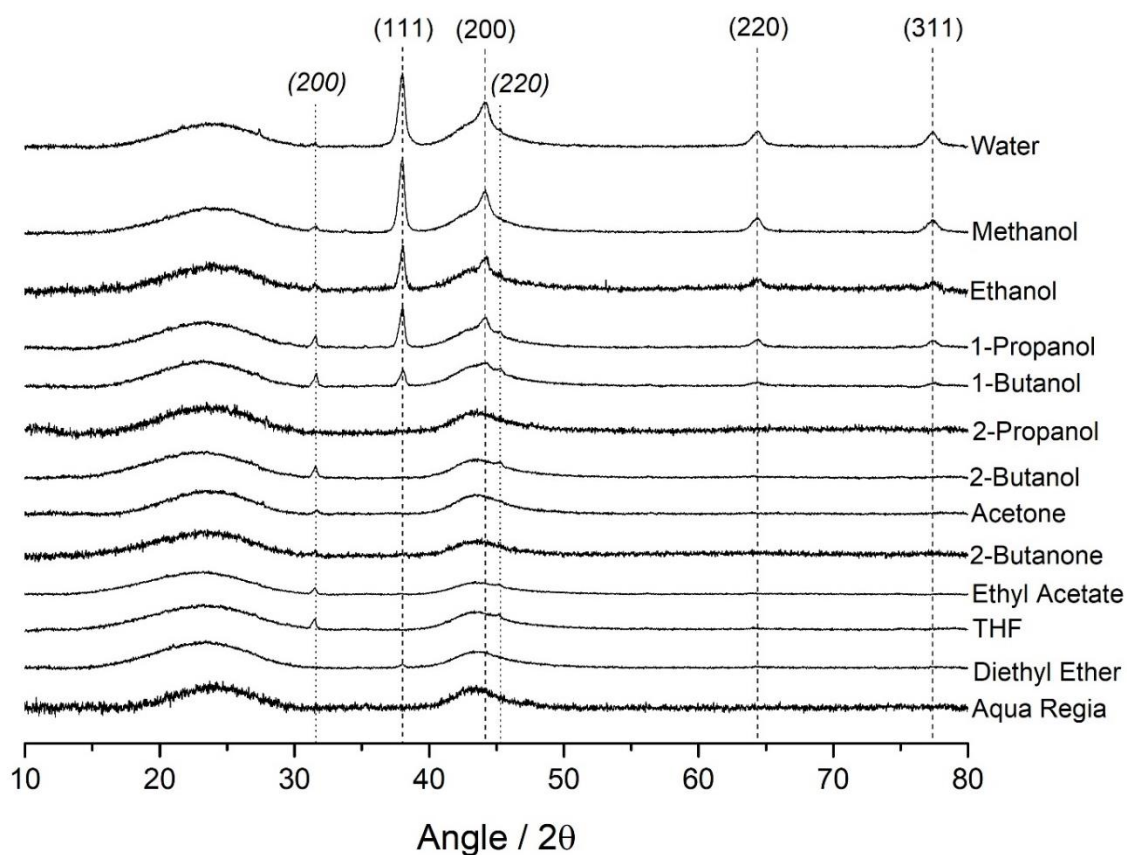


Figure 3.3. XRD patterns of all catalysts prepared with different solvents. Reflections at 38, 44, 65 and 78 / 2θ correspond to FCC metallic gold crystallites. Reflections at 32 and 46 / 2θ correspond to NaCl CCP crystallites.³⁸

3.5. Effect of drying temperature on catalytic activity

To investigate the effect of drying temperature on catalytic activity, three other low polarity solvents were used to prepare catalysts; DMSO, DMF and cyclohexanone. These solvents each had a higher boiling point than that of aqua regia and would therefore require a higher drying temperature during catalyst preparation. These solvents and their respective polarities, boiling points, drying temperatures and acetylene conversions of the catalysts prepared are listed in Table 3.2.

Table 3.2. Acetylene conversion values for low polarity, high boiling point solvents.

Catalysts	Polarity ($E_T(30)$) (kcal mol ⁻¹) ³⁷	Boiling Point (°C)	Drying temperature (°C)	Conversion of Acetylene (%)
Au/C - DMSO	45.0	189	195	14
Au/C - DMF	43.8	154	160	8
Au/C - Cyclohexanone	40.8	155	160	3
Au/C - Acetone	42.2	56	40	22
			140	27

These catalysts have a range of acetylene conversions, higher than or equivalent to that of the catalyst prepared with aqueous solvent (3 %, Figure 3.2); however, each performed worse than the catalysts of similarly low solvent polarities, such as 2-butanol, acetone and 2-butanone. The XRD patterns of these fresh catalysts shows the presence of gold nanoparticles which could account for the poor conversion, Figure 3.4.

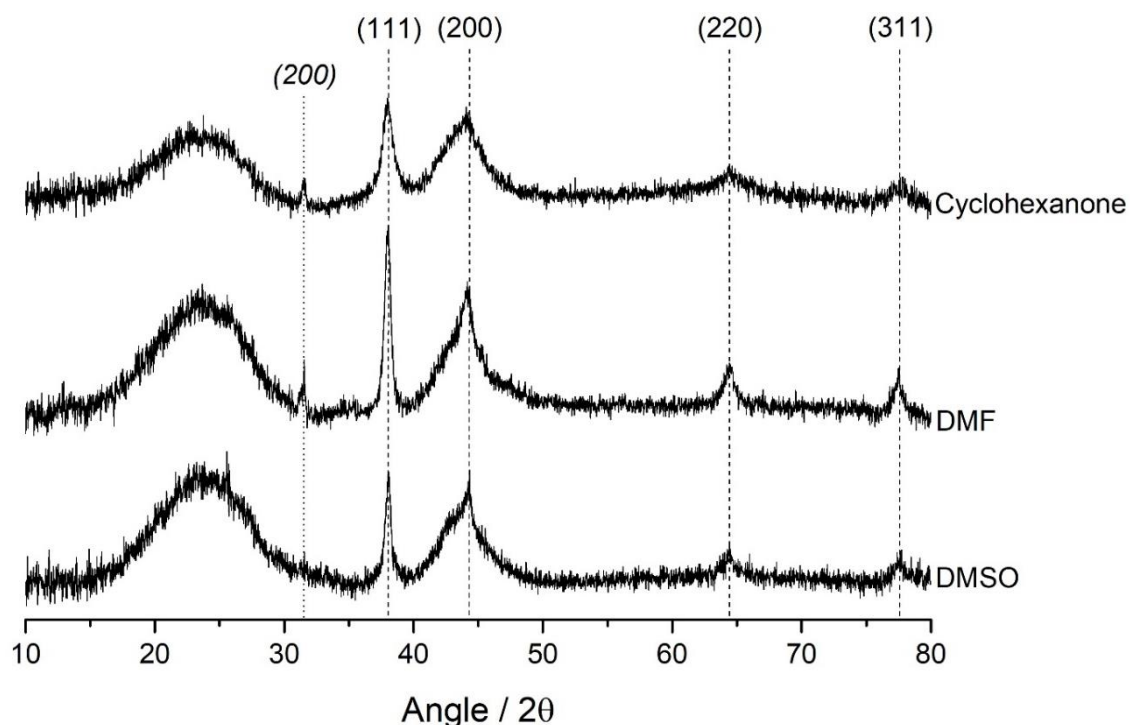


Figure 3.4. XRD patterns of the Au/C-Cyclohexanone, Au/C-DMF and Au/C-DMSO catalysts after 240 min of reaction. Reflections at 38, 44, 65 and 78 / 2θ correspond to FCC metallic gold crystallites. Reflections at 32 / 2θ correspond to NaCl CCP crystallites.³⁸

In order to determine if the drying temperature alone caused the agglomeration of gold nanoparticles, a catalyst was prepared using acetone as the solvent and dried at 140 °C; this solvent was chosen as it was cheap, non-harmful, readily available in the lab and the prepared catalyst had a stable conversion of 22 % when dried at 40 °C, similar to other catalysts prepared with low polarity solvents. As noted in Table 3.2, the initial conversion (maximum conversion within the first 30 min of reaction) of this catalyst (27 %) is higher than that of the catalyst prepared with acetone and dried at 40 °C (22 %) (Figure 3.5). However, the catalyst slowly deactivates during the 4 h reaction, resulting in a final, still decreasing conversion of 19 %.

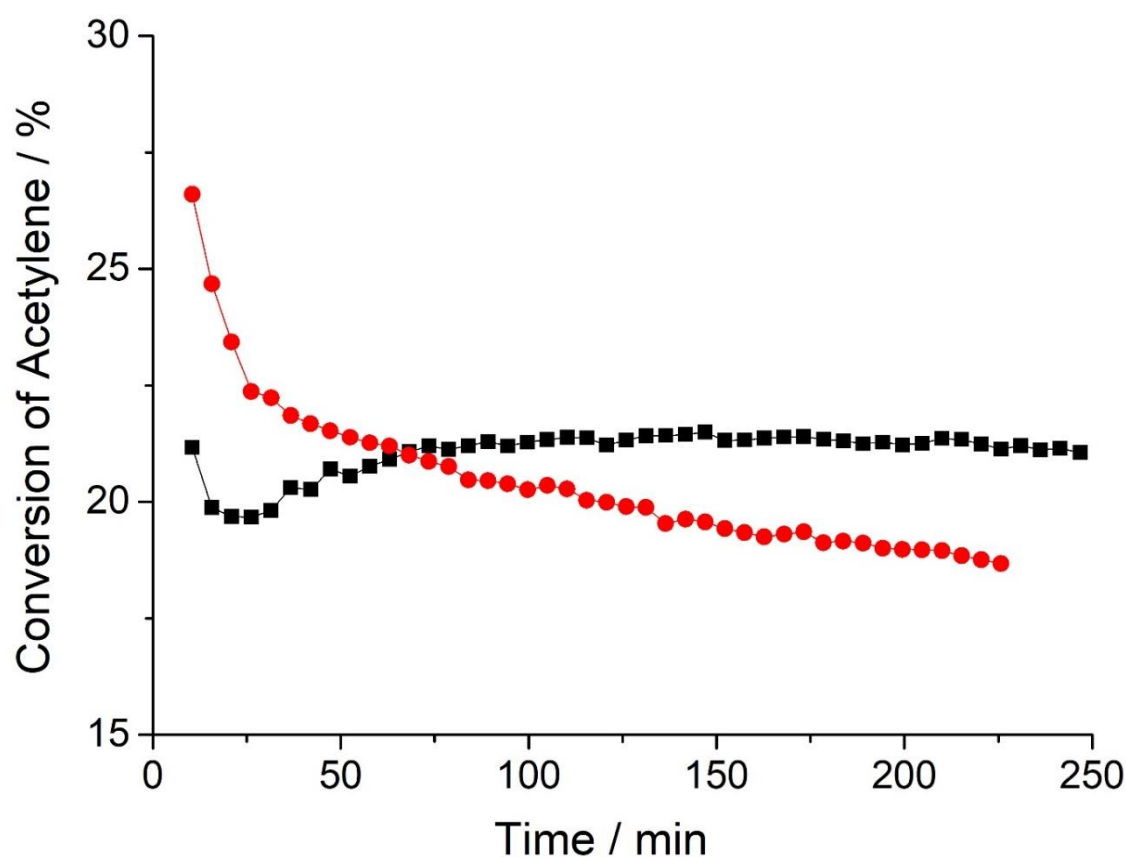


Figure 3.5. Time-on-line of Au/C-Acetone prepared at 45 °C (■) and 140 °C (●), under conditions stated in 3.3.

The XRD pattern (Figure 3.6) of the fresh catalyst shows nanoparticles are present. These become more ordered and crystalline after testing, shown by the growth and sharpening of the reflections corresponding to gold. The gold crystallite sizes were calculated using the Scherrer equation, with reference to a silicon standard. The size of the crystallites increased from 3 to 8 nm, confirming a small degree of agglomeration occurred during the reaction. Therefore, the presence of gold nanoparticles is itself not indicative of a low activity catalyst but perhaps a

contributing factor; in this case, the nanoparticles may result in lower stability shown by the steady decrease in conversion observed in this reaction. This highlights the need for an appropriate drying temperature for each solvent used; too high and gold will sinter during the drying process, leading to lower catalyst stability. Further investigation into catalyst stability was conducted, focusing on the oxidation state of the gold, discussed in section 3.7.

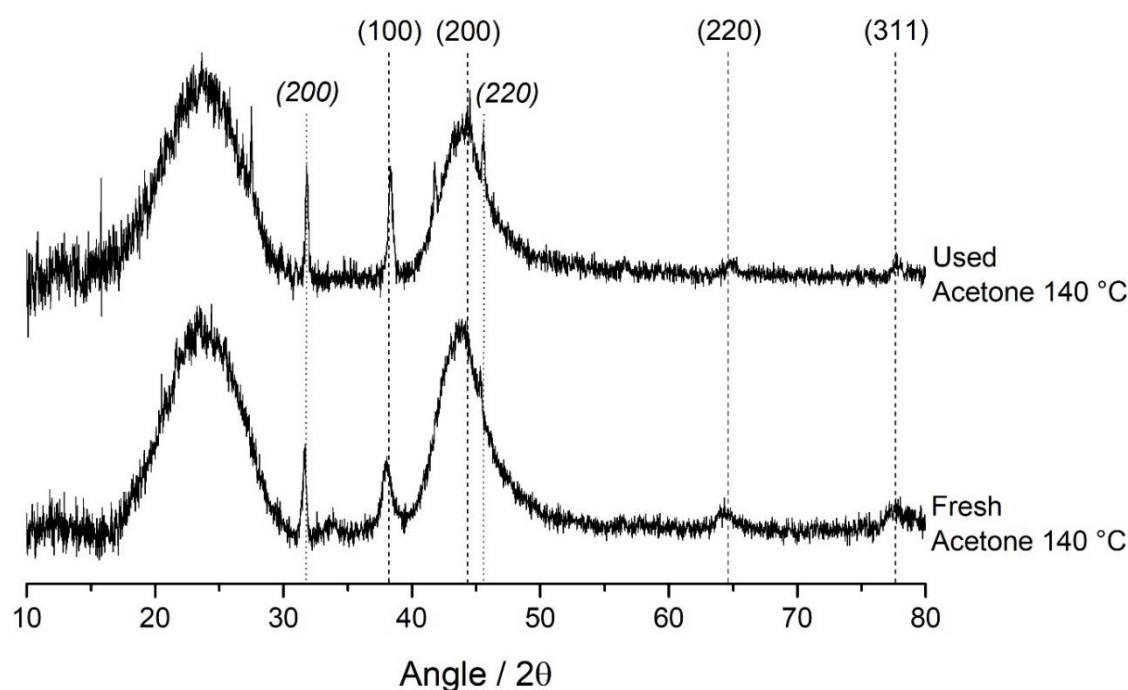


Figure 3.6. XRD patterns of fresh and used (reacted for 4 h) Au/C-Acetone catalyst dried at 140 °C. Reflections at 38, 44, 65 and 78 / 2θ correspond to FCC metallic gold crystallites. Reflections at 32 / 2θ correspond to NaCl CCP crystallites.³⁸

3.6. Effect of water introduced in preparation on catalytic activity

To determine the effect of water-containing solvents on the catalytic performance, catalysts were prepared using a water:acetone mix, with an increasing concentration of water; 0, 5, 10, 20, 50 and 100 %. Extra dry acetone was used to ensure there was no water present in the solvent before preparing the acetone:water mix.

Figure 3.7 shows the acetylene conversion versus water content. As the water content was increased, the conversion decreased until 50 %, where the catalytic activity was comparable to that of the catalyst prepared using water alone (100 %). These conversion values are comparable to that of carbon with no gold present and carbon impregnated with acetone (both 2.0 %). Previous tests have shown that preparing gold on carbon catalysts using water as a solvent

resulted in the formation of gold nanoparticles, which are inactive for the acetylene hydrochlorination reaction.²⁶ To confirm if this was the cause of the observed decreasing in conversion, XRD analysis of all fresh samples was performed, as well as carbon impregnated with acetone and dried, with no gold present, for reference (Figure 3.8).

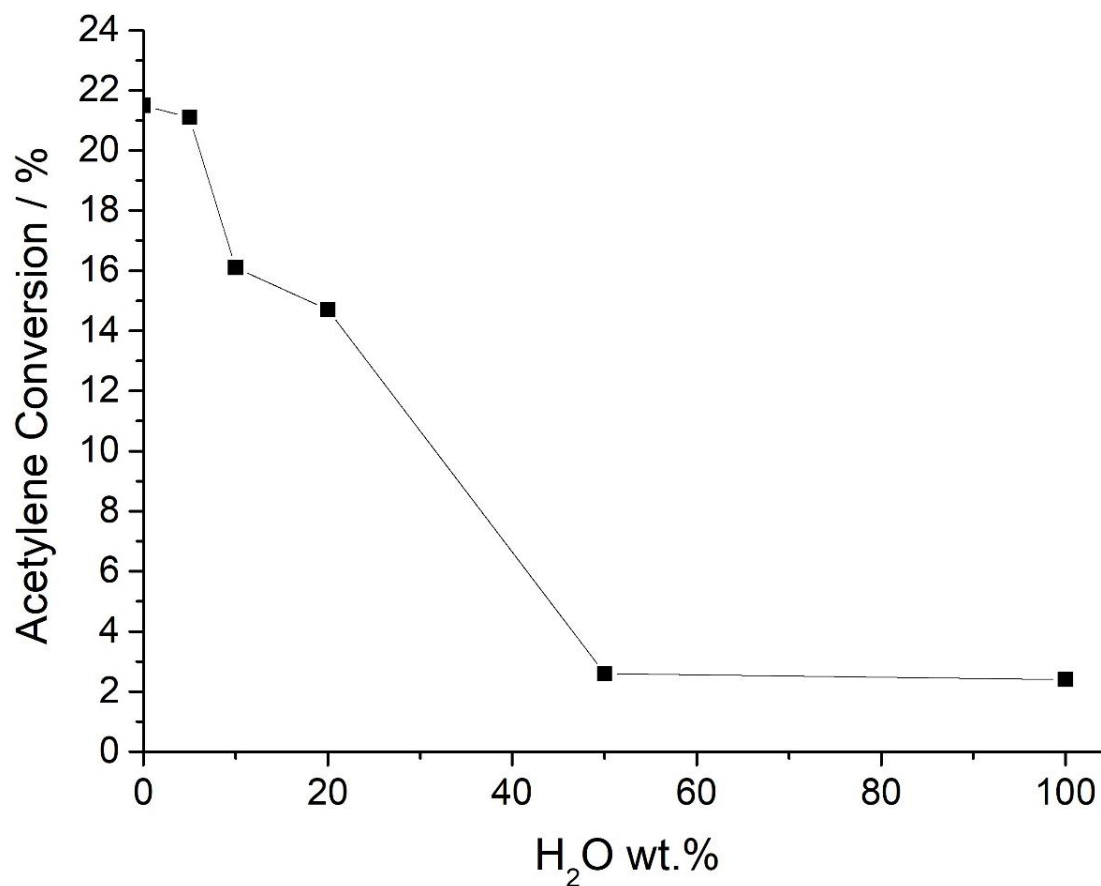


Figure 3.7. Plot of water content vs conversion for Au/C-Acetone catalysts after 240 of reaction, under conditions stated in 3.3.

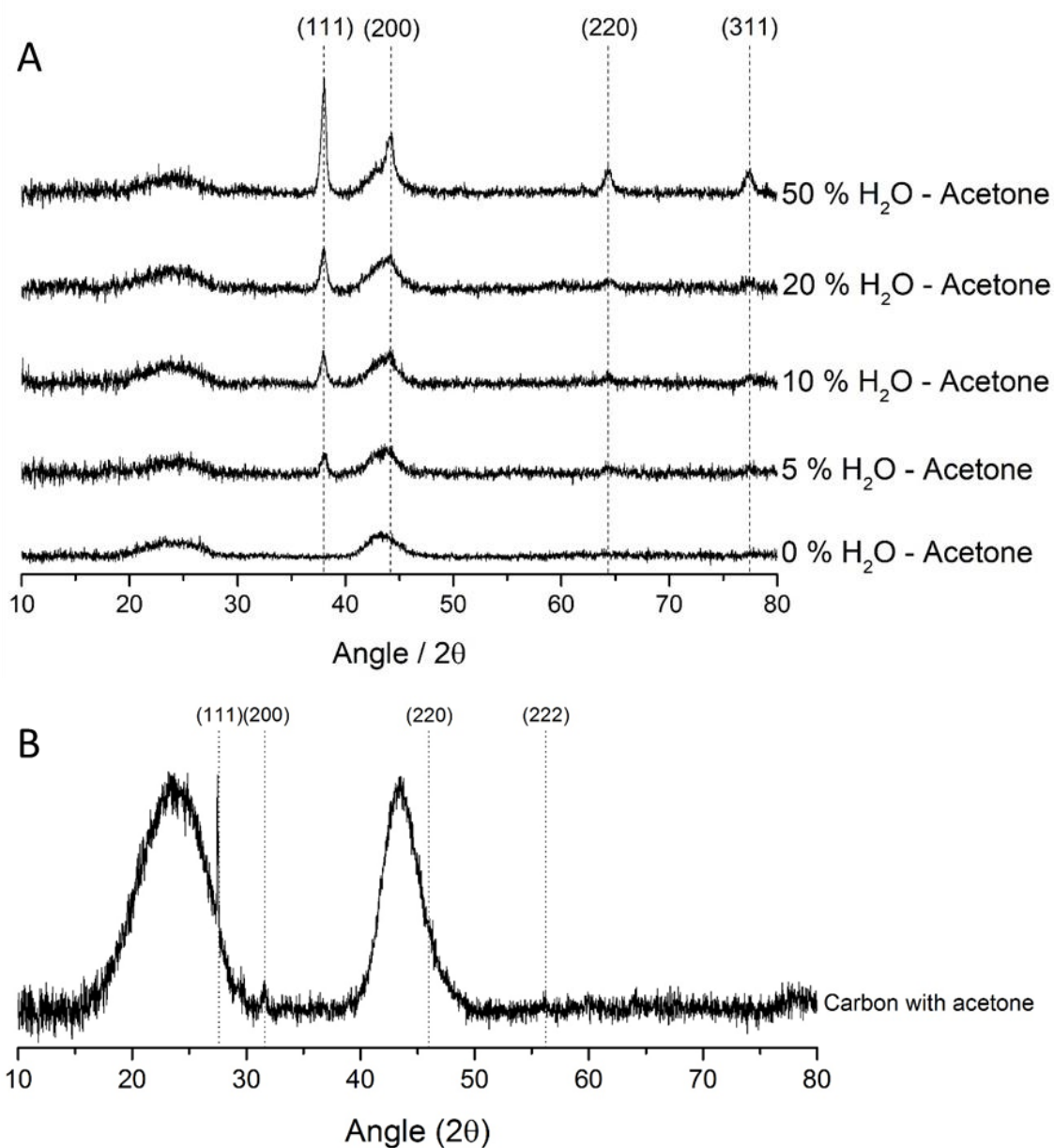


Figure 3.8. A: XRD patterns of catalysts prepared with increasing water concentration. Reflections at 38, 44, 65 and 78 / 2θ correspond to FCC metallic gold crystallites. B: XRD pattern of carbon impregnated with acetone. Reflections at 27, 32, 46 & 57 / 2θ correspond to NaCl.³⁸

The reflections attributed to gold nanoparticles increase in height as the water content increases. This is indicative of an increase in nanoparticle size, confirmed using the Scherrer equation; the calculated nanoparticle size for the catalyst prepared with 50 % water:acetone was 18 nm. Once 50 % water:acetone is reached, the acetylene conversion remains constant; therefore, it was assumed that the majority of the gold was reduced to Au(0) and any remaining surface coverage of oxidised gold was insufficient to maintain a higher conversion. The increasing size of gold nanoparticles at higher water content solvents confirmed the need for solvents to be water-free.

In order to better appreciate how little water is needed to affect the stability of the gold, STEM analysis was conducted on Au/C-Acetone catalysts prepared with two different solvents; HPLC-grade acetone and extra dry acetone. HPLC-grade acetone contains $\leq 0.1\%$ water, whereas ultra-dry acetone, sealed in a nitrogen purged bottle, contains a maximum of 0.005% water, as determined by coulometric testing.^{39,40} The microscopy images of the Au/C-HPLC Acetone catalyst shows mostly atomically dispersed gold (Figure 3.9A), with nanoparticles in areas (red arrows), some in the order of 100 nm (Figure 3.9B). Prolonged exposure to the beam, needed to adjust the magnification and resolution to acquire clear images, would have contributed to the agglomeration of gold to larger nanoparticles, though would not be solely responsible for sizes as large as 100 nm. A comparison of two points of the catalyst, using EDS, indicates that a homogeneous dispersion of atomic gold was present throughout the catalyst (box 1 in Figure 3.10A, labelled Support in Figure 3.10B), as noted by several peaks at energies corresponding to Au excitation present in the EDS. This analysis also confirmed that the large nanoparticles are comprised of gold (box 2 in Figure 3.10A, labelled Au NP in Figure 3.10B). Conversely, the Au/C-Ultra dry acetone catalyst was formed predominantly of atomically dispersed gold, with small areas of gold clusters (Figure 3.11A). Although there were some nanoparticles present, all were smaller than 5 nm (Figure 3.11B). These results show that even small quantities of water, introduced during the preparation of the catalyst, can cause large agglomeration of gold which can detrimentally affect the catalytic activity.

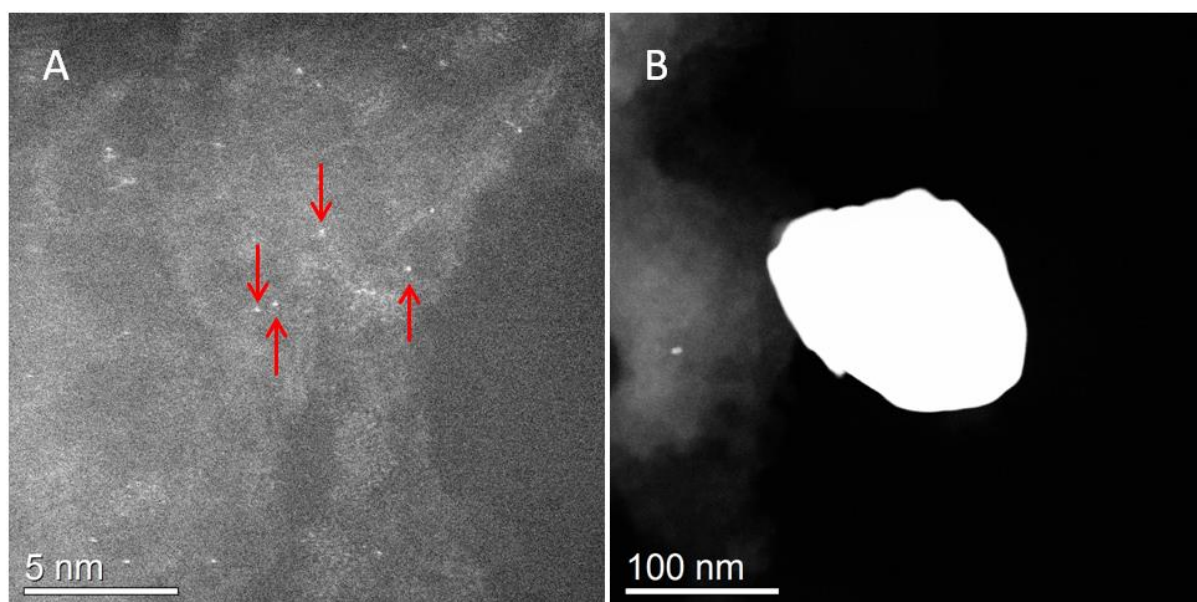


Figure 3.9. Representative STEM-HAADF images of Au/C-HPLC Au/C-Acetone catalyst.

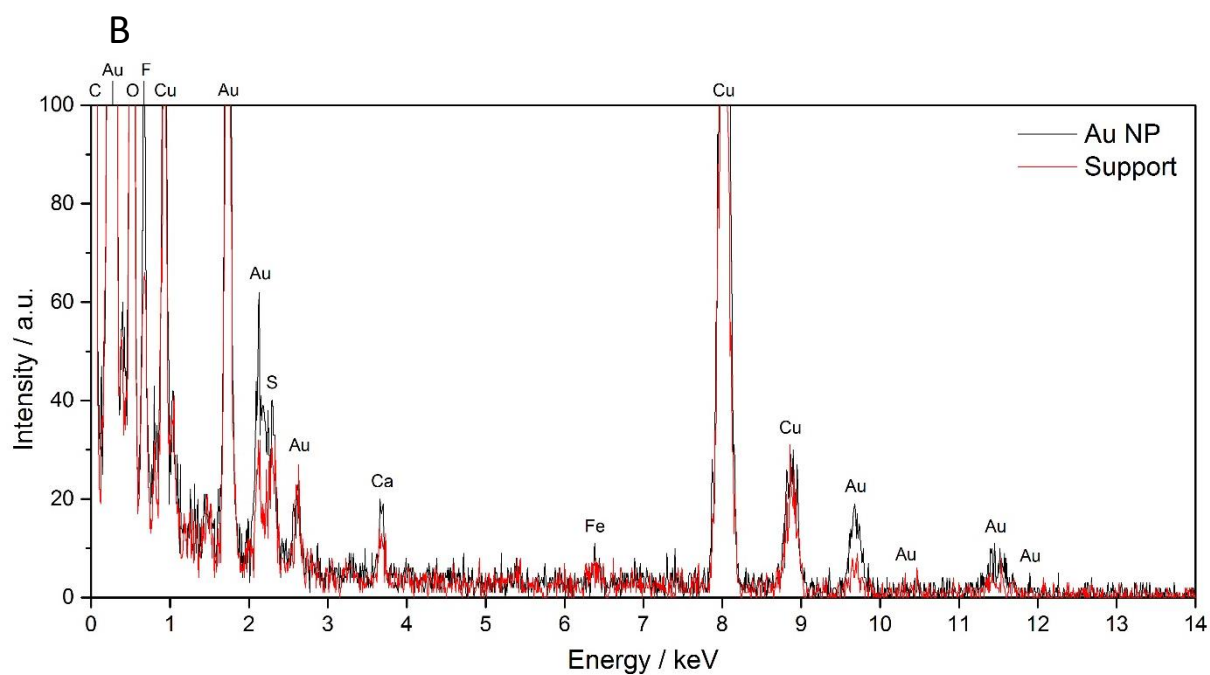
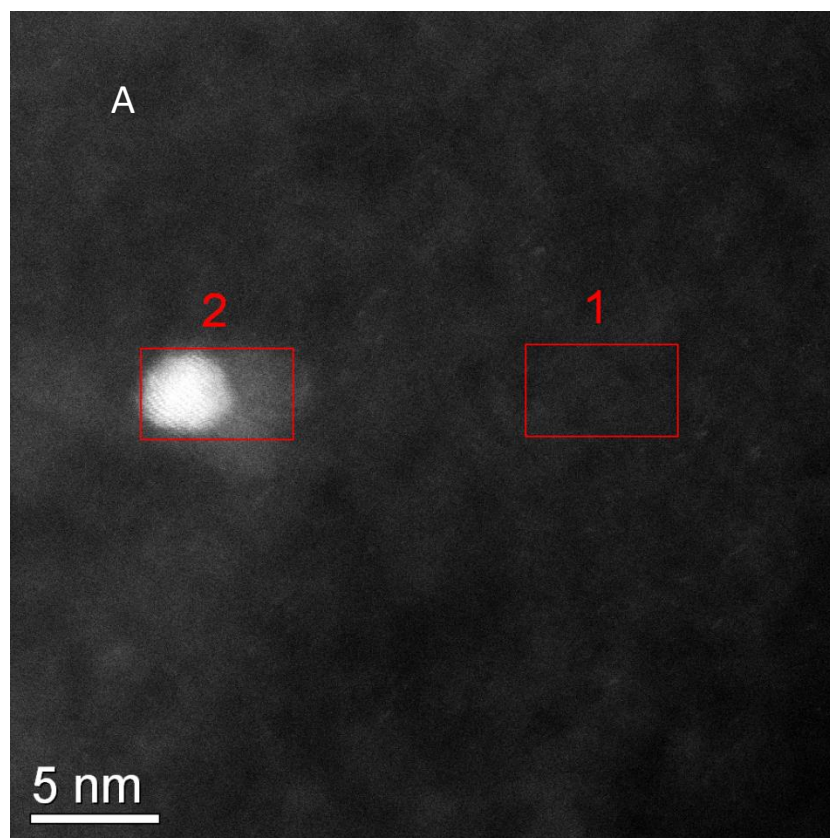


Figure 3.10. (A) Representative STEM-HAADF image and (B) corresponding EDS of Au/C-HPLC Acetone catalyst – 1 encompassing predominantly carbon support and 2 encompassing a gold nanoparticle.

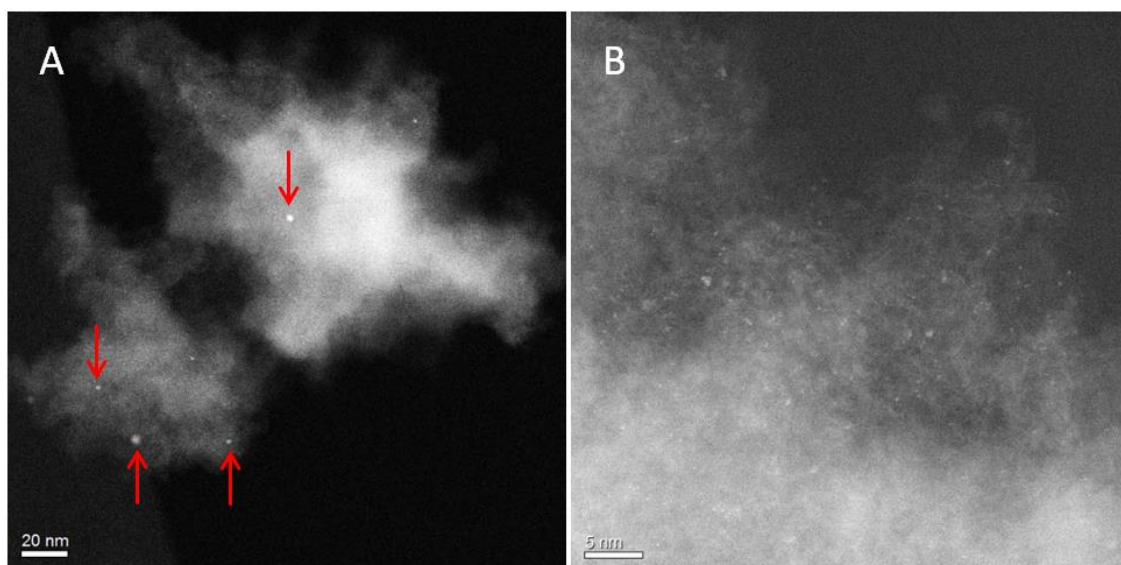


Figure 3.11. Representative STEM-HAADF image of Au/C-Ultra dry acetone catalyst.

3.7. Investigation of the catalyst stability

Stability is an important factor in the field of catalysis; by definition a catalyst should not be consumed during a reaction, therefore it must be reusable. To check the stability of the Au/C-Acetone catalyst, a reaction was carried out over two consecutive days. In this test the catalyst was heated to 200 °C in argon, subject to reaction conditions for 4 h, then cooled in argon. The following day this procedure was repeated, and the catalyst reacted for a further 3 h. For comparison, the same experiment was also carried out using the Au/C-Aqua regia catalyst. The results are shown in Figure 3.12.

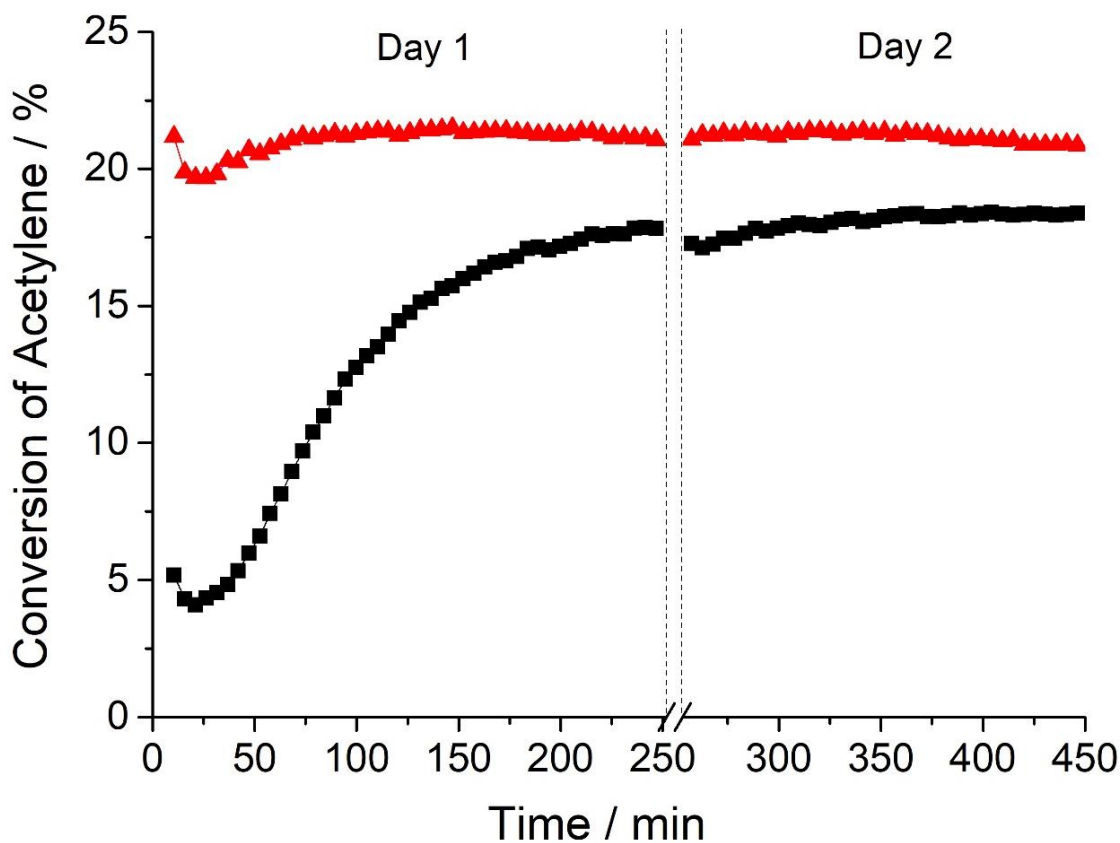


Figure 3.12. Time-on-line comparison of Au/C-Acetone (▲) and Au/C-AR (■) catalysts, each tested for a total of 7 h for the acetylene hydrochlorination reaction, under conditions stated in 3.3.

The Au/C-Acetone catalyst has a high initial conversion, with a slight fluctuation within the first 75 min, between 20 - 23 %. For the remaining 165 min of reaction on the first day, and the following 180 min the following day, the conversion remains remarkably stable. This is significantly different to the Au/C-AR catalyst, which requires 240 min on the first day to reach a stable conversion of 18 %. The following day the catalyst again experiences a small induction period, which is substantially less pronounced than the previous day, lasting 25 min before the catalyst reaches a stable conversion. XRD analysis was performed for the Au/C-Acetone catalyst at each stage of the reaction; fresh, after 4 h of reaction and after the total 7 h (Figure 3.13 and Figure 3.14).

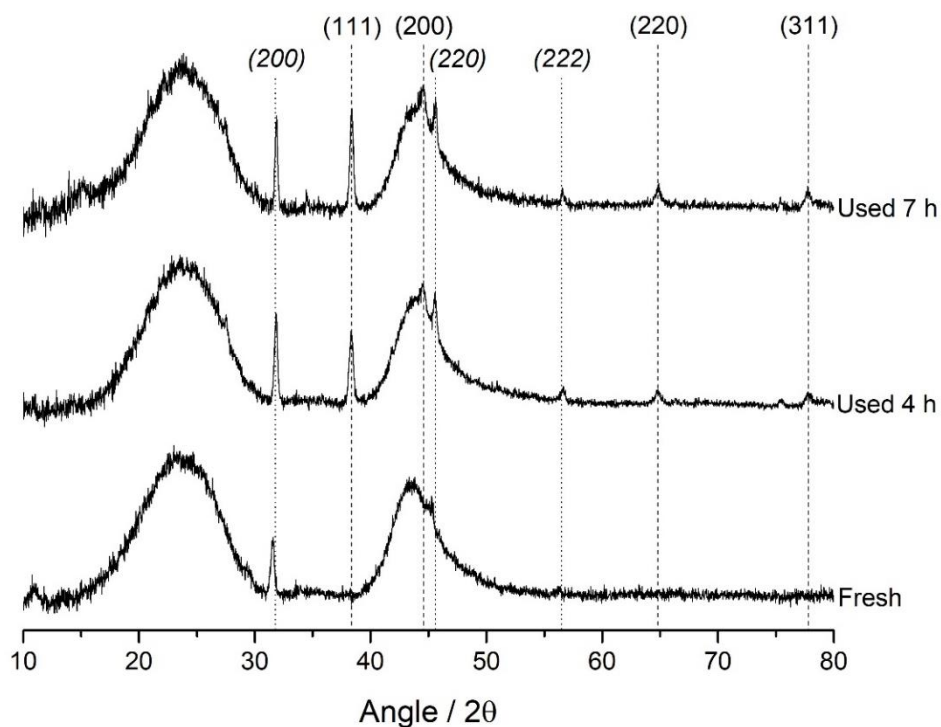


Figure 3.13. XRD patterns of the Au/C-Acetone catalyst; (fresh) before reaction, (used 4 h) after 4 hours of time-on-line, and (used 7 h) after 7 hours of time-on-line. Reflections at 38, 44, 65 and 78 / 2θ correspond to FCC metallic gold crystallites. Reflections at 32 / 2θ correspond to NaCl.³⁸

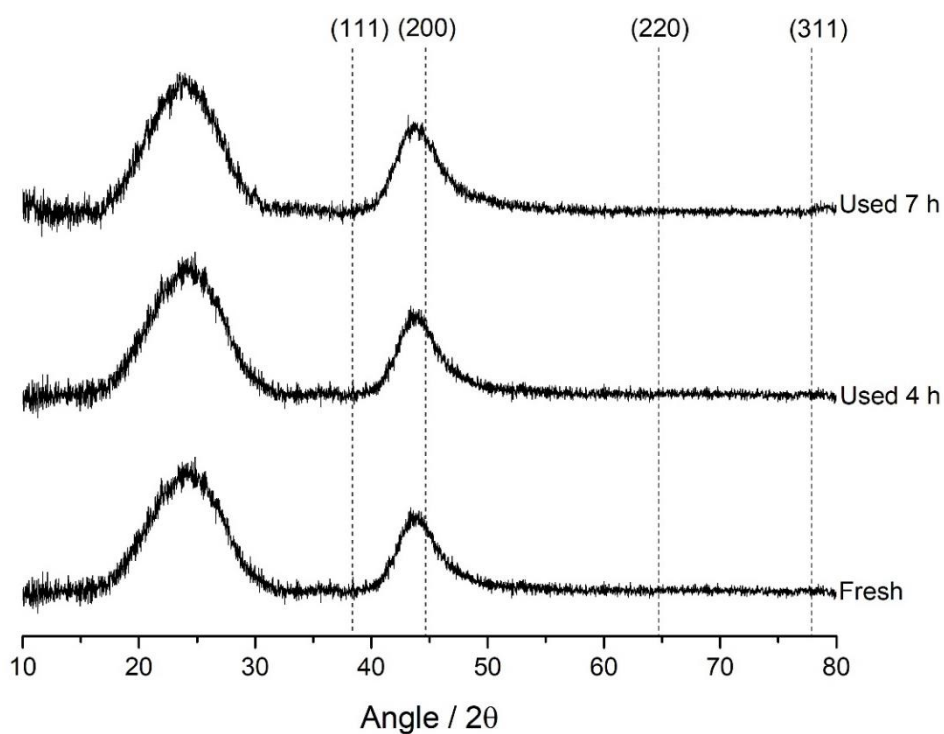


Figure 3.14. XRD patterns of the Au/C-Aqua regia catalyst; (fresh) before reaction, (used 4 h) after 4 hours of time-on-line, and (used 7 h) after 7 hours of time-on-line. Reflections at 38, 44, 65 and 78 / 2θ correspond to FCC metallic gold crystallites. Reflections at 32 / 2θ correspond to NaCl.³⁸

Analysis of the fresh Au/C-Acetone catalyst showed only reflections associated with sodium chloride crystals. Present in the carbon support, sodium chloride could have crystallised during the preparation of the catalyst due to rapid evaporation of ultra-dry solvents; this was not commonly observed in the more aqueous solvents as the NaCl was readily dissolved and dispersed before drying occurred. Future experiments could be performed to confirm this theory, using much purer carbons doped with known quantities of NaCl. After 4 h of reaction, significant reflections due to gold nanoparticles were observed in the XRD of the Au/C-Acetone catalyst, indicating reduction then agglomeration of the cationic gold to Au(0). The reflection intensities increased slightly after 7 h and became narrower, indicating further growth of gold nanoparticles.

It was shown in the time-on-line data that the conversion of the Au/C-Acetone catalyst remains constant throughout the reaction; however, it is known that the main deactivation method for gold on carbon catalysts is due to reduction of oxidised gold, forming Au(0).² Therefore the formation of metallic gold was thought to occur during the heating of the catalyst up to reaction temperature. This was confirmed by in-situ X-ray diffraction analysis; the Au/C-Acetone catalyst was steadily heated under inert conditions in 10 °C increments (1 °C min⁻¹) and held at each temperature for 40 min for an XRD scan to be performed (Figure 3.16). There were large number of reflections present in the in-situ spectra (Figure 3.16) which were not observed in the ex-situ spectra (Figure 3.13). Other than those reflections observed at 38, 44, 65 and 78 / 2 θ due to FCC gold nanocrystals, and the two broad reflections at 24, 43 and 79 2 θ due to carbon, all other reflections were caused by impurities in the cell. Figure 3.15 E.C. shows multiple sharp reflections present in the empty cell. A carbon sample impregnated with acetone was also analysed in-situ to confirm there was no change in these reflections during the analysis (Figure 3.15). Au(0) became visible at 190 °C, confirming the instability of the gold during heating. A comparison with the Au/C-Aqua regia catalyst (Figure 3.16) shows that these catalysts have very different thermal stabilities, providing further evidence of a different support-gold interaction. The Au/C-Aqua regia catalyst is stable up to 310 °C, with small reflections corresponding to gold nanoparticles apparent from this temperature.

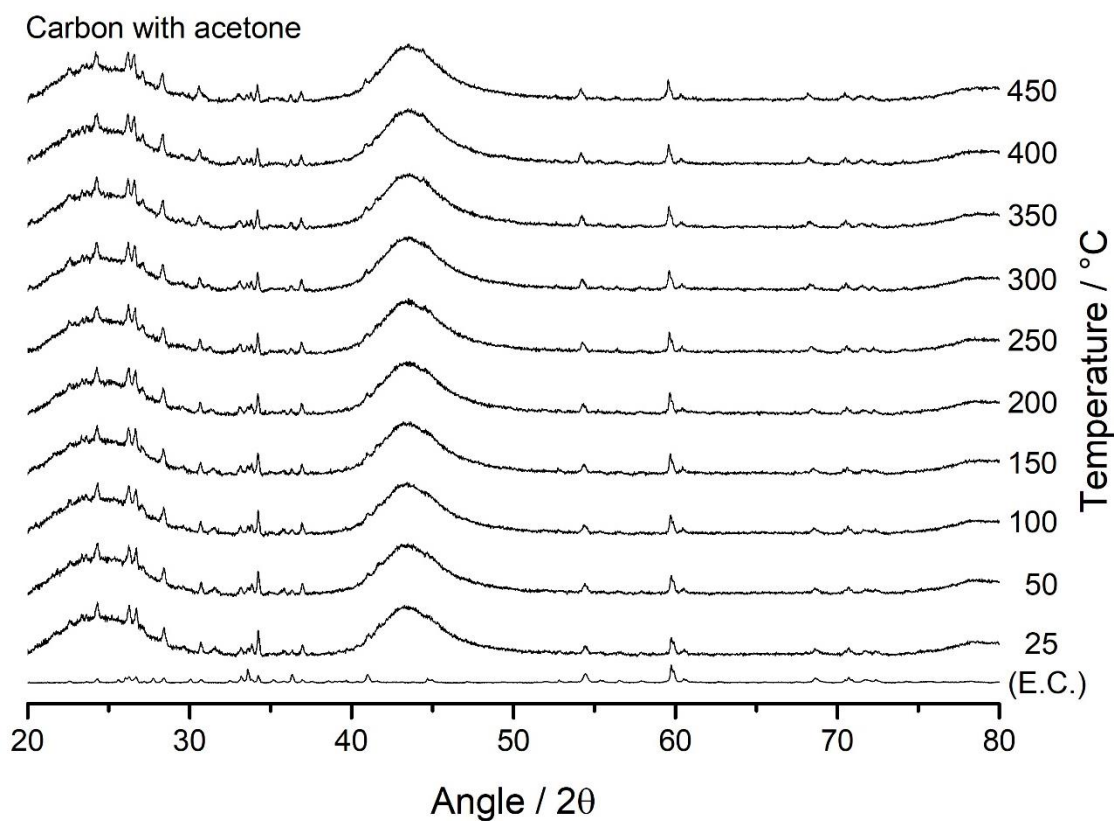
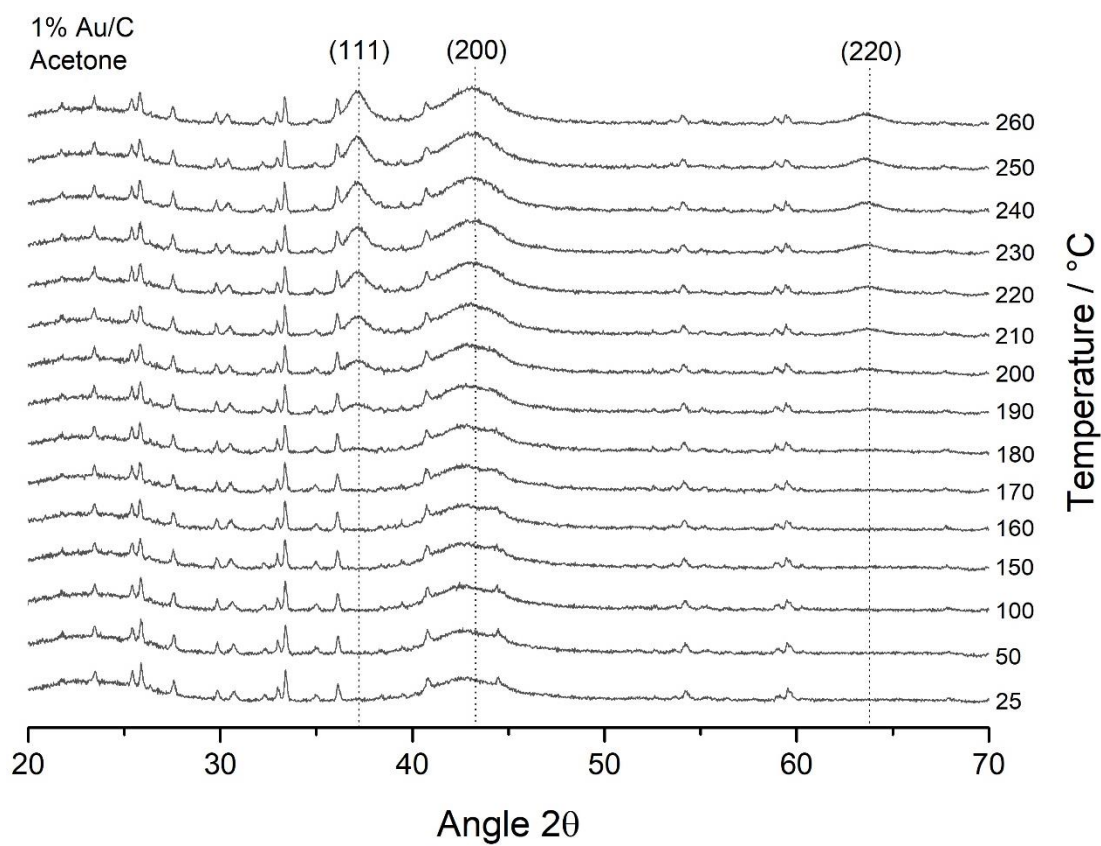


Figure 3.15. In-situ XRD pattern of carbon impregnated with acetone. E.C. indicates empty cell.



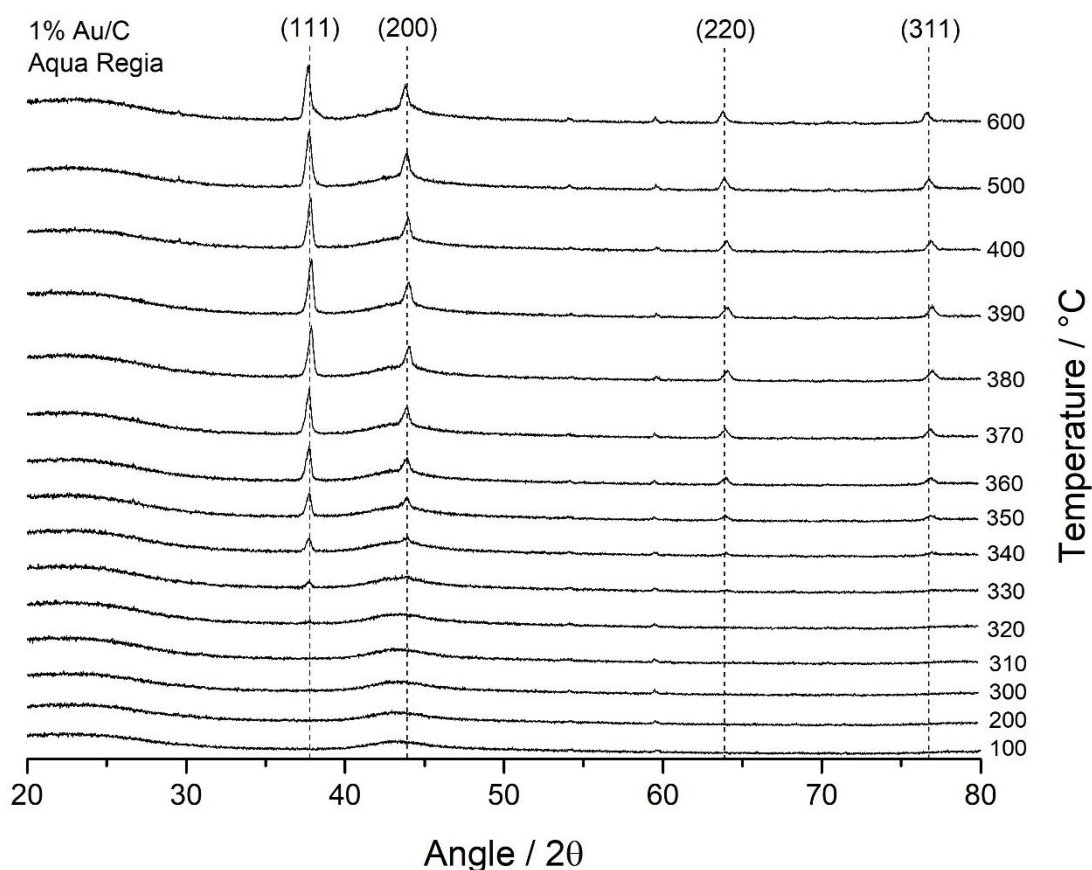


Figure 3.16. In-situ XRD patterns of Au/C-Acetone (top) and Au/C-Aqua regia (bottom) catalysts. Reflections at 38, 44, 65 and 78 / 2θ correspond to FCC metallic gold crystallites.

3.8. XAFS study of catalyst gold species

Based on previous results obtained in this group,²⁶ an optimised Au(I):Au(III) ratio is needed to achieve a consistent conversion during the reaction. The steady time-on-line reaction profile displayed by the Au/C-Acetone catalyst on both days is indicative of an optimised Au(I):Au(III) ratio even before the reaction commences. This is in contrast to the Au/C-Aqua regia catalyst; this begins the reaction with the ideal cationic gold ratio but then rapidly changes upon introduction of the reaction gas mixture. The resultant 240 min induction period then occurs to return to the optimised Au(I)/Au(III) ratio.

In order to determine the relative changes in gold oxidation states, the catalysts were compared to three gold standard materials; $\text{KAuCl}_4/[\text{AuCl}_4]^-$ (Au(III)), $[\text{AuCl}_2]^-$ (Au(I)) and gold foil (Au(0)). The gold foil reference is used in all XAFS experiments, whilst the Au(III) was obtained from previous work within the group on KAuCl_4 .⁴¹ The Au(I) standard was obtained from calculated difference spectra obtained from previously reported work on $[\text{AuCl}_2]^-$.⁴² This was a calculated value due to the instability of the AuCl compound.⁴² As described in Chapter 2, the transition at the Au L_3 -edge from Au $2p_{3/2} \rightarrow 5d$ gives rise to an appreciable peak in the XANES region, known as the

white line. The prominence of this white line is dependent on the oxidation state of the Au; Au(III) gives rise to a normalised white line height of 1.1, Au(I) 0.6 and Au(0) shows the usual gold absorption edge shape with no peak (Figure 3.17).

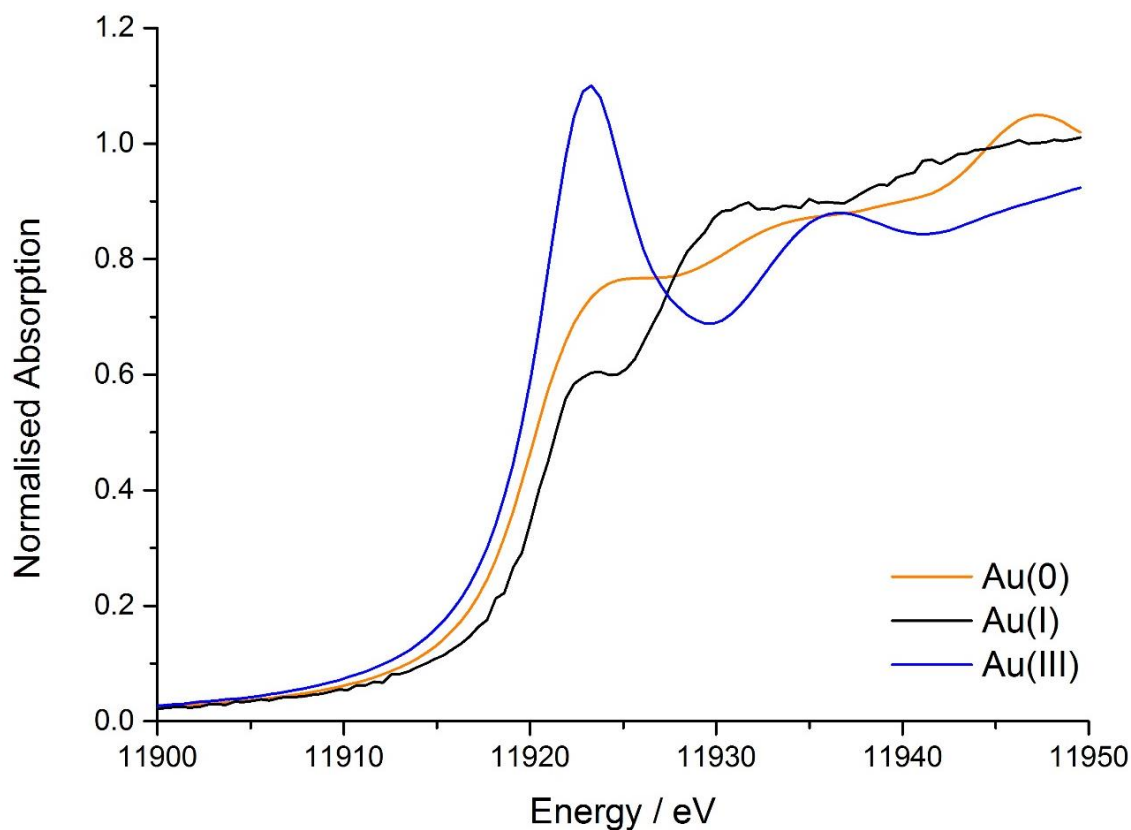


Figure 3.17. Au L_3 -edge XANES of $\text{KAuCl}_4/[\text{AuCl}_4]^-$ (Au(III)), $[\text{AuCl}_2]^-$ (Au(I)) and gold foil (Au(0)). See section 2.4.2 for experimental details.

Gold L_3 -edge XANES was used to investigate the gold oxidation state of the Au/C-Acetone catalyst and Au/C-Aqua regia catalyst. An Au/C-Acetone catalyst, which had been tested for 4 h under standard reaction conditions, was also analysed to determine the effect of reaction conditions. The results are shown in Figure 3.18, showing that the gold was in the cationic state before and after reaction, which concurs with the experimental data. The gold is predominantly Au(I) (both Fresh and Used Au/C-Acetone catalysts have a white line height of 0.7), although some of this character is lost after reaction, shown by a decrease in white line height. In comparison, the fresh Au/C-Aqua regia catalyst was comprised of a greater proportion of Au(III) shown by a greater white line height (0.8). As shown by work in this group, the white line height of the Au/C-Aqua regia catalyst changes during heating and upon introduction of the reaction gases.²⁶ However, post-reaction the catalyst has a white line height comparable to that of the Used Au/C-Acetone catalyst. The gold foil reference has no white line height, as it is composed

of only Au(0).

A linear combination fitting (LCF) of the XANES data was performed with reference to the standards (Figure 3.19) (see chapter 2 for further explanation of LCF). These results confirmed that the fresh Au/C-Acetone catalyst consisted primarily of Au(I) (77 %) and the remainder Au(III) (23 %). This also confirms that all of the gold is present in the oxidised form, similar to the Au/C-Aqua regia catalyst; Au(I) (78 %) and Au(III) (19 %). The increased Au(I) contribution of the Au/C-Acetone catalyst, compared to the Au/C-Aqua regia catalyst, is likely to contribute to the higher initial conversion of the catalyst, and the significantly steadier conversion. The used Au/C-Acetone catalyst contains a significant metallic gold contribution, Au(0) (19 %), present from the reduction of Au(I) to Au(0); therefore the Au(I) content was reduced (58 %), and the Au(III) contribution remained constant (23 %). This indicates that some of the gold has sintered due to high temperatures; this was shown previously in the in-situ XRD discussion (see Figure 3.16), confirming the instability of the Au/C-Acetone catalyst upon heating to reaction temperature.

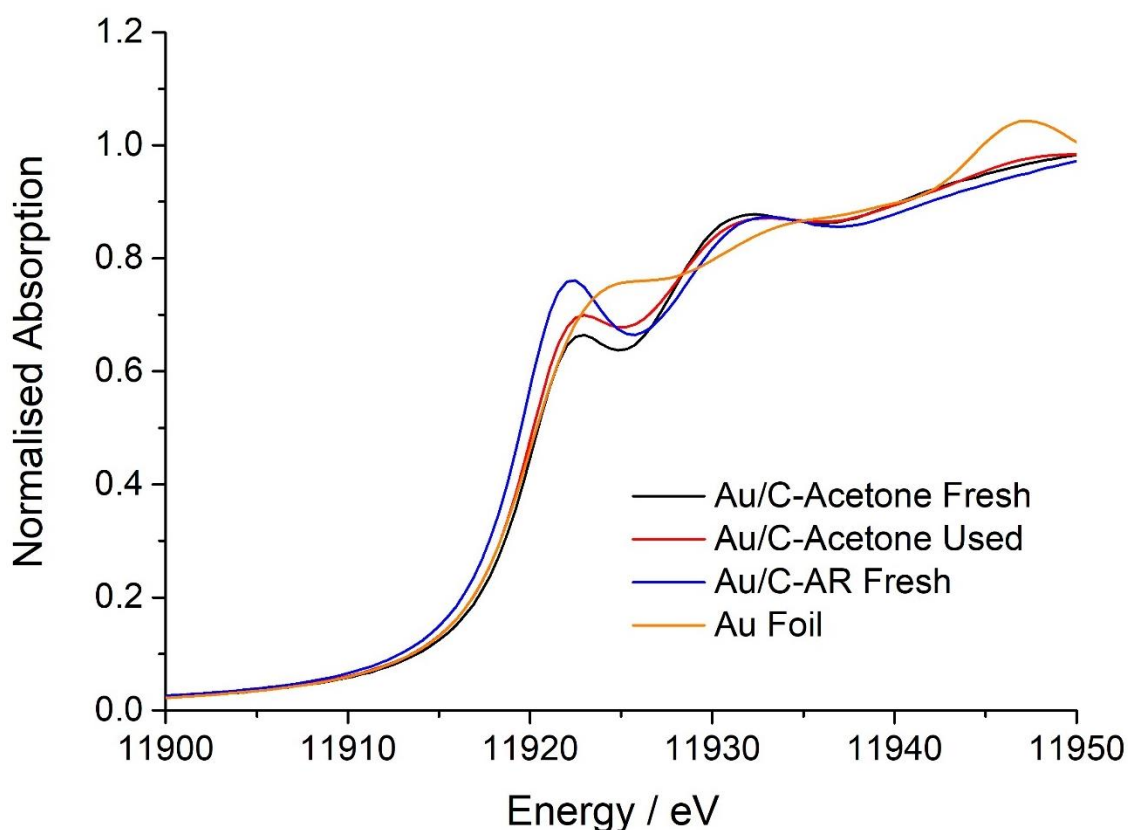


Figure 3.18. Au L₃-edge XANES of fresh and used (after 4 h of reaction) Au/C-Acetone catalysts, Au/C-Aqua regia catalyst (AR) and Au foil as reference.

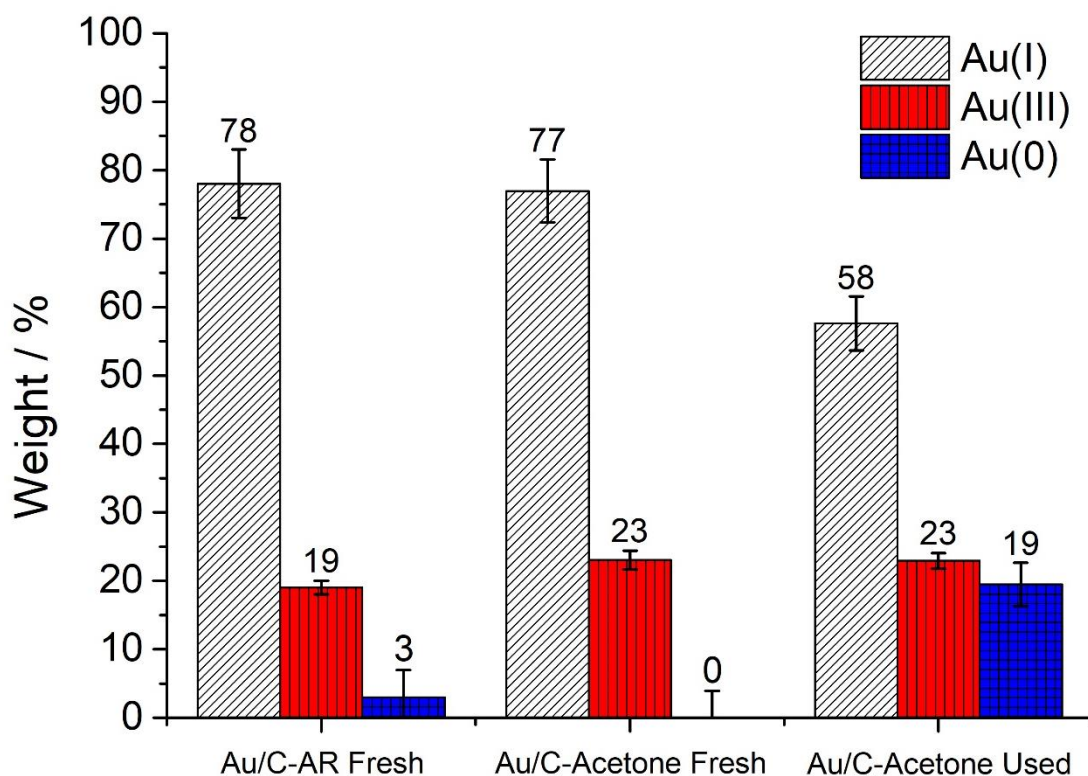


Figure 3.19. Linear combination fitting of the Au L_3 -edge XANES for the fresh Au/C-Aqua regia catalyst, fresh and used (after 4 h of reaction) Au/C-Acetone catalysts. Error bars indicate standard deviation.

EXAFS analysis was performed to determine the short-range order of the catalysts (Figure 3.20). A comparison of the fresh and used (after 4 h of reaction) Au/C-Acetone catalysts shows a decrease in the peak size at 1.8 Å, which corresponds to Au-Cl interaction, whilst concurrently the double peak at 2.5 and 3.0 Å increased in size slightly, due to an increase in metallic gold concentration. It could be deduced from this that as the nanoparticles of gold are formed, chlorine is lost from the surface of the catalyst. The Au/C-Aqua regia catalyst in contrast has a significantly higher Au-Cl character, which is likely due to the abundance of chlorine in the solvent mixture, the different gold oxidation state (more Au(III) content) as well as a different support-gold-chlorine interaction, which may account for the very different time-on-line data profile. The gold foil reference shows clearly the position of the double peak which corresponds to metallic Au(0).

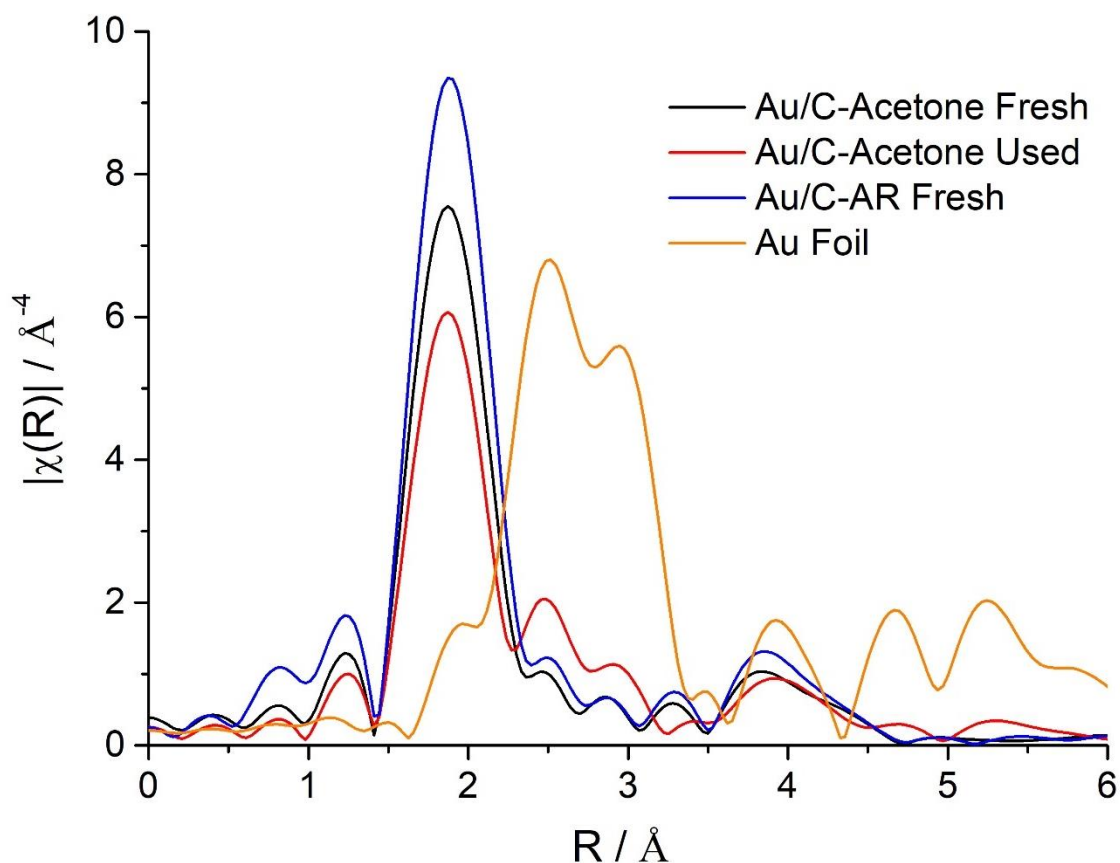


Figure 3.20. Fourier transform of the k^3 -weighted χ EXAFS data of fresh and used (after 4 h of reaction) Au/C-Acetone catalysts, Au/C-Aqua regia catalyst (AR) and Au foil as reference.

3.9. Conclusions

Single site gold on carbon catalysts prepared using solvents such as aqua regia have previously been shown to be very active for the acetylene hydrochlorination reaction, more so than its commercial predecessor, mercury on carbon. Here the use of organic solvents removes the need for highly oxidising and acidic solvents to produce single-site catalysts, which are more active whilst maintaining high selectivity.

The use of low polarity solvents resulted in catalysts with comparable acetylene conversion due to a limit of mono atomic gold dispersion. However, the use of high polarity solvents caused a decrease in catalytic activity. This was attributed to the drying temperature during catalyst preparation and the concentration of water in the solvent. High drying temperatures facilitated sintering of the monodispersed gold. Low concentrations of water resulted in reduction of gold, again leading to nanoparticle formation. Both factors therefore result in catalysts with a poor gold dispersion and hence low acetylene conversion.

The Au/C-Acetone catalyst was used for a reusability study. This catalyst displayed a much

steadier reaction profile than that of the Au/C-Aqua regia catalyst and maintained a higher conversion throughout the 7 h of reaction. Although nanoparticles were formed after 4 and 7 h of use, these were determined to have been formed during the heating of the catalyst under inert conditions and not as a result of the reaction gases used. High performance and a steady reaction profile are both desirable factors if a catalyst is to be used in commercial conditions, therefore this catalyst shows promise for industrial application. Further investigation would be required to determine if this catalyst achieves the same performance after scale-up of the preparation.

Characterisation of the fresh Au/C-Acetone catalyst using Au L₃-edge XANES confirmed the gold was present as cationic Au(I)/Au(III) on the carbon support. The high initial Au(I) content explained the reduced induction period when compared to the Au/C-Aqua regia catalyst, which must undergo a prolonged in-situ oxidation to attain a similar state. k³-weighted χ EXAFS data confirmed the presence of Au(0) post-reaction. The continued stability of the catalyst, regardless of this Au(0) content, suggests that not all of the metal is active during the reaction. This indicates that further optimisation of the reaction temperature could be explored to minimise gold reduction and hence optimise catalytic activity.

3.10. References

- 1 A. Zecchina, S. Bordiga and E. Groppo, in *Selective Nanocatalysts and Nanoscience: Concepts for Heterogeneous and Homogeneous Catalysis*, ed. A. Zecchina, Wiley-VCH Verlag GmbH & Co. KGaA, 1st edn., 2011, pp. 1–27.
- 2 G. Malta, S. A. Kondrat, S. J. Freakley, C. J. Davies, S. R. Dawson, X. Liu, L. Lu, K. Dymkowski, F. Fernandez-Alonso, S. Mukhopadhyay, E. K. Gibson, P. P. Wells, S. F. Parker, C. J. Kiely and G. J. Hutchings, *ACS Catal.*, 2018, **8**, 8493–8505.
- 3 A. A. Herzing, C. J. Kiely, A. F. Carley, P. Landon and G. J. Hutchings, *Science*, 2008, **321**, 1331–1335.
- 4 M. Crespo-Quesada, A. Yarulin, M. Jin, Y. Xia and L. Kiwi-Minsker, *J. Am. Chem. Soc.*, 2011, **133**, 12787–12794.
- 5 M. Haruta, T. Kobayashi, H. Sano and N. Yamada, *Chem. Lett.*, 2006, **16**, 405–408.
- 6 John Dunleavy, *Platin. Met. Rev.*, 2006, **50**, 110.
- 7 H. Uchida and M. R. Harada, *Sci. Eng. Hydrog. Energy Technol.*, 2019, 215–219.
- 8 M. Flytzani-Stephanopoulos, *Acc. Chem. Res.*, 2014, **47**, 783–792.
- 9 M. Yang, L. F. Allard and M. Flytzani-Stephanopoulos, *J. Am. Chem. Soc.*, 2013, **135**, 3768–3771.
- 10 J. C. J. Bart, S. Cavallaro, G. Lefebvre, M. Lazarus, A. Kollmuss, J. H. Teles, C. S. Slaten, M. Seapan, M. W. Lower, P. E. Tomlinson, M. Aoki, R. Noyori, O. A. Kholdeeva, S. H. Jung, J. S. Chang, K. Holmberg, K. Wang and J. Chen, *Science*, 2014, **346**, 1498–1502.
- 11 X.-K. Gu, B. Qiao, C.-Q. Huang, W.-C. Ding, K. Sun, E. Zhan, T. Zhang, J. Liu and W.-X. Li, *ACS Catal.*, 2014, **4**, 3886–3890.
- 12 C. Wang, G. Garbarino, L. F. Allard, F. Wilson, G. Busca and M. Flytzani-Stephanopoulos, *ACS Catal.*, 2016, **6**, 210–218.
- 13 B. Qiao, J.-X. Liang, A. Wang, C.-Q. Xu, J. Li, T. Zhang and J. (Jimmy) Liu, *Nano Res.*, 2015,

- 8, 2913–2924.
- 14 B. Qiao, J. Liu, Y. G. Wang, Q. Lin, X. Liu, A. Wang, J. Li, T. Zhang and J. Liu, *ACS Catal.*, 2015, **5**, 6249–6254.
- 15 J. C. Fierro-Gonzalez and B. C. Gates, *J. Phys. Chem. B*, 2004, **108**, 16999–17002.
- 16 S. Uchida, E.-A. Kim, K. Fujita, C. K. Kim, I. A. Firmo, M. H. Hamidian, J. C. Davis, I. Lee, H. Eisaki, M. J. Lawler, S. Mukhopadhyay, J. Lee, X. Guo, G. Fang, G. Li, H. Ma, H. Fan, L. Yu, C. Ma, X. Wu, D. Deng, M. Wei, D. Tan, R. Si, S. Zhang, J. Li, L. Sun, Z. Tang, X. Pan and X. Bao, *Science*, 2014, **344**, 612–616.
- 17 G. Vilé, D. Albani, M. Nachtegaal, Z. Chen, D. Dontsova, M. Antonietti, N. López and J. Pérez-Ramírez, *Angew. Chemie Int. Ed.*, 2015, **54**, 11265–11269.
- 18 U. Heiz, A. Sanchez, S. Abbet and W.-D. D. Schneider, *J. Am. Chem. Soc.*, 1999, **121**, 3214–3217.
- 19 J. Liu, *ACS Catal.*, 2017, **7**, 34–59.
- 20 J. Wan, W. Chen, C. Jia, L. Zheng, J. Dong, X. Zheng, Y. Wang, W. Yan, C. Chen, Q. Peng, D. Wang and Y. Li, *Adv. Mater.*, 2018, **30**, 1–8.
- 21 X. F. Yang, A. Wang, B. Qiao, J. Li, J. Liu and T. Zhang, *Acc. Chem. Res.*, 2013, **46**, 1740–1748.
- 22 T. W. Hansen, A. T. Delariva, S. R. Challa and A. K. Datye, *Acc. Chem. Res.*, 2013, **46**, 1720–1730.
- 23 J. Xu, J. Zhao, J. Xu, T. Zhang, X. Li, X. Di, J. Ni, J. Wang and J. Cen, *Ind. Eng. Chem. Res.*, 2014, **53**, 14272–14281.
- 24 C. J. Davies, *PhD Thesis*, 2012, Cardiff University.
- 25 M. Conte, C. J. Davies, D. J. Morgan, T. E. Davies, D. J. Elias, A. F. Carley, P. Johnston and G. J. Hutchings, *J. Catal.*, 2013, **297**, 128–136.
- 26 G. Malta, S. A. Kondrat, S. J. Freakley, C. J. Davies, L. Lu, S. R. Dawson, A. Thetford, E. K. Gibson, D. J. Morgan, W. Jones, P. P. Wells, P. Johnston, C. R. A. Catlow, C. J. Kiely and G. J. Hutchings, *Science*, 2017, **355**, 1399–1403.
- 27 G. Malta, S. J. Freakley, S. A. Kondrat and G. J. Hutchings, *Chem. Commun.*, 2017, **53**, 11733–11746.
- 28 W. Lin, R.-W. Zhang, S.-S. Jang, C.-P. Wong and J.-I. Hong, *Angew. Chemie Int. Ed.*, 2010, **49**, 7929–7932.
- 29 W. Lin, *Rare Met.*, 2012, **31**, 92–95.
- 30 J. Zhao, B. Wang, X. Xu, Y. Yu, S. Di, H. Xu, Y. Zhai, H. He, L. Guo, Z. Pan and X. Li, *J. Catal.*, 2017, **350**, 149–158.
- 31 H. S. Oh, J. H. Yang, C. K. Costello, Y. M. Wang, S. R. Bare, H. H. Kung and M. C. Kung, *J. Catal.*, 2002, **210**, 375–386.
- 32 M. Conte, C. J. Davies, D. J. Morgan, A. F. Carley, P. Johnston and G. J. Hutchings, *Catal. Letters*, 2014, **144**, 1–8.
- 33 M. Conte, A. F. Carley, C. Heirene, D. J. Willock, P. Johnston, A. A. Herzing, C. J. Kiely and G. J. Hutchings, *J. Catal.*, 2007, **250**, 231–239.
- 34 X. Liu, M. Conte, D. Elias, L. Lu, D. J. Morgan, S. J. Freakley, P. Johnston, C. J. Kiely and G. J. Hutchings, *Catal. Sci. Technol.*, 2016, **6**, 5144–5153.
- 35 M. Conte, C. J. Davies, D. J. Morgan, T. E. Davies, A. F. Carley, P. Johnston and G. J. Hutchings, *Catal. Sci. Technol.*, 2013, **3**, 128–134.
- 36 G. J. Hutchings, *J. Catal.*, 1985, **96**, 292–295.
- 37 C. Reichardt, *Angew. Chemie Int. Ed.*, 1979, **18**, 98–110.
- 38 Y. Qin, D. Yu and J. Zhou, *CrystEngComm*, 2017, **19**, 5356–5360.
- 39 Acetone, 99.8%, for HPLC, ACROS Organics™, <https://www.fishersci.co.uk/shop/products/acetone-99-8-hplc-acros-organics-3/p-217171#?keyword=hplc+acetone>, (accessed October 2018).
- 40 Acetone, 99.8%, Extra Dry, AcroSeal™, ACROS Organics™,

<https://www.fishersci.co.uk/shop/products/acetone-99-8-extra-dry-acroseal-acros-organics-2/p-217168#?keyword=acros+acetone>, (accessed October 2018).

41 G. Malta, PhD thesis, Cardiff University, 2018.

42 S.-Y. Chang, A. Uehara, S. G. Booth, K. Ignatyev, J. F. W. Mosselmans, R. A. W. Dryfe and S. L. M. Schroeder, *RSC Adv.*, 2015, **5**, 6912–6918.

4. Acetylene hydrochlorination using sulfur treated, carbon supported gold catalysts

4.1. Introduction

The work in this chapter initially focuses on the use of bimetallic carbon supported catalysts, with the aim of improving the catalytic activity over that of the monometallic Au/C catalyst. Previous work showed that the addition of $\text{Ce}(\text{SO}_4)_2$, a known oxidising agent,¹ could enhance the activity of Au/C catalysts.² The use of bimetallic gold catalysts has been well reported for the acetylene hydrochlorination reaction. The addition of a second metal may enhance the activity of a gold catalyst by

- Stabilising the active species, inhibiting Au(I) or Au(III) reduction.^{3–7}
- Increasing electron density of active species by electron transfer from extra metal, thereby promoting the chemisorption of HCl which in turn results in less reduction of gold by C_2H_2 .^{8–11}
- Promote a high dispersion of gold, which may generate more active sites.^{12,13}
- Decrease the extent of agglomeration of gold to nanoparticles.^{14,15}

These examples of bimetallic catalysts also incur drawbacks such as; Au-Pd/C and Au-Pt/C catalysts decrease selectivity, resulting in significant coke deposition and rapid deactivation of the catalyst,¹³ Au-Co(III)/spherical activated carbon (SAC) and Au-La(III)/SAC begin to deactivate after only 48 h online,^{4,16} Au-Ir/C, Au-Cu/C and Au-Cs/C required high loadings (>2 %) of the additional metal to achieve comparable conversions to Au/C,^{5,13,17} whilst Au-Ru/C had no effect on catalytic activity.¹³ Also, when using bimetallic catalysts, recycling the precious metals from spent catalysts becomes more difficult. Firstly, this commonly requires the use of aqua regia to leach the metals from the support, which is a very hazardous chemical for use in industrial quantities and does not result in a full metal recovery. Therefore, other pyrometallurgic processes are also required to fully extract the metals. This results in an overall loss of valuable precious metals and therefore reduces the economic viability of such catalysts.^{18,19}

Another reported method to synthesise highly active catalysts is via the use of dopants. Doping

carbon with nitrogen results in the promotion of acetylene adsorption and hence increased acetylene conversion. This is especially significant as it also results in active metal-free catalysts, although none yet as active as their metal-based counterpart.^{20–22} Further work was performed on N-doped carbon by Wang *et al.*, also introducing sulfur to the support via sulfuric acid. This increased the catalytic activity above that when using only N-doped carbon, by further promoting the adsorption of acetylene.²³ Focusing on carbon supported gold catalysts, Di *et al.* used thiourea in a simpler preparation to dope the catalyst with both N and S.²⁴ Their results indicated that sulfur served to anchor the gold and prevent the reduction of the Au(I) and Au(III), as also noted via TPR analysis.^{25,26} The addition of sulfur via ionic liquids has also been noted to increase the dispersion of gold species and inhibit carbon deposition, resulting in a highly active, long-life catalyst.²⁷ Work by P. Johnston *et al.* has shown that gold-sulfur complexes deposited on carbon can increase the activity of the catalyst when compared to Au/C alone²⁸ and the use of complexes containing soft ligands increased the stability of the catalyst over those prepared with complexes containing halides, such as chlorine. This work has been tested at an industrial scale in a pilot plant by Johnson Matthey, proving irrefutably the advantage of incorporating sulfur in Au/C catalysts.²⁹ The latter portion of this chapter, therefore, takes inspiration from the work by Johnson Matthey to determine how the addition of sulfur to a Au/C catalyst can affect the catalytic activity, with the overall aim of increasing the acetylene conversion.

4.2. Experimental Conditions

4.2.1. Preparation of pre-treated carbons

Carbons were pre-treated with a sulfate solution or dilute acid; the sulfate solutions were ammonium sulfate and sodium sulfate, the dilute acids were sulfuric acid, hydrochloric acid, nitric acid, phosphoric acid and aqua regia. In all cases, the sulfates and acids were dissolved and diluted in deionised water to form equimolar solutions, with the exception of aqua regia. When an equimolar solution was not used, this was stated in the text. 15 mL of a prepared solution was stirred on 1.15 g of activated carbon for 1 h. The solution was filtered under vacuum, washed with deionised water (100 mL) and dried at 110 °C for 16 h. All catalysts were prepared to a 1 wt. % Au loading on carbon.

4.2.2. Preparation of post-treated carbons

To prepare post-wash catalysts, a 1% Au/C catalyst was first prepared. This catalyst (1.15 g) was then stirred in a pre-prepared solution (as stated in **4.2.1**) (15 mL) for 1 h, the solution filtered under vacuum, washed with deionised water (100 mL) and dried at 110 °C for 16 h.

4.2.3. Reaction conditions

All reactions were performed using the following conditions unless stated otherwise: C₂H₂ : HCl 1:1.02, balanced in argon, total gas flow 50 mL min⁻¹, catalyst (0.09 g), 200 °C, ambient pressure.

4.3. Catalyst Nomenclature

A list of all of the catalyst names and their respective preparations.

- Pre-wash – carbon support stirred in a sulfur containing solution, followed by filtering, washing with 100 mL H₂O and drying. This modified carbon was then used to prepare a 1% Au/C catalyst via wet impregnation with aqua regia.
- Post-wash – 1% Au/C catalyst prepared by wet impregnation with aqua regia. This catalyst was then stirred in a sulfur containing solution, followed by filtering, washing with 100 mL H₂O and drying.
- No AR – A sulfur containing solution was used as the solvent for H₂AuCl₄ instead of aqua regia.
- Pre-wash, no H₂O wash – Pre-wash preparation as above, omitting the wash with 100 mL H₂O during filtering.
- Pre-wash, x mL wash – Pre-wash preparation as above, washing with x mL of H₂O instead of the typical 100 mL.
- C-x – carbon prepared by stirring the carbon in a sulfur containing solution (x), followed by filtering, washing with 100 mL H₂O and drying.
- Au/C-AR – unmodified catalyst preparation.
- Au/C-solvent – unmodified carbon catalyst prepared using named solvent instead of aqua regia.

4.4. Bimetallic catalysts

Three Au/C bimetallic catalysts were prepared by first stirring carbon in 15 mL of a saturated cobalt, manganese or iron sulfate aqueous solution, prepared by stirring 5 g of metal sulfate in 15 mL of H₂O. This was followed by washing with 100 mL of H₂O and drying. Gold was then deposited onto this modified carbon using aqua regia as the solvent as used previously for Au/C-AR. This preparation method was used to achieve a high loading of secondary metal on the carbon support, in order to use these catalysts for screening tests. Cobalt sulfate was chosen for the preparation as Co has previously been shown to enhance the activity of Au in this reaction

by increasing the relative concentration of Au(I) and Au(III) species, reducing sintering and inhibiting coke deposition.^{4,9} Mn and Fe were chosen as neighbouring transition metal elements for comparison. Each catalyst was tested for the reaction and the maximum conversion (during the 240 min test) was determined (Figure 4.1). Both the Au/C-CoSO₄ and Au/C-MnSO₄ catalysts have much higher conversions (47 and 37 %, respectively) than that of monometallic Au/C-AR (19 %); however, Au/C-FeSO₄ maintained a low conversion throughout the test (5 %). To determine if the increase in acetylene conversion was due to a synergistic effect between Au and the second metal or a possible modification of the carbon support, reactions of the modified carbons were also performed. C-CoSO₄ and C-MnSO₄ had low conversion (4 and 3 %, respectively) comparable to that of carbon (2 %), confirming that gold remained the active metal in the reaction.

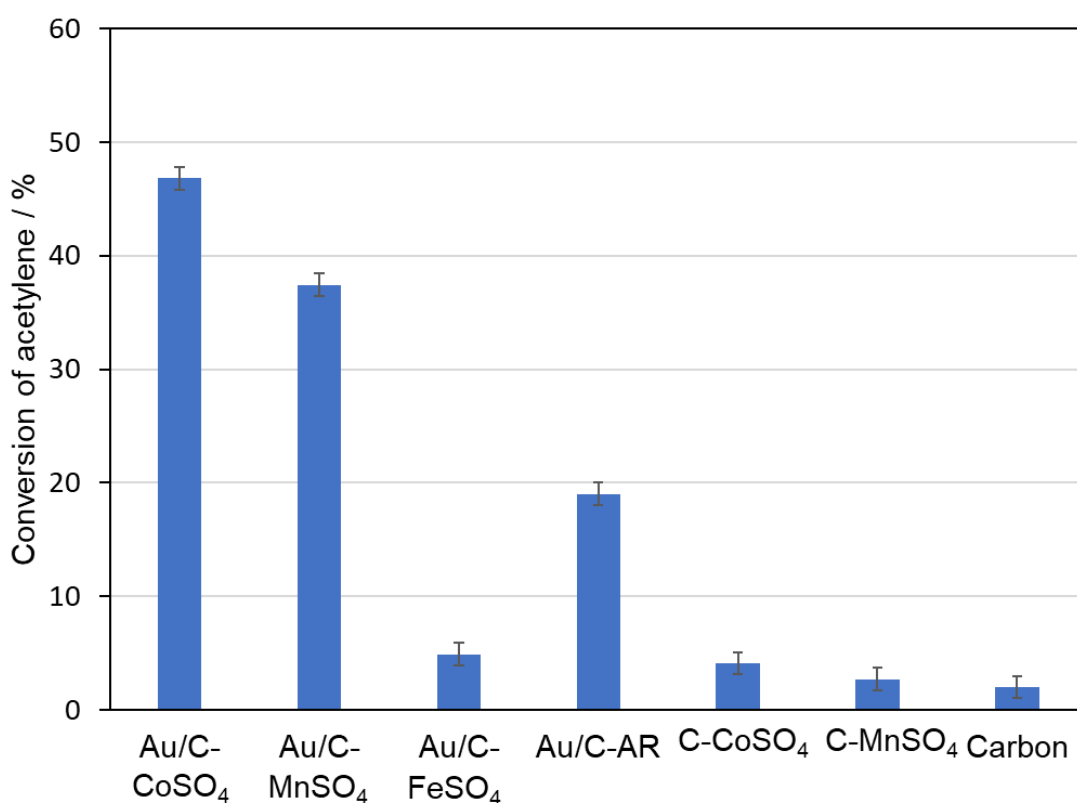


Figure 4.1. Comparison of acetylene conversions for Au/C-CoSO₄, Au/C-MnSO₄ and Au/C-FeSO₄ catalysts and their respective treated carbons, conditions as stated in section 4.2.3. Error bars indicate percentage error.

XRD analysis was performed to determine if any gold nanoparticles were present before or after reaction (Figure 4.2), as it has been suggested in previous literature that gold nanoparticles are inactive for the acetylene hydrochlorination reaction.³⁰ All three fresh bimetallic catalysts exhibited no reflections due to gold or any other metal, containing only the two broad

reflections for carbon at 24 and 44 / 2θ . However, used Au/C-FeSO₄ did contain characteristic reflections corresponding to gold nanoparticles, indicating the agglomeration of gold during the reaction. If these gold nanoparticles had formed at the start of the reaction, during heating to 200 °C or immediately upon introduction of the reactant gases, this would explain the low conversion for the remainder of the test.

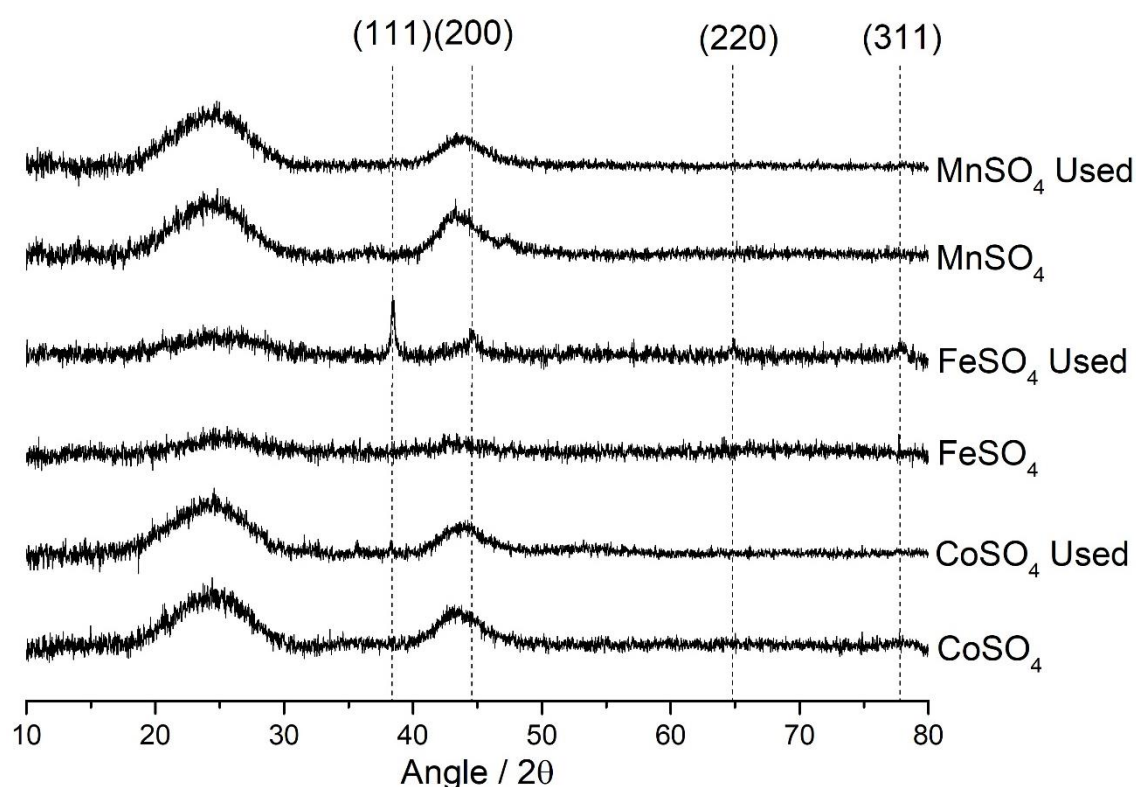


Figure 4.2. XRD patterns of Au/C-CoSO₄, Au/C-FeSO₄ and Au/C-MnSO₄ catalysts, fresh and used. Reflections at 38, 44, 65 and 78 / 2θ correspond to FCC metallic gold crystallites.

XPS analysis was performed to confirm that the secondary metal had remained on the catalyst after preparation and to determine the concentration of added metal and sulfur present on each catalyst. Table 4.1 shows that there was a significantly greater concentration of iron and sulfur on Au/C-FeSO₄ compared to Co and Mn on their respective catalysts. Such a high concentration may have covered the active species, also contributing to the low activity of the catalyst. This should be confirmed by preparing the Au/C-FeSO₄ catalyst with a solution of lower concentration FeSO₄ in order to make the iron and sulfur loadings more comparable to those of Co and Mn on Au/C-CoSO₄ and Au/C-MnSO₄, respectively.

Table 4.1. Atomic % of metal and sulfur present in Au/C-CoSO₄, Au/C-MnSO₄ and Au/C-FeSO₄ catalysts, determined via XPS.

Catalyst	Co At. %	Mn At. %	Fe At. %	S At. %
Au/C-CoSO ₄	0.1	-	-	0.3
Au/C-MnSO ₄	-	0.1	-	0.3
Au/C-FeSO ₄	-	-	1.0	1.4

The time-on-line data for Au/C-CoSO₄ (Figure 4.3) shows the initial activation of the catalyst over 100 min, reaching a maximum conversion of 47 %, followed by a gradual decline in conversion over the remaining 140 min. Au/C-AR is also shown for reference. Au/C-CoSO₄ was the most active catalyst, therefore XAFS analysis was performed to determine if the gold oxidation state was similar to that of monometallic Au/C-AR and also to potentially monitor changes in the S and Cl species present. *In-situ* gold L₃-edge XANES was performed to monitor changes in the gold oxidation state of Au/C-CoSO₄ before and during the reaction. Initially the Au was present solely as Au(III), as noted by a large white line height (Figure 4.4). When heated to 200 °C under a He atmosphere, the absorption intensity decreased, signifying increasing Au(I) content, very similar to that of the fresh Au/C-AR. Introduction of the reaction gases caused a rapid oxidation to more Au(III), which was reduced to the previous Au(I) oxidation state over the course of the 70 min induction period. Again, following from the work in the previous chapter this shows that the Au(I) state is most conducive to high acetylene conversion during the reaction.

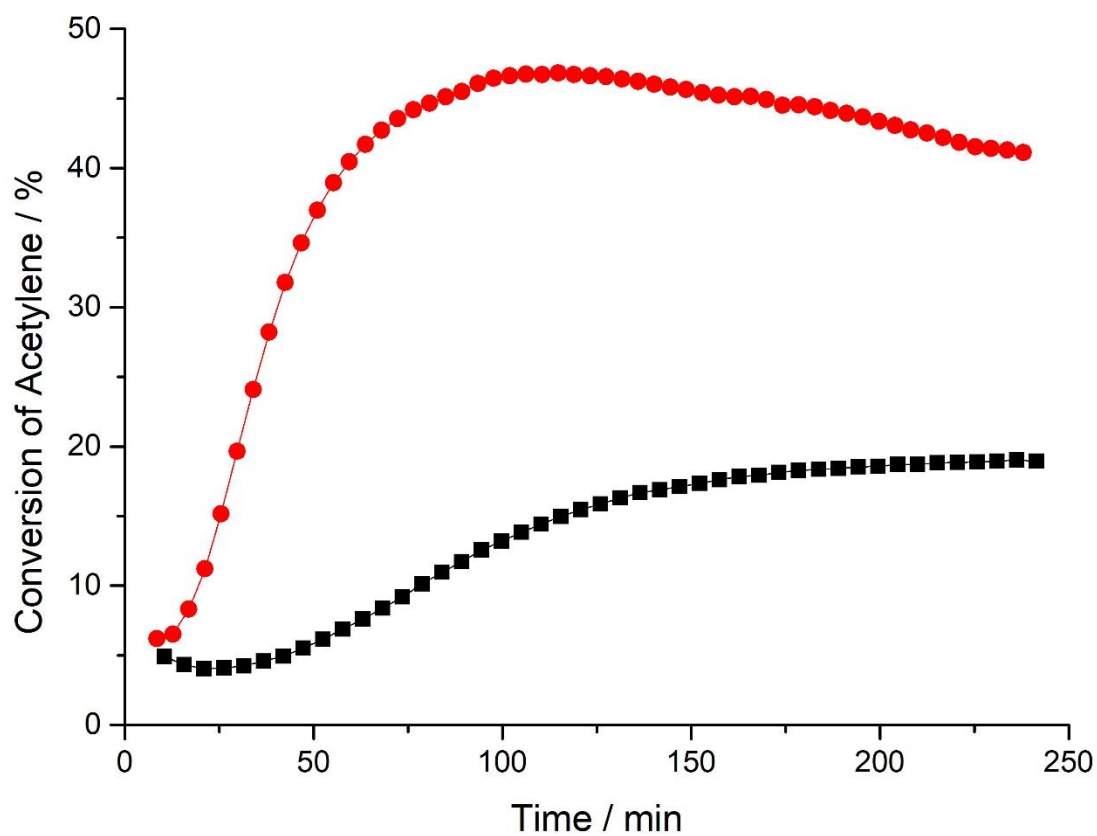


Figure 4.3. Au/C-CoSO₄ time-on-line data – Au/C-CoSO₄ (●), Au/C-AR (■), conditions stated in section 4.2.3.

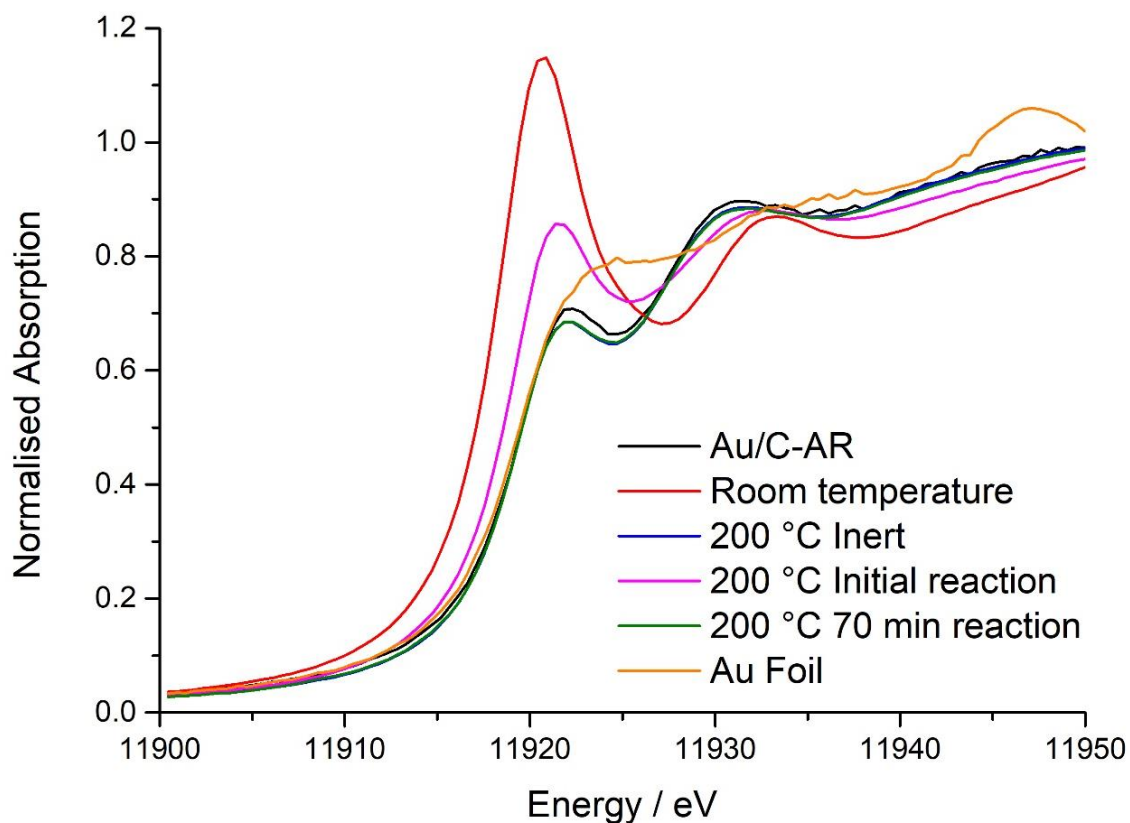


Figure 4.4. Au L_3 -edge XANES of Au/C-AR, Au/C-CoSO₄ at room temperature, after heating to 200 °C under inert conditions, after introduction of reaction gases at 200 °C, after 70 min of reaction and Au foil reference. Note that the data for 200 °C Inert (blue line) is nearly identical to and therefore hidden by the data 200 °C 70 min reaction (green line).

A linear combination fitting (LCF) of these results was performed (Figure 4.5) to quantify the proportions of gold oxidation states present, with reference to the Au(I) and Au(III) standards (discussed in 3.7, figure 17). As was clearly shown in Figure 4.4, the initial state of the catalyst at room temperature is completely Au(III), with no fractions of other oxidation states calculated. Heating to 200 °C under inert conditions reduced the Au significantly to Au(I) (74 %) and Au(III) (25 %). These fractions of Au were remarkably similar to those of Au/C-AR (Au(I) : 78 %, Au(III) : 19 %, Au(0) : 3 %). Introduction of the reaction gases cause an oxidation of gold, to Au(III) (53 %), leaving the remainder as Au(I) (46 %). However, after 70 min of reaction the gold again partially re-oxidised, Au(I) (74 %) and Au(III) (26 %), to a state similar to that of Au/C-AR under reaction conditions. In each of the reaction stages, a small percentage of Au(0) is also reported, however in all cases this is within the error of the analysis and considered negligible. The changes in oxidation states of Au/C-CoSO₄ are similar to those observed in Au/C-Ar during the initial stages of reaction³⁰; both transition from Au(I) to Au(III) upon introduction of the reactant gases and then return to Au(I) during the course of the reaction as the gold species stabilises in a more active form.

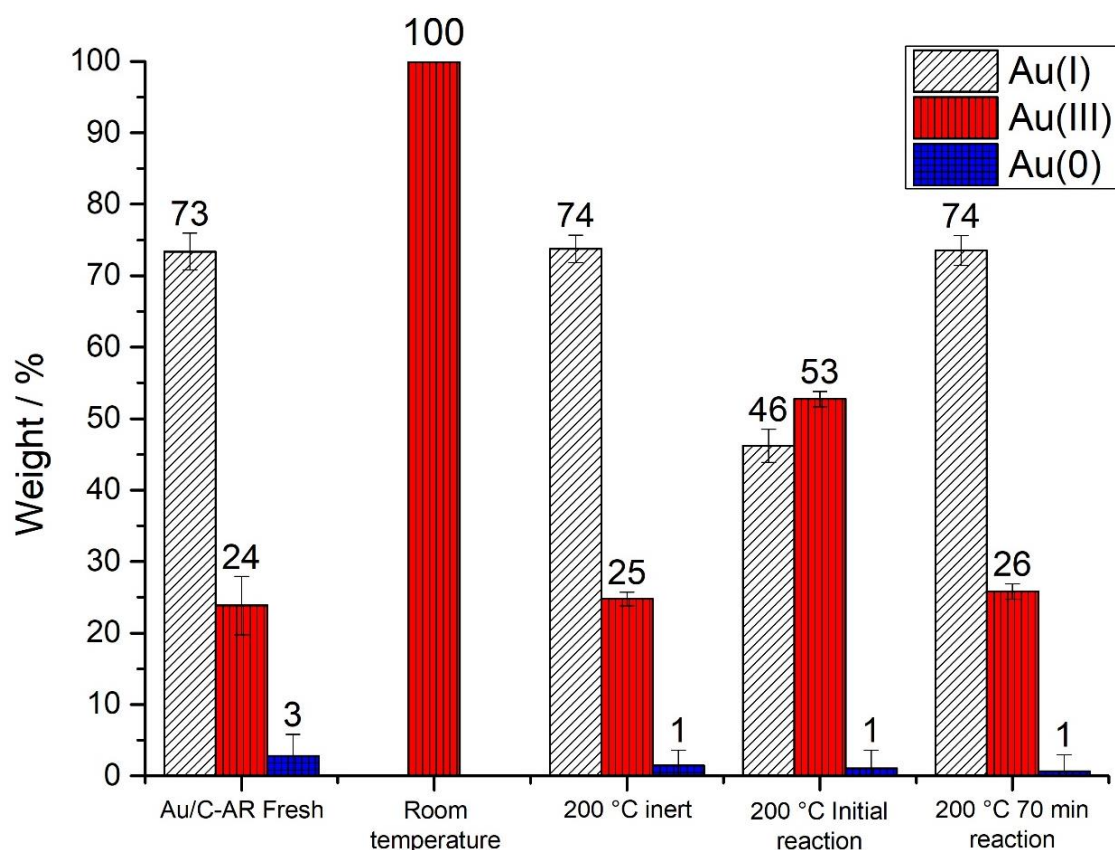


Figure 4.5. Linear combination fitting of the Au L_3 -edge XANES for Au/C-AR, Au/C-CoSO₄ at room temperature, after heating to 200 °C under inert conditions, after introduction of reaction gases at 200 °C, after 70 min of reaction and Au foil reference. Error bars indicate standard deviation.

Analysis of the EXAFS region determined the short-range order of the catalysts at the different stages of the reaction (Figure 4.6). In all cases, the catalyst showed a distinct scattering peak at 1.8 Å corresponding to Au-Cl, although the intensity of this was significantly higher in Au/C-CoSO₄ at room temperature compared to Au/C-AR. As all of these XAS measurements were taken during *in-situ* experiments, therefore all comparable conditions, this could indicate a much greater concentration of Au-Cl or Au-S, both indistinguishable via EXAFS.³⁰ However, after heating this intensity reduces to a comparable level to that of Au/C-AR, indicating a change in oxidation state. No reflections at 2.5 and 3.0 Å were detected, indicating no significant gold nanoparticle formation. This matched the data obtained from XANES and XRD, indicating no agglomeration of gold atoms under reaction conditions.

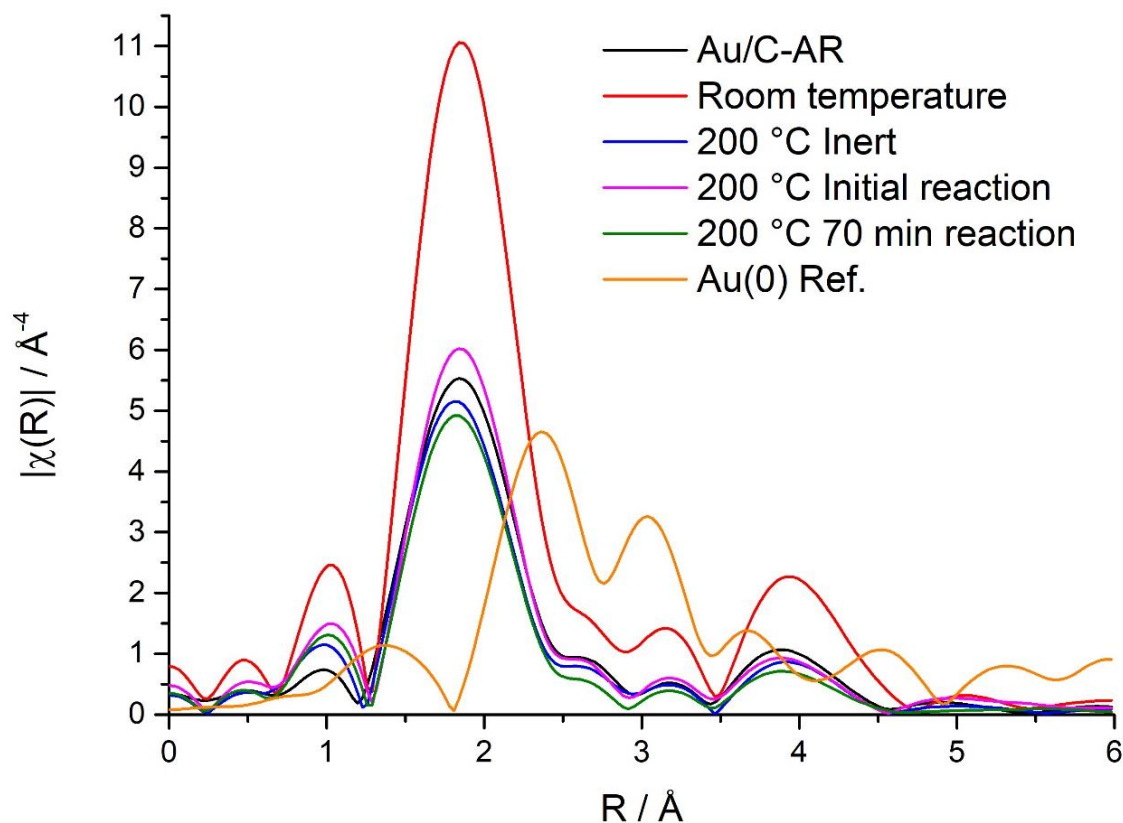


Figure 4.6. Fourier transform of the k^3 -weighted χ EXAFS data of Au/C-AR, Au/C-CoSO₄ at room temperature, after heating to 200 °C under inert conditions, after introduction of reaction gases at 200 °C, after 70 min of reaction and Au foil reference.

The combination of reaction and XAFS data showed that the addition of CoSO₄ to a Au/C catalyst increased the initial acetylene conversion, by oxidising the Au species present before reaction to Au(III). This increased the rate at which the gold reduced to the active Au(I) species, observed in the Au/C-R catalyst. However, it is important to note that the anion to Co²⁺, SO₄²⁻, may interact with the Au and hence impact the catalytic activity. Therefore, further preparations were performed, eliminating the second metal and replacing it with a simple cation to determine the effect of sulfate. This is detailed in the next section.

4.5. Catalysts prepared with salt sulfates

Two sulfate salts were chosen to replace the selection of metal sulfates used previously in order to compare the effect of sulfur on the catalytic performance; these were sodium sulfate and ammonium sulfate. For both salt sulfates, a catalyst was prepared by pre-washing the carbon in the saturated sulfate solution (5 g in 15 mL H₂O) in the same manner as performed on the metal sulfate catalysts. Gold was then added to the carbon using aqua regia as solvent to form the 1% Au/C pre-wash catalyst. Also, for each salt sulfate a post-wash catalyst was prepared. In this

case, Au/C-AR catalyst was stirred in the salt sulfate solution, followed by filtering, washing with 100 mL of H₂O and drying. Finally, a third catalyst was prepared using the salt sulfate solution instead of aqua regia. This was labelled “no AR” in figures.

4.5.1. (NH₄)₂SO₄ treatment

The catalysts prepared with (NH₄)₂SO₄ were tested for the acetylene hydrochlorination reaction and the results shown in Figure 4.7. (NH₄)₂SO₄ Pre-wash showed a much higher conversion (45 %) than that of Au/C-AR (18 %) but a similar reaction profile; an induction period lasting roughly 240 min before stabilising at a constant conversion. This suggests that sulfate is responsible for the increase in catalyst activity, as opposed to the metals introduced in the previous section. Both (NH₄)₂SO₄ post-wash and no AR had poor conversion (3 %), comparable to that of carbon with no gold present (2 %). The reactions were stopped at 100 min as the conversion was stable in both catalysts.

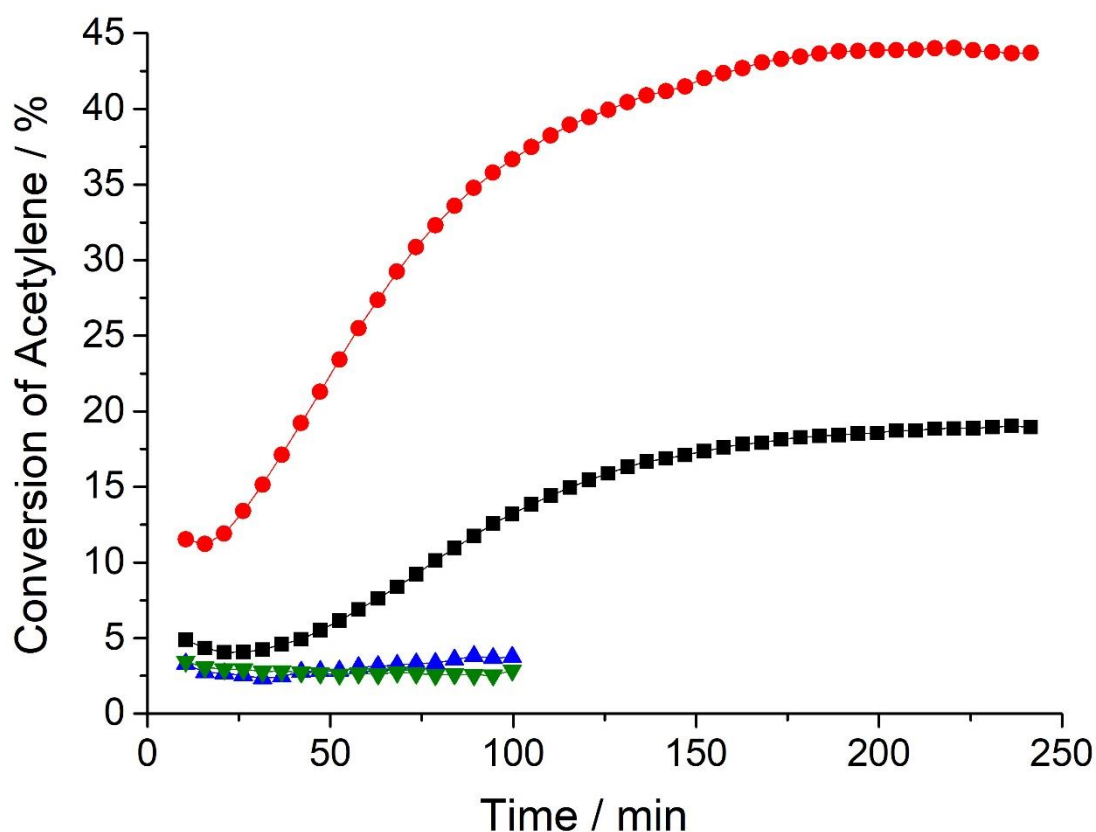


Figure 4.7. (NH₄)₂SO₄ treated catalysts time-on-line data – pre-wash (●), post-wash (▲), no AR (▼) and Au/C-AR (■), conditions stated in section 4.2.3.

XRD analysis of the three fresh catalysts determined that both (NH₄)₂SO₄ post-wash and no AR catalysts contained nanoparticles prior to reaction (Figure 4.8), whilst the pre-wash displayed

no gold reflections. This result was not unexpected in the no AR catalyst, as it is known that using water as a solvent when preparing Au/C catalysts from HAuCl_4 results in the gold being reduced on the carbon support.^{30,31} Water is not a strong enough oxidising agent to maintain the gold in its oxidised form, therefore inactive nanoparticles are readily formed.

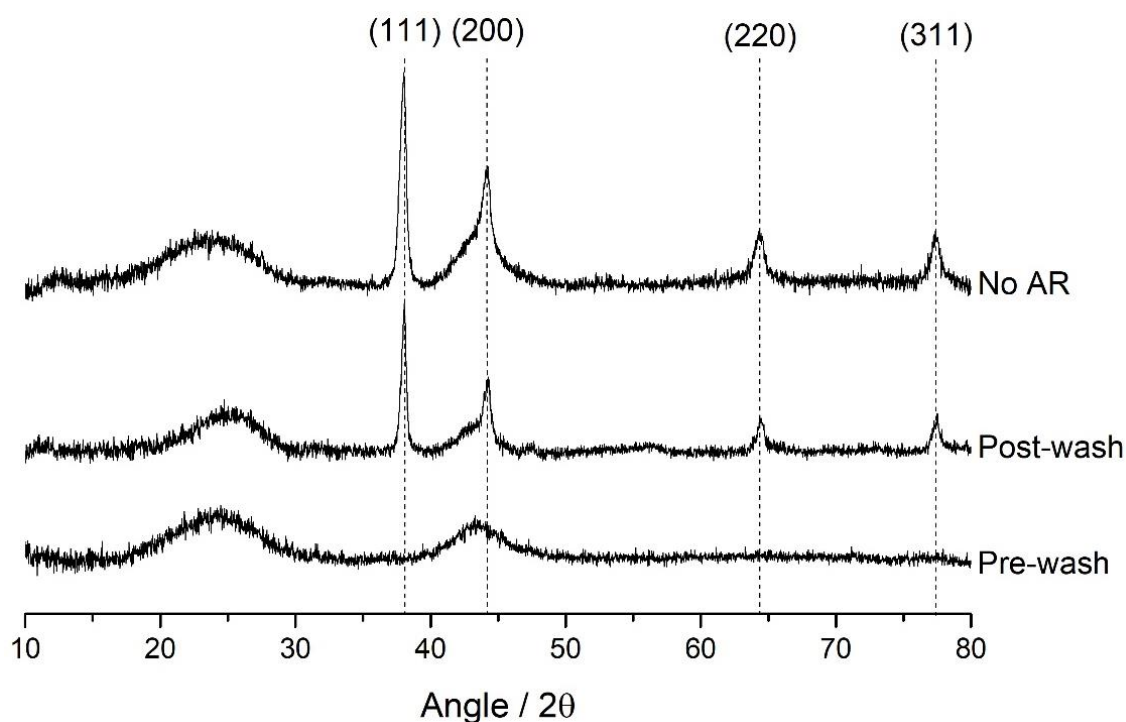


Figure 4.8. XRD patterns of fresh $(\text{NH}_4)_2\text{SO}_4$ catalysts – pre-wash, post-wash and no AR. Reflections at 38, 44, 65 and 78 / 2θ correspond to FCC metallic gold crystallites.

To determine if the salt was responsible for the nanoparticle formation or just the solvent (water), the post-wash preparation was repeated using a fresh Au/C-AR catalyst and water, instead of the $(\text{NH}_4)_2\text{SO}_4$ solution. XRD was performed which showed that just by stirring the catalyst in water and drying at 110 °C the gold was mobilised on the surface of the support and agglomerated to form nanoparticles (Figure 4.9). These nanoparticles were ~50 nm, calculated using the Scherrer equation.

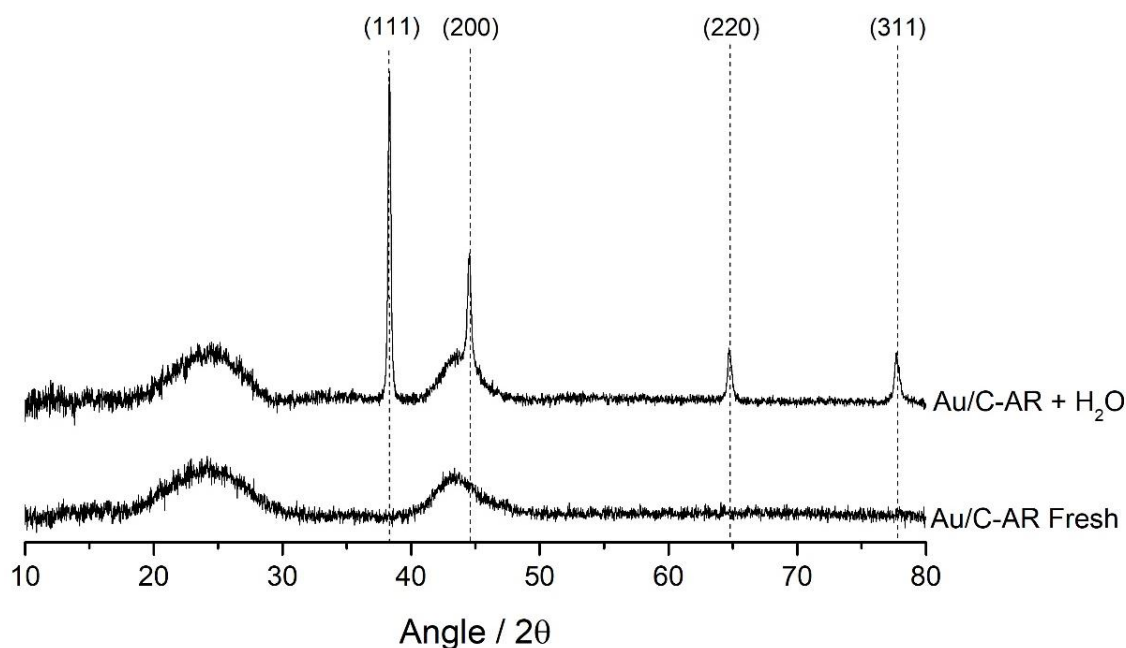


Figure 4.9. XRD patterns of fresh Au/C-AR and Au/C-AR after stirring in water for 1 h. Reflections at 38, 44, 65 and 78 / 2θ correspond to FCC metallic gold crystallites.

In combination, these results show that the introduction of sulfate resulted in an increase in acetylene conversion and also indicates that an excess of water can result in the agglomeration of gold during catalyst preparation.

4.5.2. Na_2SO_4 treatment

Reactions were performed on the three catalysts prepared with Na_2SO_4 – pre-wash post-wash and no AR (Figure 4.10). Unlike the $(\text{NH}_4)_2\text{SO}_4$ pre-wash, the pre-wash of Na_2SO_4 had no effect on the catalytic performance – Na_2SO_4 pre-wash had an almost identical reaction profile to that of Au/C-AR. Both $(\text{NH}_4)_2\text{SO}_4$ post-wash (5 %) and no AR displayed poor conversion, the latter deactivating in the short reaction time from 5 to 3 %.

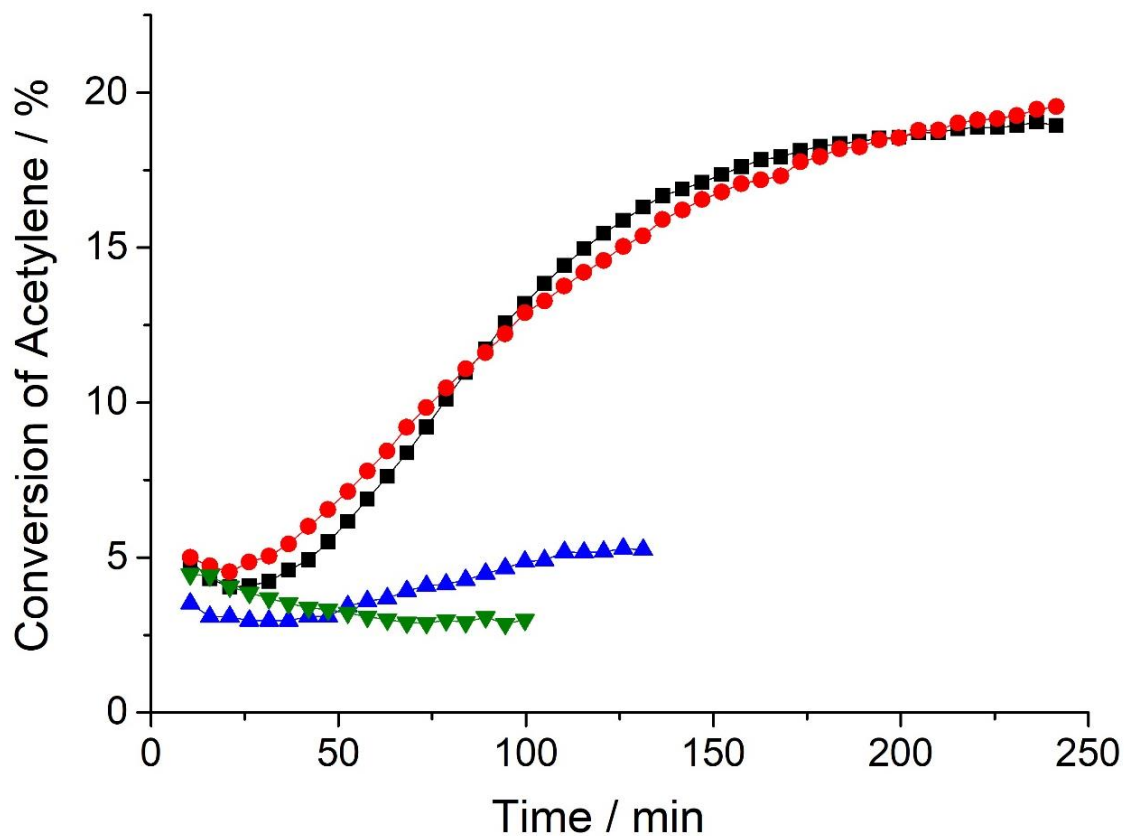


Figure 4.10. Na_2SO_4 treated catalysts time-on-line data – pre-wash (●), post-wash (▲), no AR (▼) and Au/C-AR (■).

XRD of each of the Na_2SO_4 catalysts was performed, showing very similar results to those of $(\text{NH}_4)_2\text{SO}_4$, with no nanoparticles observed in the pre-wash catalyst and nanoparticles present in both the post-wash and no AR catalysts (Figure 4.11). The same reasons for the formation of nanoparticles discussed in the $(\text{NH}_4)_2\text{SO}_4$ catalysts (4.5.1) would also explain those observed here.

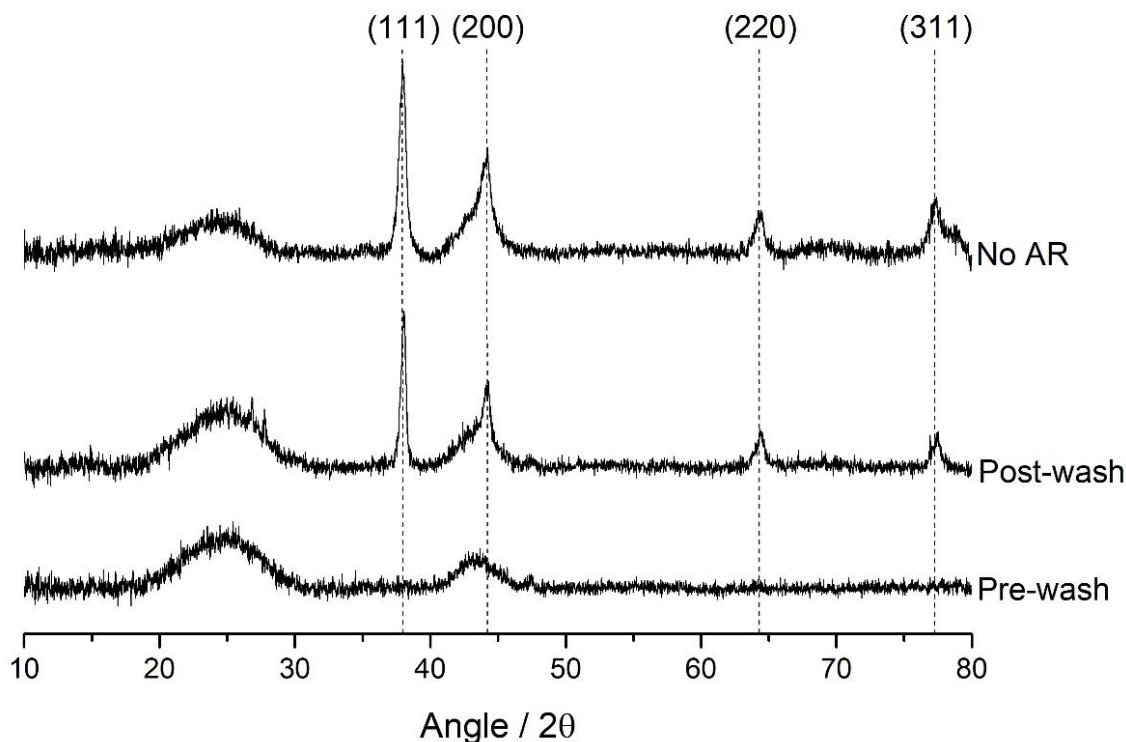


Figure 4.11. XRD patterns of fresh Na_2SO_4 catalysts – pre-wash, post-wash and no AR. Reflections at 38, 44, 65 and 78 / 2θ correspond to FCC metallic gold crystallites.

The results of these tests performed on $(\text{NH}_4)_2\text{SO}_4$ and Na_2SO_4 catalysts showed that it was possible to produce catalysts with high initial activity without the presence of another metal, merely with the addition of the sulfate anion. However, it was also shown that the choice of cation played an important role in promoting the binding of the sulfate to the support, as using NH_4^+ resulted in a more active catalyst than Na^+ . Elemental analysis of these catalysts should also be performed to determine if there was any correlation between catalytic activity and the concentration of elements present.

4.6. Sulfuric acid catalysts

In this section, sulfur was introduced to the carbon using sulfuric acid instead of metal salts. Carbon was treated using the same preparations as mentioned previously with sulfuric acid; pre-wash, post-wash and no AR. Each of the three preparations are split into their own sub-section to examine how these affected the catalytic activity.

4.6.1. Pre-treatment of carbon supports with sulfuric acid

Carbon was stirred in three dilute solutions (0.076, 0.76 and 1.52 M) of sulfuric acid to form pre-wash carbons. Gold was then deposited on these supports using aqua regia. The resulting time-

on-line data for these catalysts (Figure 4.12) shows the influence the support has on the acetylene conversion. In all three catalysts the conversion was the highest observed in any Au/C catalysts tested under the same reaction conditions; 0.76 M pre-wash achieved an initial conversion of 70 %, 1.52 M – 67 % and 0.076 M – 60 %. Each catalyst displayed very similar reaction profiles; an induction period lasting no longer than 30 min, followed by a steady decline in acetylene conversion for the remaining reaction time resulting in conversions between 49 – 52 %. Altering the concentration therefore only had a small effect on the initial conversion, with all catalysts falling to a similar conversion after 240 min.

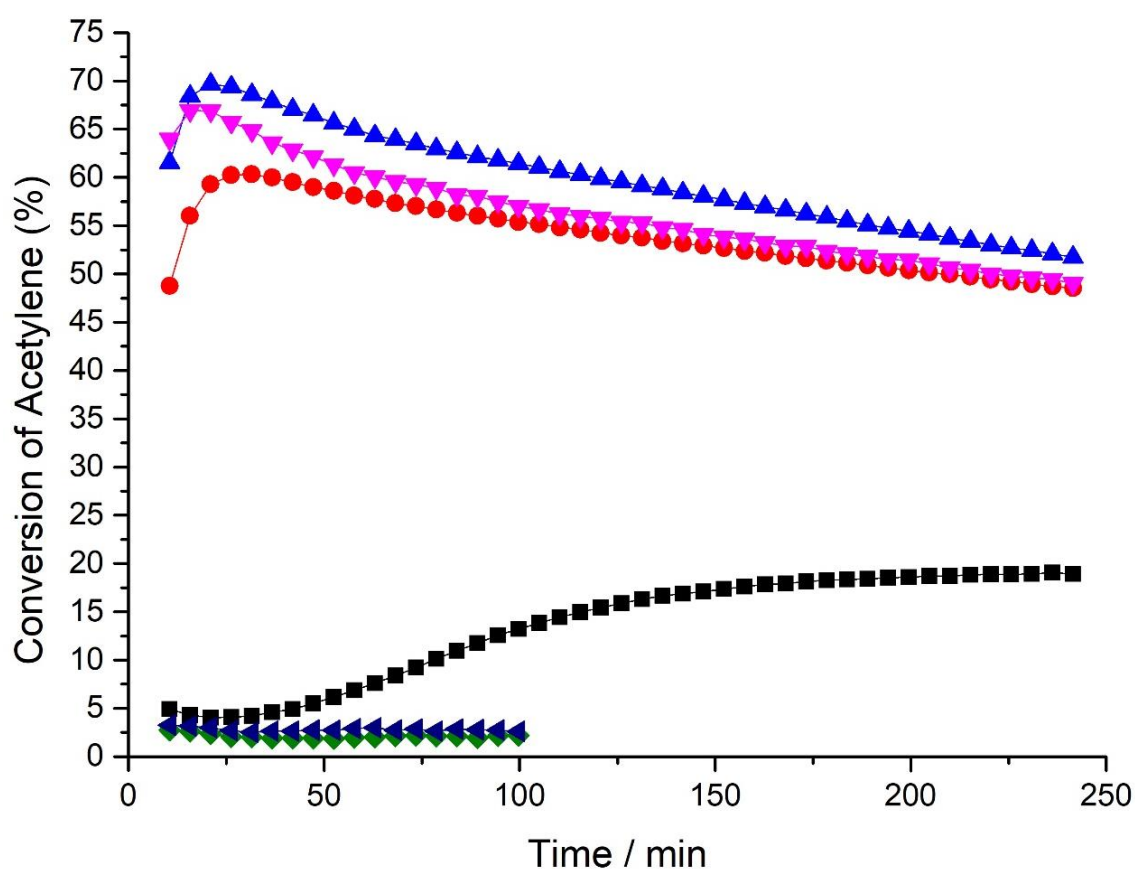


Figure 4.12. H₂SO₄ pre-wash catalysts time-on-line data – Au/C-AR (■), 0.076 M H₂SO₄ (●), 0.76 M H₂SO₄ (▲), 1.52 M H₂SO₄ (▼), 0.76 M H₂SO₄ carbon (◆) and carbon (◄), conditions stated in section 4.2.3.

XPS analysis of each fresh catalyst was performed to compare the relative concentrations of sulfur and oxygen on the H₂SO₄ catalysts using the S 2p and O 1s scans, to see if there was any correlation between these and catalytic activity. These scans showed very similar atomic concentrations of sulfur of 0.4 – 0.6 % and correspondingly similar oxygen concentrations, 7.7 – 9.4 %. These comparable values would explain the very similar acetylene conversions, as each catalyst would be likely to contain similar bonding sites. Each catalyst also showed mixtures of

Au(0), Au(I) and Au(III); however, no quantification of the proportions of gold species was performed due to the reducing nature of the XPS beam which could lead to erroneous values.³⁰ This analysis should, therefore, be performed using XANES.

Table 4.2. Sulfur and oxygen atomic concentrations of 0.076, 0.76 and 1.52 pre-wash catalysts, determined via XPS.

Catalyst	S At. %	O At. %
0.076 M Pre-wash	0.6	8.5
0.76 M Pre-wash	0.5	7.7
1.52 M Pre-wash	0.4	9.4

XRD analysis (Figure 4.13) confirmed that none of the fresh catalysts contained gold nanoparticles (only fresh 0.076M pre-wash catalyst shown for clarity, both fresh 0.76 and 1.52 M appeared identical to this), whilst the used catalysts showed only small reflections owing to nanoparticle formation, visible at $38 / 2\theta$. This indicates that not only were these catalysts highly active but the gold also remained relatively stable throughout the reaction, the majority remaining as single-site gold and not sintering at high acetylene conversion (although small clusters would remain undetectable via XRD). This is dissimilar to previously reported high activity Au/C catalysts which display significant growth of gold nanoparticles,³² suggesting that the gold is better supported on these H₂SO₄ pre-wash catalysts.

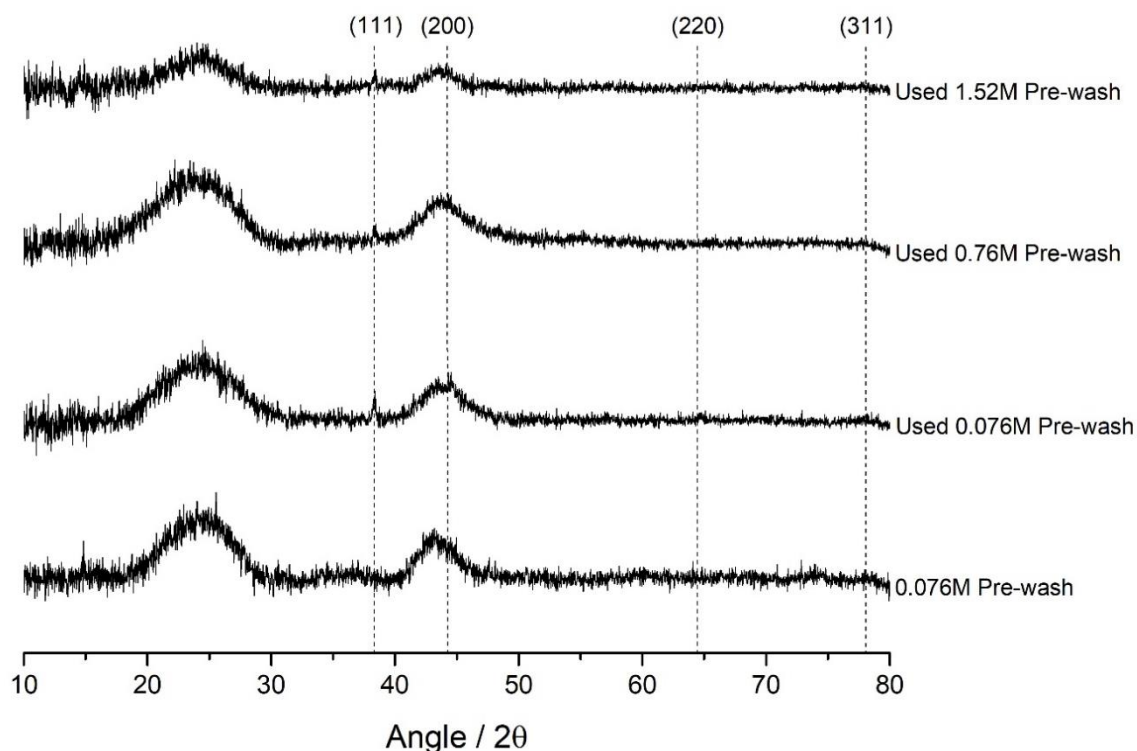


Figure 4.13. XRD patterns of fresh and used pre-wash H_2SO_4 catalysts. Reflections at 38, 44, 65 & 78 / 2θ correspond to FCC metallic gold crystallites.

Further characterisation was performed on 0.76 M pre-wash catalyst as this achieved the highest acetylene conversion. To determine whether the small proportion of gold nanoparticle formation observed in the used catalyst occurred as a result of heating or due to the reaction itself, the catalyst was heated under nitrogen whilst *in-situ* XRD analysis was performed (Figure 4.14). This showed that no reflections corresponding to gold nanoparticles were observed until 240 °C. Above this temperature, characteristic reflections at 38, 44, 65 and 78 / 2θ became visible. Therefore, the small nanoparticles observed in the used catalyst (Figure 4.13) were formed due to the introduction of the reaction gases. As sintering of gold occurred at 240 °C, this indicates that the gold was less stable than Au/C-AR, which began sintering at 320 °C (see 3.7, Figure 16 for *in-situ* XRD performed on Au/C-AR). Therefore, the addition of sulfur has reduced the stability of the catalyst at high temperatures.

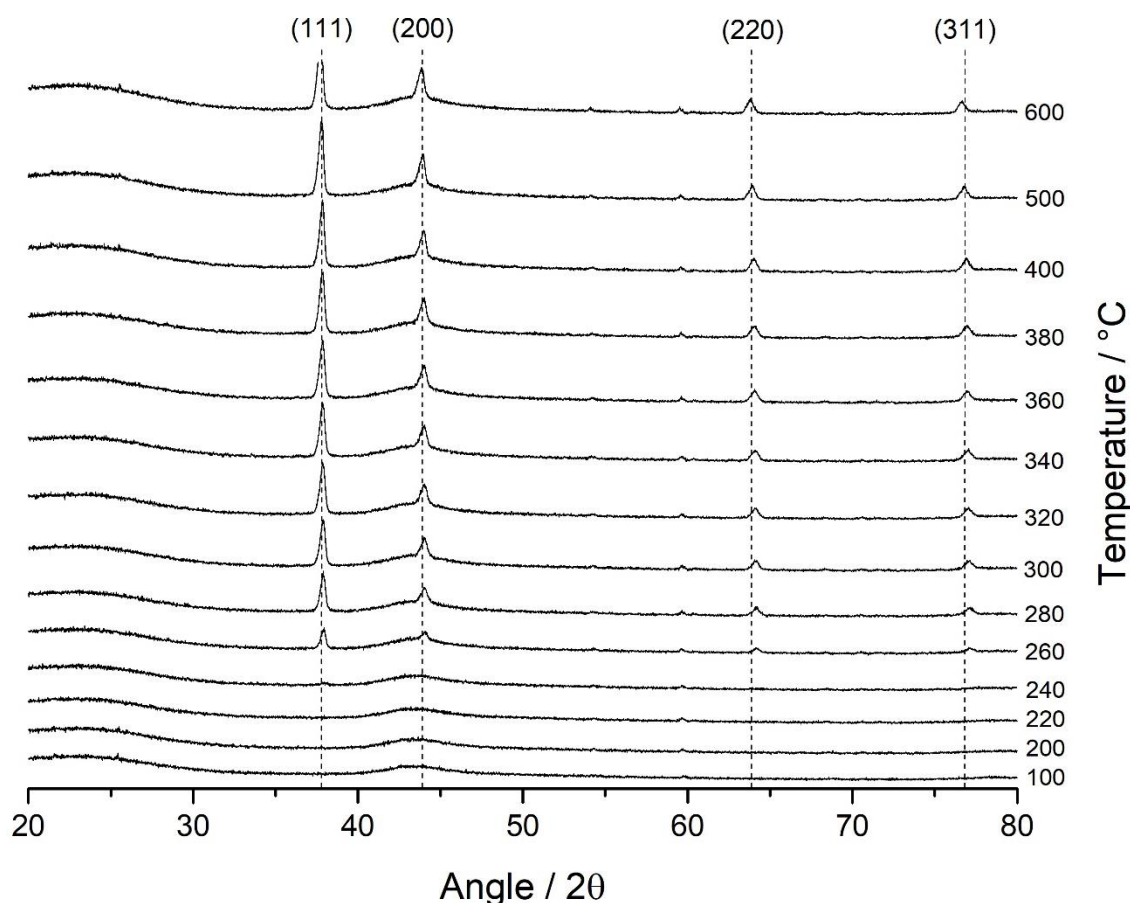


Figure 4.14. *In-situ* XRD of Fresh 0.76M H₂SO₄ Pre-wash. Reflections at 38, 44, 65 & 78 / 2θ correspond to FCC metallic gold crystallites.

Continuing to study the 0.76 M pre-wash catalyst, XPS analysis was performed at various conditions; after it had been heated to 200 °C under argon gas and then allowed to cool (labelled heated), after reaching maximum initial conversion (used, max. conversion), and after performing a reaction for 240 min (used, 240 min). These values were also compared to those obtained from Au/C-AR (Table 4.3). All of the 0.76 M pre-wash catalysts showed very little variation: sulfur concentration varied from 0.5 – 0.3 %, and variation in oxygen concentration was 8.8 – 6.6 %. Comparing these catalysts to Au/C-AR, however, shows that even after use the concentration of sulfur had remained slightly higher on 0.76 M pre-wash than on Au/C-AR (0.1 %), whilst the concentration of O was lower than that of Au/C-AR (7.6 %). From these results it can be concluded that the sulfur treatment only adds a small relative fraction of sulfur to the pre-wash catalyst, however this is still sufficient to have a remarkable enhancement in catalytic activity. This also shows that the majority of the sulfur introduced to the catalyst remains after reaction, as only a loss of 0.2 % occurs, whilst the concentration of oxygen also remains relatively constant.

Table 4.3. Sulfur and oxygen atomic concentrations of 0.76 M pre-wash catalyst at various stages of the reaction; fresh, after heating to 200 °C under argon, after reaching highest initial conversion and after 240 min of reaction, and Au/C-AR. Determined via XPS.

Catalyst	S At. %	O At. %
0.76 M Pre-wash fresh	0.5	7.7
0.76 M Pre-wash heated	0.4	7.4
0.76 M Pre-wash used, max. conversion	0.3	8.8
0.76 M Pre-wash used, 240 min	0.4	6.6
Au/C-AR fresh	0.1	7.6

This reaction was repeated with a mass-spectrometer connected to the rig, to analyse the composition of the gas stream post-reaction *in-situ*. Unfortunately, due to such low concentration of sulfur, any possible evolution of sulfur containing species was not detected. This test confirmed that the only product formed was VCM, consistently achieving > 99 % selectivity.

4.6.2. The effect of temperature on sulfuric acid pre-treated catalysts

All of the reactions performed above were tested at 200 °C to ensure that any observed changes in catalytic activity were not as a result of variation in temperature. To determine activity at temperatures comparable to those used in industrial reactors (130 – 160 °C), further tests were performed on 0.76 M pre-wash at lower temperatures. A reaction was initiated at 100 °C and the temperature increased in 25 °C increments until 175 °C. This showed that the catalyst was inactive from 100 – 150 °C, however light-off (defined in this work as when the change in acetylene conversion is greater than 0.05 % min⁻¹) occurred at 175 °C (Figure 4.15). Further tests carried out between 150 – 175 °C determined that the catalyst had a high rate of change of conversion at 160 °C and above (Figure 4.16). This light-off showed that 0.76M pre-wash was active at temperatures below that of Au/C-AR and still maintained a reduced induction period in comparison to Au/C-AR, both desirable qualities for industrial application. The test performed at 155 °C showed the catalyst to have a steadily increasing acetylene conversion. This test should be repeated to determine if the conversion would reach the same values as the higher temperature tests, albeit with a longer induction period. This temperature was determined to be the lowest at which the catalyst was active under these reaction conditions.

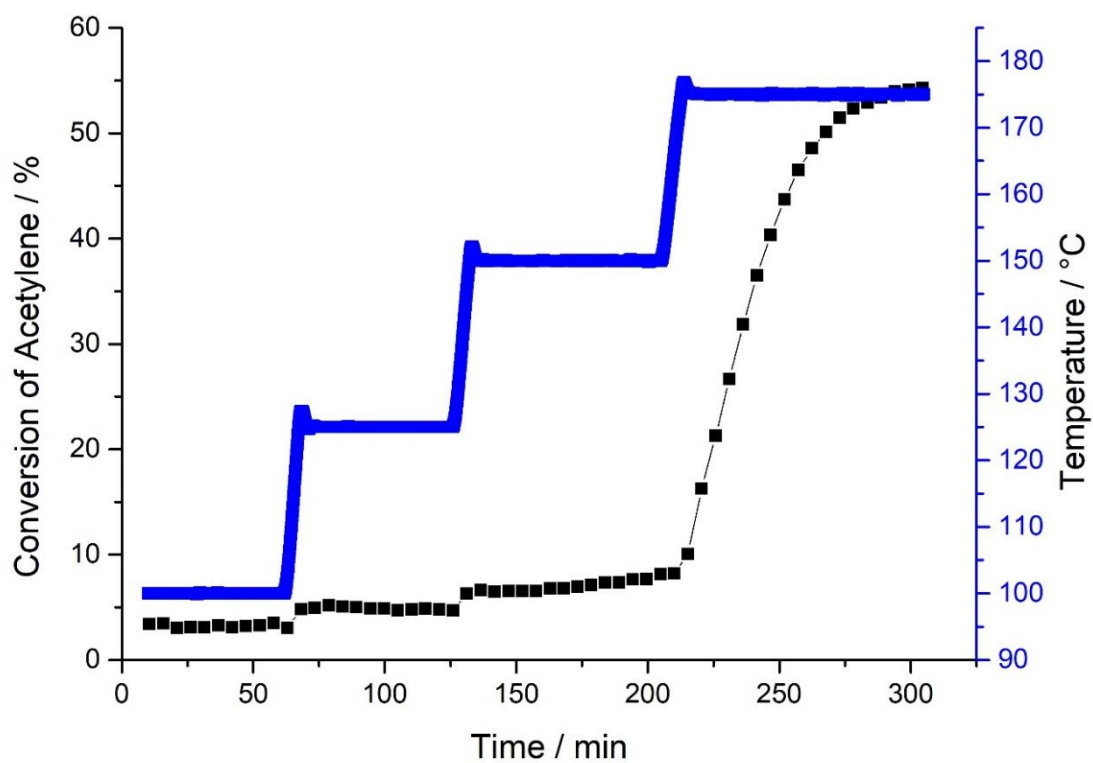


Figure 4.15. Time-on-line of Au/C – 0.76 M pre-wash, heated from 100 to 175 °C, conditions stated in section 4.2.3.

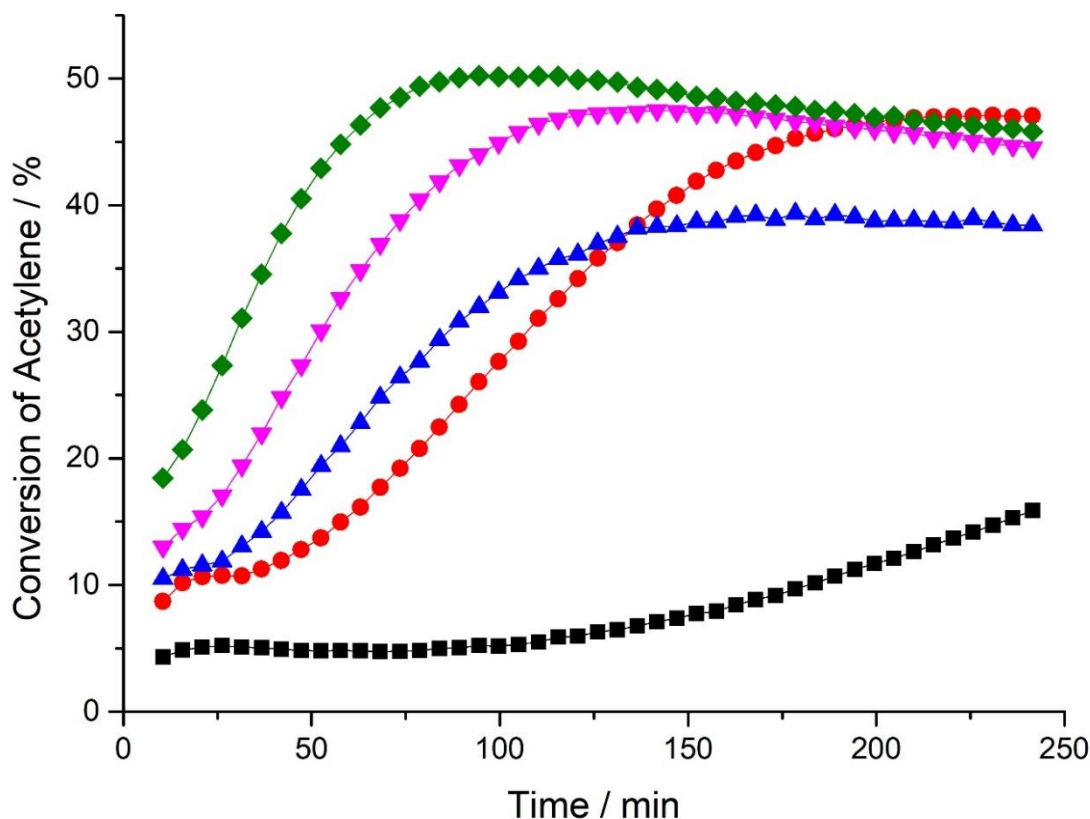


Figure 4.16. Time-on-line of Au/C – 0.76 M pre-wash, tested at 155 °C (■), 160 °C (●), 165 °C (▲), 170 °C (▼) and 175 °C (◆), conditions stated in section 4.2.3.

XANES analysis was performed to compare the gold oxidation state of the fresh 0.76 M pre-wash catalyst and those tested at 160 °C and 200 °C. These were also compared to Au/C-AR and gold foil for reference (Figure 4.17). Fresh 0.76 M pre-wash catalyst was composed of a mix of Au(I) and Au(III) states, with more Au(III) character present than observed in fresh Au/C-AR. After reaction, used 0.76 M pre-wash 160 °C was very similar to the fresh, with only a slight loss of Au(III). Increasing the temperature to 200 °C caused a further reduction, resulting in more Au(I) content, very similar to that of Au/C-AR. The conversion of Au/C-AR and used 0.76 M pre-wash (200 °C) differed by 34 % even though the oxidation states were primarily the same. This shows that another factor must contribute to the activity of the catalyst, such as dispersion of gold, availability of active sites or the interaction of the gold with reactants.

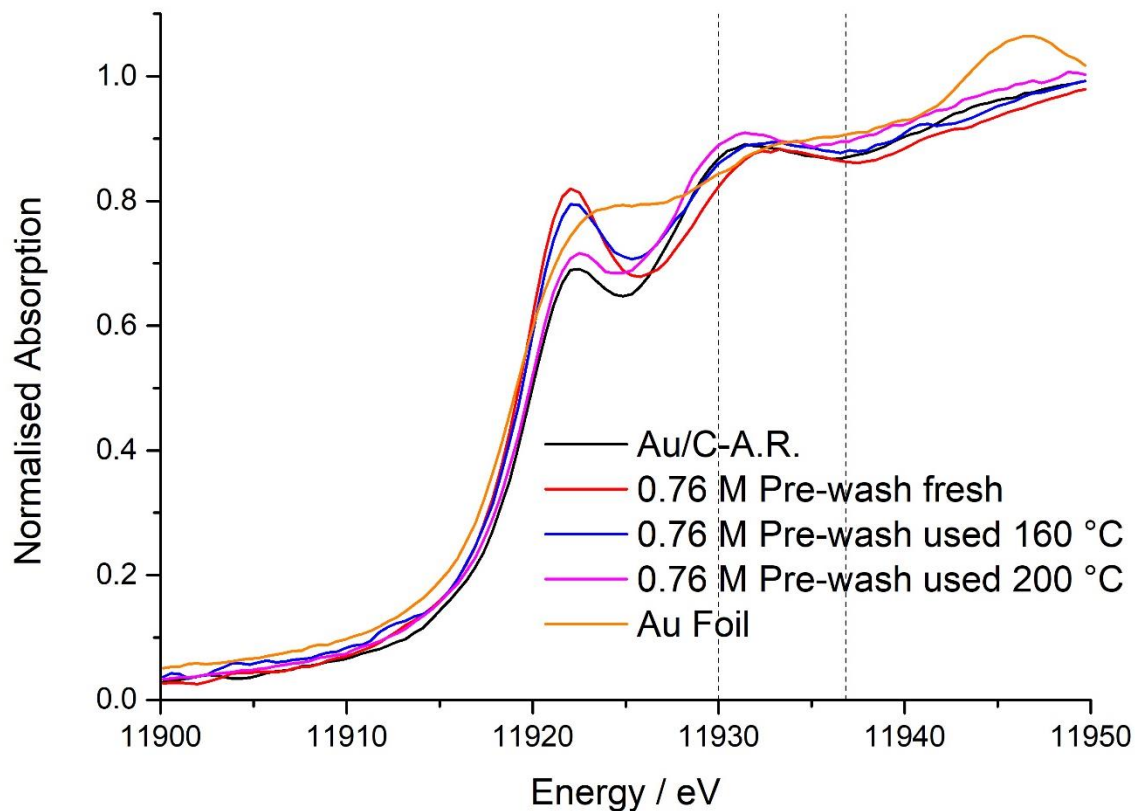


Figure 4.17. Au L_3 -edge XANES of Au/C-AR, pre-wash 0.76 M H_2SO_4 fresh, used at 160 °C, used at 200 °C and Au foil reference. Region between dashed lines (11,930 – 11936 eV) shows position of second prominent scattering feature.

LCF of the XANES data was performed to quantify the fraction of these gold oxidation states present in each catalyst (Figure 4.18). This data showed a mix of Au(I) (52 %) and Au(III) (48 %) in fresh 0.76 M pre-wash. By reacting the catalyst, the percentage of Au(I) increased, to 62 % in used 0.76 M pre-wash 160 °C and 75 % in used 0.76 M pre-wash 200 °C, matched by a corresponding decrease in Au(III). Used 0.76 M pre-wash 200 °C also had a small increase in Au(0) content (5 %).

This data does not correspond well with the XANES white line heights shown in Figure 4.17, which can be explained by the fitting of the standards to the reference materials (Figure 4.19 - Figure 4.22). In all the EXAFS analysis performed so far it was assumed that oxidised gold existed as gold chloride, as the starting material of the catalyst was $HAuCl_4$ and there was an abundance of chlorine present in the solvent, aqua regia. However, since the introduction of sulfur to the carbon support, the XANES data for the 0.76 M pre-wash catalysts no longer fit the Au-Cl references, hence the XANES absorption values not agreeing with the LCF data. In the four figures shown (Figure 4.19 - Figure 4.22) it is important to note that a smaller R-Factor (a quantitative value of the misfit of the data) and Chi-square (the statistical goodness-of-fit

parameter) value indicates a better data fit, as the maximum value of uncertainty of the fit is equal to 1.^{33,34} Using Au/C-AR as an example of “good fit” values (R-factor 0.000914, Chi-square 0.01377), the values of 0.76 M pre-wash used 160 °C and 0.76 M pre-wash used 200 °C are both over 1.5 times the R-factor and chi-square values. This does not however explain the disparity between fresh 0.76 M pre-wash (R-factor 0.000723, Chi-square 0.01043) and Au/C-AR.

It was reported that Au(I)-S and Au-Cl can be differentiated by the ligand affected scattering feature, Au(I)-S at 11,930 eV and Au-Cl having two shifts due to the different oxidation states; lower energy, 11,923 eV, with Au(I)-Cl and higher energy, 11,934 eV, with Au(III)-Cl.³⁵ A Au-S standard was not run during the XANES analysis shown in Figure 4.17; however the Au(I) and Au(III) chloride standards both show a shift in energy from 11,931 to 11,936, respectively, as shown in **3.7**, Figure 17. Comparing scattering features around the same energy range for the fresh and used 0.76 M pre-wash catalysts (region between dashed lines, 11,930 – 11,936 eV in Figure 4.17) shows a decreasing trend in energy for each catalyst, as noted in Table 4.4. This implies that fresh 0.76 M pre-wash was composed of Au-S, with a scattering energy of 11,933 eV, between those of Au(I) and Au(III). Performing the reaction at 160 °C resulted in a shift in scattering energy to 11,932 eV and increasing the temperature to 200 °C resulted in a further shift to 11,931 eV, the same as that of Au(I). Therefore, subjecting the catalyst to reaction gases and increasing the temperature may have resulted in a change of Au speciation, from Au-S to Au-Cl, or perhaps a mix of both. Further tests would be needed using appropriate Au-S standards and preferably an *in-situ* reaction to determine if this was the case.

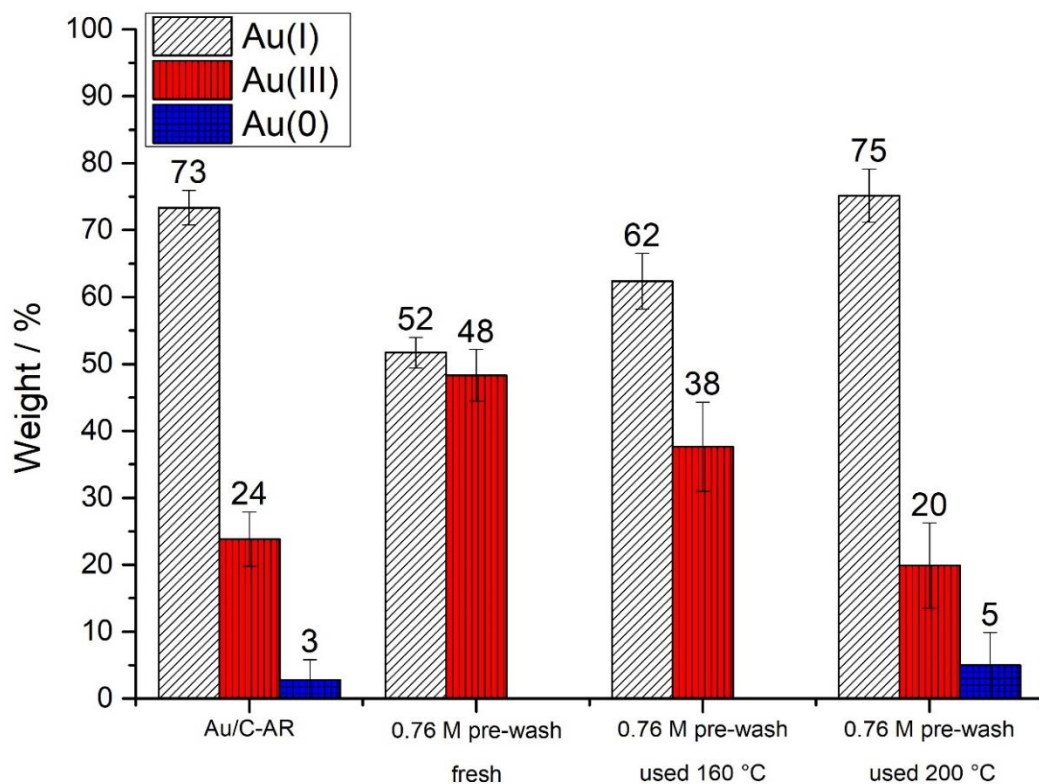


Figure 4.18. Linear combination fitting of the Au L₃-edge XANES for the fresh aqua regia catalyst, fresh and used at 160 °C and 200 °C 0.76M H₂SO₄ pre-wash catalysts. Error bars indicate standard deviation.

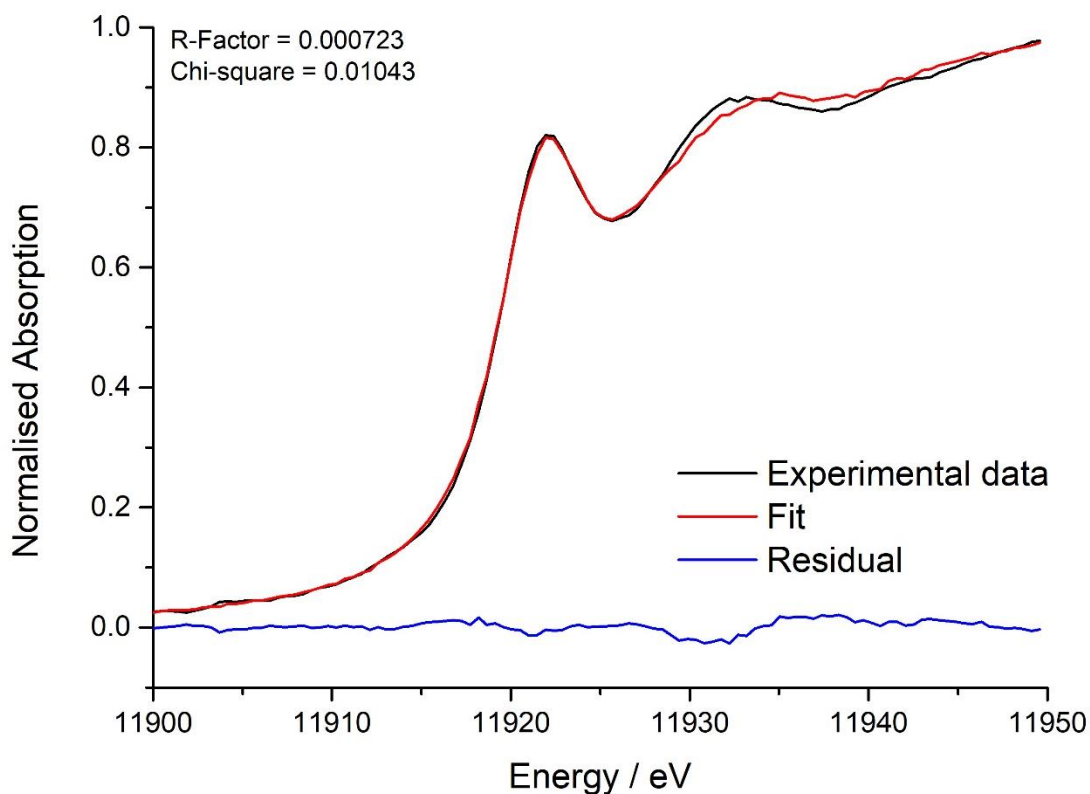


Figure 4.19. XANES data fitting for pre-wash 0.76 M pre-wash fresh.

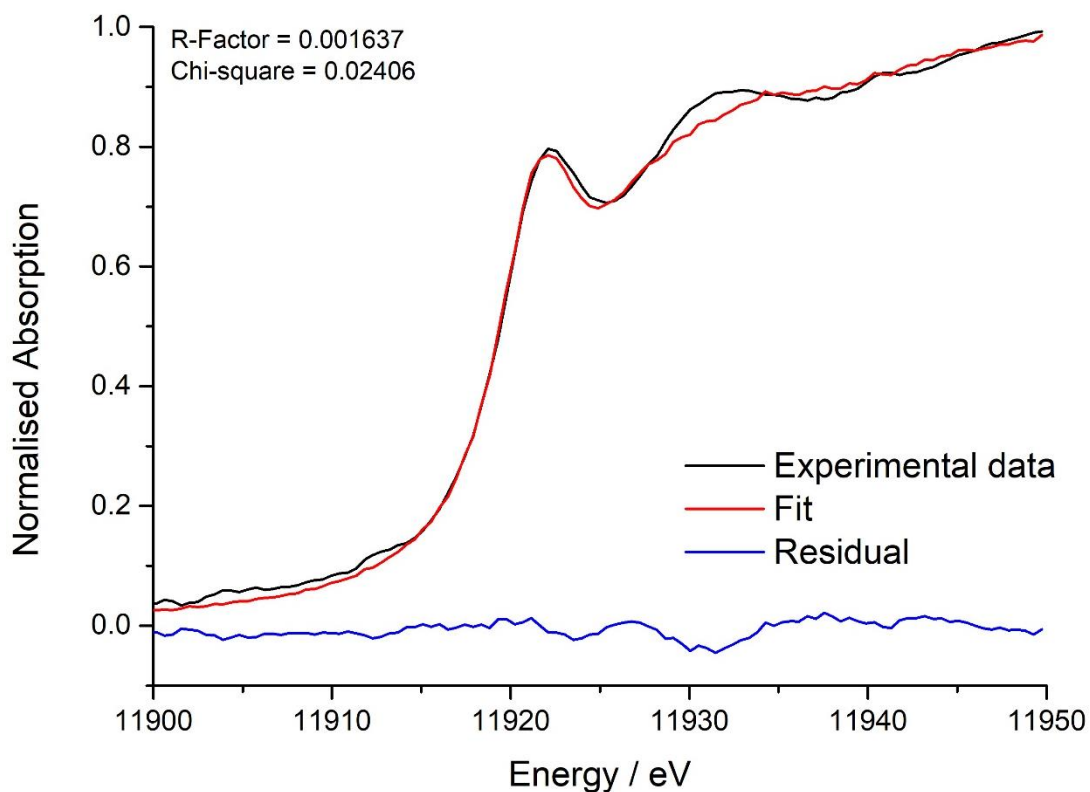


Figure 4.20. XANES data fitting for pre-wash 0.76 M pre-wash used 160 °C.

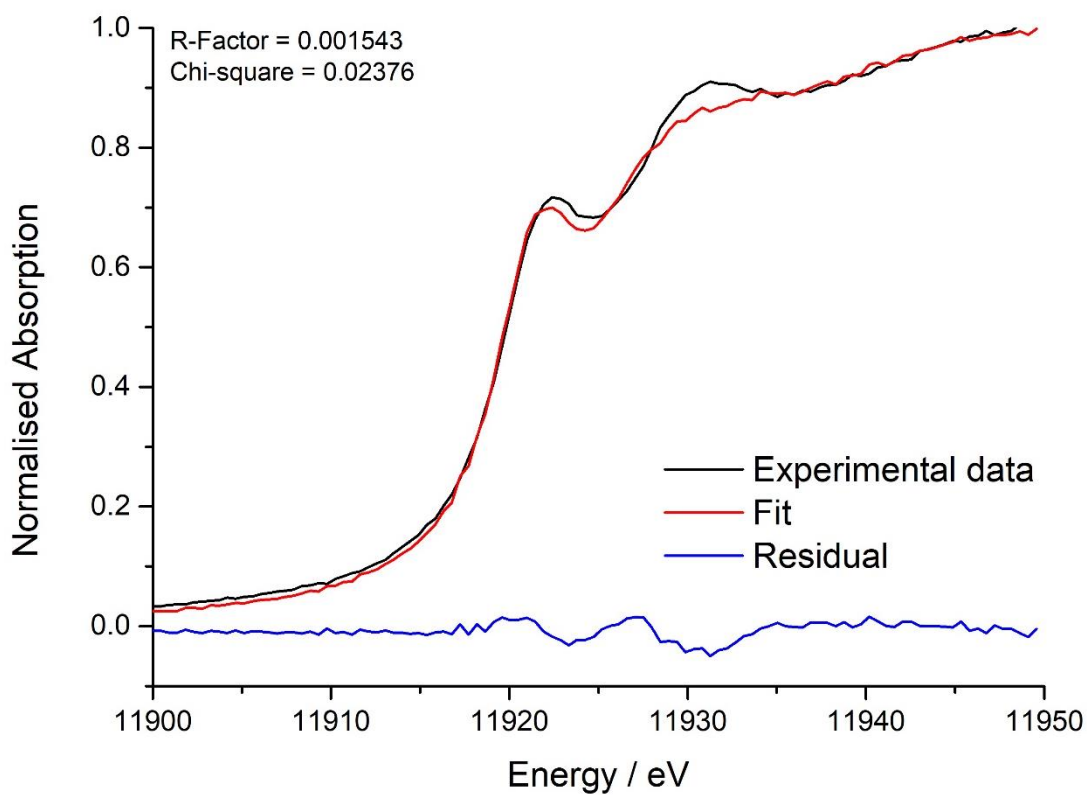


Figure 4.21. XANES data fitting for pre-wash 0.76 M pre-wash used 200 °C.

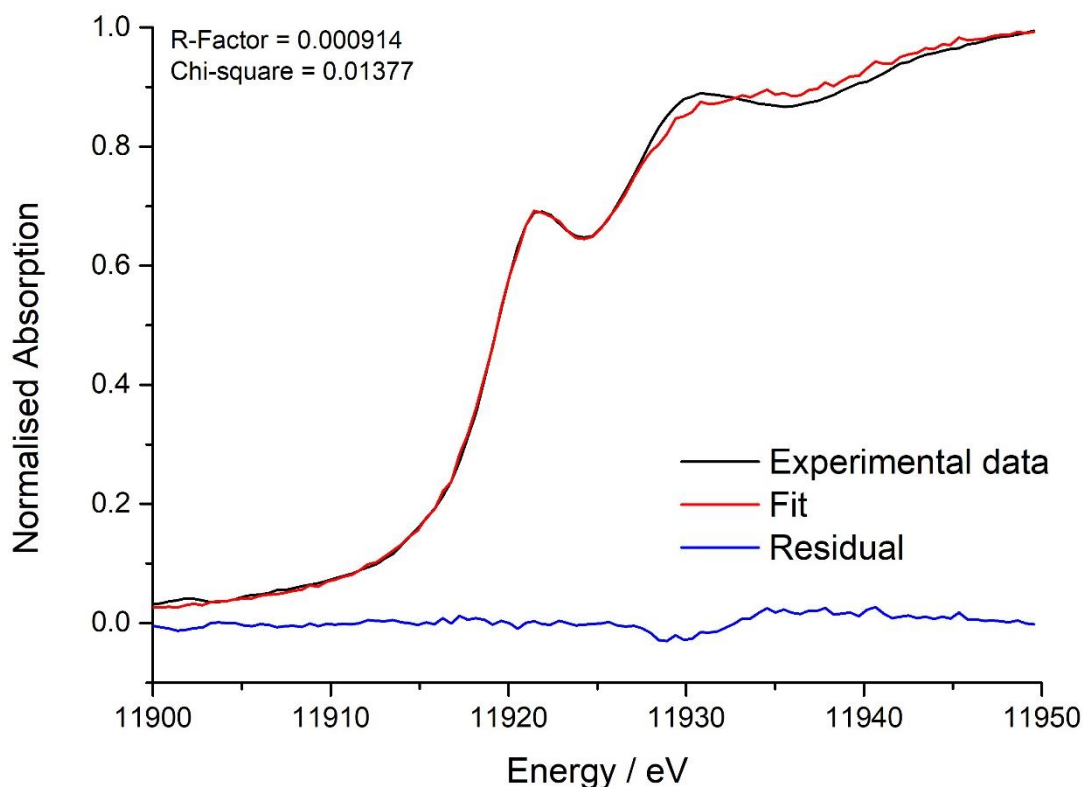


Figure 4.22. XANES data fitting for Au/C-AR.

Table 4.4. Comparison of energies of second absorption features for Au(I) and Au(III) chloride standards, pre-wash 0.76 M H₂SO₄ fresh, used at 160 °C and used at 200 °C catalysts.

Catalyst	Energy / eV
Au(I)	11,931
Au(III)	11,936
Fresh 0.76 M pre-wash	11,933
Used 0.76 M pre-wash 160 °C	11,932
Used 0.76 M pre-wash 200 °C	11,931

The EXAFS appears to show that all of the fresh and used 0.76 M pre-wash catalysts are composed of Au-Cl (Figure 4.23). Unfortunately, the scattering patterns of sulfur and chlorine appear virtually indistinguishable via EXAFS due to their atomic number differing by only one.^{30,35,36} Therefore, the results shown in Figure 4.23 for the fresh and used 0.76 M pre-wash catalysts only show a sharp scattering path at 1.8 Å, identified as the interaction of Au with a lighter element, in this case chlorine or sulfur. These results do show a much higher intensity of oxidised gold in fresh 0.76 M pre-wash than in Au/C-AR, perhaps owing to the higher concentration of S. However, after reaction at 160 and 200 °C the intensity of the scattering was the same as that Au/C-AR, suggesting a loss of this new species. This same trend was observed

in Au/CoSO₄ (4.4, Figure 4.6) albeit with a much higher initial intensity of Au-Cl/Au-S, therefore it is reasonable to suggest that the decrease in Au-Cl/Au-S intensity occurred during heating. No scattering associated with Au-Au was observed. As EXAFS is a global averaging technique, the small presence of nanoparticles detected by XRD in Figure 4.13 may not have been observed here due to the abundance of oxidised gold present.

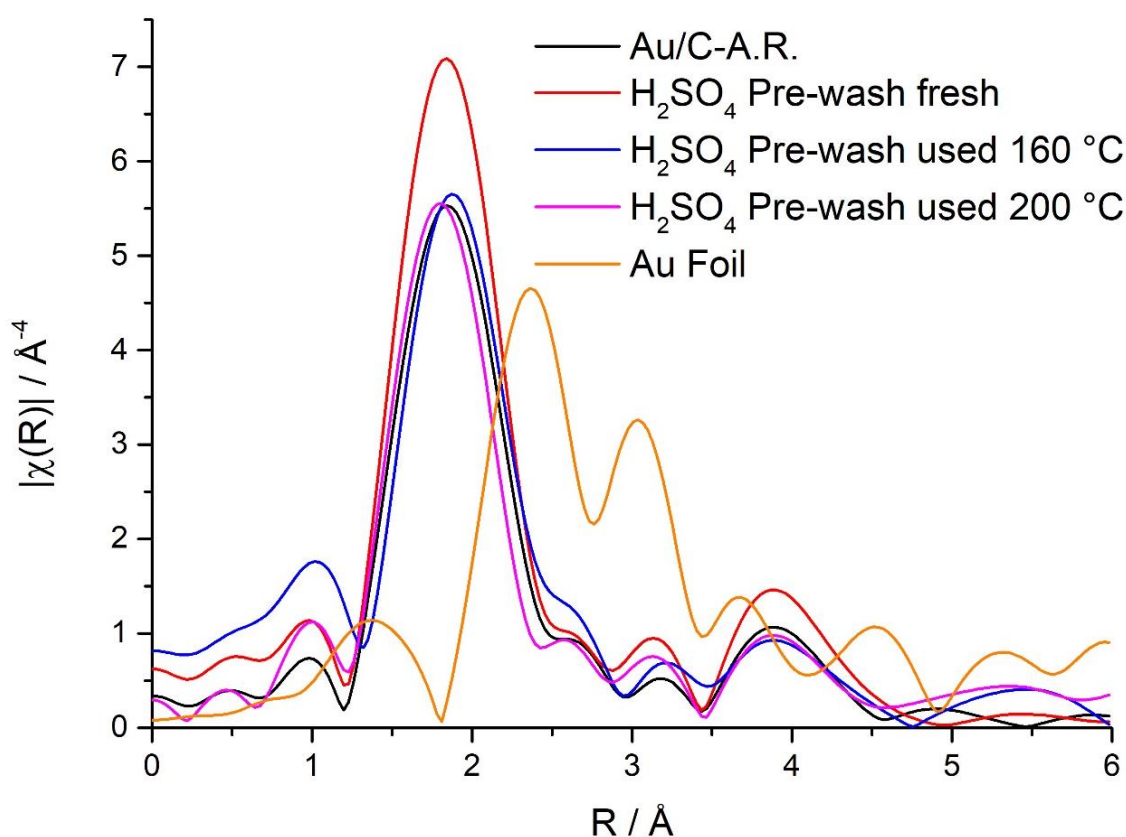


Figure 4.23. Fourier transform of the k^3 -weighted χ EXAFS data of Au/C-AR, pre-wash 0.76 M H₂SO₄ Fresh, used at 160 °C, used at 200 °C and Au foil reference.

4.6.3. The effect of water washing on pre-treated carbon supports

To prepare the pre-wash catalysts, the carbon was stirred in a 0.76 M H₂SO₄ solution, then washed with 100 mL H₂O whilst filtering, dried and used as the support. In this section, the volume of water used to wash the carbon was varied to determine what effect it may have on the sulfur concentration. To compare the activity of the catalysts, four extra 0.76 M H₂SO₄ supports were prepared using 0, 50, 500 and 1000 mL of water to wash the carbon. HAuCl₄ was then added to the supports to make 1% Au/C catalysts using aqua regia. These were compared to Au/C-AR and 0.76 M pre-wash prepared using 100 mL H₂O, as shown previously and in Figure 4.24. Using high volumes of H₂O (1000 and 500 mL) results in a small decrease in maximum initial

conversion (58 and 55 %, respectively) compared to 100 mL (70 %). This would be expected as a higher volume of water would result in the removal of excess, unbound sulfur from the support, thereby removing anchoring points for gold. This could lead to a decrease in dispersion of gold cations, reducing the activity of the catalyst. The catalyst washed with 50 mL of H₂O initially achieved a conversion the same as that of 1000 mL (58 %), but this decreased at a greater rate, resulting in a catalyst which had a lower final conversion (42 %, compared to 48 %). This catalyst may have contained too much acid on the support, hence the more rapid onset of deactivation. This was observed in the catalyst that was not washed with H₂O (0 mL), which showed a rapid deactivation, followed by a stable, low conversion of 5 %. Acid sites are a known cause of Au/C catalyst deactivation, due to acid catalysed acetylene polymerisation which coats the surface of the catalyst, blocking the active sites and rendering the catalyst inactive.^{28,32}

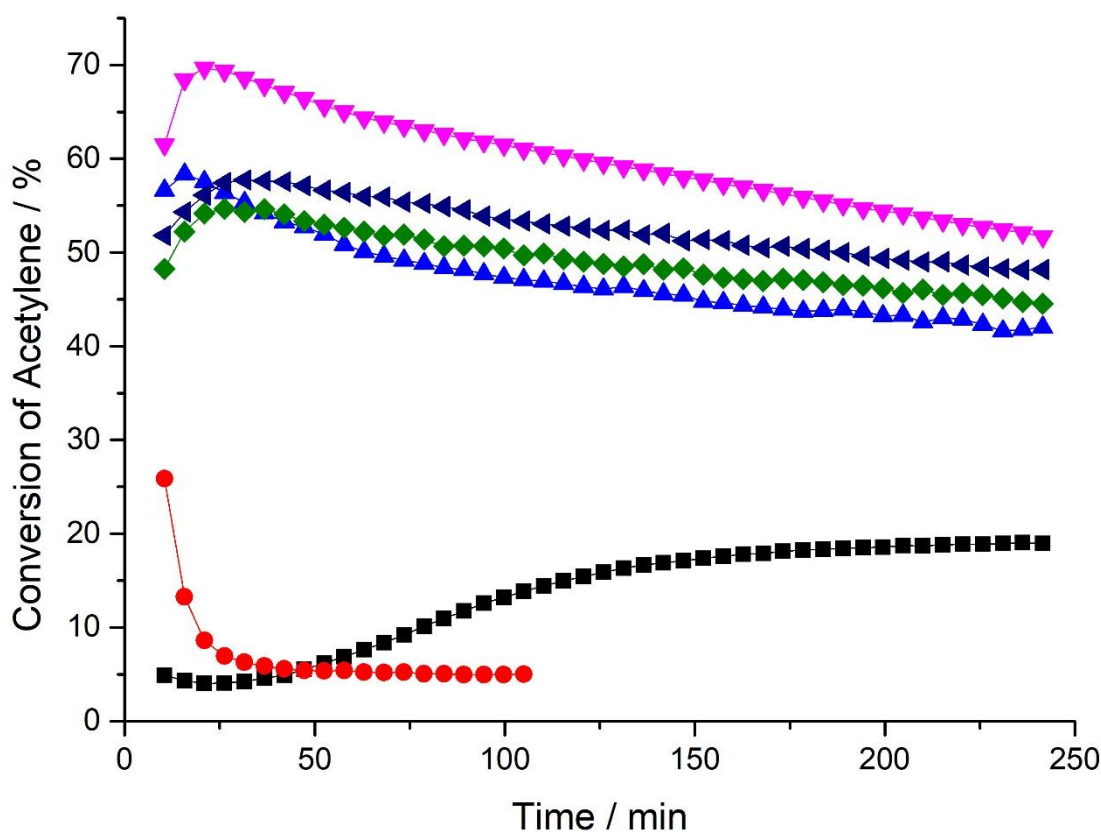


Figure 4.24. Acid pre-wash catalysts with varying volumes of H₂O wash time-on-line data – Au/C-AR (■), 0 mL wash (●), 50 mL wash (▲), 100 mL wash (▼), 500 mL wash (◆) and 1000 mL wash (◄), conditions as stated in section 4.2.3.

MP-AES of the filtrate of these carbons was performed to determine the mass of sulfur removed from the supports during the washing process. The results (Figure 4.25) show that the mass of sulfur removed increases significantly with increasing wash volume from 50 to 100 mL (234 and

304 mg respectively). However, after increasing the volume to 500 mL and 1000 mL there is only a small increase in mass of sulfur removed, to 332 and 372 mg, respectively. These results show that the catalyst washed with 50 mL of H₂O removed 1.3 times less sulfur than that washed with 100 mL. One could suggest therefore that a much greater mass of sulfur remained on the catalyst, which may explain the more rapid deactivation of the 50 mL washed catalyst. Using volumes of water greater than 100 mL continued to decrease the concentration of sulfur but had less effect on the catalyst conversion as only unbound sulfur would be removed, hence the similar reaction profiles observed in Figure 4.24.

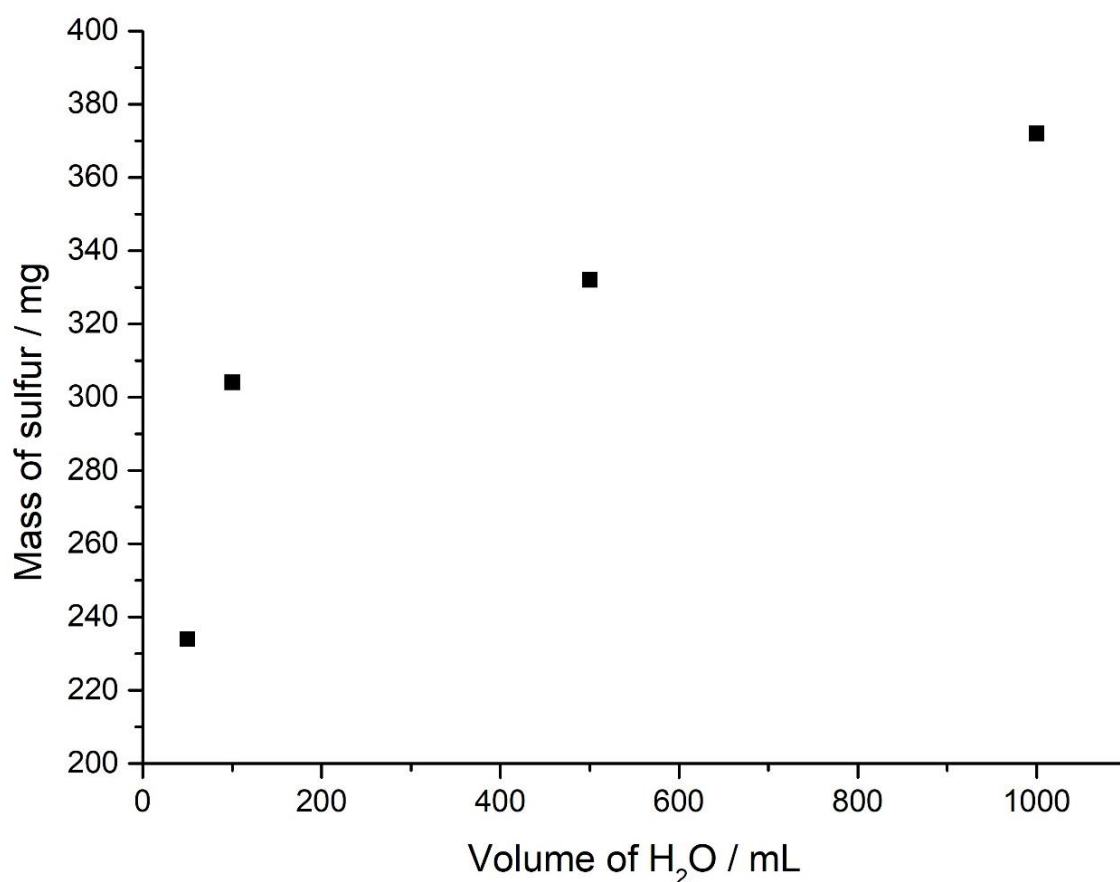


Figure 4.25. Mass of sulfur removed from 0.76 M H₂SO₄ pre-wash catalyst versus volume of water used to wash catalyst.

These MP-AES results fit well with XPS analysis performed on the same catalysts. Table 4.5 shows that the catalyst washed with 50 mL H₂O contains the highest concentration of sulfur (0.8 %), whilst the catalysts washed with 100, 500 and 1000 mL H₂O had very similar atomic concentrations (0.5 – 0.6 %) These measurements were at the limit of the XPS detection, therefore the 22 % difference between the MP-AES values of 100 and 1000 mL would be difficult to distinguish via XPS. The change in oxygen concentrations did not match those of sulfur,

suggesting that more than just oxygen containing sulfate species were present on the support. This was unsurprising, given the high concentration of oxygen present when no sulfur was introduced to the catalyst (Au/C-AR, Table 4.3 – 7.6 %).

Table 4.5. Sulfur and oxygen atomic concentrations of H₂SO₄ pre-wash catalysts washed with 50, 100, 500 and 1000 mL H₂O, determined via XPS.

Volume of H ₂ O / mL	S At. %	O At. %
50	0.8	8.7
100	0.5	7.7
500	0.6	9.4
1000	0.6	8.5

4.6.4. Post-treatment of catalyst with sulfuric acid

A series of post-wash H₂SO₄ catalysts were also prepared varying the concentrations of H₂SO₄ to determine if the activity of the catalyst could be changed after preparing Au/C-AR. As performed for the pre-wash H₂SO₄ catalysts, initially three concentrations of acid were chosen; 0.076, 0.76 and 1.52 M. However, unlike the pre-wash catalysts, varying the concentration of H₂SO₄ in the post-wash resulted in significant changes in catalytic activity (Figure 4.26). 0.076 M post-wash showed a time-on-line profile very similar to that of Au/C-AR but a slightly lower final conversion (16 % and 19 %, respectively). Increasing the concentration to 0.76 M resulted in an increase in conversion (35 %), followed by a stable conversion for the remaining reaction time. Increasing the concentration again to 1.52 M increased the initial conversion further, to 57 %, however this was then followed by a slow deactivation, as was observed for all of the pre-wash H₂SO₄ catalysts. As the conversion increased with increasing H₂SO₄ concentration, a higher concentration still was used (7.6 M) to determine if this trend would continue. The typical procedure for preparing the post-wash catalysts involved stirring Au/C-AR in the sulfur solution, filtering, washing with 100 mL H₂O and drying. Due to the high acidity of 7.6 M H₂SO₄, this catalyst was centrifuged after stirring in acid to separate the solvent from the solid catalyst, then 100 mL of H₂O added and centrifuged again, and finally dried. This method was used as the filter paper was readily dissolved in the acid. Figure 4.26 shows that such a high concentration of acid resulted in a catalyst with a much more rapid deactivation than the other post-wash catalysts. It was hypothesised that this deactivation could be ascribed to the introduction of more acid sites due to the concentration of acid, which would catalyse the polymerisation of VCM, again

blocking the active gold species.^{37,38} However, XPS showed little variation in the oxygen atomic concentration (Table 4.6) and the oxygen species present in each of the post-wash catalysts which could indicate a greater concentration of acid species on the catalyst surface.³⁹ The acidity of the carbon could be measured using techniques such as the Boehm's titration, however, as discussed in 5.3.3 this technique has reported reproducibility issues, and problems determining total oxygen content in activated carbons, therefore was not performed.^{40,41}

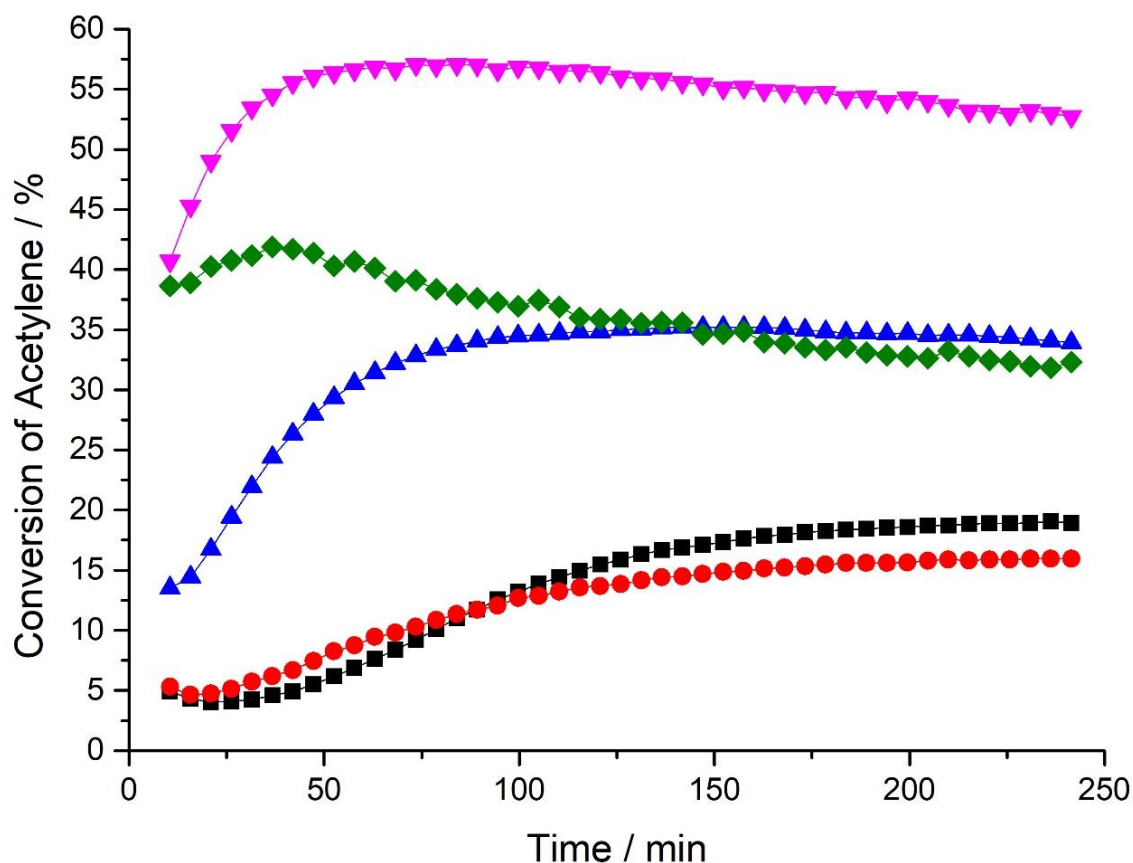


Figure 4.26. H₂SO₄ post-wash catalysts time-on-line data – Au/C-AR (■), 0.076 M H₂SO₄ (●), 0.76 M H₂SO₄ (▲), 1.52 M H₂SO₄ (▼) and 7.6 M H₂SO₄ (◆), conditions as stated in section 4.2.3.

Table 4.6. Sulfur and oxygen atomic concentrations of 0.076, 0.76, 1.52 and 7.6 M pre-wash catalysts, determined via XPS.

Catalyst	S At. %	O At. %
0.076 M Post-wash	0.5	7.9
0.76 M Post-wash	0.4	7.2
1.52 M Post-wash	0.5	8.2
7.6 M Post-wash	0.6	8.3

XRD analysis of each of the fresh and used H₂SO₄ post-wash catalysts was performed to determine how the reaction conditions affected the stability of the gold (Figure 4.27). 0.076 M post-wash contained nanoparticles before and after reaction. The solution used was a very dilute acid, therefore contained a high water content. As shown in **4.5.1**, Figure 4.9, stirring the catalyst in an aqueous solution results in the formation of nanoparticles; however, the activity profile shown in Figure 4.26 confirms that seemingly enough oxidised gold was stabilised on the support to produce an active catalyst. This also suggests that not all the gold present on Au/C-AR is active in the reaction as the same metal loading was used in all of the catalysts studied. The reaction also did not result in nanoparticle growth, confirming the stability of 0.076 M post-wash.

0.76 M post-wash did not contain any nanoparticles before reaction however they were present in the used catalyst. 1.52 M not only has a similar reaction profile to that of the pre-wash catalysts (**4.6.1**, Figure 4.12) but also had a similar lack of nanoparticles present before and after reaction. This shows that this catalyst was able to maintain a high concentration of oxidised gold when achieving high acetylene conversion. The nanoparticles observed in fresh and used 7.6 M post-wash are roughly of the same order as those of 0.076 M; however, both catalysts display very different activity profiles. The 7.6 M catalyst was thought to deactivate at a quicker rate than that of 0.076 M due to the high number of acid sites that facilitate acetylene polymerisation,^{28,32} as opposed to the agglomeration of gold (Table 4.6).

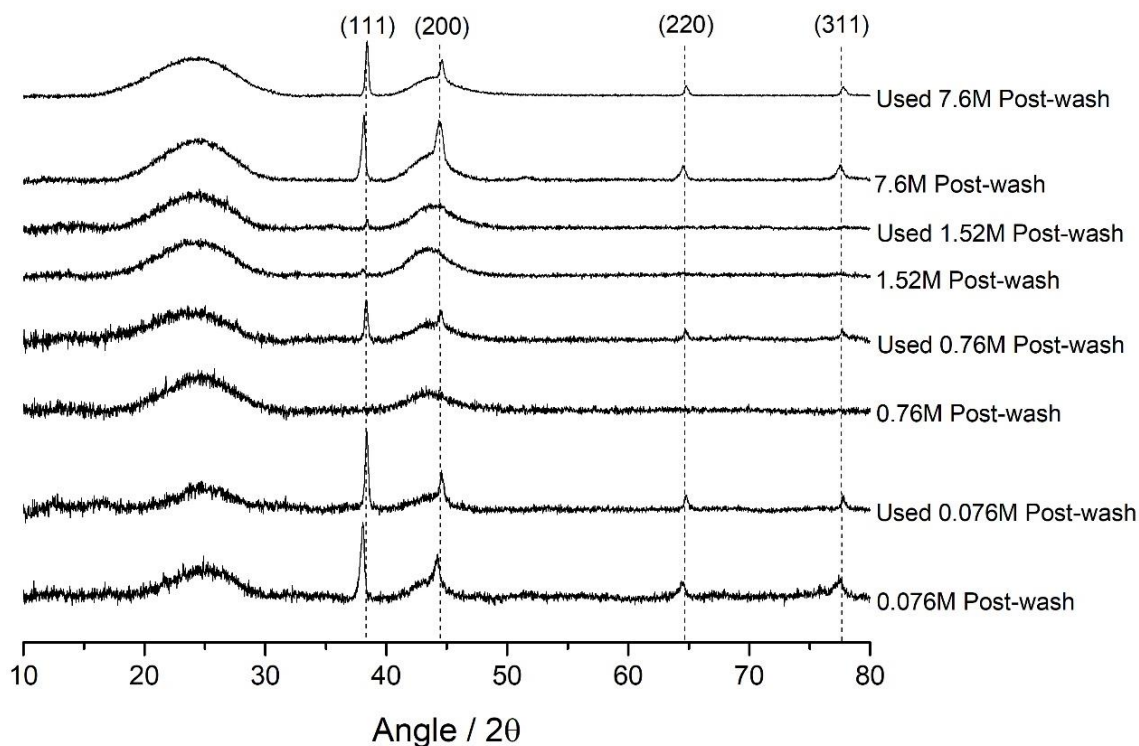


Figure 4.27. XRD of Post-wash H_2SO_4 catalysts. Reflections at 38, 44, 65 & 78 / 2θ correspond to FCC metallic gold crystallites.

These results show that variation in the concentration of H_2SO_4 post-wash had a much more significant effect on the catalytic activity than the pre-wash. The size of gold nanoparticles and hence the activity of the catalysts was directly affected by the water content of the solvent, in the case of 0.076 M and the acidity of the solvent, for 7.6 M. These factors must be controlled to produce active catalysts with steady conversion values.

4.6.5. Other sulfuric acid treatments

Two more variations in the preparation of H_2SO_4 catalysts were introduced to confirm the role of sulfur in the preparation. Firstly, a catalyst was prepared using 0.76 M H_2SO_4 as a solvent for HAuCl_4 (Au/C-0.76 M H_2SO_4 solvent). This was to determine whether H_2SO_4 had the oxidising ability to prepare a monodispersed gold on carbon without the aid of aqua regia. Secondly the carbon pre-wash support (C-0.76 M H_2SO_4) was tested without gold, to ensure that gold was necessary for the catalyst to be active. Figure 4.28 shows that the both materials had low conversions. For Au/C-0.76 M H_2SO_4 solvent, the low conversion was ascribed to the presence of large gold nanoparticles (>50 nm, calculated via the Scherrer equation) as determined by XRD analysis (Figure 4.29). These nanoparticles were present before the reaction, due to the highly aqueous based solvent which would not maintain gold in its oxidised form,³⁰ and grew upon

introduction to reaction conditions. C-0.76 M H₂SO₄ displayed a low conversion as there was no gold present. This confirms the role of gold as the active metal.

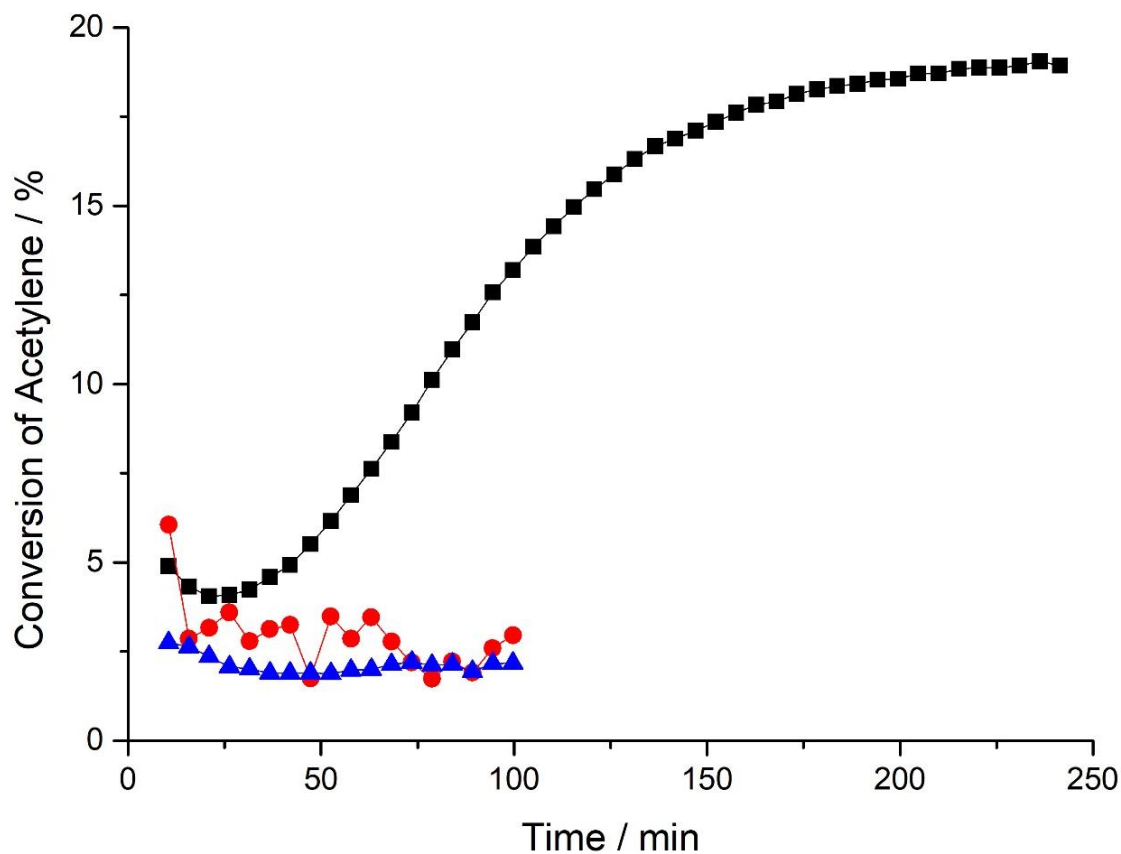


Figure 4.28. H₂SO₄ catalysts time-on-line data – Au/C-AR (■), Au/C-0.76 M H₂SO₄ solvent (●) and Carbon-0.76 M H₂SO₄ (▲), conditions as stated in section 4.2.3.

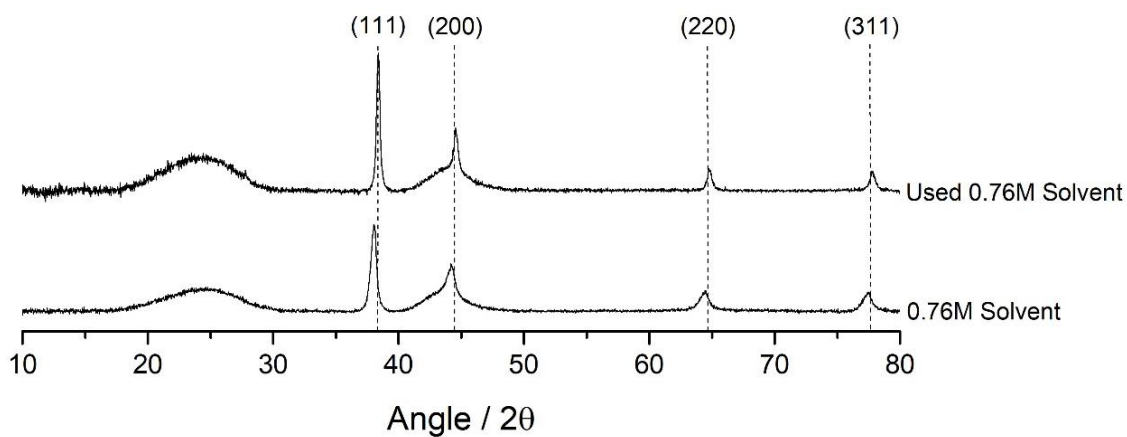


Figure 4.29. XRDs of catalysts prepared with 0.76M H₂SO₄ in place of aqua regia. Reflections at 38, 44, 65 & 78 / 2θ correspond to FCC metallic gold crystallites.

4.7. Acid treated catalysts

As H_2SO_4 had proven to be such an effective promoter for Au/C catalysts, three more acids were chosen to observe their oxidising ability. In each case, the carbon was pre-washed with 0.76 M acid and then gold added using aqua regia as the solvent.

Figure 4.30 shows that by pre-washing the support with HCl and HNO_3 , the acetylene conversion can be improved over that of Au/C-AR (22, 25 and 19 %, respectively). However, using aqua regia to pre-wash the carbon increases the conversion further (27 %), as would be expected due to a combined effect of using both acids. In each of these cases, the acid may serve to remove unwanted contaminants from the support. It is common practice, when preparing catalysts with a carbon support, to first wash the support using either dilute hydrochloric or nitric acid.⁴²⁻⁴⁴ This can be performed by stirring the carbon in the acidic solution, followed by filtering and further washing with water and finally drying, as performed above. The aim of the wash is to remove any surface contaminants, such as sodium, iron, or copper, which may act as a poison for the active metal species.⁴⁵

A H_3PO_4 pre-wash was also performed, resulting in a catalyst with a steadily increasing initial conversion, which then begins a steady decline after reaching a maximum of 55 %. The rate of decline was greater than that observed for the H_2SO_4 pre-wash catalyst, owing to a large agglomeration of gold nanoparticles, as determined via XRD (Figure 4.31). H_3PO_4 is a weak oxidising agent and therefore would not be expected to have stabilised the oxidised gold sufficiently to maintain the high activity throughout the reaction.⁴⁶ XRD also confirmed that the catalysts prepared with HCl, HNO_3 and aqua regia also contained no nanoparticles before and after use. (For clarity only fresh catalysts were shown for HCl, HNO_3 and aqua regia as the XRD patterns of the used catalysts appeared identical to those of the fresh).

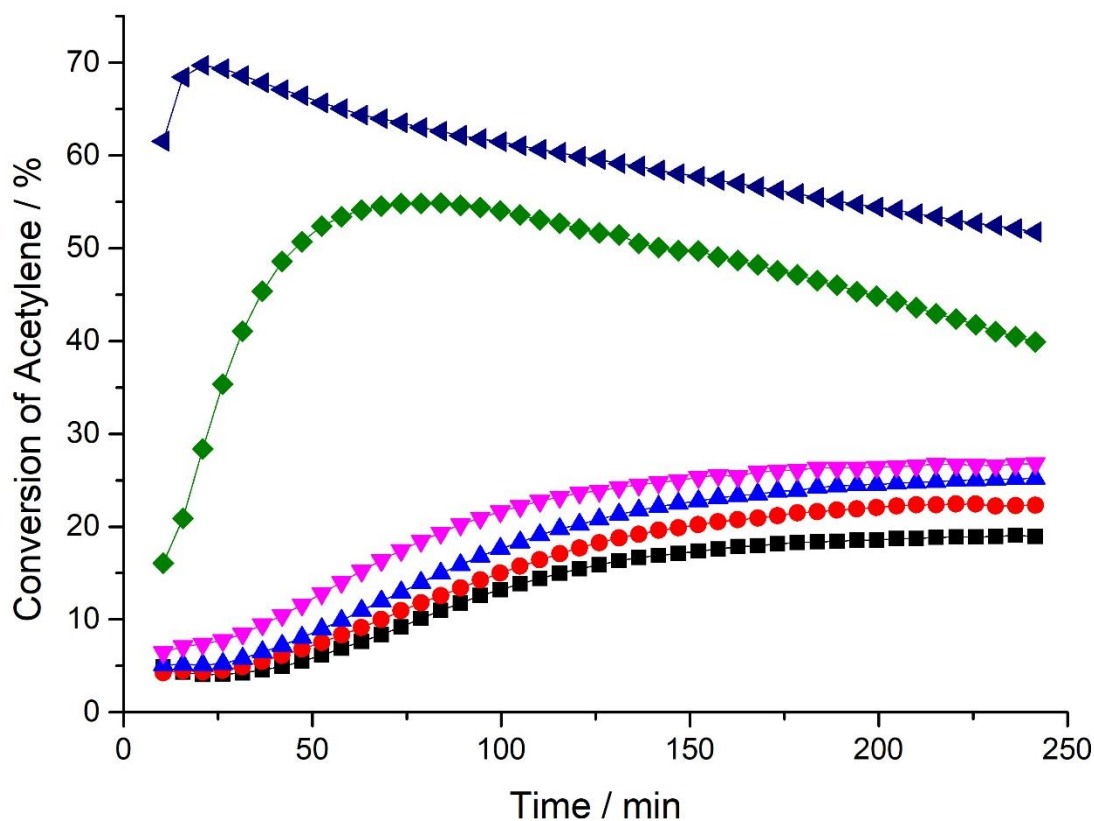


Figure 4.30. Acid pre-wash catalysts time-on-line data – Au/C-AR (■), HNO₃ (●), HCl (▲), aqua regia (▼), H₃PO₄ (◆) and H₂SO₄ (◄), conditions as stated in section 4.2.3.

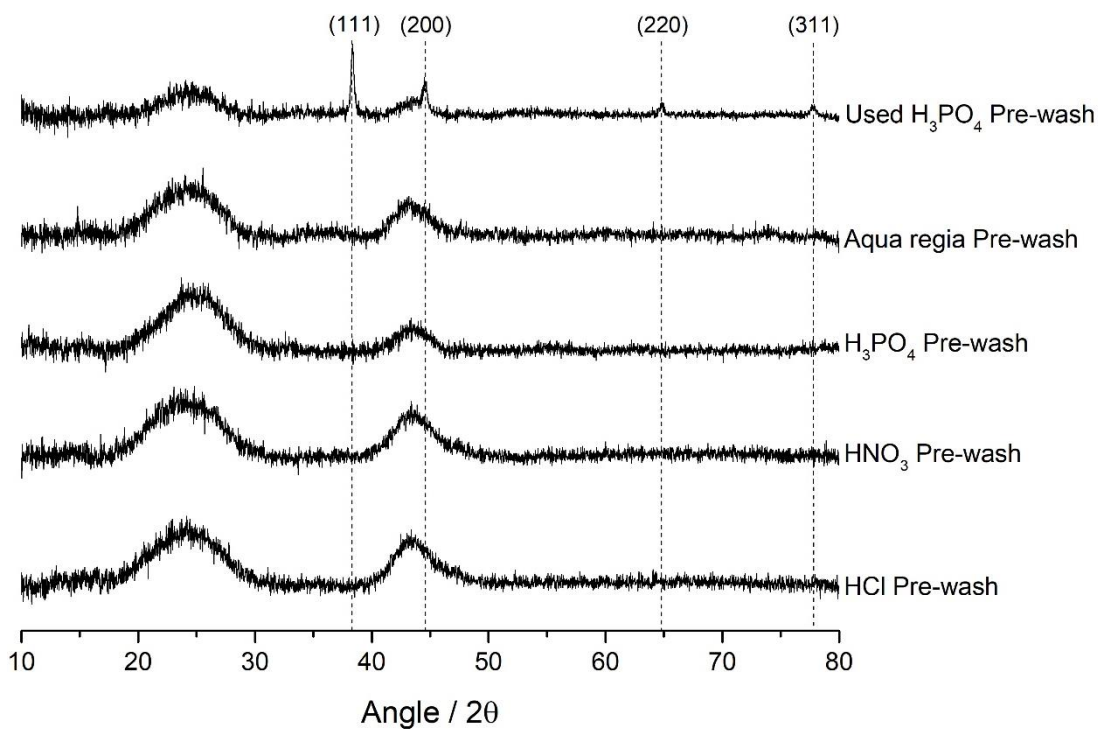


Figure 4.31. XRDs of catalysts prepared acid pre-washes; fresh HCl, fresh HNO₃, fresh aqua regia, fresh and used H₃PO₄. Reflections at 38, 44, 65 & 78 / 2θ correspond to FCC metallic gold crystallites.

4.8. Conclusions

In this work, Au/C carbon was doped with sulfur to produce highly active catalysts for the acetylene hydrochlorination reaction. Although bimetallic catalysts prepared with chloroauric acid and metal sulfates were found to be active, eliminating the second metal suggested that sulfur was the crucial species for producing highly active catalysts. Furthermore, the acetylene conversion could be increased further with the use of an appropriate sulfur containing solution, with selected cations helping to stabilise the sulfur on the support.

Pre-washing carbon in sulfuric acid resulted in catalysts with a high initial activity, which decreased slowly over a 4 h reaction period. XPS showed that a marginal increase in sulfur concentration, compared to Au/C-AR (0.1 to 0.5 At. %), had a large effect on the conversion, whilst XRD and XAFS confirmed that the catalyst was still predominately comprised of monodispersed cationic gold before and after reaction. This dispersion was consistent with previous data on Au/C-AR; however, the high catalytic activity may be the result of a slight change in oxidation state towards an initially greater proportion of Au(III). EXAFS also indicated the presence of another interaction other than Au-Cl, most likely to be that of Au-S species, although further analysis using appropriate standards would be needed to confirm. Significantly, changing the concentration of acid in the pre-wash had little effect on the acetylene conversion, owing to the volume of water used to wash the support before completing the catalyst preparation.

Alternative methods of treating the catalyst, such as using a post-wash, or sulfuric acid as a solvent instead of aqua regia, consistently resulted in catalysts with a poorer performance than the pre-wash. Therefore, in order to maximise the interaction of gold with sulfur, the carbon should be first pre-treated and aqua regia should remain the solvent of choice for the introduction of gold. A small study was also performed on the use of different acids to pre-wash the support. This confirmed that sulfuric acid was the most effective at enhancing the catalytic activity but also showed the potential of phosphoric acid.

Future work should focus on two main areas; the determination of sulfur loading and the specific interaction of gold with sulfur. A more reliable and sensitive method should be employed to quantify the sulfur loading, using a technique such as gas chromatography equipped with a pulsed flame photometric detector (PFPD), which is typically employed for determining sulfur content of petrochemical samples,⁴⁷ or x-ray fluorescence (XRF), used to determine bulk sulfur content in coal for example.⁴⁸ This could help to determine if there is an optimum sulfur loading for high activity catalysts. STEM analysis combined with EDX measurements could provide information on the dispersion of sulfur throughout the catalyst. It would be especially useful to

determine how this impacted the dispersion of gold. Further analysis of the pre-wash H₂SO₄ catalyst should also be performed to elucidate the exact nature of the gold-sulfur species present before, during and after reaction. A greater appreciation of the gold sulfur interaction could then be used to tailor this somewhat crude catalyst preparation with the use of specific solvents, with a focus towards producing more stable but still highly active gold on carbon catalysts.

4.9. References

- 1 N. N. Greenwood and A. Earnshaw, *Chemistry of the elements*, Butterworth-Heinemann, 1997.
- 2 C. J. Davies, *PhD Thesis*, 2012, Cardiff University.
- 3 H. Zhang, W. Li, X. Li, W. Zhao, J. Gu, X. Qi, Y. Dong, B. Dai and J. Zhang, *Catal. Sci. Technol.*, 2015, **5**, 1870–1877.
- 4 H. Zhang, B. Dai, X. Wang, W. Li, Y. Han, J. Gu and J. Zhang, *Green Chem.*, 2013, **15**, 829–836.
- 5 J. Zhao, J. Xu, J. Xu, J. Ni, T. Zhang, X. Xu and X. Li, *Chempluschem*, 2015, **80**, 196–201.
- 6 Y. Pu, J. Zhang, X. Wang, H. Zhang, L. Yu, Y. Dong and W. Li, *Catal. Sci. Technol.*, 2014, **4**, 4426–4432.
- 7 J. Zhao, S. Gu, X. Xu, T. Zhang and X. Di, *RSC Adv.*, 2015, **5**, 101427–101436.
- 8 Y. Dong, H. Zhang, M. Li, WeiSun, C. Guo and J. Zhang, *J. Ind. Eng. Chem.*, 2016, **35**, 177–184.
- 9 H. Zhang, B. Dai, W. Li, X. Wang, J. Zhang, M. Zhu and J. Gu, *J. Catal.*, 2014, **316**, 141–148.
- 10 C. Huang, M. Zhu, L. Kang, X. Li and B. Dai, *Chem. Eng. J.*, 2014, **242**, 69–75.
- 11 J. Zhang, Z. He, W. Li and Y. Han, *RSC Adv.*, 2012, **2**, 4814.
- 12 C. J. Davies, P. J. Miedziak, G. L. Brett and G. J. Hutchings, *Chinese J. Catal.*, 2016, **37**, 1600–1607.
- 13 M. Conte, A. F. Carley, G. Attard, A. A. Herzing, C. J. Kiely and G. J. Hutchings, *J. Catal.*, 2008, **257**, 190–198.
- 14 S. Q. Zhang and X. Li, *Catal. Sci. Technol.*, 2015, **5**, 4973–4984.
- 15 J. Zhao, Y. Yu, X. Xu, S. Di, B. Wang, H. Xu, J. Ni, L. L. Guo, Z. Pan and X. Li, *Appl. Catal. B Environ.*, 2017, **206**, 175–183.
- 16 H. Zhang, B. Dai, X. Wang, L. Xu and M. Zhu, *J. Ind. Eng. Chem.*, 2012, **18**, 49–54.
- 17 S. Wang, B. Shen and Q. Song, *Catal. Letters*, 2009, **134**, 102–109.
- 18 M. Zhu, Q. Wang, K. Chen, Y. Wang, C. Huang, H. Dai, F. Yu, L. Kang and B. Dai, *ACS Catal.*, 2015, **5**, 5306–5316.
- 19 C. Hagellüken, in *Handbook of Heterogeneous Catalysis*, Wiley-VCH Verlag GmbH & Co. KGaA, Weinheim, Germany, 2008, pp. 1846–1863.
- 20 X. Li, X. Pan and X. Bao, *J. Energy Chem.*, 2014, **23**, 131–135.
- 21 K. Zhou, B. Li, Q. Zhang, J. Q. Huang, G. L. Tian, J. C. Jia, M. Q. Zhao, G. H. Luo, D. S. Su and F. Wei, *ChemSusChem*, 2014, **7**, 723–728.
- 22 X. Li, Y. Wang, L. Kang, M. Zhu and B. Dai, *J. Catal.*, 2014, **311**, 288–294.
- 23 J. Wang, F. Zhao, C. Zhang, L. Kang and M. Zhu, *Appl. Catal. A Gen.*, 2018, **549**, 68–75.
- 24 X.-X. X. Di, J. Zhao, Y. Yu, X.-L. L. Xu, S.-C. C. Gu, H.-H. H. He, T.-T. T. Zhang and X.-N. N. Li, *Chinese Chem. Lett.*, 2016, **27**, 1567–1571.
- 25 J. Zhao, B. Wang, X. Xu, Y. Yu, S. Di, H. Xu, Y. Zhai, H. He, L. Guo, Z. Pan and X. Li, *J. Catal.*, 2017, **350**, 149–158.
- 26 H. He, J. Zhao, B. Wang, Y. Yue, G. Sheng, Q. Wang, L. Yu, Z.-T. Hu and X. Li, *Materials*

- (*Basel*), 2019, **12**, 1310.
- 27 X. Qi, W. Chen and J. Zhang, *RSC Adv.*, 2019, **9**, 21931–21938.
- 28 P. Johnston, N. Carthey and G. J. Hutchings, *J. Am. Chem. Soc.*, 2015, **137**, 14548–14557.
- 29 C. University, *Res. Excell. Framew.*, 2014, **321**, 1–3.
- 30 G. Malta, S. A. Kondrat, S. J. Freakley, C. J. Davies, L. Lu, S. R. Dawson, A. Thetford, E. K. Gibson, D. J. Morgan, W. Jones, P. P. Wells, P. Johnston, C. R. A. Catlow, C. J. Kiely and G. J. Hutchings, *Science*, 2017, **355**, 1399–1403.
- 31 X. Liu, M. Conte, D. Elias, L. Lu, D. J. Morgan, S. J. Freakley, P. Johnston, C. J. Kiely and G. J. Hutchings, *Catal. Sci. Technol.*, 2016, **6**, 5144–5153.
- 32 G. Malta, S. A. Kondrat, S. J. Freakley, C. J. Davies, S. R. Dawson, X. Liu, L. Lu, K. Dymkowski, F. Fernandez-Alonso, S. Mukhopadhyay, E. K. Gibson, P. P. Wells, S. F. Parker, C. J. Kiely and G. J. Hutchings, *ACS Catal.*, 2018, **8**, 8493–8505.
- 33 C. H. Booth and Y.-J. Hu, *J. Phys. Conf. Ser.*, 2009, **190**, 1–6.
- 34 Athena XAS Data Processing,
<http://bruceravel.github.io/demeter/documents/Athena/examples/aucl.html>,
(accessed June 2017).
- 35 Z. Song, J. P. L. Kenney, J. B. Fein and B. A. Bunker, *Geochim. Cosmochim. Acta*, 2012, **86**, 103–117.
- 36 M. F. Lengke, B. Ravel, M. E. Fleet, G. Wanger, R. A. Gordon and G. Southam, *Environ. Sci. Technol.*, 2006, **40**, 6304–6309.
- 37 B. Nkosi, N. J. Coville, G. J. Hutchings, M. D. Adams, K. Friedl and F. E. Wagner, *J. Catal.*, 1991, **128**, 366–377.
- 38 B. Nkosi, N. J. Coville, G. J. Hutchings, M. D. Adams, J. Friedl and F. E. Wagner, *J. Catal.*, 1991, **128**, 378–386.
- 39 C. Diverchy, S. Hermans, V. Dubois and M. Devillers, *Grafting of coordination compounds onto functionalized carbon supports as precursors for bimetallic Pd-Ru/C catalysts*, Elsevier Masson SAS, 2006, vol. 162.
- 40 H. P. Boehm, *Carbon N. Y.*, 2002, **40**, 145–149.
- 41 J. L. Figueiredo, M. F. R. Pereira, M. M. A. Freitas and J. J. M. Órfão, *Carbon N. Y.*, 1999, **37**, 1379–1389.
- 42 Y. Jia, R. Hu, Q. Zhou, H. Wang, X. Gao and J. Zhang, *J. Catal.*, 2017, **348**, 223–232.
- 43 J. Zhang, W. Sheng, C. Guo and W. Li, *RSC Adv.*, 2013, **3**, 21062–21068.
- 44 H. Zhang, W. Li, Y. Jin, W. Sheng, M. Hu, X. Wang and J. Zhang, *Appl. Catal. B Environ.*, 2016, **189**, 56–64.
- 45 M. Conte, A. F. Carley, C. Heirene, D. J. Willock, P. Johnston, A. A. Herzing, C. J. Kiely and G. J. Hutchings, *J. Catal.*, 2007, **250**, 231–239.
- 46 E. Wiberg, N. Wiberg and A. F. Holleman, *Inorganic chemistry*, Academic Press, 2001.
- 47 L. Chambers and M. L. Duffy, *J. Chromatogr. Sci.*, 2003, **41**, 528–534.
- 48 T. Cechák and L. Thinová, *Radiat. Phys. Chem.*, 2001, **61**, 759–761.

5. Acetylene Hydrochlorination using oxidised carbon supported gold catalysts

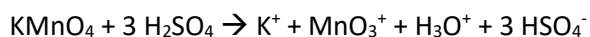
5.1. Introduction

This chapter focuses on the use of oxidised carbons as a support for the Au/C catalyst. As was discussed in the introduction (chapter 1.5), the nature of the carbon support has a significant impact on the catalytic performance. Since the early 1900s, carbon has been used almost exclusively as a support in the catalyst preparation for this reaction, due to its high surface area and stability under harsh reaction and catalyst preparation conditions. A wide range of functional groups with often complex surface chemistry can make the characterisation of these supports difficult; however, it is reported in literature that surface functionalities, introduced by simple oxidations, can be correlated with catalytic activity for certain reactions.¹⁻⁵

Previous work performed by Conte *et al.* has shown that aqua regia oxidises both gold and carbon in the preparation of Au/C catalysts, resulting in a mixture of active Au(I)/Au(III) on the surface of the support.⁶ However, in more recent work by Conte *et al.* has shown that more active catalysts can be produced by first oxidising the carbon and then using aqua regia as a solvent. By refluxing the support in nitric acid, surface oxygen groups were introduced.^{7,8} These functional groups were quantified by deconvolution of TG-MS data from CO₂ and CO evolution upon heating the support. An increase in activity and stability was correlated with an increase in phenol-, ether- and carbonyl-groups.

Herein, harsher methods of oxidation were investigated, building on the work mentioned above, to study the effect of higher oxygen concentrations on the support surface on the activity of the catalyst. The primary method of oxidation used was that developed by Hummers.⁹ Oxidation methods began with a focus on the production of graphitic oxide from graphite, as detailed by Brodie in 1859.¹⁰ Further developments by Staudenmaier¹¹ and Hofmann¹² lead to more efficient methods; however, both remained quite dangerous, with the high risk of explosion from the reaction side product chlorine dioxide. Work by Hummers and Offeman updated the method again,⁹ using a mixture of potassium permanganate and concentrated sulfuric acid, combined with sodium nitrate used to form nitric acid *in-situ*. This preparation still results in the formation of potentially explosive dimanganese heptoxide upon reaction of manganite with sulfuric acid; however, when performed at low temperatures and with sequential addition of permanganate, this was considered much safer than those performed previously and therefore became the

widely accepted method still used today, although much work has since been performed to optimise this further.¹³⁻¹⁷ Hummers oxidation proceeds via the following reactions:



Oxidation occurs via the oxidative separation of graphene layers due to dimanganese heptoxide and the permanganyl cation.^{18,19}

In this work, a series of carbons have been oxidised using Hummers' method, using different amounts of KMnO_4 per 5 g of carbon, in order to determine the optimum oxygen loading for active Au/C catalysts. Characterisation, including XAFS, XPS and SEM, was performed to elucidate the functional groups responsible for changes in activity recorded. These catalysts were then compared to two more catalysts, prepared using carbons oxidised with milder preparation methods.

5.2. Experimental conditions

5.2.1. Treatment of carbon via modified Hummers' method

Ground activated carbon (AC) was oxidised according to a modified version of the previously reported Hummers' method.⁹ Activated carbon (5 g) was added to a mixture of concentrated sulfuric (87.5 ml) and nitric acid (27.5 ml) under vigorous stirring and the mixture was allowed to cool to 10 °C in an ice bath. Nitric acid was used in place of the reported sodium nitrate to remove sodium from the reaction. Potassium permanganate (0.5-10 g) was added stepwise over a period of 2 h with the temperature maintained below 10 °C. The mixture was then allowed to reach room temperature over a period of 4 h, followed by heating to 35 °C for 30 min. Deionized water (250 ml) was added, causing the temperature to rise to 70 °C. A further portion of deionized water (1 L) was added, followed by addition of 3% hydrogen peroxide to quench any residual potassium permanganate. The mixture was allowed to settle overnight, after which the sample was separated and washed repeatedly via centrifugation until a neutral pH was obtained. The sample was finally dried at 30 °C under vacuum for 16 h.

5.2.2. Reaction conditions

All reactions were performed using the following conditions, unless stated otherwise: C_2H_2 : HCl = 1:1.02, total gas flow of 50 mL min⁻¹, 0.09 g catalyst, temperature 200 °C, ambient pressure.

5.3. Oxidising carbons via modified Hummers' method

5.3.1. Effect of amount of oxidant on catalytic activity

To determine the effect of the carbon oxidation on the final catalytic performance, seven catalysts were prepared via the Hummers' oxidation method. In each case, the mass of KMnO_4 used in the preparation of the carbon was changed (0.50, 1.25, 2.50, 3.75, 5.00, 7.50 and 10.00 g), resulting in varying amounts of oxidation of the support. The conversion of each catalyst was compared (Figure 5.1).

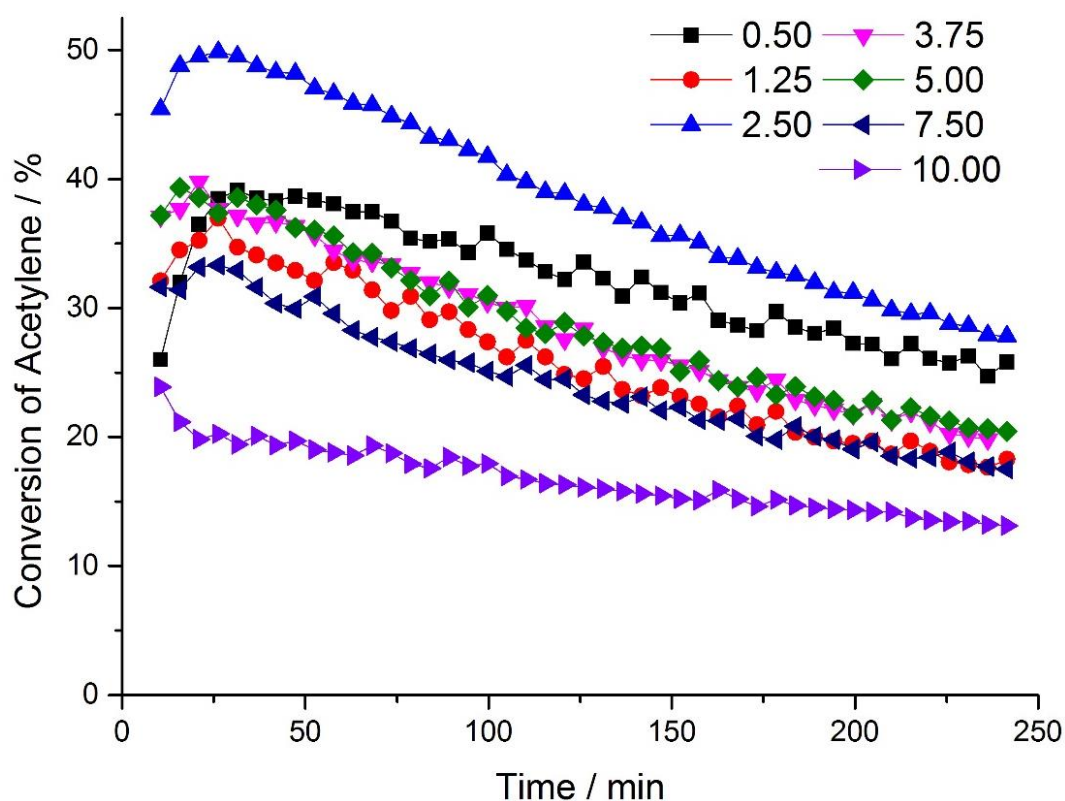


Figure 5.1. Comparison of acetylene conversions over time using catalysts prepared with different masses (g) of KMnO_4 per 5 g of carbon, denoted 0.50 - 10.00; 0.50 (■), 1.25 (●), 2.50 (▲), 3.75 (▼), 5.00 (◆), 7.50 (◄) and 10.00 (►).

Each of the catalysts exhibit the same overall trend; a brief induction period of 15 - 20 min followed by a steady decline in conversion, although a much more gradual decrease in the catalyst prepared with 10.00 g of KMnO_4 . A comparison of the final conversion of each catalyst after 4 h would not yield significant insight into the catalytic performance, as none of these catalysts had reached a stable conversion at this point. A plot of maximum initial conversion (taken at 30 min of reaction) versus mass of KMnO_4 per 5 g of carbon would prove more useful (Figure 5.2).

This comparison shows that increasing the mass of KMnO_4 from 0.5 g up to 2.50 g per 5 g of carbon results in an increase in initial acetylene conversion from 37 – 50 %. A further increase in mass of KMnO_4 from 2.50 g to 10.00 g has a detrimental effect on conversion, decreasing from 50 – 20 %.

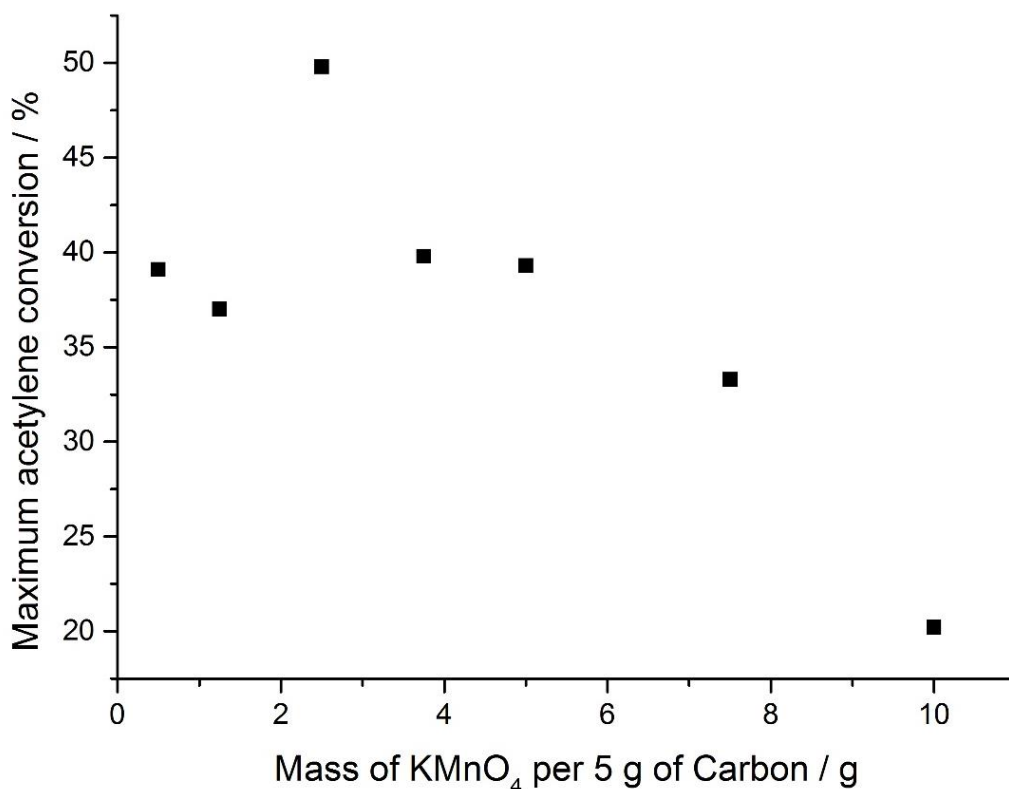


Figure 5.2. Maximum initial acetylene conversion (recorded at 30 min of reaction) of oxidised carbon catalysts prepared with different masses of KMnO_4 from 0.50 g to 10.00 g per 5 g of carbon.

Although this figure demonstrates a clear trend, the mass of KMnO_4 used per 5 g of carbon is not a suitable representative variable for comparison of the different catalysts; analysis of the atomic percentage of oxygen, determined via XPS, of these oxidised carbon catalysts when compared with the mass of KMnO_4 per 5 g of carbon does not show a linear correlation (Figure 5.3).

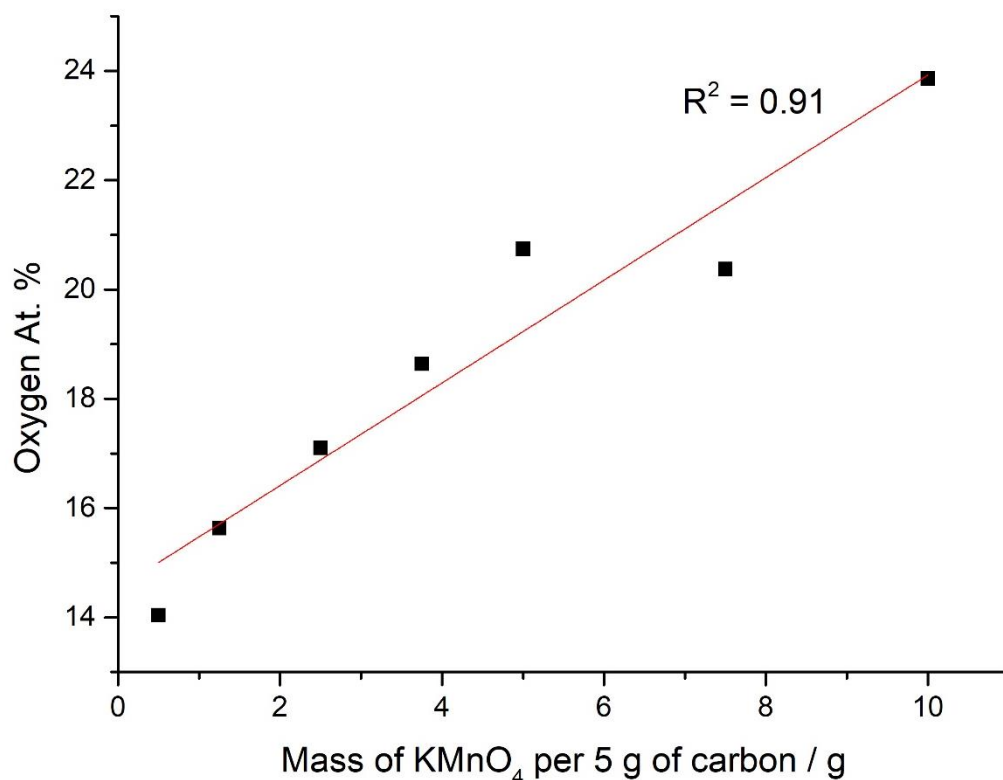


Figure 5.3. Oxygen atomic % versus mass of KMnO₄ per 5 g of carbon.

An investigation into the reproducibility of the catalysts prepared using oxidised carbons as support was performed comparing a series of catalysts prepared with 2.50 g of KMnO₄ per 5 g of carbon. This showed that repeat preparations of the same catalyst resulted in a large variation of oxygen atomic percent in the final material (Figure 5.4). This variation has previously been observed when using the Hummers oxidation method²⁰ and is attributed to the effervescent nature of the synthesis, which can result in loss of reagents during preparation. Such variation proved to have an impact on the catalytic performance, therefore making the mass of KMnO₄ an unreliable descriptor of these catalysts. For this reason, the data were replotted, using the oxygen atomic percentage to define each catalyst (Figure 5.5). For clarity, the mass of KMnO₄ used in the preparation was included as a label in subsequent figures. Comparing these data shows that a loading of 17 atomic percent oxygen results in the highest acetylene conversion.

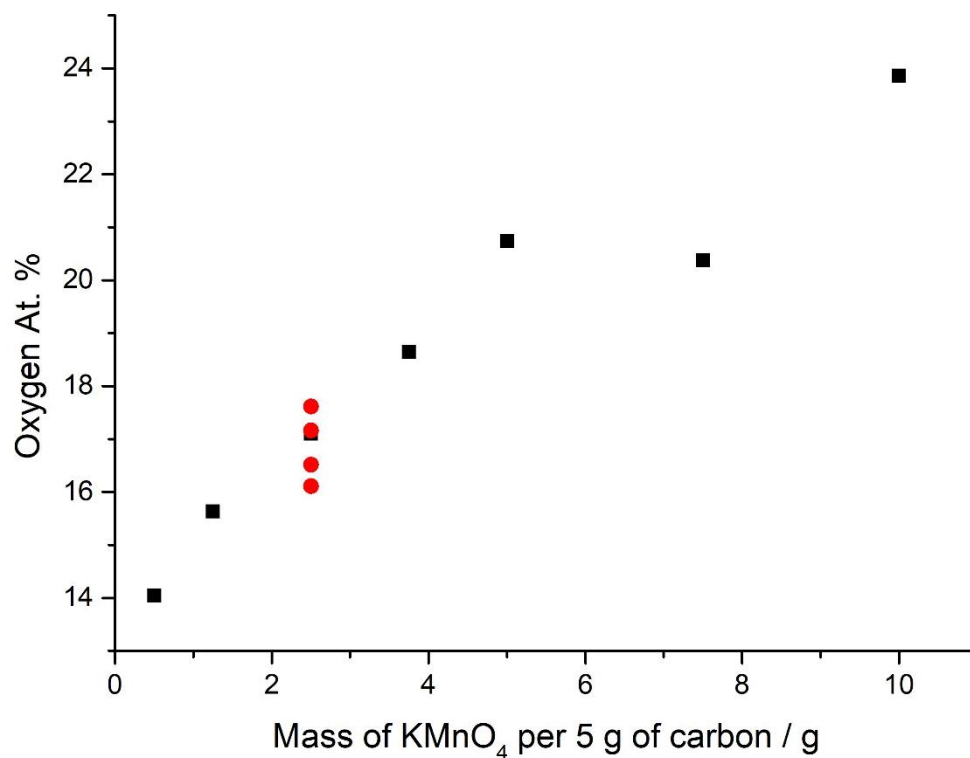


Figure 5.4. Mass of KMnO_4 per 5 g of carbon versus oxygen atomic % (■). Repeat preparations of catalysts prepared with 2.50 g of KMnO_4 (●).

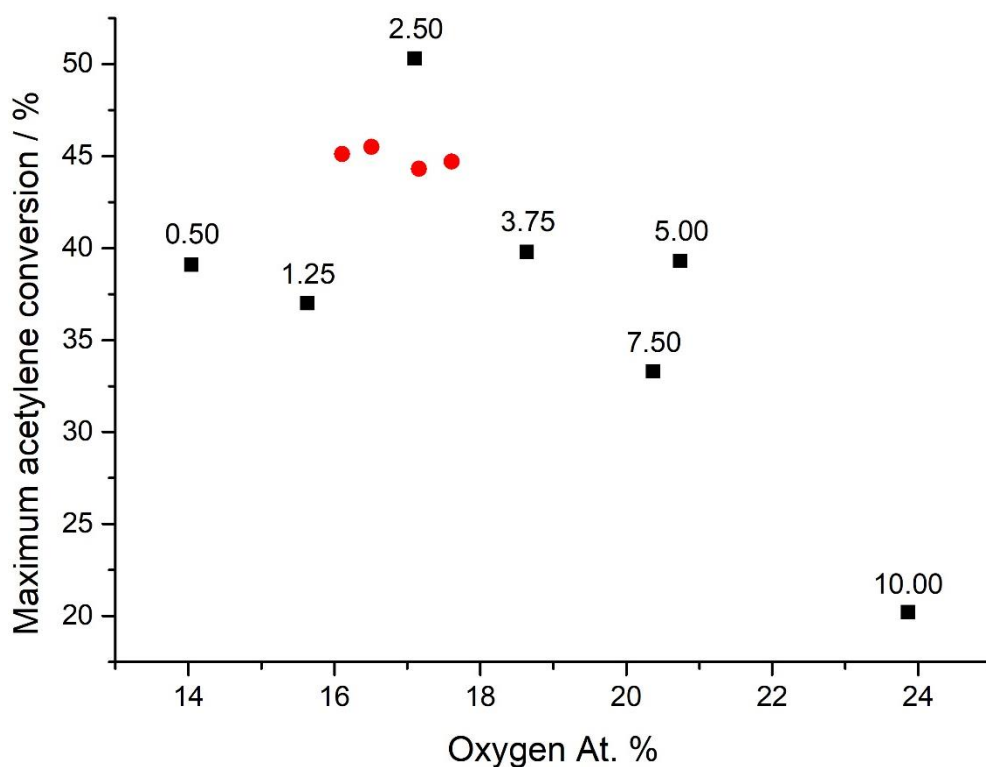


Figure 5.5. Oxygen atomic percent of the oxidised carbon catalysts versus maximum acetylene conversion (■). Number labels denote the mass of KMnO_4 per 5 g of carbon used in the preparation. (●) denotes catalysts prepared with 2.50 g of KMnO_4 .

Figure 5.6 includes unmodified carbon and 1% Au/C prepared with unmodified carbon. These extra data points highlight three key details:

- Untreated carbon still contains oxygen (5 at. %) but is inactive for the reaction.
- Gold on untreated carbon contains 8 at. % oxygen. This increase in oxygen content upon addition of gold is attributed to the use of aqua regia as a solvent, which, compared to Hummers' method, is a relatively mild oxidant. Nevertheless, this oxidation is crucial for producing oxidised gold species, thereby generating the active cationic catalytic species.
- 2.50 g of KMnO_4 provides the optimum loading of oxygen to produce catalysts with a high initial activity. The oxidised carbon without gold is as inactive as untreated carbon.

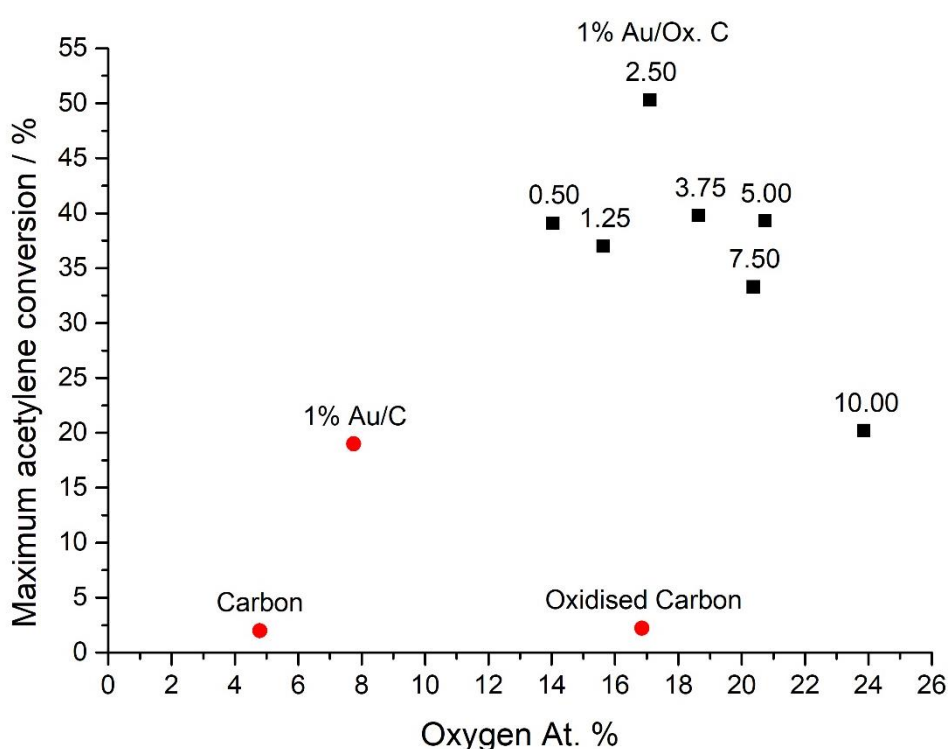


Figure 5.6. Oxygen atomic percent of the oxidised carbon catalysts versus maximum acetylene conversion (■). (●) denotes untreated carbon, 1% Au/C prepared with untreated carbon and oxidised carbon prepared with 2.50 g of KMnO_4 .

5.3.2. Characterisation via XPS

Further characterisation was performed to determine the specific oxygen groups present as a result of using Hummers' oxidation method. XPS analysis was performed on each of the oxidised carbon catalysts in an attempt to differentiate the different carbons and oxygen functional groups present on the surface of the support, which may interact with gold.⁶ The C 1s spectra were fitted using Casa XPS to determine the concentrations of the following functional groups

and hybridised species: sp^2 , $\pi\text{-}\pi^* + \text{CF}_x$ (fluorinated carbon oligomers), $\pi\text{-}\pi^*$, C=O, C-O, sp^3 and O-C=O (Figure 5.7).

The concentration of both sp^2 and sp^3 carbon decreased slightly with increasing atomic oxygen %, due to the formation of new oxygen containing functionalities upon oxidation. The concentration of C=O also decreased, from 6 to 3 %. Conversely both the concentrations of C-O and O-C=O increased from 4 to 9 % and 2 to 9 %, respectively, in accordance with the increase in oxygen content. The concentrations of $\pi\text{-}\pi^* + \text{CF}_x$ decreased slightly from 7 to 5 % whilst the $\pi\text{-}\pi^*$ remained constant throughout. It should be noted that these changes in concentrations were all minimal and are only marginally outside of experimental error, ± 1 %.

The O 1s spectra were fitted to determine the concentrations of the following functional groups: carbonyl, ether, $\text{H}_2\text{O}/\text{H}_2\text{O}_2$, satellite and ester-satellite. Figure 5.5 shows that the oxygen weight % increased with increasing mass of KMnO_4 used in the preparation. However, the relative concentration of the different functionalities did not follow the same trend (Figure 5.8). The concentration of ether increased with increasing atomic oxygen % from 47 to 55 % however, all the other functional groups remained constant, within error, fluctuating by only ± 2 %.

None of the changes in carbon or oxygen species concentrations match the trend of acetylene conversion observed in Figure 5.6. It can be deduced that when the carbons were treated with increasing masses of KMnO_4 , the amount of oxidation increased but the functional groups that may have been responsible for the peak in catalytic activity, which occurs in the catalyst prepared with 2.5 g of KMnO_4 , remained unknown. As multiple binding sites were available in all catalysts, it is more likely that the increase in conversion was a result of a combination of different sites and could not be solely attributed to one site.

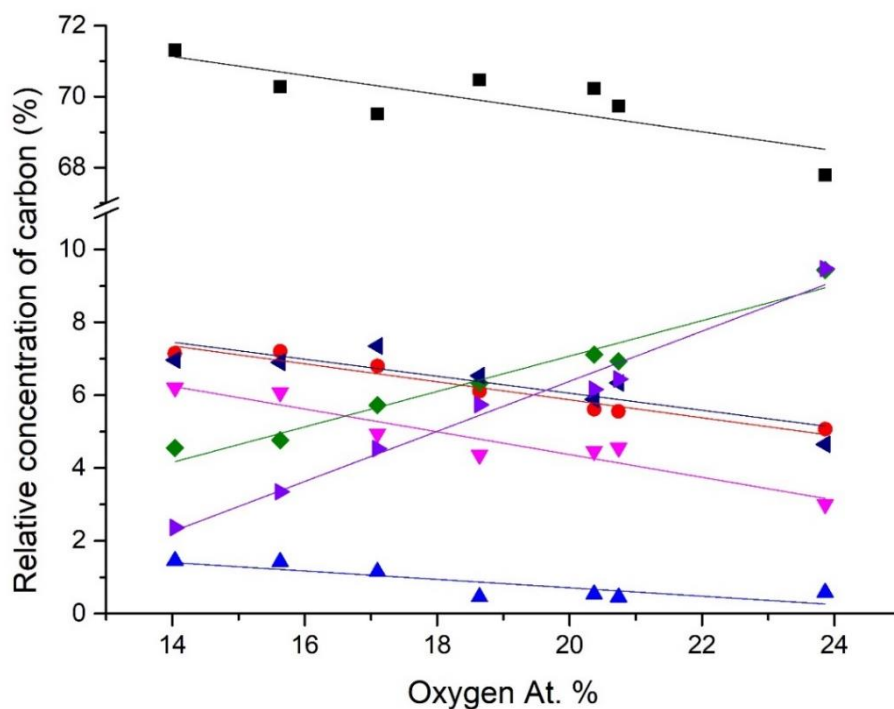


Figure 5.7. Comparison of relative concentrations of carbon species for catalysts prepared with different oxygen atomic %, determined by XPS. sp² (■), pi-pi* + CF_x (●), pi-pi* (▲), C=O (▼), C-O (◆), sp³ (◄) and O-C=O (►).

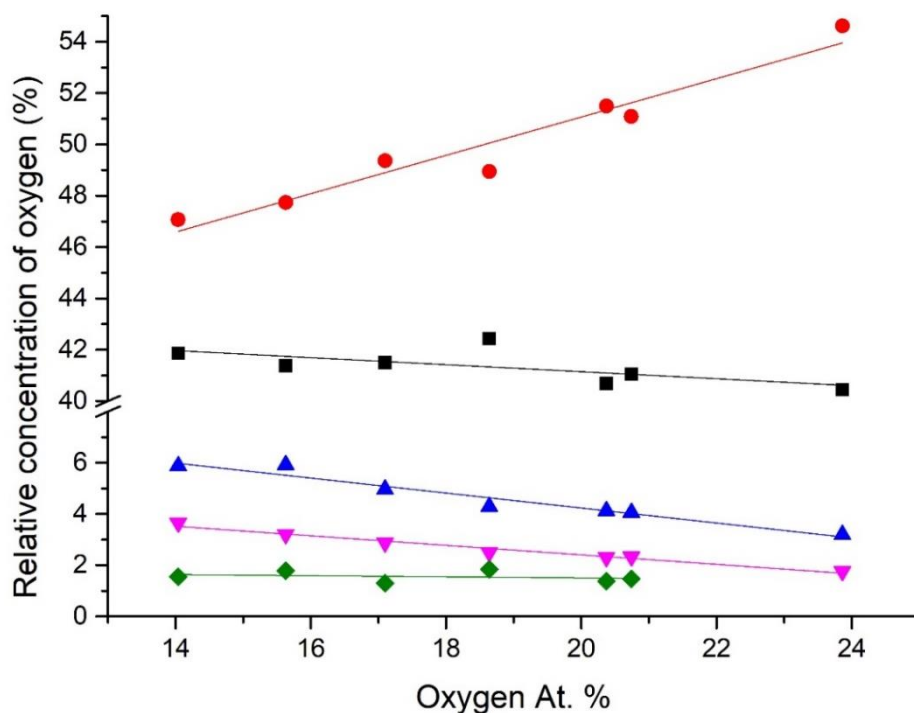


Figure 5.8. Comparison of relative concentrations of oxygen 1s species for catalysts prepared with different oxygen atomic %, determined by XPS. Carbonyl (■), ether (●), H₂O/H₂O₂ (▲), satellite (▼) and ester-satellite (◆).

Previous work performed by C. Buono *et al.* provided an insight into the effect of oxygen groups on a model highly ordered pyrolytic graphite (HOPG).²¹ The results showed that an increase in hydroxyl groups acted as nucleation points for the formation of Au(0), whereas, after a subsequent acid treatment and heating of the hydroxylated support, the presence of ether groups increased the concentration of cationic gold, both Au(III) and Au(I). In all of the oxidised carbon catalysts shown in this chapter, the Au 4f peaks between 82 – 92 eV consisted of a mixture of predominantly Au(I) and Au(III) states, with some Au(0) also present. This concentration of cationic gold would explain the high initial conversion of the oxidised carbon catalysts, as a high oxidised gold content has been observed in active Au/C-AR catalysts.²²

It has been previously reported that, during XPS analysis, oxidised gold is reduced by the electron beam, leading to an overestimate of the Au(0) content (Figure 5.9).²² Therefore, XPS was only used to confirm the presence of the active, oxidised gold species and not reported quantitatively. Further analysis of the gold speciation was performed with XAFS and discussed later in this work (chapter 5.3.4).

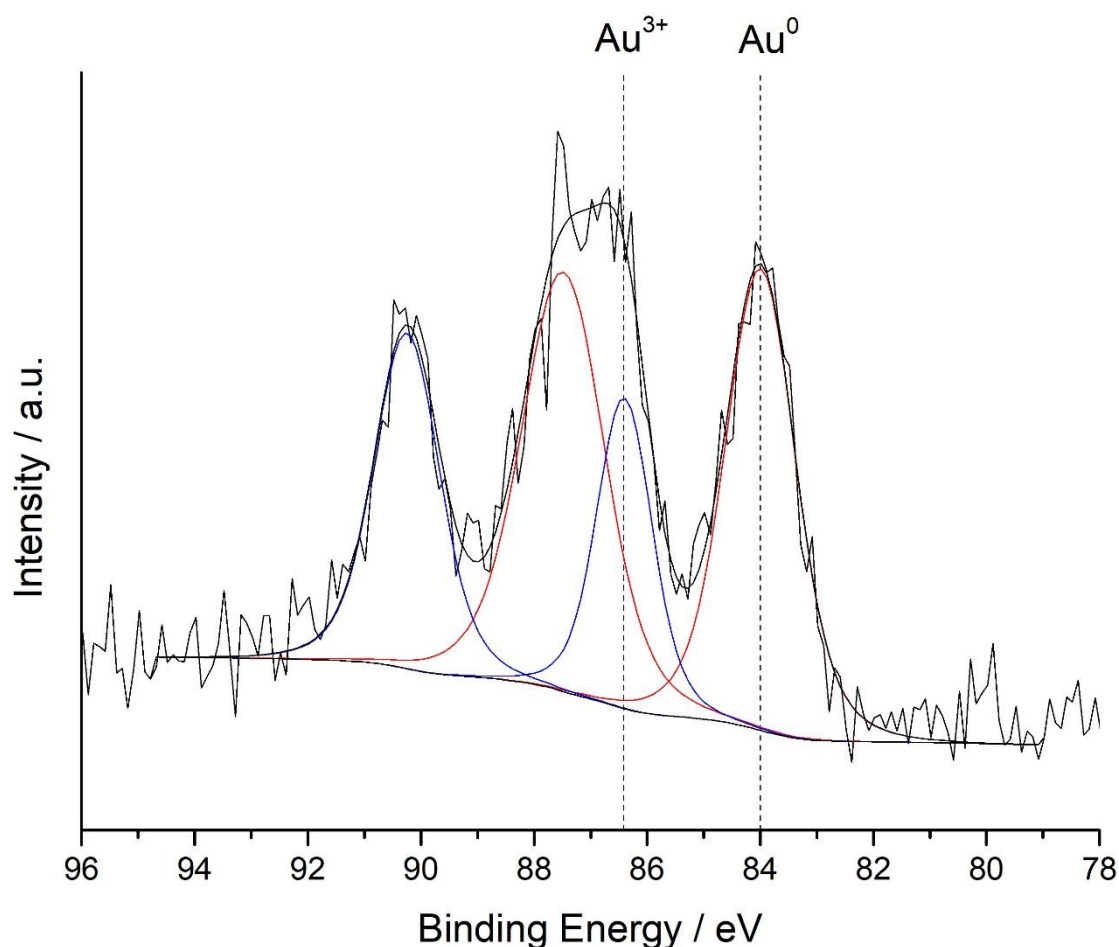


Figure 5.9. XPS Au(4f) spectrum of Au/C-AR, showing Au⁰ at 84.0 and 87.5 eV (red) and Au³⁺ at 86.0 and 90.2 eV (blue).

Further analysis of the oxidised carbon catalysts was performed using XPS. It is common practice, when preparing catalysts with a carbon support, to first wash the support using either dilute hydrochloric or nitric acid.^{23–25} This can be performed by stirring the carbon in the acidic solution, followed by filtering and further washing with water and finally drying. The aim of the wash is to remove any surface contaminants, such as sodium, iron, or copper, which may act as a poison for the active metal species.²⁶ K and Mn were both introduced during use of Hummers' oxidation method of the carbons. In order to confirm that neither of these elements remained on the support surface after catalyst preparation, which could interact with gold, analysis of each oxidised catalyst was performed at the K and Mn binding energies. These showed no peaks corresponding to the presence of either element. This was also confirmed via ICP-MS. Analysis of the oxidised carbon support prepared with 2.5 g of KMnO₄ showed that of the original 2.5 g of KMnO₄, < 3 mg of K and < 1 mg of Mn remained. It was assumed that such low quantities would have no influence on the catalytic activity.

5.3.3. Other characterisation techniques

In order to determine the oxygen content of the carbon materials, analysis could have been performed via Boehm titration²⁷ which could provide information on the different oxygen-containing surface groups present. However, this technique was not attempted due to known problems with the technique reported in literature, such as reproducibility issues when using small sample masses, long equilibrium times for microporous materials and only up to 50 % of the total oxygen content being analysed in activated carbons.²⁸

FTIR analysis is another technique employed for the characterisation of carbon materials to determine the surface functionality. Characteristically black in colour, it can often prove problematic to obtain clear spectra of carbons as the sample may absorb almost all infra-red radiation. In addition, different groups have multiple bands, resulting in overlap which can make quantification difficult;²⁸ however, in general the assignment of the following vibrational bands is consistent; the $\nu(\text{O-H})$ vibration at around 3400 cm^{-1} , the $\nu(\text{C-H})$ vibrations between $2960\text{--}2860\text{ cm}^{-1}$, the $\nu(\text{CO}_2)$ at 2340 cm^{-1} , the $\nu(\text{C=O})$ band at around 1700 cm^{-1} and the $\nu(\text{C=C})$ at $1610\text{--}1630\text{ cm}^{-1}$.^{29–31} A qualitative approach was taken to characterise unmodified carbon, carbon treated with aqua regia, carbon oxidised via Hummers' method using 2.5 g of KMnO_4 , 1% Au/C-AR catalyst and 1% Au/Ox C catalyst prepared with 2.5 g KMnO_4 .

The infrared spectrum shown in Figure 5.9 shows few differences between the four samples. There is a small absorption at 1700 cm^{-1} in the oxidised carbon due to C=O, which increases slightly upon addition of gold, in both the unoxidised and oxidised carbon catalysts. The absorption in the unoxidized sample was due to the increase in carbon-oxygen groups present as a result of using Hummers' oxidation preparation. The further increase apparent in the oxidised carbon catalysts was due to the catalyst preparation in aqua regia. There was also an increase in absorption in the samples containing gold, between $1300\text{--}1380\text{ cm}^{-1}$; however, as this feature was common to both catalysts it was ruled out as a functionality that would result in one catalyst being more active than the other.

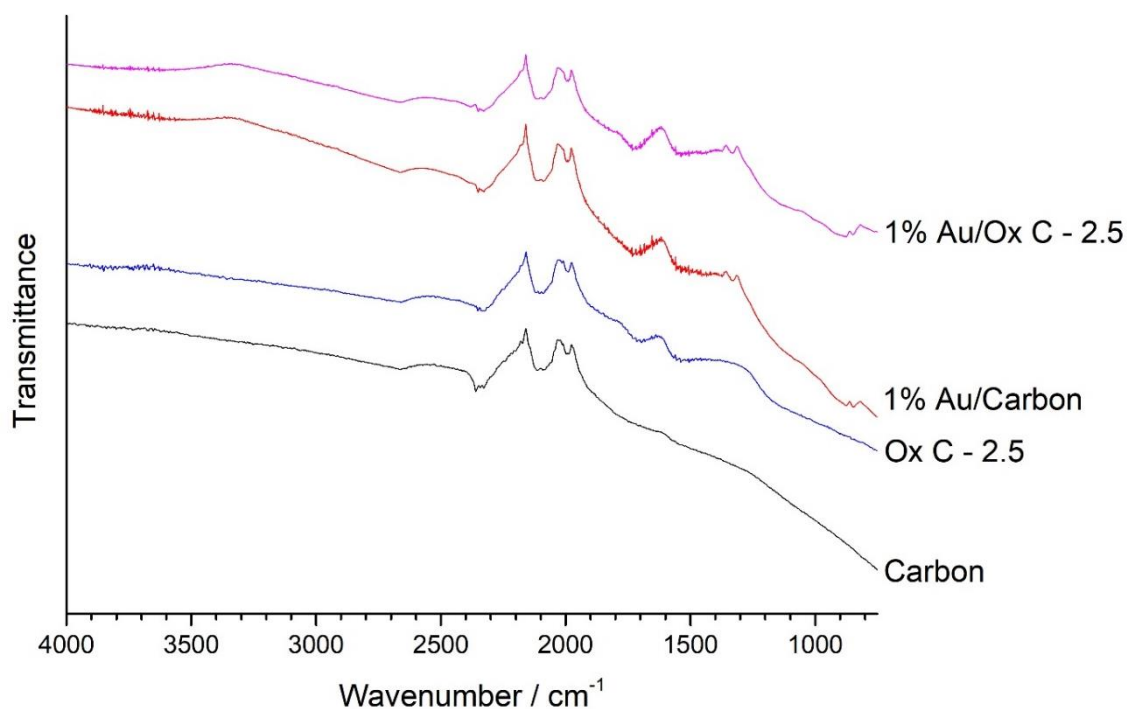


Figure 5.10. Comparison of the Infra-red spectra of the untreated carbon (Carbon, black), the 1 % Au/C-AR catalyst (1 % Au/Carbon, red) , the oxidised carbon prepared with 2.5 g of KMnO_4 per 5 g of carbon (Ox C - 2.5, blue) and the 1% Au/Ox C catalyst (1% Au/Ox C, purple).

Figure 5.10 compares a range of oxidised carbons and their subsequently prepared 1 % Au catalysts. These samples were chosen because of their differences in both catalytic activities and oxygen content (Figure 5.5). 1 % Au/Ox C - 0.5 and 1 % Au/Ox C - 5 catalysts both have a similar conversion (39 %) but 7 % difference in oxygen wt. %, whilst the 1 % Au/Ox C - 5 and 1 % Au/Ox C - 10 catalysts both have very different conversions (39 and 20 %, respectively) and a difference of 4 oxygen wt. %. However, these differences could not be discerned via IR analysis. All 6 samples appeared near identical apart from slight variation in the absorptions at 2340 and 1700 cm^{-1} , due to CO_2 and C=O, respectively.

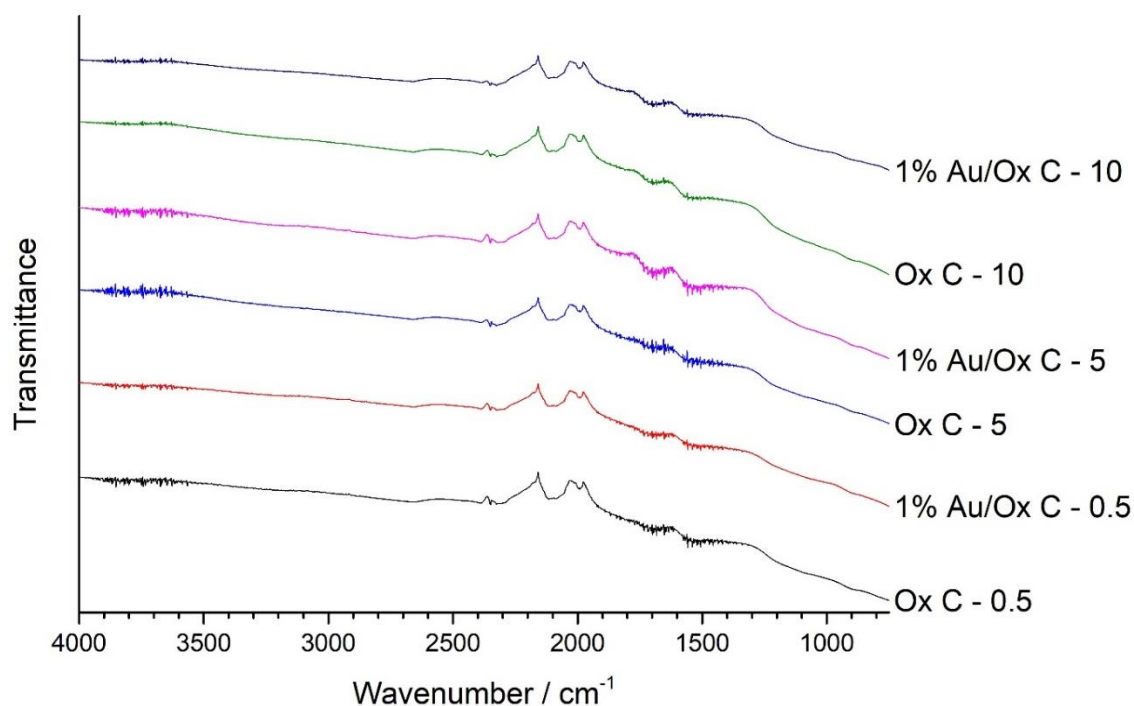


Figure 5.11. Comparison of the Infra-red spectra of oxidised carbon supports (Ox C - 0.5, black, Ox C - 5, blue, Ox C - 10, green) and oxidised carbon catalysts (1 % Au/Ox C - 0.5, red, 1 % Au/Ox C - 5, purple, 1 % Au/Ox C - 10, dark blue). Number labels denote mass of KMnO_4 per 5 g of carbon used in the preparation.

TG-MS has been used to determine the functionality of carbon surface species by monitoring the MS signal of CO_2 , CO and H_2O during heating.^{28–30,32,33} The decomposition temperature of groups such as carboxylic acids, carboxyl anhydrides and lactones from the CO_2 MS signal are reliably found in the ranges shown in Figure 5.11.²⁸ Anhydride, phenol and carbonyl functionality can also be reliably determined from the CO decomposition temperature. Work by R. Schlögl *et al.* noted that the decomposition of groups which formed water could be used to confirm an increase in carbon oxidation, as the carboxyl groups bind to water thereby forming anhydrides at higher temperatures.³² TG-MS was employed to further study differences in the untreated and oxidised carbon catalysts, with limited success.

The Au catalyst prepared with 2.5 g KMnO_4 /5 g of carbon (1 % Au/Ox C - 2.5) was heated under a helium atmosphere to 850 °C and compared to 1 % Au/C-AR. The evolution of CO_2 was detected by mass spectrometry and the signal normalised with reference to the mass of 1% Au/C prepared on unmodified carbon. The results shown in Figure 5.11 confirm the increase in oxidation of the oxidised carbon, as seen by a significant increase in the signal at temperatures corresponding to the decomposition of carboxyl groups and a slight increase in lactones, when compared to the unmodified carbon-supported catalyst.

Due to equipment limitations, both the MS signals for H₂O and CO were contaminated with atmospheric gases; H₂O and N₂ saturated the H₂O and CO signals respectively, rendering these data unusable. For this reason, TG-MS was used solely to confirm that the oxidised carbon catalyst contained greater oxygen functionality, and no further characterisation by this method was performed. A comparison of the different oxidised carbon catalysts would prove useful in determining changes in the surface oxygen-containing groups present, therefore future work should focus on comparing a range of these catalysts using the appropriate equipment, as described in the literature, to determine quantifiable differences between catalyst functionalities.

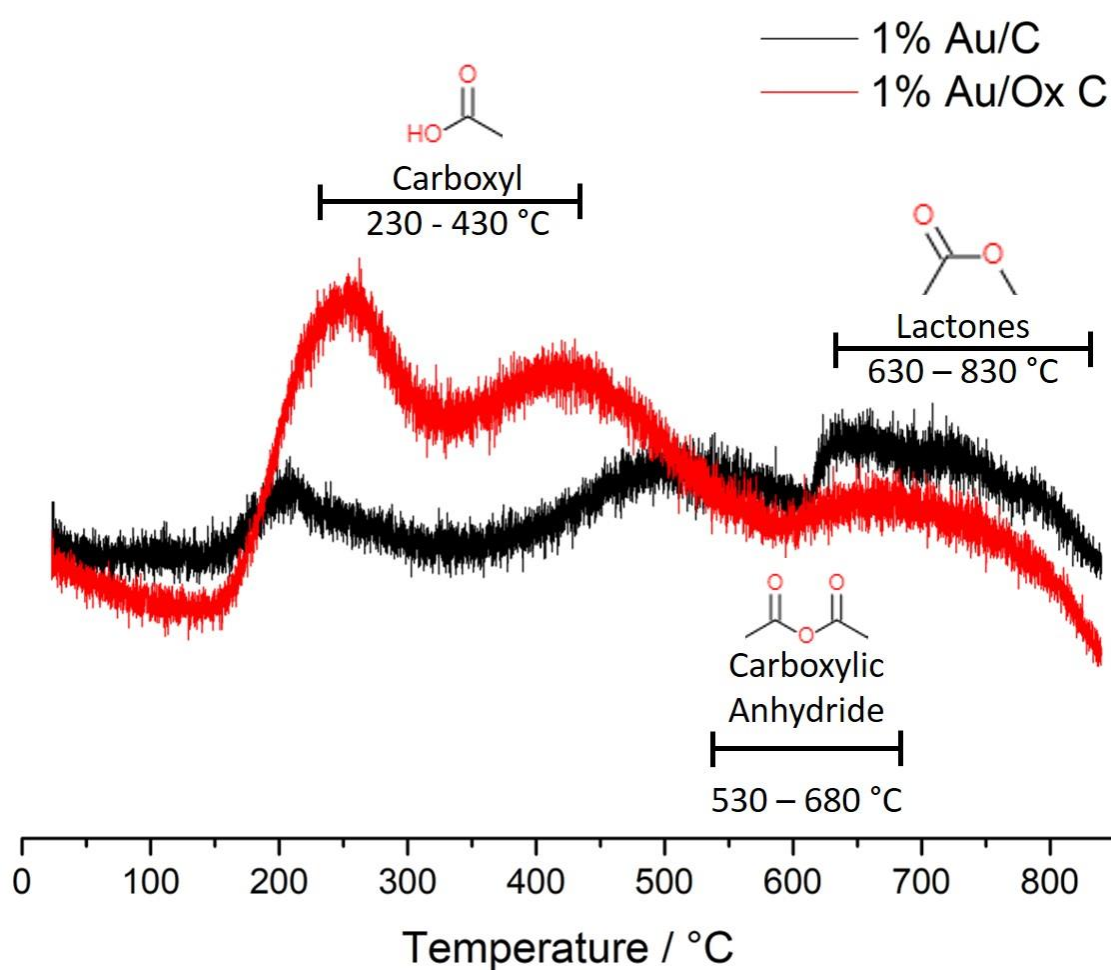


Figure 5.12. Normalised TG-MS of 1% Au/C-AR (black) and 1% Au/Ox C prepared with 2.5 g of KMnO₄ per 5 g of carbon (red). Relative signals denote the evolution of CO₂ during heating.

In order to gain an appreciation of the distribution of gold on the surface of the oxidised carbon, XRD analysis was performed on all of the fresh and used catalysts (Figure 5.12). All of the fresh catalysts have the same pattern as that observed for carbon, which is two broad reflections at 25 and 43 / 2 θ corresponding to a turbostratic arrangement of carbon (a random stacking of

parallel layers).^{34,35} This implies that all the gold distributed on the surface has been dispersed in a homogenous manner, resulting in no formation of nanoparticles. Post-reaction, nanoparticles were apparent in all the used catalysts, as noted by the reflections at 38, 44, 65 & 78 / 2θ . The size of reflections corresponding to Au and hence nanoparticle size increased from 1% Au/Ox C – 0.50 to 1% Au/Ox C – 3.75; however, no trend was observed between nanoparticle size and acetylene conversion or atomic concentration of oxygen. The formation of nanoparticles has been previously observed in high gold loading, high activity catalysts under reaction conditions,³⁶ due to the abundance of gold readily sintering after reduction of Au-Cl to Au(0), which lead to catalyst deactivation. It could be assumed that, due to the high conversion of these catalysts, the deactivation mechanism for the oxidised carbon catalysts is the same. This is suggested due to the observed formation of Au nanoparticles and subsequent reduction in acetylene conversion.

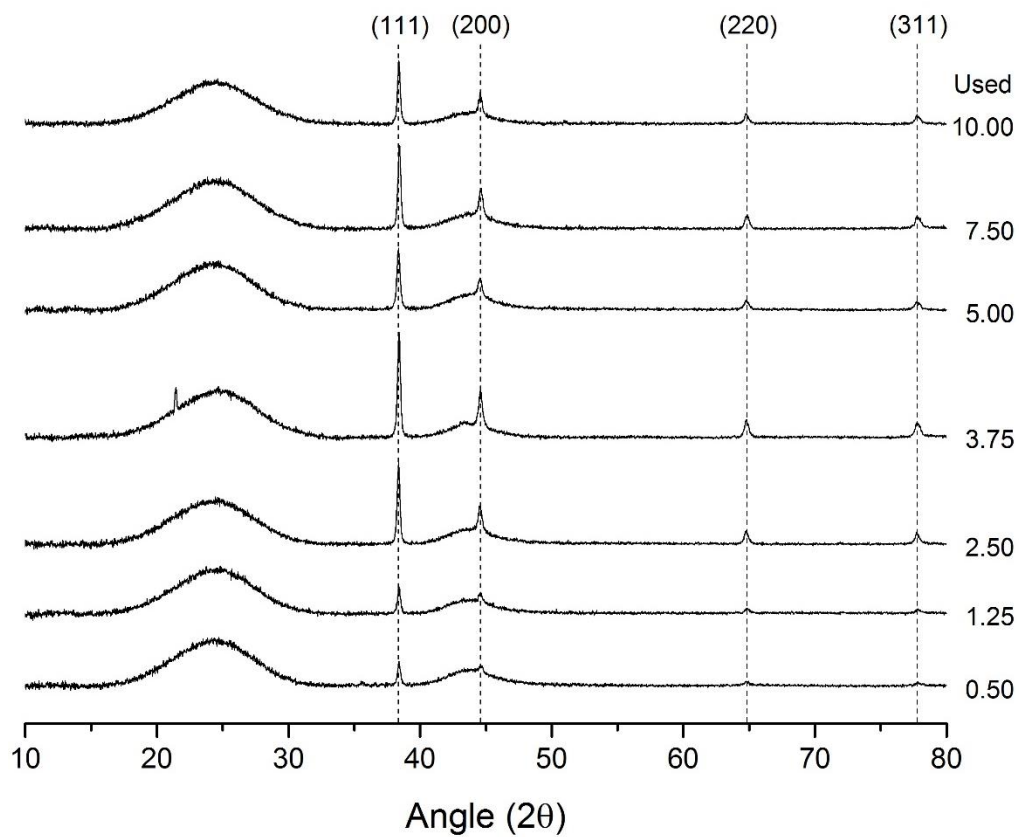
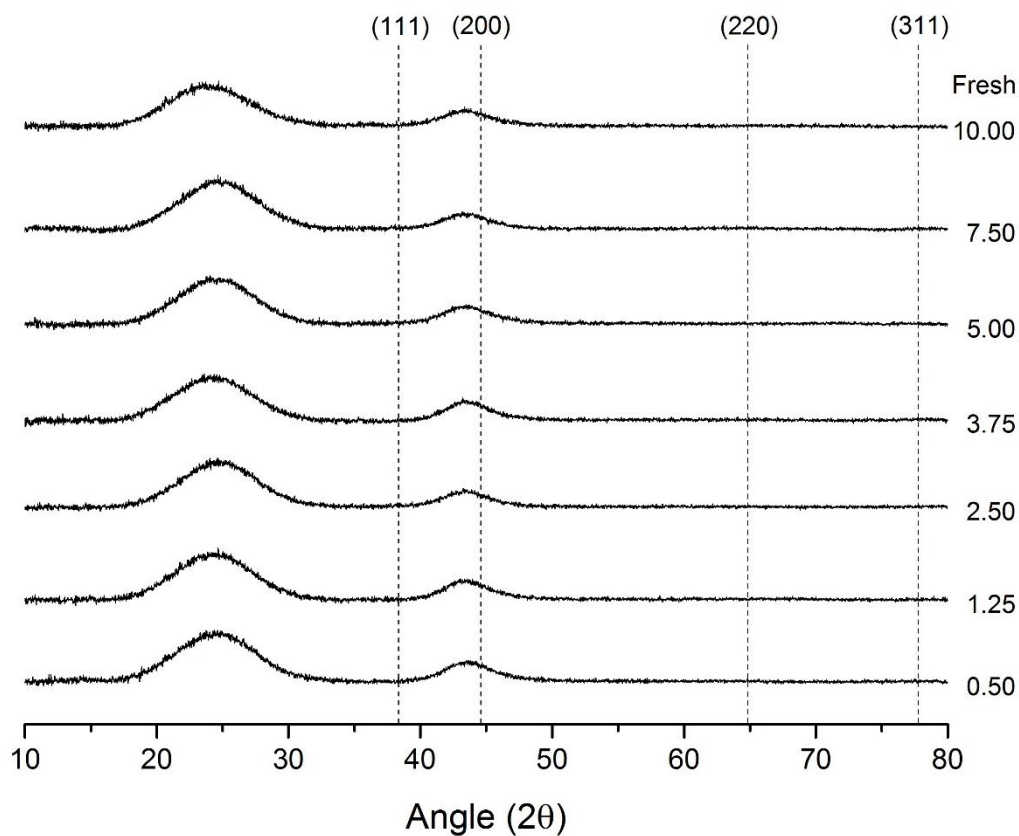


Figure 5.13. XRD pattern of fresh oxidised carbon catalysts (top) and catalysts used at 200 °C for 240 min (bottom). Number labels denote mass of KMnO_4 per 5 g of carbon, used in Hummers' oxidation preparation. Reflections at 38, 44, 65 & 78 / 2θ correspond to FCC metallic gold crystallites.

BET surface area analysis of fresh and used 1 % Au/Ox C – 0.5, 2.5, 5.0 and 10 was performed to determine if there was any correlation between surface area and catalytic performance; however, no trend was observed.

5.3.4. Effect of temperature on catalytic activity of 1 % Au/Ox C – 2.5

The temperature of the acetylene hydrochlorination reaction, as in nearly all catalysed reactions, has a significant impact on the performance of the catalyst. Gold catalysts undergo deactivation via two pathways, dependant on the temperature of the reaction; at low temperature, gold facilitates the polymerisation of acetylene, resulting in long polymers that block the active site, thereby deactivating the catalyst; at high temperatures, the gold undergoes sintering, resulting in large, inactive gold nanoparticles.³⁷ Naturally in industry, where cost is a primary concern when performing reactions, catalysts are applied at the lowest feasible reaction temperature without compromising the productivity of the catalyst. In order to determine the lowest active temperature of the catalyst, tests were carried out at varying temperatures on the 1 % Au/Ox C – 2.5 catalyst (Figure 5.13).

When tested at 200 °C, the catalyst begins with a high acetylene conversion of 50 % before decreasing and stabilising at 20 % after 250 min. Decreasing the temperature to 160 °C causes the catalyst to undergo an initial induction period of 75 min, followed by stabilisation at 32 %. (This reaction was not continued for the standard 4 h as the catalyst was removed from the reactor in order to characterise the active, stable gold species.) Decreasing the temperature further to 130 °C and 120 °C resulted in a prolonged induction period that had not stabilised after 4 h of reaction. The test performed at 130 °C was continued for a further 3.5 h to determine if the catalyst would stabilise or deactivate (Figure 5.14); after this time, the conversion reached 27 %, close to that of the same catalyst tested at 160 °C, and was increasing, albeit at a marginal rate. The test performed at 120 °C was also increasing, reaching 15 % conversion after 280 min. Tests performed at 110 °C or lower resulted in a low, stable conversion of 3 %, comparable to that of carbon with no gold present. Induction of gold on carbon catalysts at such low temperatures had not previously been observed, therefore, further characterisation of these used catalysts was performed to elucidate the nature of the gold species after reaction.

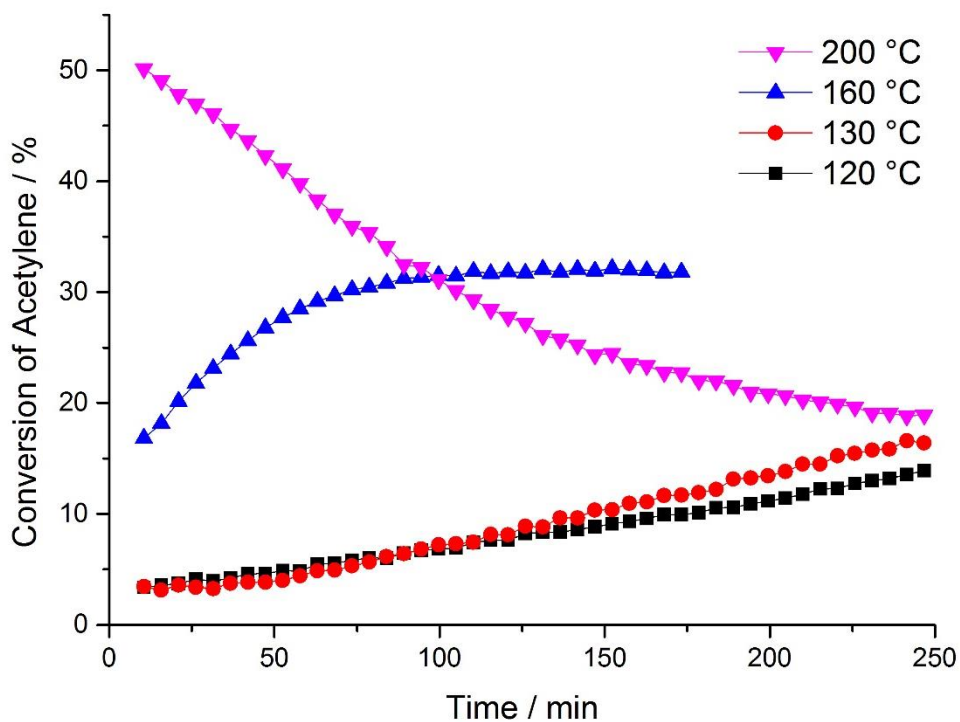


Figure 5.14. Time on-line study of 1 % Au/Ox C – 2.5, tested at 200, 160, 130 and 120 °C for the acetylene hydrochlorination reaction, tested for 250 min.

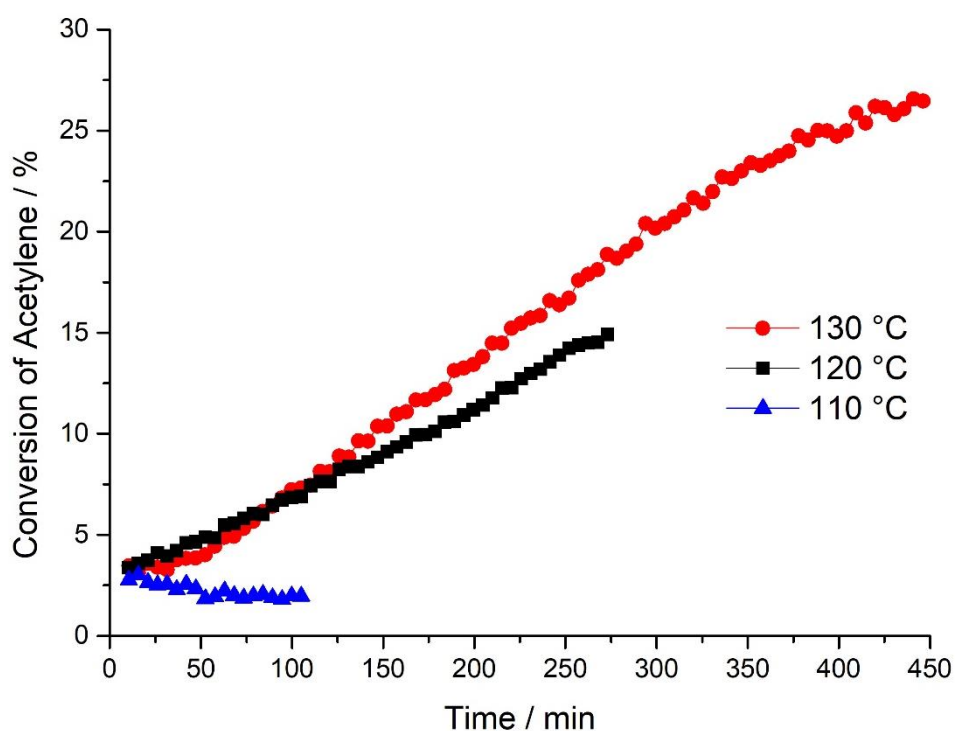


Figure 5.15. Time on-line study of 1 % Au/Ox C – 2.5 tested at 130, 120 and 110 °C for the acetylene hydrochlorination reaction, tested for 450 min.

SEM analysis of the fresh catalyst and those used at 130, 160 and 200 °C was performed to determine the dispersion of gold before and after reaction. Figure 5.15 shows the fresh catalyst.

At this stage, the gold is predominately atomically dispersed and therefore not visible via SEM, as shown by image A. However, in a few small areas, gold nanoparticles are clearly visible, as shown by the black dots in image B. These nanoparticles are all smaller than 10 nm and congregated in distinct areas, hence not observed via XRD which calculates an average particle size using the Scherrer equation. It would be interesting to determine if there is a correlation between the agglomeration of gold and the distribution of oxygen species introduced during the oxidation of the carbon; however, in order to perform such an analysis, a detector such as the Silicon Drift would be required. This is because oxygen is a light element, therefore in order to detect slight variations in oxygen weight percent an instrument of high precision is required. Unfortunately, this was not possible for the work in this chapter.

After testing under reaction conditions at 130 °C, the gold dispersion remained predominantly the same as that of the fresh; mostly homogeneously monodispersed with a few small areas of gold nanoparticles (Figure 5.16), confirmed with EDX. The combination of low temperature and steady induction period therefore did not result in significant gold agglomeration.

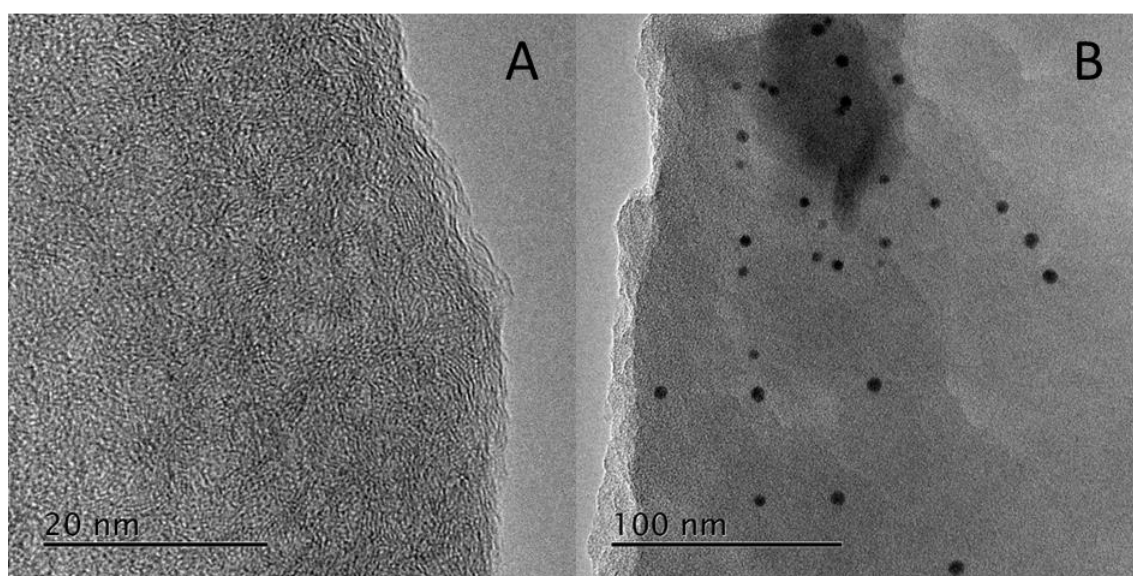


Figure 5.16. SEM images of fresh 1% Au/Ox C - 2.5; carbon with not visible monodispersed gold (A) and black dots of gold nanoparticles on carbon (B).

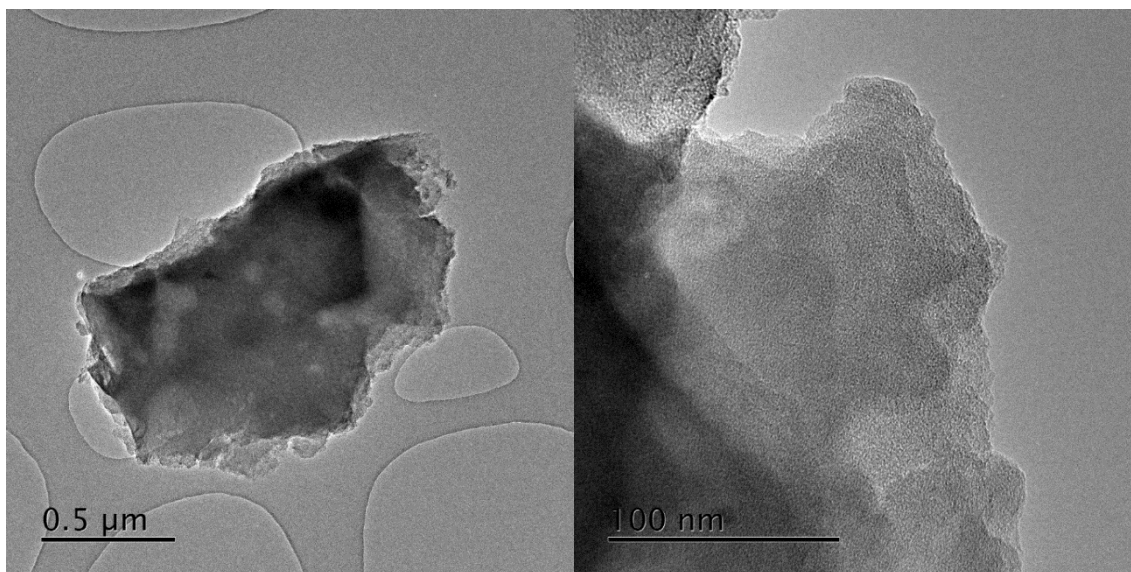


Figure 5.17. SEM images of 1% Au/Ox C - 2.5 tested at 130 °C, both images showing carbon with not visible monodispersed gold.

After testing the catalyst at 160 °C, the gold distribution had changed significantly. Image A of Figure 5.17 shows an area of catalyst with a high quantity of large nanoparticles. This is apparent in many areas of the sample; image B shows an area where the gold is assumed to be monodispersed (not visible in the SEM image but detected by EDX) however the predominant distribution is now that of image A. Image C shows a large (> 0.5 μm) gold nanoparticle. This nanoparticle has been completely removed from the carbon support, highlighting the dramatic change in gold speciation. Another large nanoparticle is shown in image D; however, this nanoparticle has facilitated the growth of carbon nanotubes, shown by the long grey “string-like tails” formed on the left of the nanoparticle. Such nanotube growth is one of the main forms of gold catalyst deactivation in the acetylene hydrochlorination reaction as the tubes can grow to such an extent that they cover the active gold species.^{37,38} This typically occurs during extended reactions due to acid sites introduced by acidic solvents, such as aqua regia, causing acid-catalysed polymerisation of acetylene.³⁹ Regardless of this, such a large nanoparticle is unlikely to be active for the reaction as it will be in the inactive Au(0) state (which should be confirmed with further characterisation such as XPS or XAFS).²² Although the conversion of the catalyst remained stable for 75 min after the initial induction period, it would be expected that the conversion would decrease as a result of the carbon nanotube and Au(0) formation after a prolonged time period. Figure 5.18 shows the catalyst after reaction at 200 °C. As was the case after testing at 160 °C, much of the gold had sintered (image A) whilst some areas of monodispersed gold remained (image B).

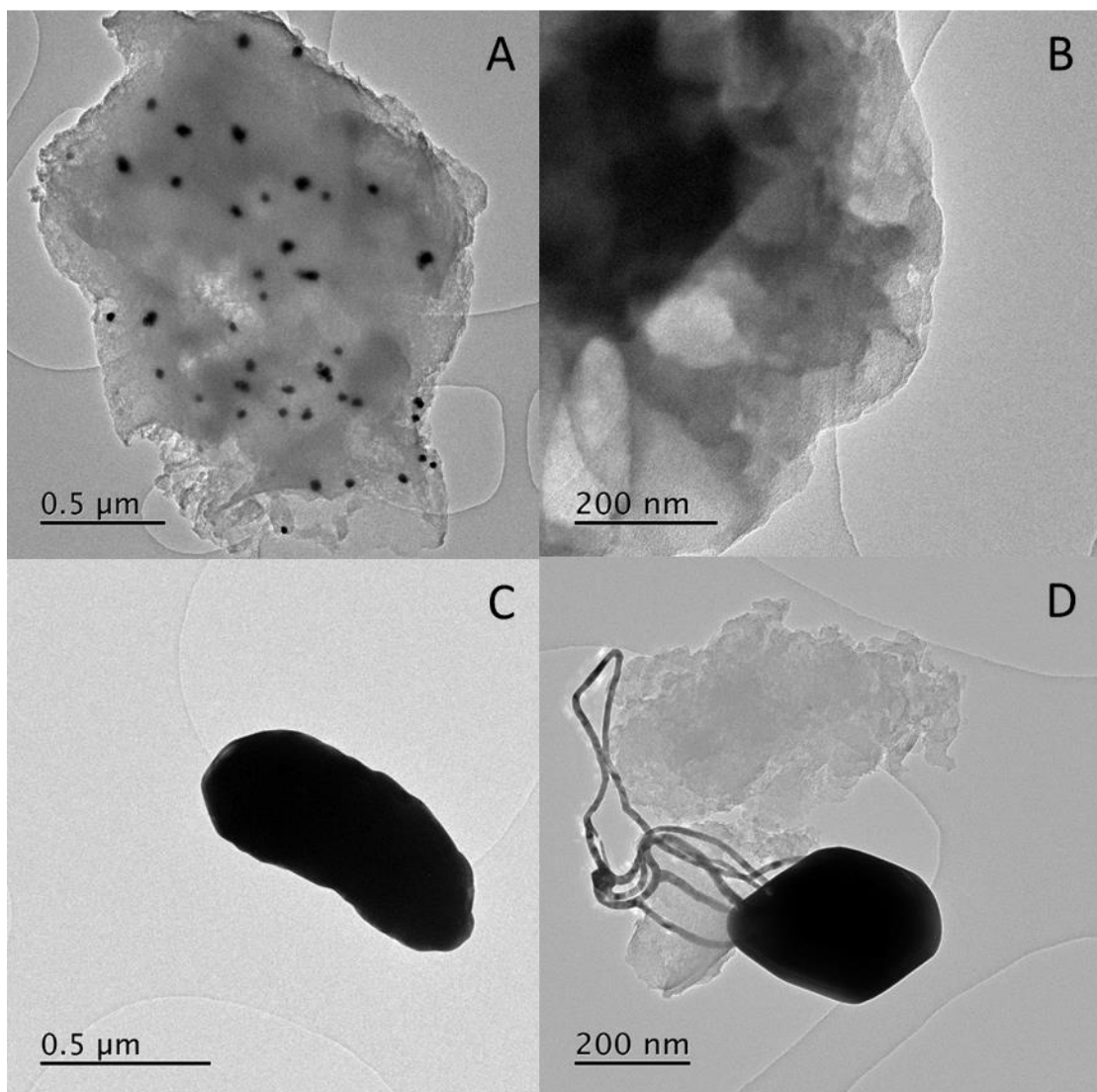


Figure 5.18. SEM images of 1% Au/Ox C - 2.5 tested at 160 °C; black dots of gold nanoparticles on carbon (A), carbon with not visible monodispersed gold (B), large gold nanoparticle detached from carbon support (C) and large nanoparticle with "tails" of carbon nanotubes on carbon (D).

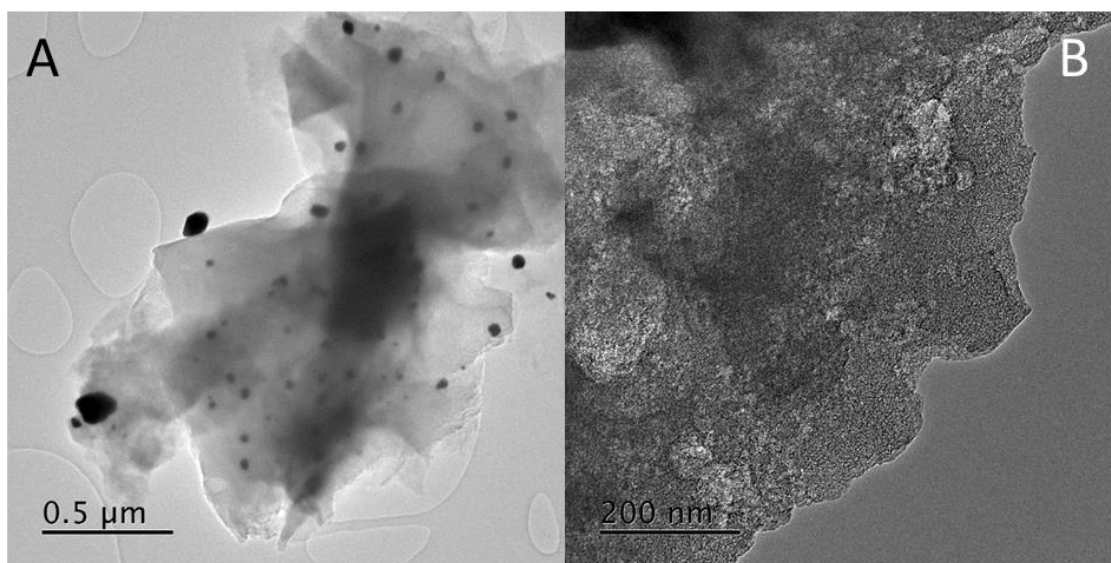


Figure 5.19. SEM images of 1% Au/Ox C - 2.5 tested at 200 °C; black dots of gold nanoparticles on carbon (A), carbon with not visible monodispersed gold (B).

5.3.4.1. Effect of temperature on gold oxidation state

Analysis of the fresh 1 % Au/Ox C – 2.5 catalyst using *ex-situ* XANES (Figure 5.19) showed the Au species to be very similar to that of the catalyst prepared with unmodified carbon, primarily in the Au(I) state. This is shown by the single peak at 11,920 eV with a normalised absorption of 0.7, with reference to metallic Au(0).

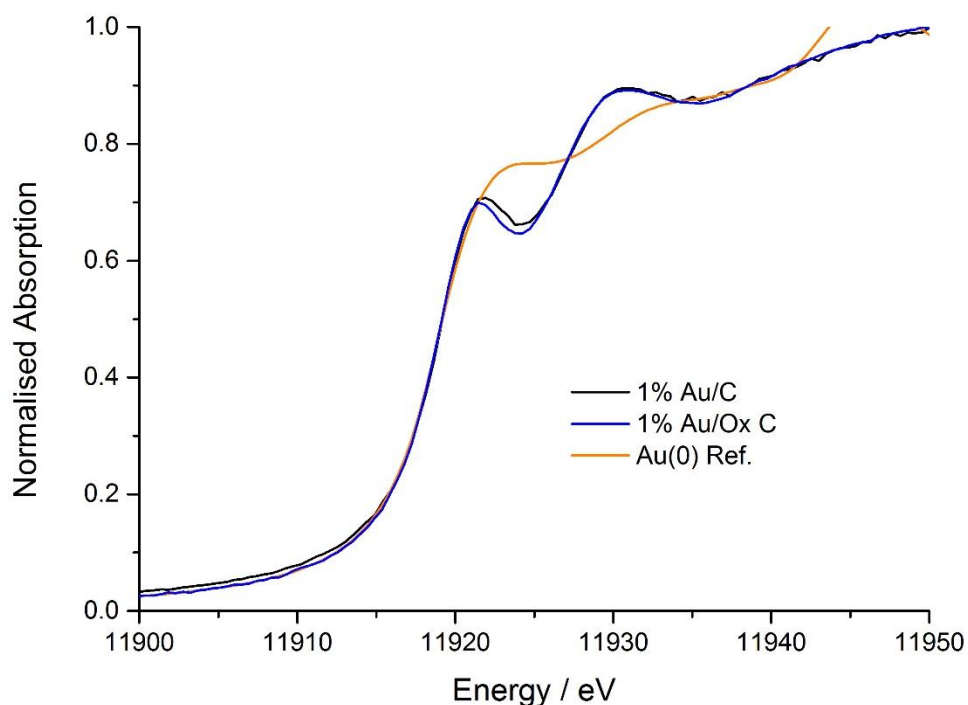


Figure 5.20. *Ex-situ* Au L₃ edge-normalised XANES spectra of 1% Au/C-AR, 1% Au/Ox C – 2.5 and a gold-foil reference material.

Comparison of the fresh 1% Au/Ox C – 2.5 catalyst with those used at various temperatures showed significant changes in the gold oxidation states (Figure 5.20). When tested at 200 °C the absorption peak becomes shallower indicating the formation of Au(0), comparable to the Au(0) gold foil reference of Figure 5.19. This is indicative of the deactivation of the catalyst, as observed in the time on-line plot (Figure 5.13). The catalyst tested at 160 °C has also undergone reduction to Au(0), to a greater extent than that of the catalyst tested at 200 °C. The gold on the catalyst tested at 130 °C however has been oxidised during the reaction, resulting in a more Au(III) like species than any of the other fresh or used catalysts as shown by a greater normalised absorption (0.9). It has previously been shown that a greater proportion of Au(III) results in a lower acetylene conversion and that conversion increases with greater Au(I) content;²² however, the results shown on the time-on-line plots (Figure 5.13 and Figure 5.14) show the acetylene conversion to be steadily increasing over time, which could either indicate that this catalyst is undergoing a very long transition period, or that if the Au(III) content is given sufficient reaction time, it can also be as active as a Au(I) catalyst.

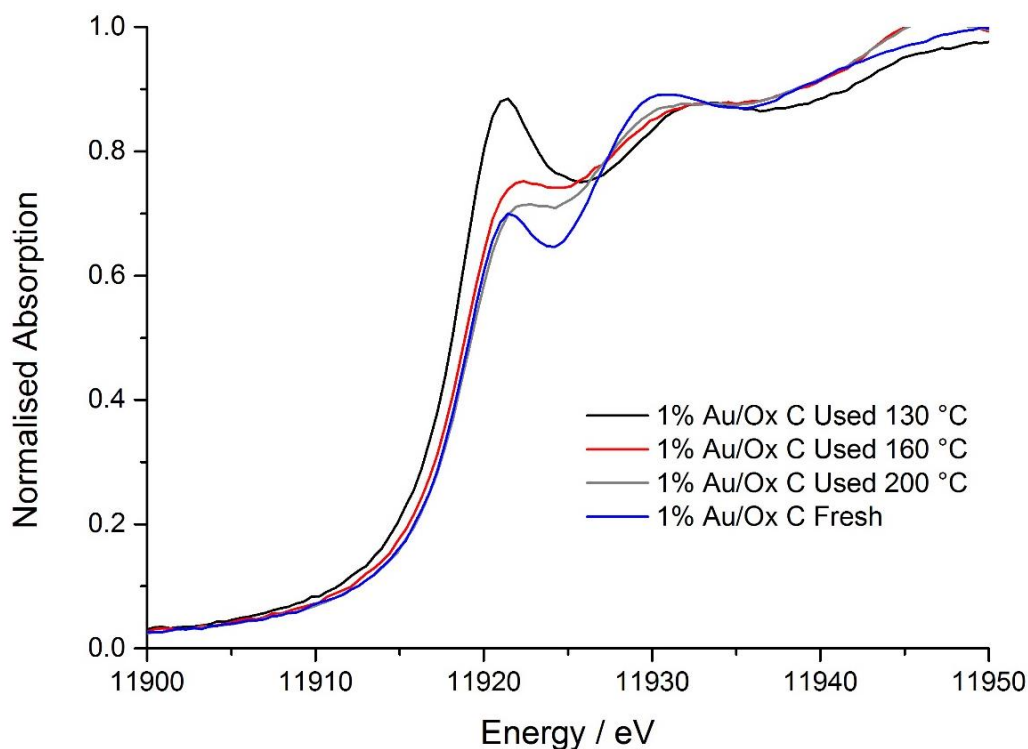


Figure 5.21. *Ex-situ* Au L₃ edge-normalised XANES spectra of 1% Au/Ox C – 2.5 Fresh and the same catalyst used at 130, 160 and 200 °C.

A linear combination fitting of the XANES results was performed in order to quantify the proportion of each gold species, Au(I), Au(III) and Au(0), in the fresh and used catalysts (Figure 5.21). In accordance with analysis performed on 1 % Au/C-AR, this catalyst is comprised predominantly of Au(I) (78 %), with Au(III) (19 %) forming the remaining oxidised gold species and 3 % Au(0). The fresh 1 % Au/Ox C – 2.5 catalyst had a very similar gold speciation; again comprised of the same proportion of Au(I) (78 %), and similar Au(III) (22 %) with no Au(0). As the oxidised carbon catalyst is instantly active at the start of the reaction when tested at 200 °C, it could be assumed that this mixture of gold states is that which results in the high initial activity. This in turn suggests that oxidising the carbon has resulted in differing surface species to those of the unoxidised carbon, which are able to stabilise these initial gold oxidation states, albeit briefly, giving rise to such a different reaction profile.

Previous *in-situ* analysis showed that, when tested at 200 °C, the Au/C-AR undergoes an initial rapid change in oxidation state from predominately Au(I) to Au(III), upon introduction of the reaction gases, followed by a steady stabilisation back to Au(I). The Au oxidation state then remains stable for as long as the reaction was continued.²² Analysis of the 1 % Au/Ox C – 2.5, also tested at 200 °C, reveals a different ratio of gold oxidation states to those of the 1 % Au/C-AR; 41 % Au(I), 10 % Au(III) and 49 % Au(0). This indicates a significant reduction of the high abundance of Au(I) present in the fresh catalyst, as well as some of the Au(III), to form Au(0).

The combination of high conversion and reaction conditions appear to be favourable for the sintering of Au, as was observed in an initially highly active, 2% Au/C catalyst studied previously.³⁶ This is in agreement with the SEM characterisation (Figure 5.18) and also the evidence that formation of Au(0) results in a decrease of catalytic activity due to catalyst deactivation.^{22,36,40}

Decreasing the reaction temperature to 160 °C results in reduction of Au(I) and Au(III) to a larger proportion of Au(0) (63 %) in 1 % Au/Ox C – 2.5. This is contradictory to the time-on-line plot (Figure 5.13) in which the catalyst conversion remains stable for 75 min. In this reaction, as in all reactions performed in this work, the VCM counts closely correlated with the acetylene conversion values, indicating that VCM was the only product formed. This strange result requires further investigation therefore, a prolonged time on-line analysis should be performed at this temperature to determine if this would be the case.

The 1 % Au/Ox C – 2.5 catalyst tested at 130 °C also shows a large proportion of Au(0) (46%) compared to the fresh catalyst; however, this catalyst also contains a significantly higher proportion of Au(III) (44 %) and a loss of Au(I) (10 %). This change in oxidation state is similar to that observed in the 1 % Au/C-AR at the start of the reaction, where oxidation of Au(I) to Au(III) occurs, although in the case of 1 % Au/Ox C – 2.5 the change was accompanied by the formation of Au nanoparticles. At temperatures below 100 °C, polymerisation of acetylene is facilitated. This is especially apparent in catalysts prepared with acidic solvents such as aqua regia as the resulting acid sites contribute to polymer formation.^{37,38} By correlating the production of VCM (using counts from GC analysis) with conversion of acetylene it was determined that this was not the case for this reaction; the VCM production correlates well with loss of acetylene for the duration of the reaction at 130 °C. Even at low conversions, this catalyst formed gold nanoparticles, indicating that the gold was mobile on the surface of the oxidised carbon and readily reduced. This also indicates that the amount of single-site oxidised gold remaining was sufficient to maintain a steadily increasing acetylene conversion. Therefore, it could be assumed that not all of the gold on the surface of the catalyst is active in the reaction, as Au(0) is known to be inactive.³⁹

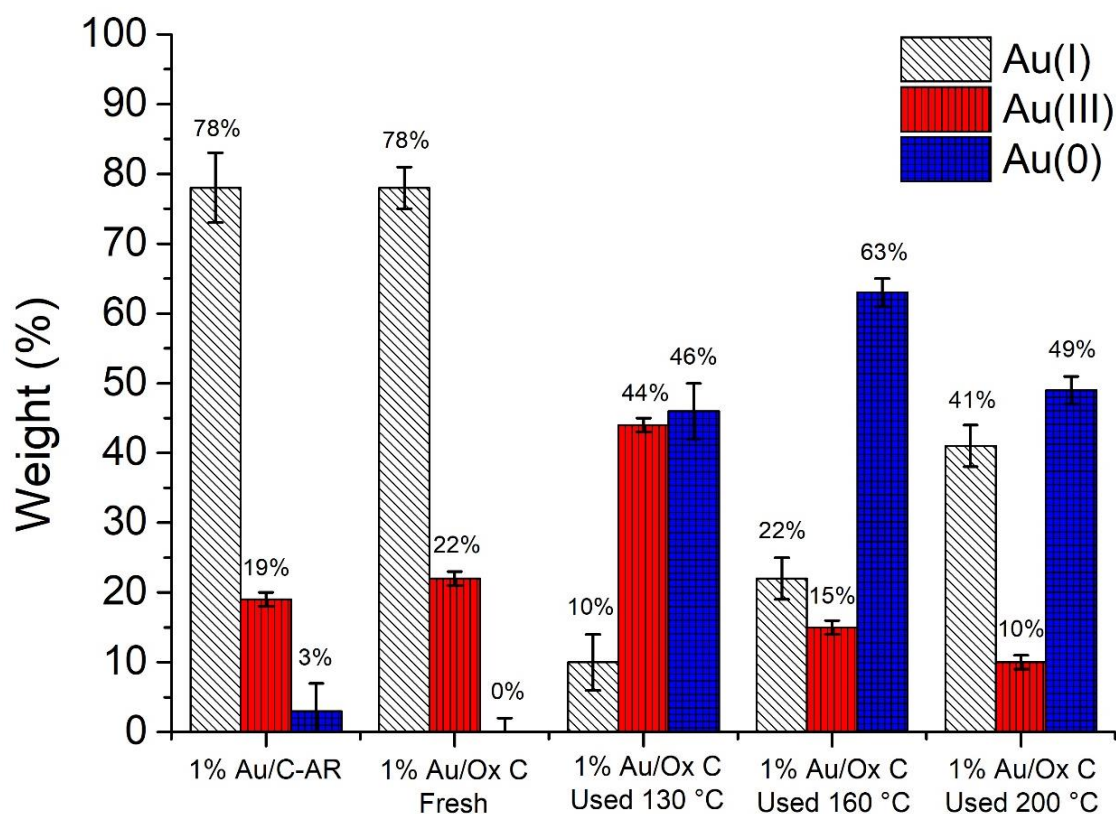


Figure 5.22. Linear combination fitting of the Au L₃-edge XANES for the fresh Au/C-AR catalyst, fresh and used at 130, 160 and 200 °C 1 % Au/Ox C – 2.5 catalysts. Error bars indicate standard deviation.

Analysis of these catalysts via EXAFS was performed in order to determine the change in Au-Cl speciation and monitor the formation of Au(0). Figure 5.22 shows the k^3 - weighted χ EXAFS Fourier transform data of the fresh Au/C-AR and 1 % Au/ Ox C – 2.5 catalysts. Both show a single peak at 1.8 Å, indicating Au-Cl scattering, and have a negligible double peak at 2.4 and 3.0 Å, indicating little Au-Au scattering and hence few/no gold nanoparticles present. This data is in accordance with the XANES – both fresh catalysts have an almost identical initial gold oxidation state and distribution. Work performed on the hydration of $[\text{AuCl}_4]^-$ suggests that the coordination of Au-O and Au-Cl can be distinguished in EXAFS. Whilst the exact values of the scattering peaks vary between sources, Au-O consistently exhibited a peak at 0.3 Å lower radial distance than that of Au-Cl.^{41–44} Unfortunately, as was shown in Figure 5.22, only Au-Cl was observed, with no clear differences between the Au/C-AR and 1 % Au/Ox C – 2.5 catalysts. This is due to a weaker intensity of back-scattering from the Au-OH species, as oxygen has fewer electrons than chlorine with which to cause scattering,⁴¹ and due to the high concentration of chlorine present in the starting material (HAuCl_4) and introduced in the solvent (aqua regia).

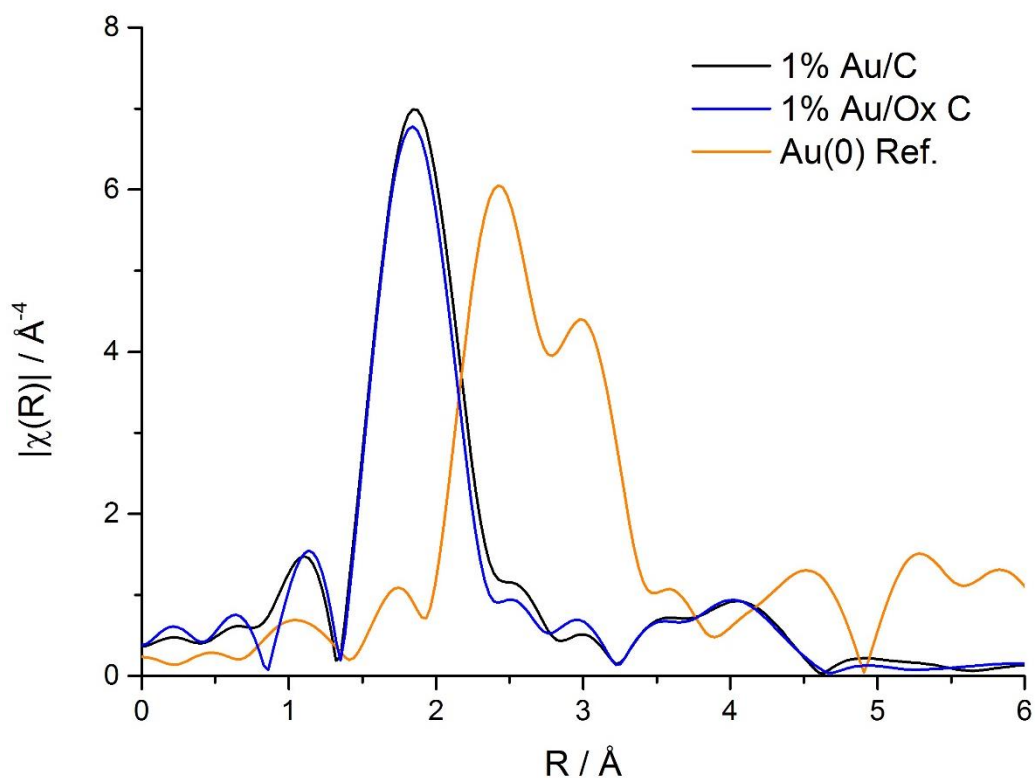


Figure 5.23. k^3 -weighted χ EXAFS Fourier transform data of 1% Au/C-AR, 1% Au/Ox C – 2.5 and a gold-foil reference material.

Figure 5.23 compares the EXAFS of the 1% Au/Ox C – 2.5 catalysts used at various temperatures to that of the fresh 1 % Au/Ox C – 2.5. All of the used catalysts have peaks at 2.4 and 3.0 Å, indicating Au(0) formation. The increase in Au(0) is concurrent with a reduction in the proportion of Au-Cl; the catalysts used at 130 °C contains the most Au-Cl and the least Au(0) whereas the catalyst used at 160 °C contains the least Au-Cl and most Au(0), closely matching the LCF data.

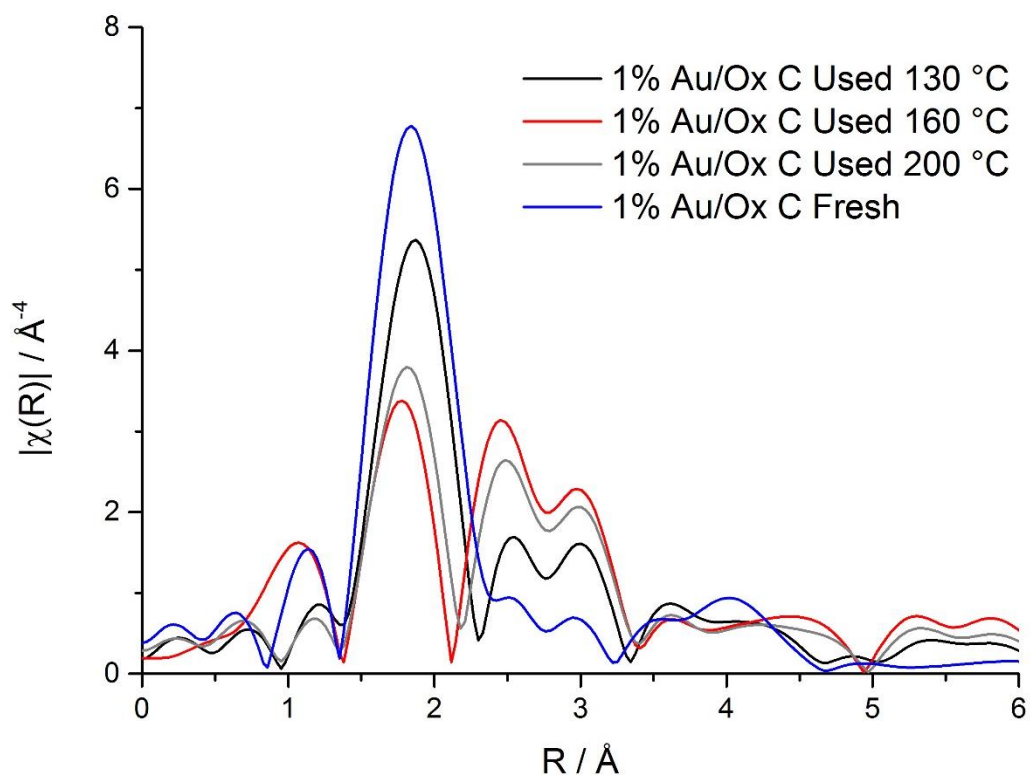


Figure 5.24. k^3 -weighted χ EXAFS Fourier transform data of 1% Au/Ox C – 2.5 Fresh and the same catalyst used at 130, 160 and 200 °C.

Analysis of the fresh and used catalysts via XPS provides some insight to the change in carbon and oxygen functionality upon reaction. Comparison of the carbon functionality shows no trend between the fresh catalyst and those tested at different reaction temperatures (Figure 5.24). Increasing the reaction temperature resulted in progressively greater sp^3 content, especially in the catalyst used at 200 °C. This gain of sp^3 carbon was mirrored by a loss of sp^2 . All the remaining functionalities remained constant, providing no further insight to the optimised functionality of the catalyst tested at 160 °C.

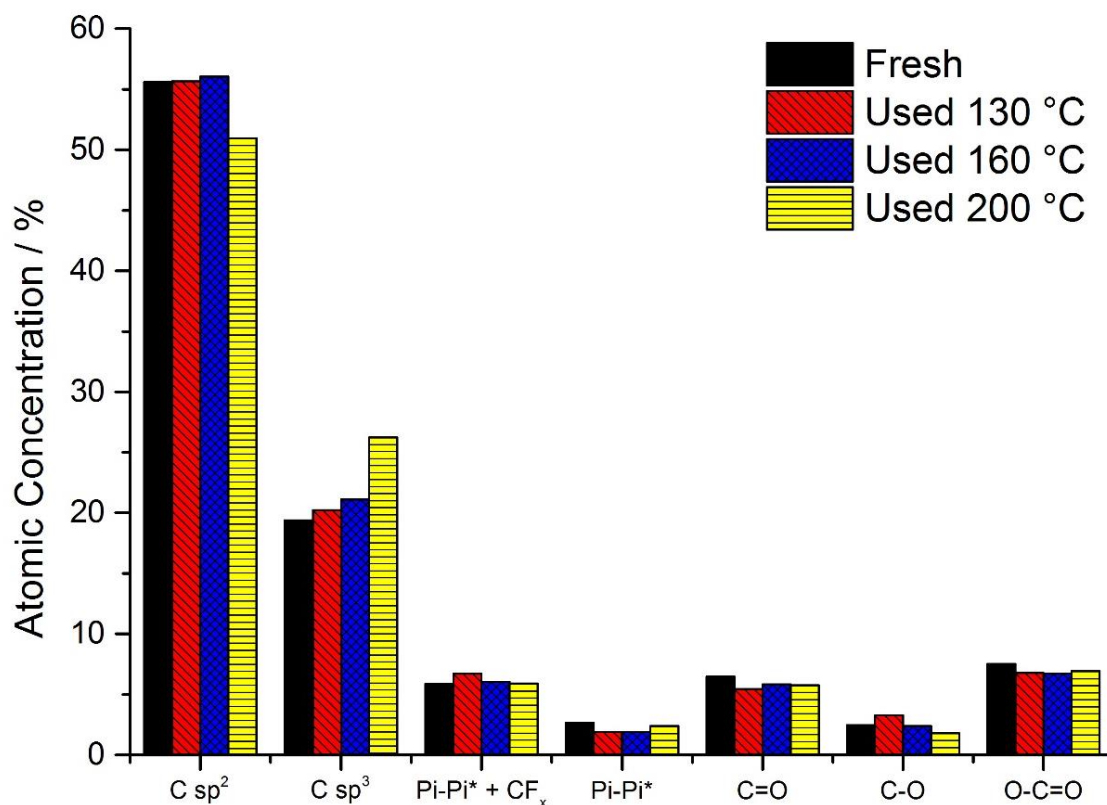


Figure 5.25. XPS of different carbon functional groups present in the oxidised carbon catalyst, fresh and tested at 130, 160 and 200 °C.

Comparing the oxygen functionality with the conversion of the catalysts after 240 min showed significant trends (Figure 5.25). The final acetylene conversion was highest when tested at 160 °C, followed by 200 and then 130 °C. The most abundant oxygen group in the catalyst tested at 160 °C was the ether. The atomic concentration of ether decreased in the 1 % Au/C – 2.5 catalyst tested at 200 °C and decreased again when tested at 130 °C. This is inversely proportional to the carbonyl group, where the catalyst tested at 160 °C had the lowest concentration of carbonyl and the concentration increased in the catalyst tested at 200 °C, increasing again when tested at 130 °C and in the fresh 1 % Au/C – 2.5. Both the satellite and ester satellite groups match this trend also, with the lowest concentration of these groups found in the catalyst tested at 160 °C and the highest concentration in the fresh catalyst. It could be inferred from these results that at higher temperatures the carbonyl/ester groups lose oxygen to form ethers; however, this would require further confirmation with repeat tests and characterisation. This led to different gold bonding, whereby the most stable catalytic species is that achieved at 160 °C. The concentration of water/peroxide species remained relatively constant at each reaction temperature.

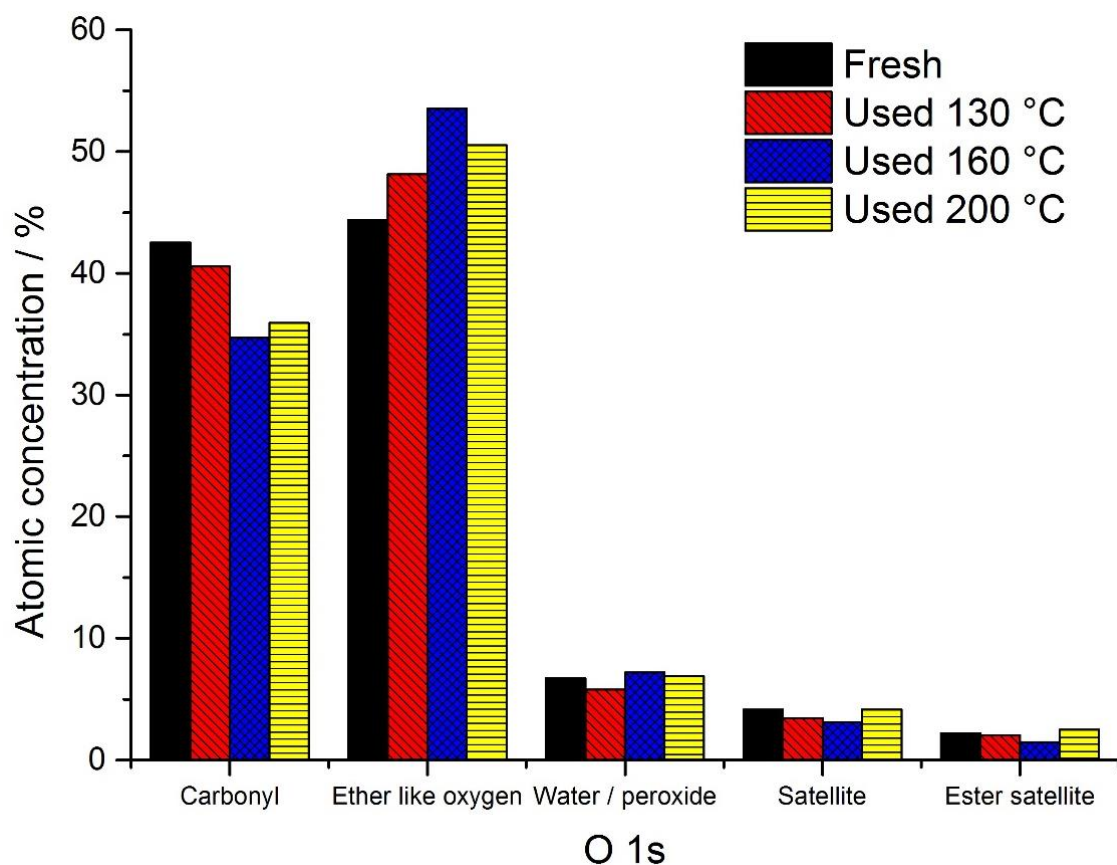


Figure 5.26. XPS of different oxygen functional groups present in the 1 % Au/Ox C – 2.5, fresh and tested at 130, 160 and 200 °C

The oxidised carbon catalysts prepared with varying amounts of KMnO_4 (0.50 – 10.00) were each tested at successive temperatures in order to determine the light-off temperature of the catalyst, ie. the minimum temperature needed to activate the catalytic reaction. Each catalyst was initially heated to 130 °C, then subject to reaction gases and the temperature periodically increased in 10 °C increments until acetylene conversion increased by $\geq 1\%$ / 20 min. A representative time-on-line plot of Au/C-AR is shown in Figure 5.26, showing light-off occurring at 190 °C. All temperature tests on oxidised carbon catalysts were performed in the same manner. The light-off temperatures are given in Table 5.2. All the oxidised carbon catalysts have a light-off temperature 30 – 50 °C lower than that of the Au/C-AR catalyst. This indicates that the interaction of the gold with the oxidised carbon support leads to a decrease in activation energy for the reaction. It should be noted that the light-off temperature for the catalyst prepared with 2.50 g of KMnO_4 was 150 °C, which was because, although the catalyst previously lit-off at 120 °C (Figure 5.13), subsequent preparations resulted in catalysts that were unable to achieve the same low light-off temperature. Future work should focus on the reproducibility of

the catalyst preparation in order to determine the cause of the change in activation temperature.

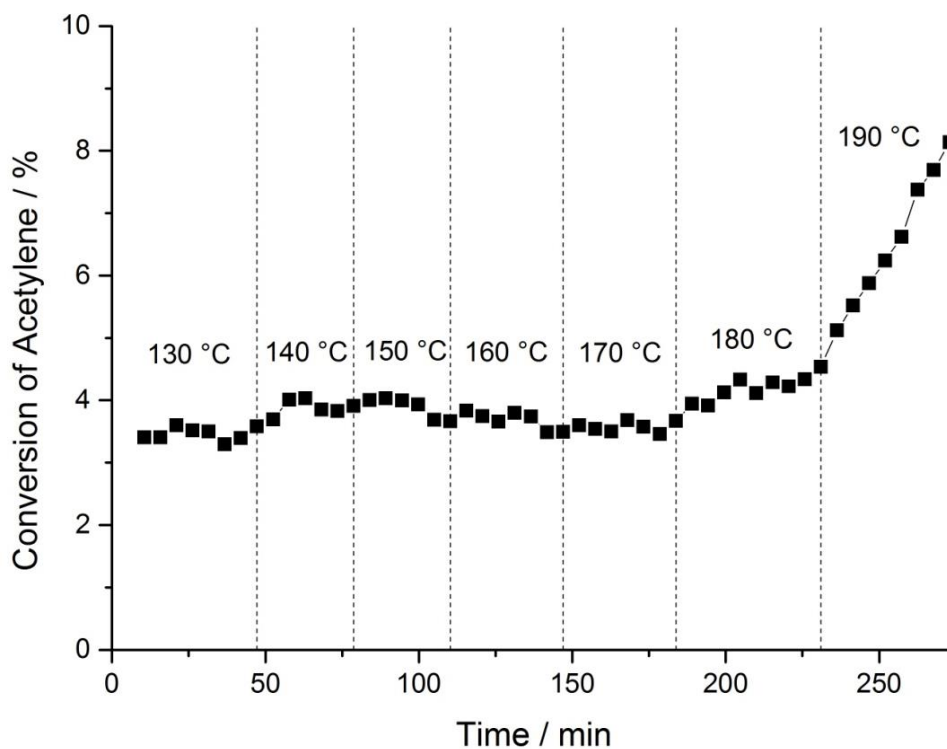


Figure 5.27. Time-on-line plot of 1% Au/C-AR, tested at increasing temperatures under standard reaction conditions as stated in section 5.2.2.

Table 5.1. Comparison of light-off temperatures for the Au/C-AR catalyst (0.00 g of KMnO_4) and oxidised carbon catalysts.

Mass of KMnO_4 / g	O At. %	Light-off Temp / °C
0.00	9.57	190
0.50	14.04	160
1.25	15.63	150
2.50	17.10	150
3.75	18.64	150
5.00	20.95	150
7.50	20.50	150
10.00	23.86	140

5.3.5. Effect of varying temperature on catalytic activity of 1 % Au/Ox C – 5

Further testing was carried out on the oxidised carbon catalyst prepared with 5.00 g of KMnO_4 . 1 % Au/Ox C – 5 was tested at temperature from 160 – 200 °C. In all of the tests performed, the catalyst began with a higher initial conversion than that achieved by the 1 % Au/C-AR catalyst, indicating an optimised gold state even before the reaction gases had been introduced. The data shown in Figure 5.27 shows that as the reaction temperature is increased, the induction period gradually reduces, up to the catalyst tested at 200 °C, which has no induction period. After a period of conversion higher than that of the Au/C-AR catalyst, all of the 1 % Au/Ox C – 5 catalysts tested began to deactivate. Unfortunately, due to time constraints, most of the reactions were not performed for longer than 240 min; of those that were, each showed a continued deactivation, resulting in a conversion similar to that of the Au/C-AR catalyst (18 %). This could imply that, although the oxidised carbon catalysts are initially able to attain much higher conversion than the untreated catalyst, the optimised gold oxidation state of the catalyst and hence general final conversion is still that of the 1 % Au/C-AR. XRD analysis shows that 1 % Au/Ox C – 5 initially contained gold nanoparticles and testing at the various temperatures resulted in sintering (Figure 5.28).

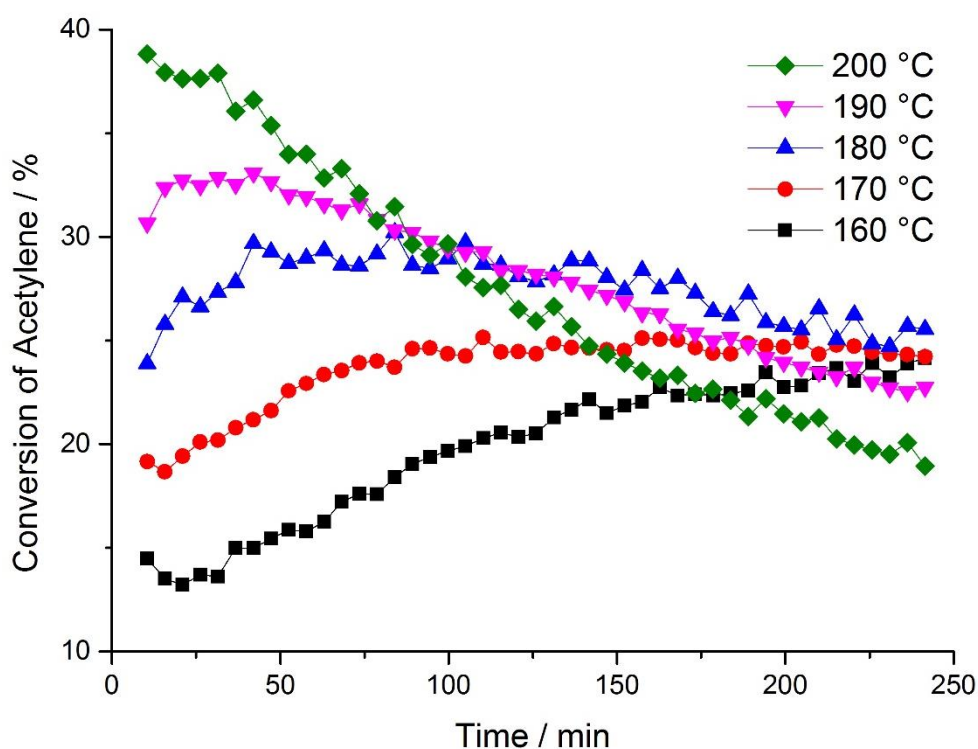


Figure 5.28. Time-on-line of Au/Ox C – 5, tested at various temperatures from 160 – 200 °C, reaction conditions as stated in section 5.2.2.

Nanoparticle formation and catalyst deactivation occurred in all tests performed on the 1 % Au/Ox C – 5 catalyst. XRD analysis of this catalyst was performed to determine if the instability was a result of the reaction gases or the heating of the catalysts. The catalyst was heated under argon to 200 °C, then allowed to cool and analysed. Figure 5.28 shows sintering of the gold, indicating that the metal was not stable at high temperatures. This was also observed in the acetone catalyst detailed in Chapter 3. The sintering of the gold before reaction does not in itself result in unstable catalysts, as the acetone-prepared catalyst was stable for at least 7 h of reaction. Work on the acetone-prepared catalyst indicated that a small proportion of Au(0) had no negative impact on the activity, presumably owing to the large proportion of oxidised gold remaining on the surface of the catalyst. Therefore, it could be concluded that either the high catalytic activity or an as-yet unknown factor was the cause of catalyst deactivation.

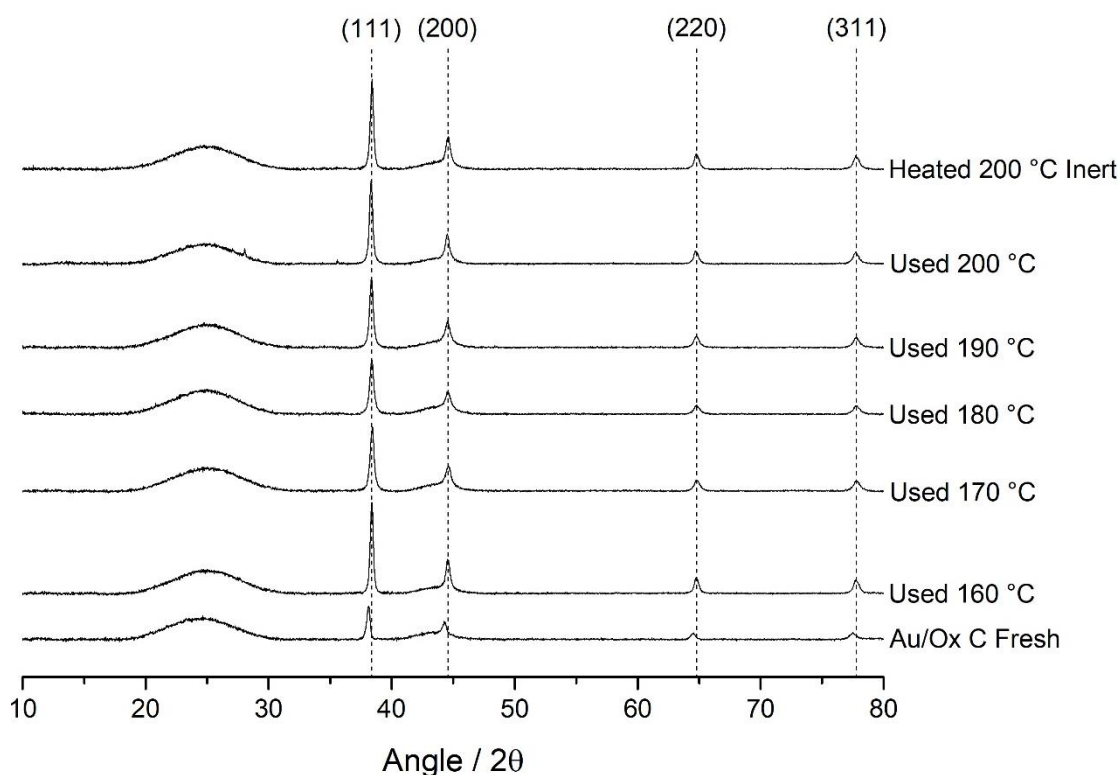


Figure 5.29. XRD pattern of Fresh Au/Ox C – 5 catalyst, used at 160-200 °C and heated at 200 °C under inert conditions. Reflections at 38, 44, 65 & 78 / 2 θ correspond to FCC metallic gold crystallites.

TGA was performed on the fresh 1 % Au/Ox C – 5 catalyst, and the same catalyst tested at 160, 180 and 200 °C. These were compared to the 1 % Au/C-AR catalyst. Figure 5.29 shows that there was an initial mass loss between 30 – 100 °C, due to evaporation of adsorbed water present on all the catalysts; however, comparison of the data above 100 °C shows minor differences between any of the catalysts. Both the unoxidised and oxidised catalysts had similar mass loss

profiles between 100 – 200 °C, indicating good functional group stability at the reaction temperatures used in this work. Literature suggests that the mass losses above 100 °C were due to carboxylic groups between 150 – 350 °C, hydroxyl groups between 350 – 500 °C and thermal oxidation of the remaining carbon above 500 °C.^{45,46} The XPS analysis (Figure 5.7 & 5.8) showed only minor differences in concentration of the various oxygen groups, which would explain the lack of observed differences in TGA profiles between the untreated and oxidised carbon catalysts. The used catalysts also have very similar TG profiles, indicating good stability of the functional groups throughout the reaction.

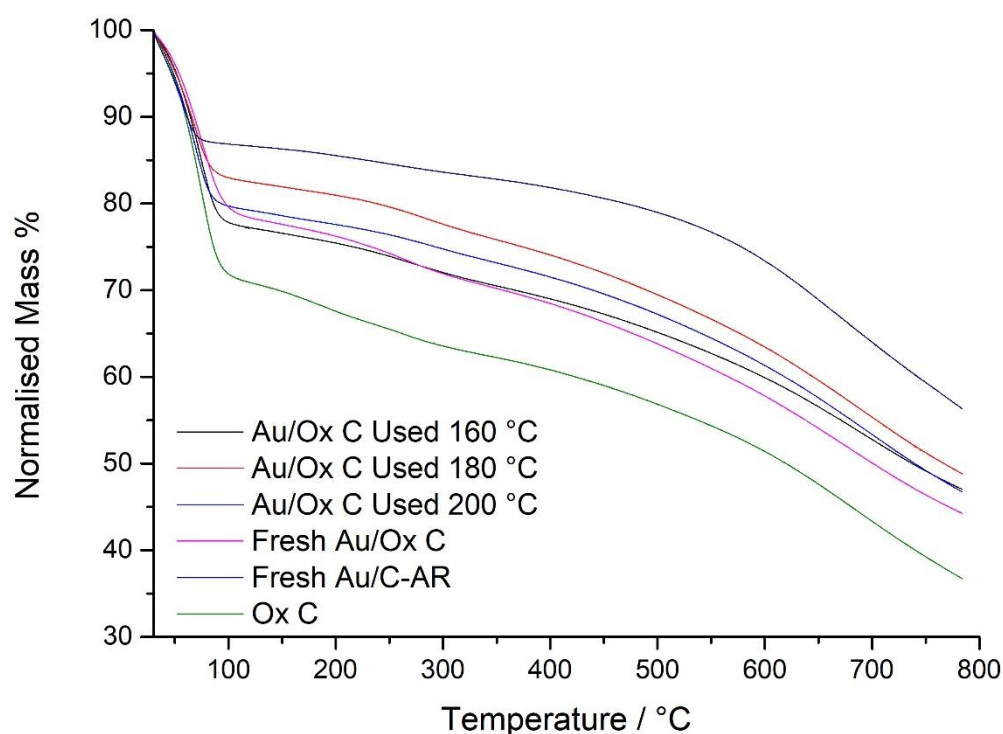


Figure 5.30. TGA profiles of oxidised carbon, fresh Au/C-AR, fresh Au/Ox C catalyst, used Au/Ox C tested at 160, 180 and 200 °C.

5.4. The effect of washing the carbon

In order to ensure that it was the oxidation of the carbon that caused the increase in activity of the oxidised carbon catalysts, the carbon was stirred in water for 1 h, filtered and dried. In this way, the preparation mimicked the latter washing stages of Hummers' preparation method. 1 % gold was then added to this "washed" carbon with aqua regia as normal. The 1 % Au/C-washed catalyst achieved an initial conversion of 42 % (Figure 5.30), which decreased to 29 % after 240 min of reaction. Again, a high initial conversion resulted in sintering of the gold, hence

deactivation of the catalyst, second only to the 1 % Au/Ox C – 2.5 catalyst; however the oxygen weight % was only slightly higher (11 wt. %) than that of the Au/C-AR catalyst (10 wt. %).

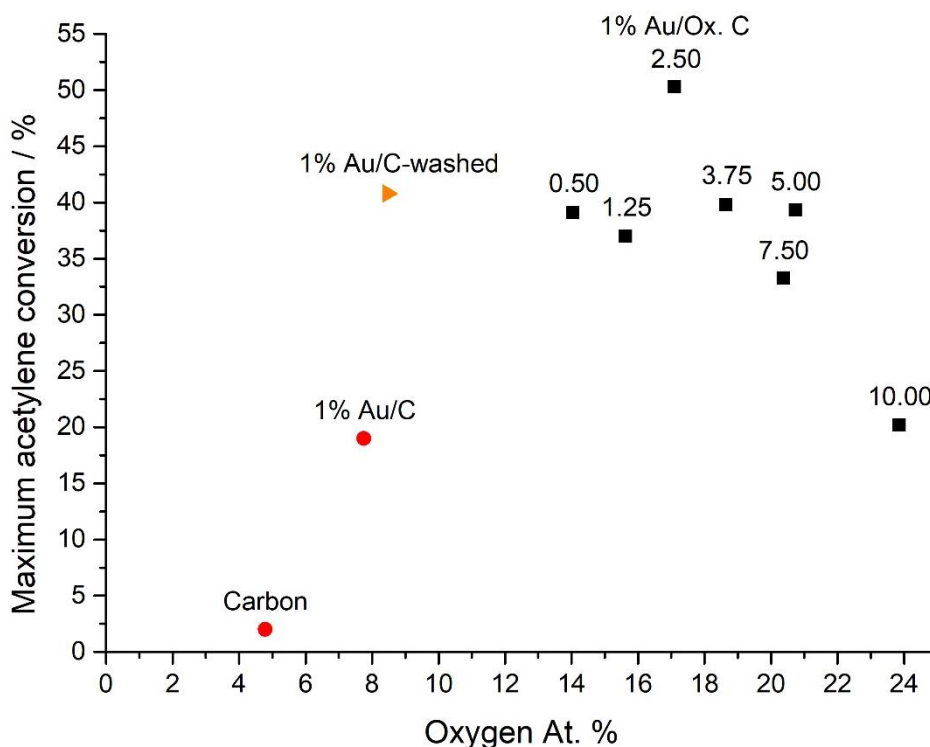


Figure 5.31. Oxygen atomic percent of the oxidised carbon catalysts versus maximum acetylene conversion (■). Number labels denote the mass of KMnO_4 per 5 g of carbon used in the preparation. (●) denotes untreated carbon and 1% Au/untreated carbon, (▶) denotes 1% Au/C-washed catalyst prepared on washed carbon.

The results of the SEM analysis (Figure 5.31) show no differences between unoxidised carbon and washed carbon. Visually, both comprised large grains of amorphous carbon. Small bright spots indicate trace, high mass elements. EDX analysis of these supports shows a slight variation in atomic composition, reported in Table 5.3. Both contain a large variety of different elements typically introduced during the preparation of the carbon.⁴⁷ The variation in mass of oxygen was included in italics as limitations in the equipment resulted in erroneous and misleadingly different values. Three elements were detected in the washed carbon that were not present in unoxidised carbon; Na, Cl and K. Although it could be argued that these elements were not present in high concentrations to begin with, introduction or omission of trace elements can have a significant impact on catalytic activity and stability. Sodium for example is a known poison for the acetylene hydrochlorination reaction,²⁶ therefore the lack of this element may have directly influenced the activity of the 1 % Au/C-washed catalyst. Further investigation should be undertaken to determine the effect, if any, of these elements on the catalytic activity before any confident conclusions can be stated.

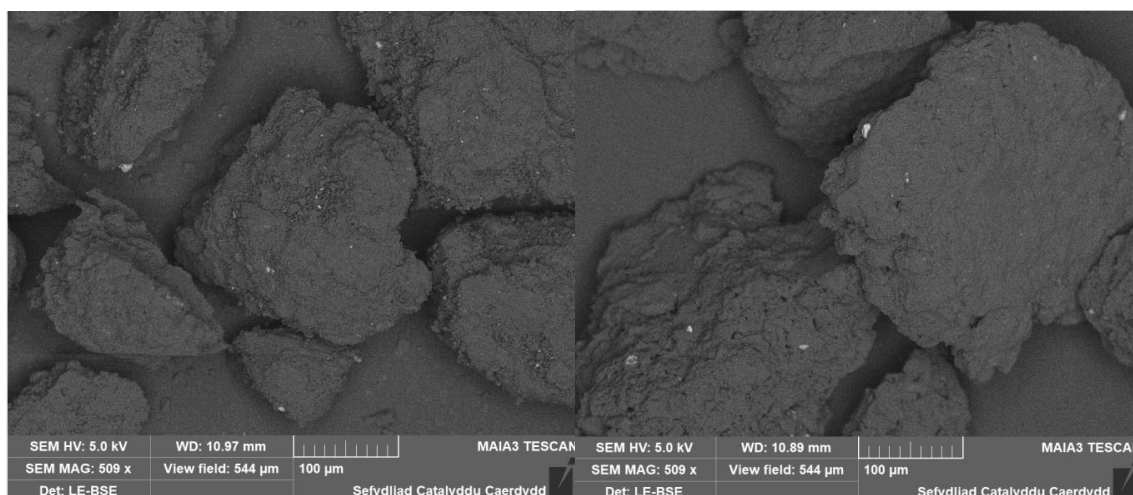


Figure 5.32. SEM images of unoxidised carbon (left) and washed carbon (right).

Table 5.2. Elemental compositions of untreated carbon and unoxidised carbon, determined by EDX. Each value was formed from an average of four separate analyses.

	Weight %	
	Unoxidised carbon	Washed carbon
C	94.07	99.12
O	6.62	0.00
Na	0.20	0.02
Mg	0.02	0.00
Al	0.04	0.05
Si	0.24	0.35
S	0.32	0.47
Cl	0.07	0.00
K	0.07	0.00
Ca	0.05	0.07
Co	0.00	0.02

5.5. Combining oxidised carbon supports with acetone

A 1% Au/C catalyst was prepared using an oxidised carbon support (prepared with 2.5 g of KMnO_4 per 5 g of carbon) and acetone as the solvent. This catalyst, labelled 1% Au/Ox C Acetone, was then tested at 200 °C and compared to the 1 % Au/Ox C catalyst prepared with aqua regia (1 % Au/Ox C AR, Figure 5.32). The use of acetone as a solvent reduced the initial conversion of

the catalyst from 37 to 31 % (note the lower than previously reported conversion of the aqua regia prepared oxidised carbon catalyst, which are due to reproducibility issues, noted and discussed in Figure 5.5). Contrary to the acetone catalyst reported in Chapter 3, 1 % Au/Ox C Acetone was not stable throughout the reaction, owing to the initial increase in acetylene conversion which resulted in sintering of gold and catalyst deactivation, as observed in the oxidised carbon catalysts discussed previously (sections 5.3.3 and 5.3.5). After a steady decrease in conversion over 260 min, both catalysts reached a similar conversion of 26/25 %. As was observed in the 1 % Au/Ox C – 5 (Figure 5.27), the conversion tends towards that of the Au/C-AR catalyst, again implying that even if an initially different oxidised state is present on the surface, the gold will eventually reach the same steady state conversion. Longer reactions should be performed to confirm this observation.

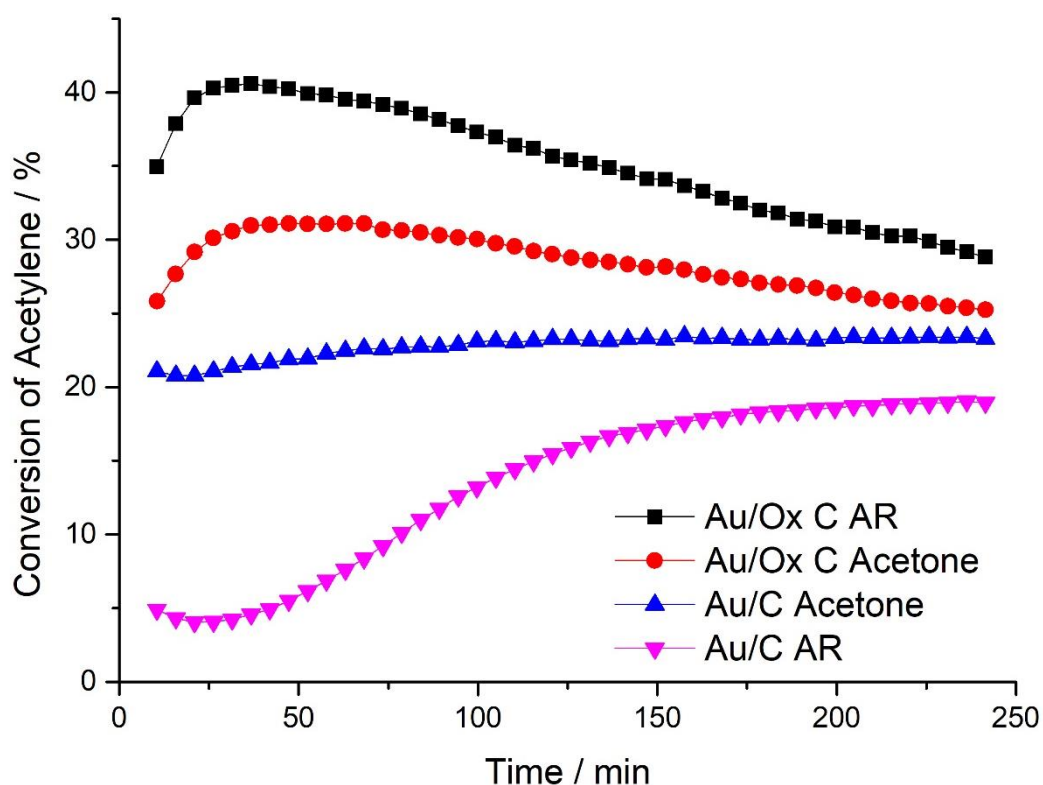


Figure 5.33. Time-on-line data of Au/Ox C AR, Au/Ox C Acetone, Au/C Acetone and Au/C AR, reaction conditions as stated in section 5.2.2.

5.6. Oxidising the support via different methods

Recent reports have suggested that by performing alternative oxidations of the carbon, or using different oxidising solvents to aqua regia, the activity of the Au/C catalyst can be increased.^{8,33} To compare the activity of two of these catalysts to those prepared with Hummers' oxidation

method, two catalysts were prepared as follows: the first was prepared by refluxing carbon in concentrated HNO_3 , followed by gold wet impregnation using aqua regia, to produce a 1% gold catalyst, denoted Au/C- HNO_3 . The second was prepared using a 1:3 mix of H_2O_2 :HCl as solvent to dissolve HAuCl_4 , followed by wet impregnation on untreated carbon to form a 1% gold catalyst, denoted Au/C- H_2O_2 /HCl. These catalysts were prepared in the same manner as those reported in literature by K. C. O'Connell⁸ and J. Zhao,³³ respectively. Each catalyst was analysed via XPS to determine the oxygen atomic percent. The initial conversion of each catalyst versus oxygen atomic percent is shown in Figure 5.33. Both catalysts have the same conversion as that of the Au/C-AR catalyst (18 %); however, each has different oxygen atomic percentage.

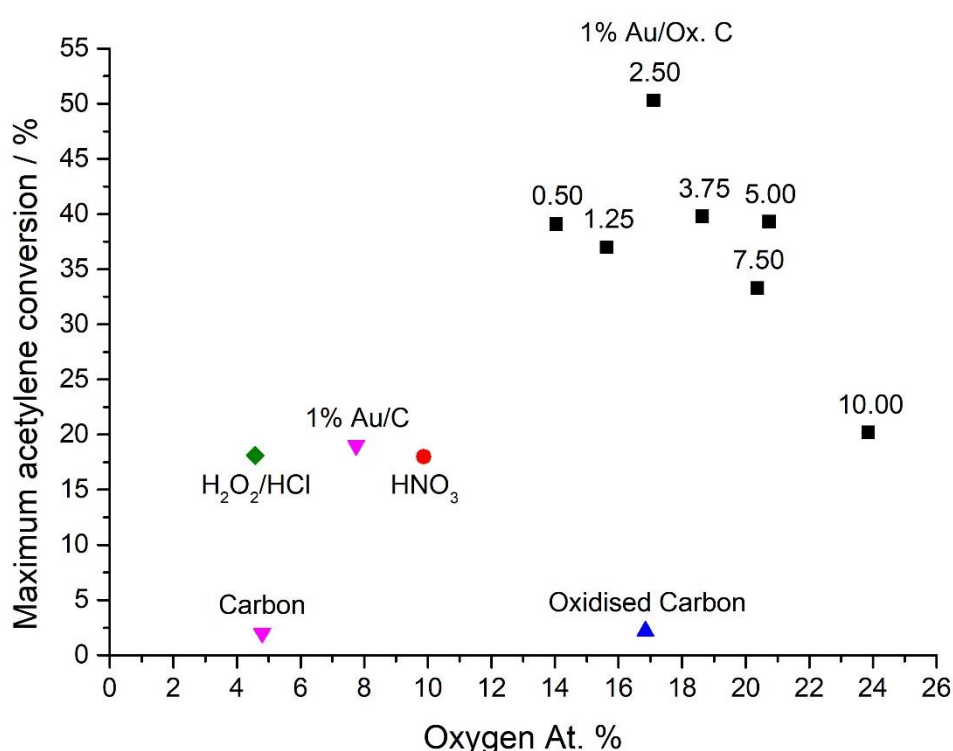


Figure 5.34. Oxygen atomic percent of the oxidised carbon catalysts versus maximum acetylene conversion (■). (▼) denotes untreated carbon, (▼) 1% Au/C prepared with unoxidised carbon and (▲) oxidised carbon prepared with 2.50 g of KMnO_4 , (◆) Au/C- H_2O_2 /HCl and (●) Au/C- HNO_3 .

Au/C- HNO_3 has a higher oxygen content than the Au/C-AR catalyst, as one would expect after refluxing the carbon in an acidic, oxidising environment. Au/C- H_2O_2 /HCl has a lower oxygen content than the Au/C-AR catalyst, slightly lower than (but within error) of that of unoxidised carbon with no gold present. The lack of oxygen was attributed to this catalyst preparation not including aqua regia; as was reported in Zhao's work, the use of aqua regia results in a greater total concentration of surface-oxygen groups than the H_2O_2 /HCl solvent mixture.³³

Although the conversion of each of the catalysts was comparable to the Au/C-AR catalyst, the

initial activation of each was significantly shorter than 240 min (Figure 5.34). Both reached a stable conversion within 100 min of reaction and remained at a constant conversion for the remaining time.

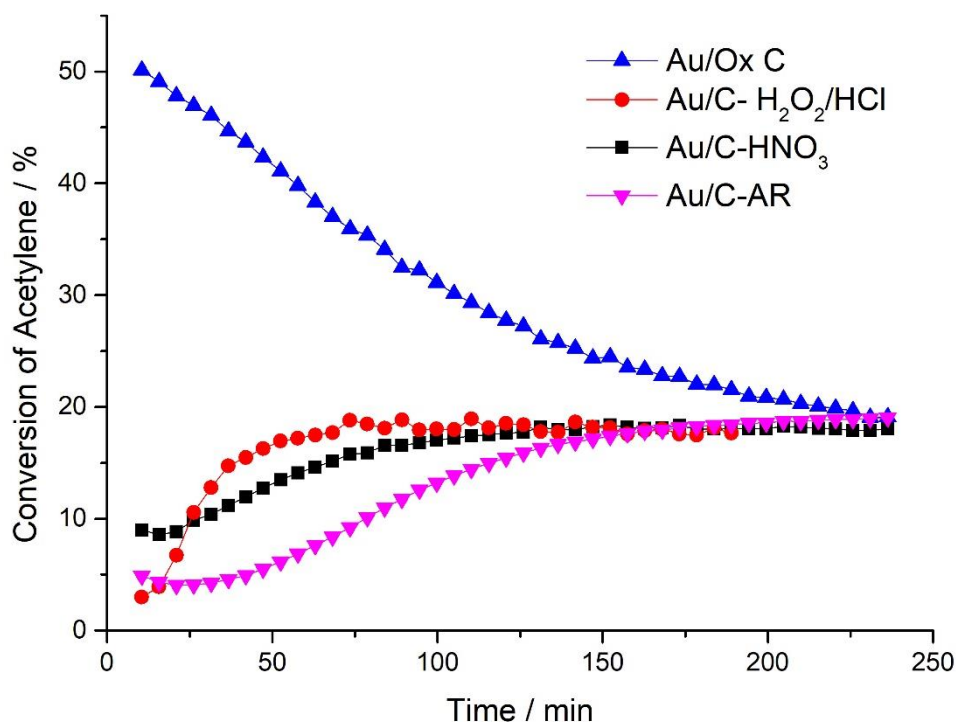


Figure 5.35. Time-on-line data of Au/Ox C, Au/C-H₂O₂/HCl, Au/C-HNO₃ and Au/C-AR, reaction conditions as stated in 5.2.2.

The light-off temperature of the Au/C-H₂O₂/HCl and Au/C-HNO₃ catalysts was determined and compared to those of the oxidised carbon catalysts, as shown in Table 5.4. Both have a lower light-off temperature than the Au/C-AR catalyst but higher than any of the oxidised catalysts. This is especially significant given that Au/C-H₂O₂/HCl had a lower oxygen weight percent than the Au/C-AR catalyst yet is still active at 20 °C lower temperature. Given the changes in atomic oxygen percent and acetylene conversion, this indicates that the oxygen atomic weight is not the sole reason for differences in the reaction profile or activation energy of the catalyst and hence light-off temperature. Further investigation would be required to determine the specific functionality that is responsible for these changes.

Table 5.3. Comparison of light-off temperatures for Au/C-AR, oxidised carbon catalysts, Au/C-H₂O₂/HCl and Au/C-HNO₃.

Mass of KMnO ₄ / g	O At. %	Light-off Temp / °C
0.00	9.57	190
0.50	14.04	160
1.25	15.63	150
2.50	17.10	150
3.75	18.64	150
5.00	20.95	150
7.50	20.50	150
10.00	23.86	140
Au/C-H ₂ O ₂ /HCl	5.73	170
Au/C-HNO ₃	13.73	180

XPS analysis of these catalysts was performed to determine the abundance of different carbon (Figure 5.35) and oxygen (Figure 5.36) functionalities on the supports. Analysis of the carbon region showed a much higher concentration of sp² carbon in both Au/C-HNO₃ (77 %) and Au/C-H₂O₂/HCl (80 %) compared to the oxidised carbon catalysts (<72 %) and a slight increase in pi-pi* - CF_x, within error (±1 %). Lower sp³, C=O and C-O concentration was observed in both catalysts, suggesting that the increase in sp² concentration was not attributed to an increase in oxygen functionality. pi-pi* and O-C=O content also remained low.

The oxygen region concurred with the carbon results; a decrease in carbonyl concentration was observed in both Au/C-HNO₃ (35 %) and Au/C-H₂O₂/HCl (39 %) compared to the oxidised carbon catalysts, as well as a low ether content. The concentration of H₂O/H₂O₂ increased to 10 % in Au/C-H₂O₂/HCl, as would be expected due to the solvent. The concentration of the satellites remained relatively constant for all catalysts. Therefore, catalytic stability, in this case the ability of the gold to remain anchored and active on the support surface, may be attributed to a higher concentration of sp² hybridised carbon and a decrease in the oxygen functionalities. This provides further credence to the hypothesis that higher oxygen concentration decreases the stability of the gold on the support (discussion on Table 5.1).

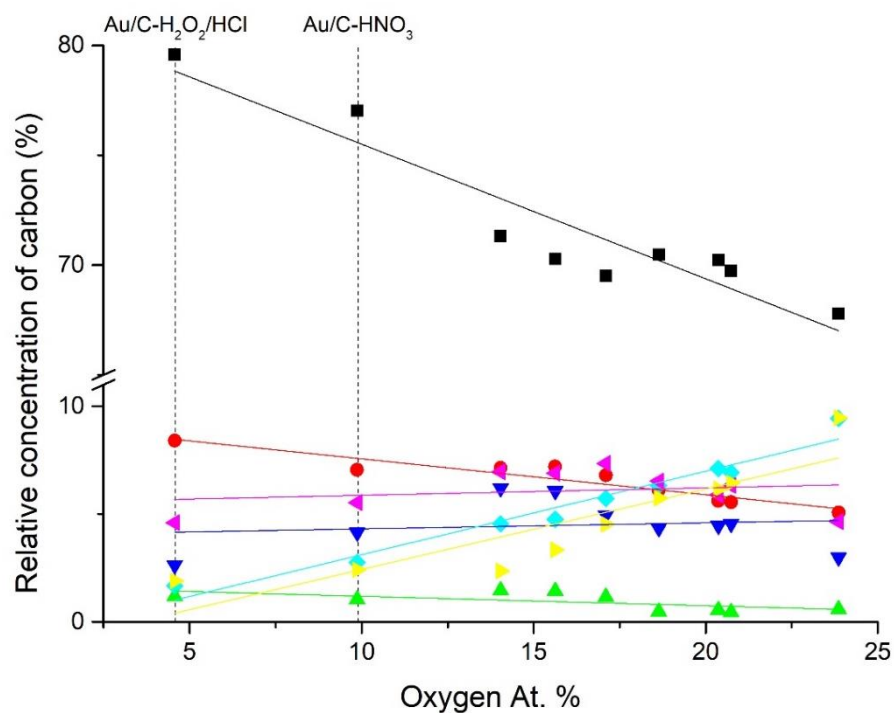


Figure 5.36. Comparison of relative concentrations of carbon species for catalysts prepared with different oxygen atomic %, determined by XPS. sp² (■), pi-pi* + CF_x (●), pi-pi* (▲), C=O (▼), C-O (◆), sp³ (◄) and O-C=O (►).

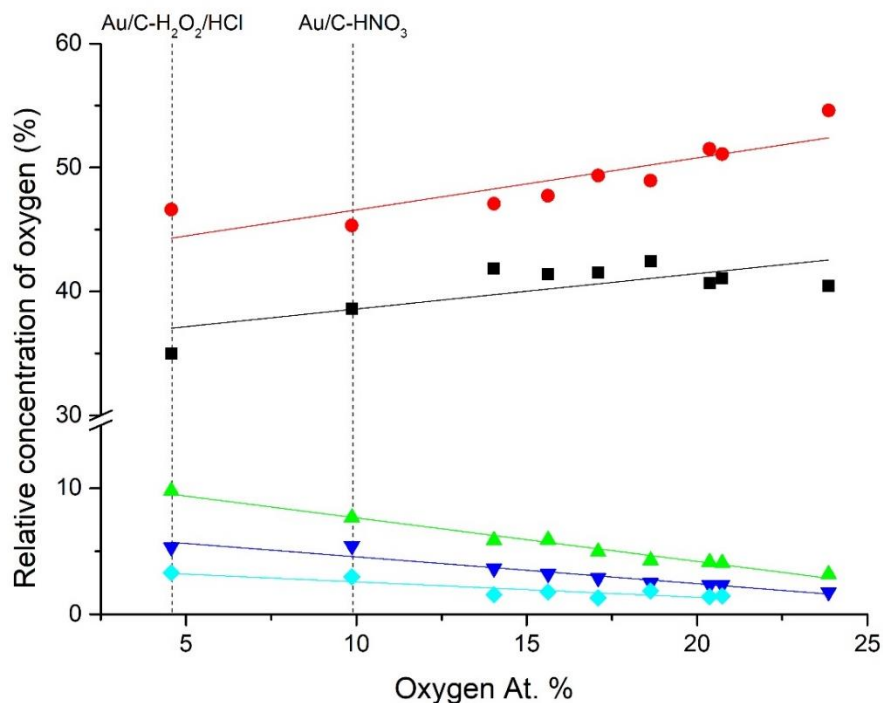


Figure 5.37. Comparison of relative concentrations of oxygen species for catalysts prepared with different oxygen atomic %, determined by XPS. Carbonyl (■), ether (●), H₂O/H₂O₂ (▲), satellite (▼) and ester-satellite (◆).

Gold L_3 -edge XANES analysis of Au/C-HNO₃ was performed to determine the oxidation state of the gold present. Figure 5.37 shows that the oxidation state of Au/C-HNO₃ was very similar to that of Au/C-AR, noted by normalised white line heights of 0.8 and 0.7 respectively. Future work should include a comparison of the fresh and used catalysts, as this was not performed; however, given that the reaction profile of Au/C-HNO₃ was so similar to Au/C-AR, it would not be unreasonable to suggest that the white line height of the used catalyst would also be similar to that of the fresh and used Au/C-AR (both 0.8).

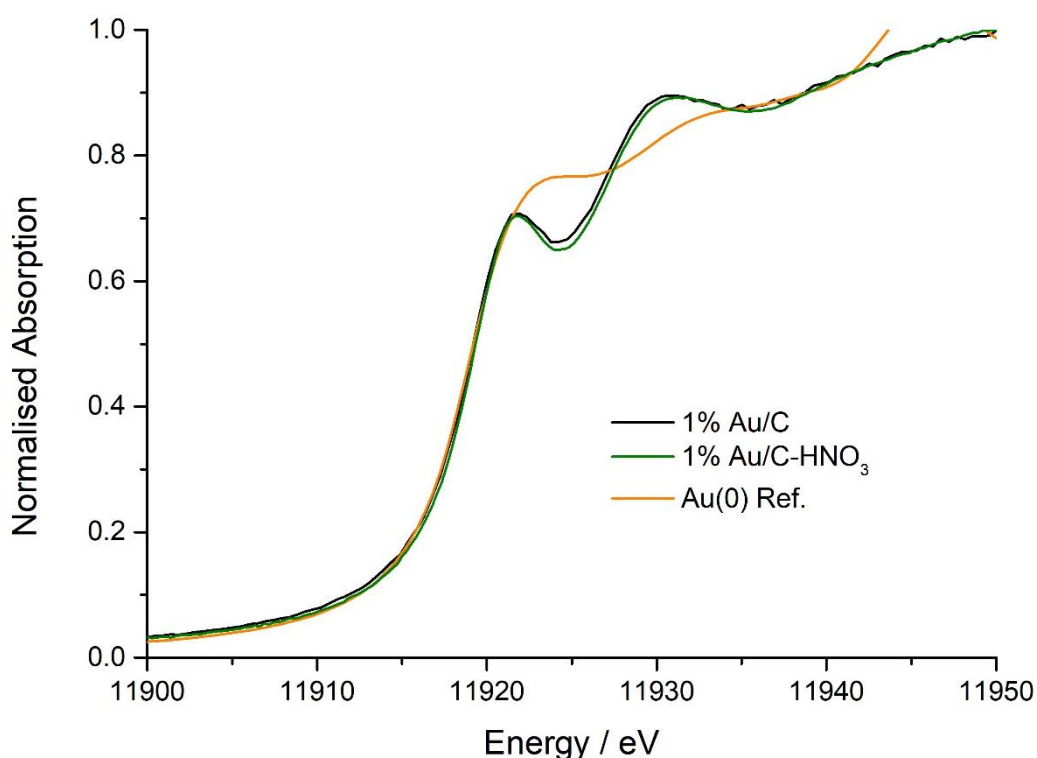


Figure 5.38. *Ex-situ* Au L_3 edge-normalised XANES spectra of 1% Au/C-AR, 1% Au/C-HNO₃ and a gold-foil reference material.

LCF of the XANES data was performed, confirming the relative abundance of gold oxidation states was near identical to that of both the fresh Au/C-AR and 1 % Au/Ox C – 2.5 [75 % Au(I), 25 % Au(III), 0 % Au(0)]. Given that the gold speciation is so similar to that of Au/C-AR, an *in-situ* XANES study would be useful to determine if Au/C-HNO₃ undergoes the same change in oxidation states, albeit at a much faster rate. The lack of Au(0) confirmed the homogenous dispersion of gold on the support, observed in all of the catalysts prior to reaction.

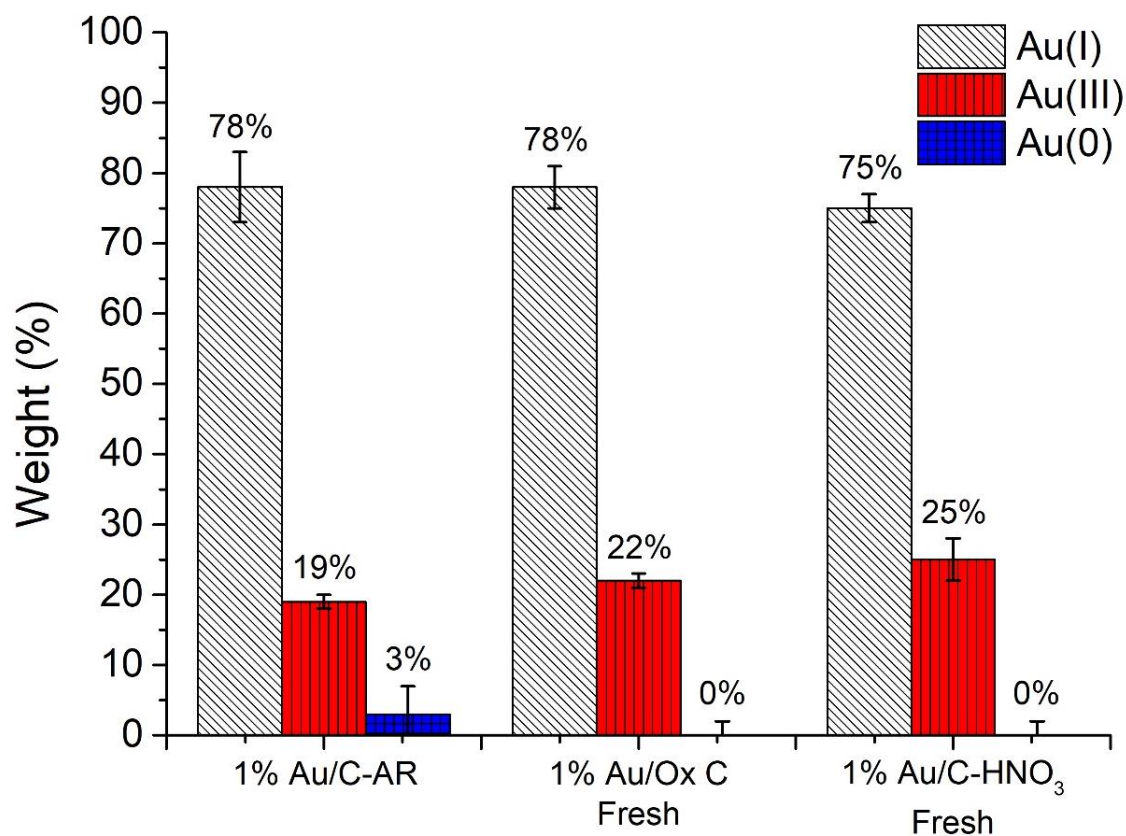


Figure 5.39. Linear combination fitting of the Au L₃-edge XANES for the fresh Au/C-AR, fresh Au/Oxidised C and fresh Au/C-HNO₃ catalysts. Error bars indicate standard deviation.

Similar to the XANES, EXAFS analysis also showed virtually no differences between Au/C-HNO₃ and Au/C-AR (Figure 5.39). Both displayed a single sharp peak at 1.8 Å corresponding to Au-Cl, with no Au-Au scattering paths observed around 2.5 – 3.0 Å.

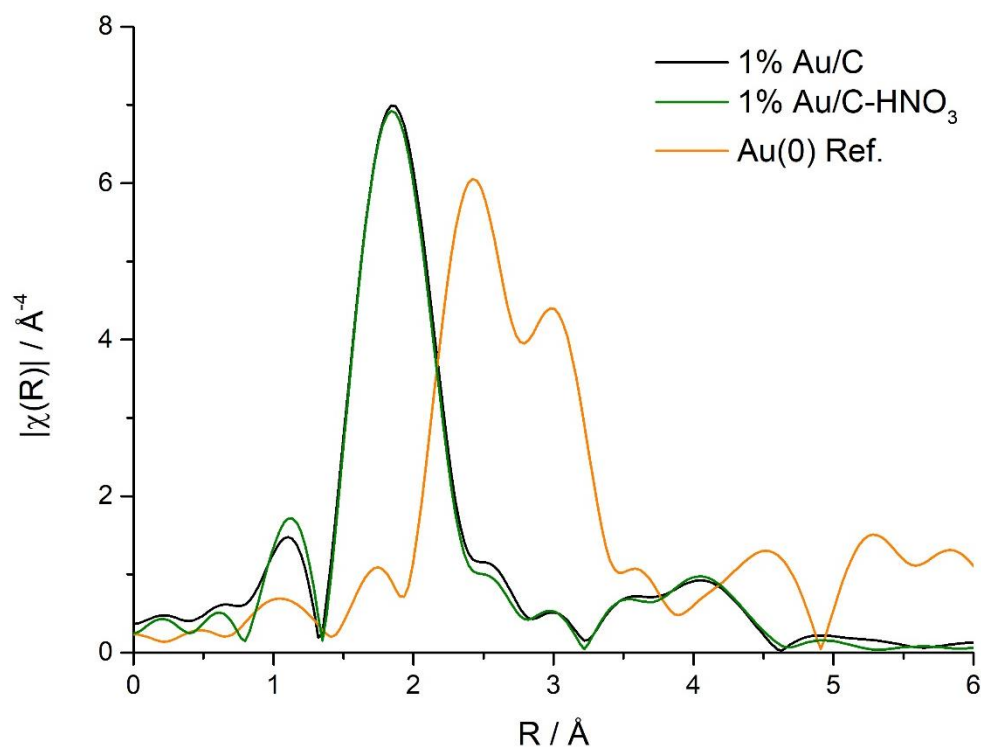


Figure 5.40. k^3 - weighted χ EXAFS Fourier transform data of 1% Au/C-AR, 1% Au/C-HNO₃ and a gold-foil reference material.

5.7. Conclusions and future work

A series of 1 wt. % Au/C catalysts were prepared by oxidising the carbon support via Hummers' oxidation method. Each of these catalysts achieved a much higher initial conversion when compared with the Au/C-AR catalyst (prepared with untreated carbon) and were able to light-off at lower reaction temperatures. Comparing the oxygen content of each catalyst, as determined by XPS, with the acetylene conversion, revealed an optimum oxygen atomic percent of 21. Masses of oxygen greater or lower than this resulted in lower activity catalysts.

XRD concluded that nanoparticles were formed in all catalysts during the reaction, facilitating the deactivation of each catalyst. This was attributed to the high conversion exhibited by all oxidised catalysts, facilitating the sintering of cationic gold to form metallic Au(0). The temperature of the reaction had a significant impact on the activity of the oxidised catalyst prepared with 2.50 g of KMnO₄. Decreasing the temperature to 130 °C resulted in much longer induction period; however, the catalyst managed to achieve an acetylene conversion higher than that of Au/C-AR. SEM analysis confirmed that the catalyst maintained a homogeneous cationic gold dispersion throughout the reaction. After reaction, this catalyst was comprised of a greater Au(III) character than displayed in Au/C-AR, suggesting why the catalyst did not achieve

a steady conversion during the reaction. Further reduction of the catalyst would be needed to achieve the desired, stable predominantly Au(I) species present in Au/C-AR. Increasing the reaction temperature to 160 °C and 200 °C reduced the Au(III) content whilst increasing the Au(I), also increasing the acetylene conversion. Gold nanoparticles were observed at the higher temperatures, explaining the deactivation observed in the test at 200 °C. XPS analysis suggested that ether groups may be responsible for high acetylene conversion, whilst the presence of carbonyls resulted in the lowest conversion.

Reactions performed on a catalyst prepared by washing the carbon had a high conversion with a low oxygen content. Analysis of the carbon suggested that removal of elements such as Na, K and Cl, present in the original carbon, may have contributed to the increase in activity. Catalysts should be prepared on "clean" carbons (those without large concentrations of contaminants) doped with known quantities of Na, K and Cl, independently, to determine the effect, if any, of these elements on the catalytic activity. This could help to understand the high conversion with low oxygen content.

Two catalysts were prepared using mild oxidation methods, refluxing in HNO₃ and using H₂O₂/HCl as a solvent. Both catalysts had a rapid induction period followed by a final conversion comparable to that of Au/C-AR. Characterisation showed that Au/C-HNO₃ had a higher oxygen concentration, whilst Au/C-H₂O₂/HCl had a lower oxygen concentration than Au/C-AR. Therefore, it was concluded that the concentration of oxygen itself did not dictate the activity of the catalyst; in accord with literature the specific oxygen functional groups would be responsible for changes in gold speciation.

From these results, much future work could be performed to determine the exact cause of the increased acetylene conversion exhibited by the oxidised carbon catalysts. Firstly, the TG-MS method should be optimised to detect the concentration of CO removed from the catalyst upon heating; this would provide further insight to the differences in functionality introduced upon oxidation, to complement the CO₂ data. STEM analysis of the oxidised carbon catalysts should be performed with a silicon drift detector to determine if there is a correlation between the distribution of oxygen and agglomeration of gold; this would indicate whether the increased oxygen concentration affects the distribution of gold during the reaction. Finally, significant attention should be directed towards the reproducibility of the oxidised catalysts, especially that prepared with 2.50 g of KMnO₄. Although 1 % Au/Ox C – 2.5 catalyst was able to light-off at temperatures as low as 120 °C, subsequent preparations of the catalyst resulted in a higher temperature of 150 °C. This would be facilitated by the future work mentioned above; if the functional groups responsible for the increased catalytic activity could be determined, the

preparation method may be tailored towards these functionalities.

5.8. References

- 1 M. F. R. Pereira, J. J. M. Órfão and J. L. Figueiredo, *Appl. Catal. A Gen.*, 1999, **184**, 153–160.
- 2 O. V. Netskina, O. V. Komova, E. S. Tayban, G. V. Oderova, S. A. Mukha, G. G. Kuvshinov and V. I. Simagina, *Appl. Catal. A Gen.*, 2013, **467**, 386–393.
- 3 C. Moreno-Castilla, F. Carrasco-Marín, C. Parejo-Pérez and M. V. López Ramón, *Carbon N. Y.*, 2001, **39**, 869–875.
- 4 T. Y. Xu, Q. F. Zhang, H. F. Yang, X. N. Li and J. G. Wang, *Ind. Eng. Chem. Res.*, 2013, **52**, 9783–9789.
- 5 B. F. Machado, M. Oubenali, M. Rosa Axet, T. Trang Nguyen, M. Tunckol, M. Girleanu, O. Ersen, I. C. Gerber and P. Serp, *J. Catal.*, 2014, **309**, 185–198.
- 6 M. Conte, C. J. Davies, D. J. Morgan, T. E. Davies, D. J. Elias, A. F. Carley, P. Johnston and G. J. Hutchings, *J. Catal.*, 2013, **297**, 128–136.
- 7 J. Xu, J. Zhao, J. Xu, T. Zhang, X. Li, X. Di, J. Ni, J. Wang and J. Cen, *Ind. Eng. Chem. Res.*, 2014, **53**, 14272–14281.
- 8 K. C. O’Connell, J. R. Monnier, J. R. R. Regalbuto, K. C. O’Connell, J. R. Monnier and J. R. R. Regalbuto, *Appl. Catal. B Environ.*, 2018, **225**, 268–272.
- 9 W. S. Hummers and R. E. Offeman, *J. Am. Chem. Soc.*, 1958, **80**, 1339.
- 10 B. C. Brodie, *Philos. Trans. R. Soc. London*, 1859, **149**, 249–259.
- 11 L. Staudenmaier, *Berichte der Dtsch. Chem. Gesellschaft*, 1898, **31**, 1481–1487.
- 12 U. Hofmann and E. König, *Zeitschrift für Anorg. und Allg. Chemie*, 1937, **234**, 311–336.
- 13 C. Yu, C. F. Wang and S. Chen, *Sci. Rep.*, 2016, **6**, 1–7.
- 14 D. C. Marcano, D. V. Kosynkin, J. M. Berlin, A. Sinitskii, Z. Sun, A. Slesarev, L. B. Alemany, W. Lu and J. M. Tour, *ACS Nano*, 2010, **4**, 4806–4814.
- 15 J. Sun, N. Yang, Z. Sun, M. Zeng, L. Fu, C. Hu and S. Hu, *ACS Appl. Mater. Interfaces*, 2015, **7**, 21356–21363.
- 16 J. Chen, B. Yao, C. Li and G. Shi, *Carbon N. Y.*, 2013, **64**, 225–229.
- 17 H. Yu, B. Zhang, C. Bulin, R. Li and R. Xing, *Sci. Rep.*, 2016, **6**, 1–7.
- 18 J. H. Kang, T. Kim, J. Choi, J. Park, Y. S. Kim, M. S. Chang, H. Jung, K. T. Park, S. J. Yang and C. R. Park, *Chem. Mater.*, 2016, **28**, 756–764.
- 19 A. M. Dimiev and J. M. Tour, *ACS Nano*, 2014, **8**, 3060–3068.
- 20 S. D. Pattison, *PhD Thesis*, 2015, Cardiff University.
- 21 C. Buono, P. R. Davies, R. J. Davies, T. Jones, R. Lewis, D. J. Morgan, N. Robinson and D. J. Willock, *Faraday Discuss.*, 2014, **173**, 257–272.
- 22 G. Malta, S. A. Kondrat, S. J. Freakley, C. J. Davies, L. Lu, S. R. Dawson, A. Thetford, E. K. Gibson, D. J. Morgan, W. Jones, P. P. Wells, P. Johnston, C. R. A. Catlow, C. J. Kiely and G. J. Hutchings, *Science*, 2017, **355**, 1399–1403.
- 23 Y. Jia, R. Hu, Q. Zhou, H. Wang, X. Gao and J. Zhang, *J. Catal.*, 2017, **348**, 223–232.
- 24 J. Zhang, W. Sheng, C. Guo and W. Li, *RSC Adv.*, 2013, **3**, 21062–21068.
- 25 H. Zhang, W. Li, Y. Jin, W. Sheng, M. Hu, X. Wang and J. Zhang, *Appl. Catal. B Environ.*, 2016, **189**, 56–64.
- 26 M. Conte, A. F. Carley, C. Heirene, D. J. Willock, P. Johnston, A. A. Herzing, C. J. Kiely and G. J. Hutchings, *J. Catal.*, 2007, **250**, 231–239.
- 27 H. P. Boehm, *Carbon N. Y.*, 2002, **40**, 145–149.
- 28 J. L. Figueiredo, M. F. R. Pereira, M. M. A. Freitas and J. J. M. Órfão, *Carbon N. Y.*, 1999, **37**, 1379–1389.
- 29 J. L. Figueiredo and M. F. R. Pereira, *Catal. Today*, 2010, **150**, 2–7.

- 30 J. L. Figueiredo, M. F. R. R. Pereira, M. M. A. A. Freitas, J. J. M. M. Órfão, L. Figueiredo, M. F. R. R. Pereira, M. M. A. A. Freitas, J. L. Figueiredo, M. F. R. R. Pereira, M. M. A. A. Freitas and J. J. M. M. Órfão, *Ind. Eng. Chem. Res.*, 2007, **46**, 4110–4115.
- 31 C. Rodríguez-valencia, S. Chiussi, M. López-álvarez, S. Stefanov, S. Chiussi, J. Serra and P. González, *Inst. Civ. Eng.*, 2014, **3**, 106–114.
- 32 S. Reiche, N. Kowalew and R. Schlögl, *ChemPhysChem*, 2015, **16**, 579–587.
- 33 J. Zhao, B. Wang, Y. Yue, S. Di, Y. Zhai, H. He, G. Sheng, H. Lai, Y. Zhu, L. Guo and X. Li, *J. Catal.*, 2018, **365**, 153–162.
- 34 M. Inagaki, in *Handbook of Advanced Ceramics*, ed. S. Somiya, Academic Press, 2nd edn., 2013, pp. 25–60.
- 35 M. Pawlyta, J.-N. Rouzaud and S. Duber, *Carbon N. Y.*, 2015, **84**, 479–490.
- 36 G. Malta, S. A. Kondrat, S. J. Freakley, C. J. Davies, S. R. Dawson, X. Liu, L. Lu, K. Dymkowski, F. Fernandez-Alonso, S. Mukhopadhyay, E. K. Gibson, P. P. Wells, S. F. Parker, C. J. Kiely and G. J. Hutchings, *ACS Catal.*, 2018, **8**, 8493–8505.
- 37 B. Nkosi, M. D. Adams, N. J. Coville and G. J. Hutchings, *J. Catal.*, 1991, **128**, 378–386.
- 38 B. Nkosi, N. J. Coville, G. J. Hutchings, M. D. Adams, J. Friedl and F. E. Wagner, *J. Catal.*, 1991, **128**, 378–386.
- 39 P. Johnston, N. Carthey and G. J. Hutchings, *J. Am. Chem. Soc.*, 2015, **137**, 14548–14557.
- 40 G. Malta, S. J. Freakley, S. A. Kondrat and G. J. Hutchings, *Chem. Commun.*, 2017, **53**, 11733–11746.
- 41 A. Uehara, S.-Y. Chang, S. G. Booth, S. L. M. Schroeder, J. F. W. Mosselmans and R. A. W. Dryfe, *Electrochim. Acta*, 2016, **190**, 997–1006.
- 42 K. Paclawski, D. A. Zajac, M. Borowiec, C. Kapusta and K. Fitzner, *J. Phys. Chem. A*, 2010, **114**, 11943–11947.
- 43 X. Chen, W. Chu, D. Chen, Z. Wu, A. Marcelli and Z. Wu, *Chem. Geol.*, 2009, **268**, 74–80.
- 44 Z. Song, J. P. L. Kenney, J. B. Fein and B. A. Bunker, *Geochim. Cosmochim. Acta*, 2012, **86**, 103–117.
- 45 V. Datsyuk, M. Kalyva, K. Papagelis, J. Parthenios, D. Tasis, A. Siokou, I. Kallitsis and C. Galiotis, *Carbon N. Y.*, 2008, **46**, 833–840.
- 46 M. Tang, H. Dou and K. Sun, *Polymer (Guildf.)*, 2006, **47**, 728–734.
- 47 C. L. Bianchi, S. Biella, A. Gervasini, L. Prati and M. Rossi, *Catal. Letters*, 2003, **85**, 91–96.

6. Conclusions and future work

The use of gold catalysts for the acetylene hydrochlorination reaction has increased significantly since its discovery and development by Hutchings et al. This work focused on the effect of changing the solvent and the support in order to improve the catalytic activity, detailing significant steps towards removing the need for harmful highly oxidising solvents and improving the initial catalytic activity.

6.1. Carbon supported single-site gold catalysts prepared using low polarity solvents

Aqua regia is often used as solvent to prepare gold on carbon catalysts for the acetylene hydrochlorination reaction, due to the solvent's ability to prepare catalysts with a high dispersion of oxidised gold species on the support surface; however, the environmental and safety implications of this solvent make it unsuitable for use in industrial scale preparations. This work shows that low polarity solvents can offer a suitable alternative to aqua regia. Their use in the preparation of the catalyst can result in active catalysts with a reduced induction period, when compared with those prepared with aqua regia. Furthermore, when using acetone, the drying temperature is significantly reduced and the solvent is neither toxic nor corrosive, resulting in a much greener catalyst preparation method.

The activity of the catalyst was correlated with the polarity of the solvent, as decreasing the polarity resulted in a higher acetylene conversion. When using high polarity solvents, two variables were considered before preparation of the catalyst; the concentration of water in the solvent and the drying temperature. A greater water concentration resulted in the formation of gold nanoparticles (monitored using XRD), which have been shown to be inactive for the acetylene hydrochlorination reaction. Therefore, where possible, extra dry solvents should be used. Increasing the drying temperature, especially to temperatures greater than 140 °C facilitated gold nanoparticle formation via sintering, hence should also be avoided.

When using acetone as a solvent, the catalyst displayed stable conversion for 4 h and maintained the same conversion upon re-use for a further 3 h, indicating potential viability for industrial use. This was attributed to the oxidation state of the gold, as determined via XANES spectroscopy: the oxidation state changed rapidly from a mixture of Au(I)/Au(III) to predominately Au(I), the species which is considered responsible for high activity in Au/C catalysts during this reaction.

Future work should focus on the scale-up of the catalyst, to determine whether it could be utilised in industry and also to determine whether the formation of Au(0) could be reduced further, to possibly attain a higher conversion from the Au/C-Acetone catalyst.

6.2. Sulfur treated, carbon supported gold catalysts

The addition of sulfur increased the activity of the Au/C catalyst. By pre-washing the carbon in a dilute solution of H₂SO₄, the atomic concentration of sulfur increased from 0.1 to 0.5 %, determined via XPS and this increase more than trebled the initial acetylene conversion, whilst also removing the induction period associated with Au/C catalysts prepared with aqua regia. Altering the preparation method, via a post-wash or using H₂SO₄ as the solvent instead of aqua regia, resulted in a poorer catalytic performance. Therefore, pre-washing the carbon was the best method to introduce sulfur. This method should be optimised, perhaps whilst concurrently changing the gold loading, to attain an optimal gold-sulfur interaction. This interaction was suggested due to EXAFS analysis; however, without the use of appropriate standards or other characterisation techniques it was not possible to determine the exact sulfur species present. Pre-washing the carbon with hydrochloric or nitric acid had only a minor affect on acetylene conversion. Phosphoric acid resulted in a similar activity profile to that of sulfuric acid; a rapid initial increase in conversion followed by a quick deactivation. It would be useful to study this catalyst in order to better appreciate the deactivation mechanism, which could lead to a greater understanding of how to stabilise the cationic gold species.

Future work should include comparing the sulfuric acid treated catalyst to appropriate sulfur standards, to determine the sulfur species present. This may help to understand the interaction of sulfur with gold, to determine why this catalyst was so active. The dispersion of the gold and sulfur before and after reaction, monitored via STEM, may also lead to a greater appreciation of this interaction. Methods with a greater degree of accuracy should be employed to determine the exact sulfur concentration on the pre-wash catalyst. For example, gas chromatography equipped with a pulsed flame photometric detector, or x-ray fluorescence, both techniques regularly used for sulfur analysis. A greater understanding of the above issues could help to improve the catalyst preparation with an aim towards stabilising the gold species during the course of the reaction.

6.3. Oxidised carbon supported gold catalysts

The carbon support was oxidised using a modified Hummers' method, thereby introducing greater oxygen functionality that could interact with the gold. This oxidation resulted in both a

high initial acetylene conversion and, significantly, activation of the catalyst at temperatures below 200 °C. This is especially important for the hydrochlorination of acetylene performed under industrial reaction conditions, where reducing energy consumption is advantageous and a constant goal.

XPS analysis determined the optimum oxygen concentration to be 21 %. Increasing or decreasing this concentration resulted in a lower acetylene conversion. High conversion was attributed to the presence of ether groups introduced via the oxidation, whilst carbonyls decreased the conversion. The catalyst prepared with 21 % oxygen was active at 130 °C, which resulted in a much longer induction period but the resulting acetylene conversion was higher than that achieved by unmodified Au/C. Interestingly a catalyst prepared by washing the carbon with water before deposition of gold also had a high initial acetylene conversion. This was attributed to the loss of traces of Na, K and Cl.

Alternative oxidation methods, refluxing the carbon in HNO₃ and using H₂O₂/HCl as a solvent, resulted in varying oxygen concentrations but the same acetylene conversion as unmodified Au/C. This showed that the concentration of oxygen was not the key factor in determining conversion but the oxygen groups themselves would be responsible for changes in conversion. Future work should be aimed at determining the functionality responsible for the changes in acetylene conversion. STEM analysis should be performed to monitor the distribution of gold and oxygen throughout the reaction. A study should be performed to determine the effect of elements such as Na, K and Cl. The preparation method should be optimised to ensure reproducibility, in order that the catalyst will light off at 130 °C, which will aid in future studies.